Absorption sélective de gaz par des liquides ioniques basés sur des anions carboxylates ou des anions tris (pentafluoroethyl) trifluorophosphates

Stéphane Stevanovic

▶ **To cite this version:**

Stéphane Stevanovic. Absorption sélective de gaz par des liquides ioniques basés sur des anions carboxylates ou des anions tris (pentafluoroethyl) trifluorophosphates. Autre. Université Blaise Pascal - Clermont-Ferrand II, 2012. Français. NNT : 2012CLF22294 . tel-00822155

HAL Id: tel-00822155
https://theses.hal.science/tel-00822155

Submitted on 14 May 2013

HAL is a multi-disciplinary open access archive for the deposit and dissemination of scientific research documents, whether they are published or not. The documents may come from teaching and research institutions in France or abroad, or from public or private research centers.

L'archive ouverte pluridisciplinaire **HAL**, est destinée au dépôt et à la diffusion de documents scientifiques de niveau recherche, publiés ou non, émanant des établissements d'enseignement et de recherche français ou étrangers, des laboratoires publics ou privés.

N^{O} d'Ordre : D.U. 2297

UNIVERSITE BLAISE PASCAL

U.F.R. Sciences et Technologies

ECOLE DOCTORALE DES SCIENCES FONDAMENTALES

N^{0} 732

THESE

présentée pour obtenir le grade de

DOCTEUR UNIVERSITAIRE

Spécialité : Chimie Physique

Par **STEVANOVIC Stéphane**

ABSORPTION SELECTIVE DE GAZ PAR DES LIQUIDES IONIQUES BASES SUR DES ANIONS CARBOXYLATES OU DES ANIONS TRIS(PENTAFLUOROETHYL)TRIFLUOROPHOSPHATES

Soutenue publiquement le 28/11/2012, devant la commission d'examen.

Directeurs :	Costa Gomes Margarida	Examinateurs :	Coxam Jean Yves
	Padua Agilio		Santini Catherine
Rapporteurs :	Herri Jean-Michel	Invités :	Carrette Pierre-Louis
	Jacquemin Johan		Husson Pascale

Résumé

Différentes familles de liquides ioniques ont été sélectionnées pour leur capacité d'absorption de gaz et plus particulièrement de dioxyde de carbone. L'objectif de ces travaux est de définir les liquides ioniques les plus à même d'être utilisés en tant qu'absorbants dits alternatifs dans les procédés de captage de gaz, l'enjeu principal étant à terme de diminuer les coûts de production des procédés industriels.

Les systèmes retenus sont des liquides ioniques purs issus de la combinaison de cations imidazolium, pyrrolidinium et phosphonium avec des anions de type carboxylate ou tris(pentafluoroethyl)trifluorophosphate ainsi que des mélanges binaires de liquides ioniques avec anion carboxylate + eau.

L'absorption de différents gaz - dioxyde de carbone, azote, protoxyde d'azote et éthane - dans les liquides ioniques purs ainsi que dans les mélanges liquide ionique + eau a été mesurée dans une gamme de températures comprises entre 303.15 et 353.15 K et pour des pressions proches de l'atmosphérique. La sélectivité des liquides ioniques pour l'absorption de dioxyde de carbone par rapport aux autres gaz a pu être déterminée. La caractérisation de l'absorption de gaz est fonction des systèmes étudiés, les interactions entre les gaz et certains liquides ioniques (ou certains mélanges liquide ionique + eau) étant uniquement de type physique alors que dans d'autres systèmes, l'absorption est le résultat à la fois d'interactions physiques mais également de la présence de réaction chimique.

Mots clefs : Captage de gaz, dioxyde de carbone, liquides ioniques, propriétés thermophysiques, absorption, mécanismes de solvatation.

Abstract

Different classes of ionic liquids have been selected for their ability to solubilize gases and more particularly carbon dioxide. The objective of this work is to define the ionic liquids which are most likely to be used as alternative absorbents in capture processes of gases, the main issue is to reduce the costs of production of the industrial processes.

The systems used are the pure ionic liquids from the combination of imidazolium, phosphonium and pyrrolidinium cation with carboxylate or tris (pentafluoroethyl) trifluorophosphate anion and binary mixtures of ionic liquids with carboxylate anion + water.

The absorption of different gases - carbon dioxide, nitrogen, nitrous oxide and ethane – in pure ionic liquids as well as in mixtures of ionic liquid + water was measured in a temperature range of between 303.15 and 353.15 K and pressures close to atmospheric. The selectivity of ionic liquids for the absorption of carbon dioxide from other gases could was determined. Characterization of gas absorption is a function of the studied system, since the interactions between gas and ionic liquid (or mixture ionic liquid + water) are of the physical type for some systems, while in other, the absorption is the result of both physical interaction and chemical reaction.

Keywords: Gas capture, carbon dioxide, ionic liquid, thermophysical properties, absorption, mechanisms of solvation.

Remerciements

Ces travaux se sont déroulés à l'Institut de Chimie de Clermont-Ferrand (ICCF) – UMR 6296 de l'Université Blaise Pascale Clermont Ferrand et du CNRS.

Je tiens à remercier les nombreuses personnes qui ont été impliquées dans ce projet :

Mes directeurs de thèse Margarida F. Costa Gomes et Agilio Padua pour m'avoir permis d'intégrer l'équipe liquides ioniques et avoir encadré cette thèse,

Jean Yves Coxam et Karine Ballerat-Busseroles, de l'équipe captage du CO_2 qui ont également contribué à ce projet,

Johan Jacquemin et Jean Michel Herri pour avoir accepté d'être les rapporteurs de ces travaux ainsi que les autres membres du jury à savoir Pierre Louis Carrette, Pascale Husson et Catherine Santini,

Les différentes personnes du projet ACACIA qui ont collaboré à ces travaux : Paul Broutin, Ilham Mokbel et Dominique Picq,

Laure Pison qui a été d'une aide précieuse notamment lors des travaux expérimentaux effectués au cours de cette thèse ainsi que les autres personnes qui ont contribué de près ou de loin à ce travail : Claude Forano, Sabine Sarraute,

Tous les postdoctorants, doctorants et stagiaires qui ont pu participer à ces travaux : Dimitrios Almantariotis, Yohann Coulier, Yun Deng, Olivia Fandino, Maxime Francais, Leila Moura, Alfonso S. Pensado et Ajda Podgorsek.

Sommaire

1. INTRODUCTION

1.1 Contexte

Les principaux gaz à effet de serre (GES) présents à l'état « naturel » dans l'atmosphère sont la vapeur d'eau (H_2O) pour 55 %, le dioxyde de carbone (CO_2) pour 39 %, le méthane (CH_4) pour 2 %, l'ozone (O_3) pour 2 % et le protoxyde d'azote (N_2O) pour 2 %. Les six GES d'origine industrielle listés dans le protocole de Kyoto sont le dioxyde de carbone, le méthane, le protoxyde d'azote, les hydrofluorocarbones (HFC), les hydrocarbures perfluorés (PFC) et l'hexafluorure de soufre (SF_6). Le pouvoir de réchauffement global (PRG), visant à comparer la contribution d'un gaz à effet de serre au réchauffement climatique par rapport à celle du CO_2, sur une période donnée, permet d'exprimer les émissions de gaz à effet de serre en équivalent CO_2. Ces émissions de GES d'origine anthropique ont fortement augmenté depuis l'époque préindustrielle, passant de 28.7 milliards de tonnes-équivalent CO_2 ($GtCO_2eq$) en 1970 à 49.0 $GtCO_2eq$ en 2004 soit une hausse de 70 %[1] (Figure 1). Le dioxyde de carbone est le gaz à effet de serre le plus important par le volume de ses émissions, celles-ci ayant augmenté de 80 % en 34 ans, et représentant 77 % des émissions de gaz à effet de serre en 2004. Ceci est à mettre en relation avec le développement de l'utilisation des combustibles fossiles par les industries.

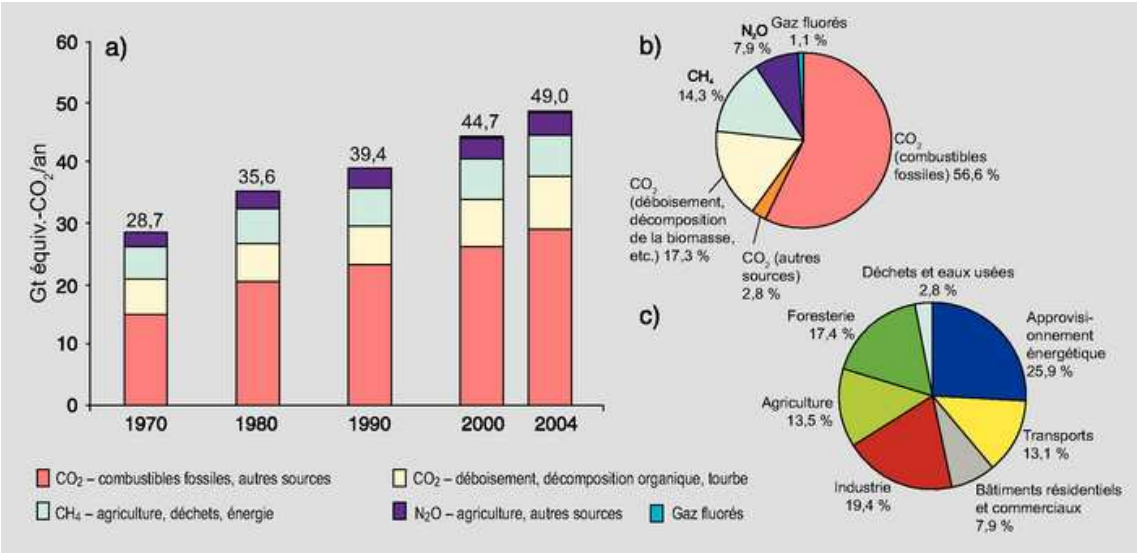

Figure 1. a) Émissions annuelles mondiales de gaz à effet de serre (GES) anthropiques sur la période 1970 - 2004. b) Parts respectives des différents GES anthropiques dans les émissions totales de 2004, en équivalent - CO_2. c) Contribution des différents secteurs aux émissions totales de GES anthropiques en 2004, en équivalent - CO_2.[1]

Afin de limiter les émissions de dioxyde de carbone dans l'atmosphère, plusieurs mesures sont apparues. Le protocole de Kyoto, signé en 1997 par 188 pays et ratifié en 2005 va dans ce sens. Il vise à réduire de 5.2 % les émissions de dioxyde de carbone des 38 pays les plus industrialisés entre 2008 et 2012 par rapport à leur niveau de 1990.[2] Depuis la signature du protocole de Kyoto, l'Union Européenne s'est engagée à réduire de 8 % ses émissions globales de dioxyde de carbone et a mis en place un marché de permis d'émissions négociables à parti du 1er janvier 2005. La Commission européenne a également présenté, dans le cadre du « Paquet Energie-Climat » une procédure visant entres autres à réduire de 20 % les émissions de gaz à effet de serre d'ici 2020.

Une des voies envisagées pour réduire les émissions de gaz à effet de serre est le développement des technologies de captage de dioxyde de carbone. Le principe consiste à capter le dioxyde de carbone au niveau d'installations industrielles fixes émettrices de grandes quantités de gaz dans l'atmosphère. Les émissions issues des fumées étant généralement constituées d'un mélange de dioxyde de carbone mais également de vapeur d'eau, d'azote et d'oxygène, il est nécessaire, dans un premier temps, de séparer le dioxyde de carbone des autres gaz. Les trois principales techniques utilisées pour le captage de dioxyde de carbone sont illustrées dans la Figure 2.

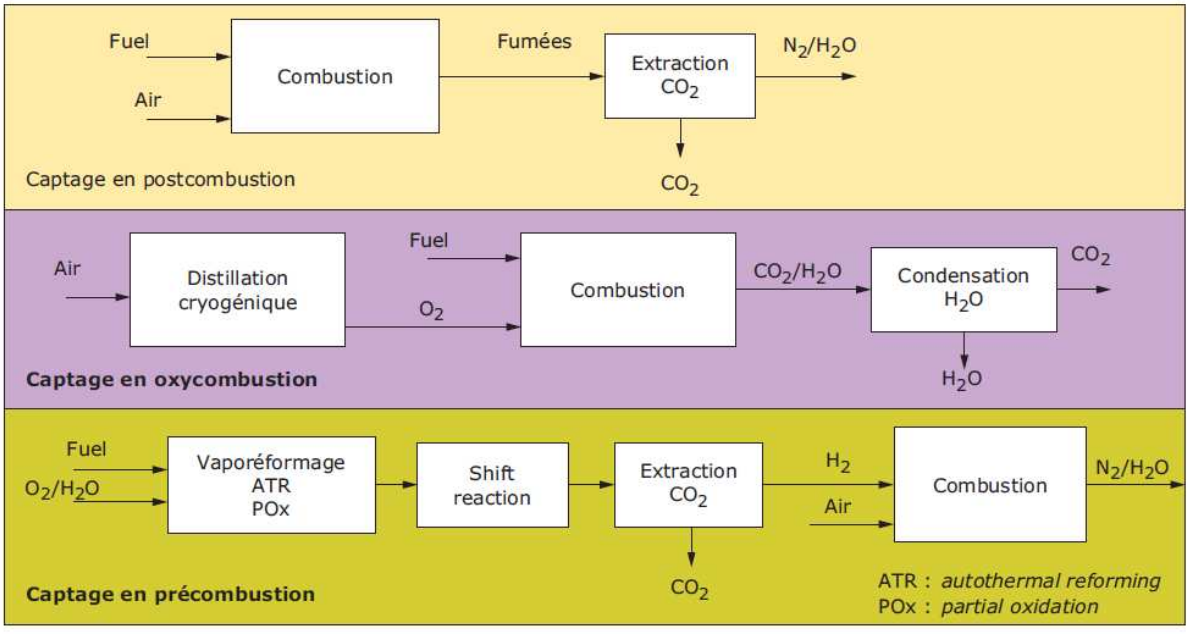

Figure 2. Principales techniques de captage du dioxyde de carbone.[3]

Le captage en oxycombustion[4] consiste à faire une combustion en présence d'oxygène pur ou dilué par du dioxyde de carbone. Les fumées produites sont composées uniquement de dioxyde de carbone et de vapeur d'eau.

Le captage en précombustion[5] consiste à convertir le combustible initial en gaz de synthèse, constitué d'un mélange de dioxyde de carbone et d'hydrogène. Le gaz de synthèse est ensuite transformé en présence d'eau ce qui permet de séparer le dioxyde de carbone et l'hydrogène.

Enfin le captage en postcombustion[6] consiste à séparer le dioxyde de carbone contenu dans les fumées de combustion en sortie d'installation. Dans ce cas, les fumées sont traitées à pression atmosphérique et les volumes sont très importants. Le dioxyde de carbone est relativement dilué, de 3 à 20 % en concentration volumique et doit être séparé des autres gaz présents dans les fumées. Différentes technologies sont actuellement en développement pour le captage en postcombustion tels que l'adsorption, la séparation membranaire, la cryogénie et l'absorption aux solvants. L'absorption peut se faire à l'aide de solvants physiques ou hybrides (physique + chimique).

1.2 Projet ACACIA

Le projet ACACIA (Amélioration du Captage du CO_2 Industriel et Anthropique), s'inscrit dans cette thématique de captage de gaz. Ce projet, d'une durée de 36 mois s'étalant d'octobre 2008 à octobre 2011, a été financé par le FUI (Fonds Unique Interministériel). Ce projet, faisant intervenir à la fois des partenaires industriels (RHODIA, IFP, ARKEMA, LAFARGE, SOLVAY, GDF, VEOLIA) et académiques (ICCF, LMOPS, LSA, Université Claude Bernard Lyon 1) est à la recherche de solutions pour diminuer les émissions de dioxyde de carbone dans l'atmosphère. L'objectif principal du projet est de développer des méthodes de captage en post combustion avec comme enjeu principal la réduction des coûts des procédés existants. Plusieurs solutions ont été envisagées dans ce projet. Le captage du dioxyde de carbone par voie liquide en est une. Les travaux exposés ici vont s'intéresser à des solvants dits alternatifs et pouvant interagir physiquement ou chimiquement avec le dioxyde de carbone. C'est dans ce contexte que le sous projet SP2.5, concernant l'étude de la capture du dioxyde de carbone par des liquides ioniques, a été mis en place.

1.3 Liquides ioniques

Les liquides ioniques sont des composés constitués uniquement d'ions, un cation organique et un anion organique ou inorganique généralement volumineux[7], et dont la température de fusion est inferieure à 100°C.[8] La combinaison des différents cations et anions permet d'obtenir une grande variété de liquides ioniques, plusieurs centaines de liquides ioniques différents étant actuellement commercialisés.[9] Les cations et les anions les plus fréquemment utilisés sont regroupés dans la figure ci dessous.[10]

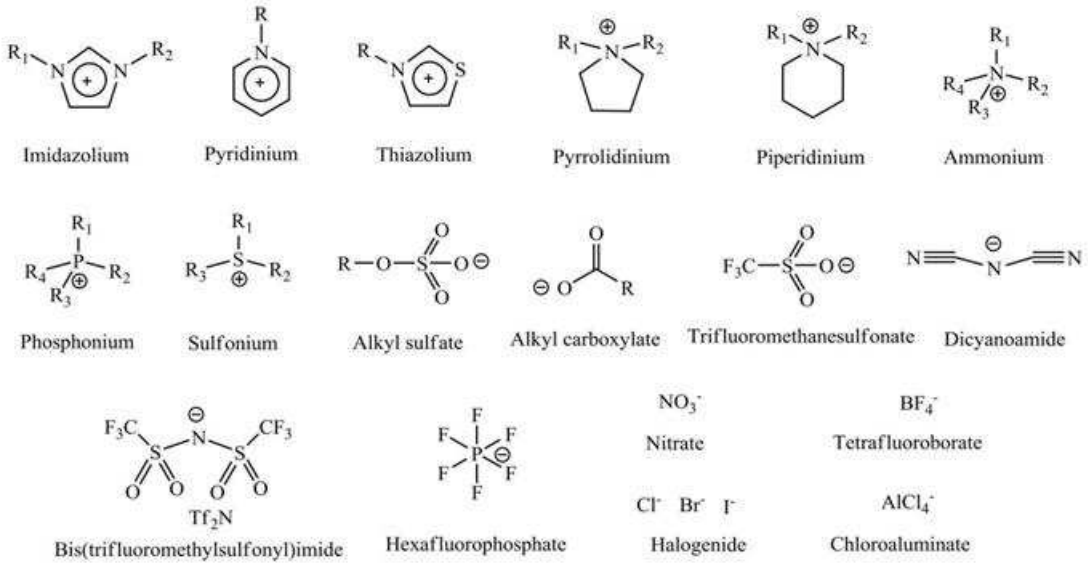

Figure 3. Exemple de cations et d'anions formant les liquides ioniques.

L'association de cations et d'anions de tailles différentes confère aux liquides ioniques des structures moléculaires asymétriques ainsi qu'une grande flexibilité et une très faible tension de vapeur.[11] La variété des combinaisons cation/anion possibles influe également sur les propriétés physico-chimiques des liquides ioniques (conductivité, température de fusion, densité, viscosité, miscibilité avec de l'eau…)[12,13] ainsi que sur leur propriété à solubiliser des composés organiques, inorganiques ou des gaz.[14]

Le caractère modulable des liquides ioniques fait qu'ils peuvent être utilisés dans de nombreuses applications telles que les techniques de séparation, la chimie analytique, l'électrochimie, la catalyse, la biocatalyse et la chimie synthétique.[15]

1.4 Objectifs

Les travaux présentés ici consistent à comparer la capacité d'absorption de gaz et plus principalement de dioxyde de carbone dans différentes familles de liquides ioniques purs ainsi que dans des mélanges binaires liquides ioniques + eau. Le terme d'absorption regroupe deux notions, premièrement la notion de solubilité, associée à des phénomènes purement physiques et deuxièmement, la notion de réaction chimique. L'objectif principal est de contribuer au développement de l'utilisation de liquides ioniques qui satisfont à un ensemble de contraintes dans les processus industriels de captage de dioxyde de carbone. En effet, le solvant utilisé devra posséder une grande capacité d'absorption et de régénération, une importante sélectivité du dioxyde de carbone par rapport aux autres gaz, une cinétique rapide tout en ayant une stabilité thermique suffisante et des capacités de transport compatibles avec une utilisation dans un procédé industriel. La détermination de l'absorption en fonction de la température a permis d'accéder aux propriétés thermodynamiques de solvatation des gaz dans des liquides ioniques à savoir l'énergie de Gibbs de solvatation, l'enthalpie de solvatation et l'entropie de solvatation. Ceci aide à comprendre la manière dont les liquides ioniques interagissent avec les autres composés et comment ils se structurent autour de ces molécules autrement dit la façon dont les solutés se solubilisent dans le solvant. D'un point de vue pratique, la connaissance de l'enthalpie de solvatation permet d'estimer la quantité d'énergie nécessaire à la régénération du solvant lors du fonctionnement du procédé.

Ces travaux ont également consisté dans un premier temps à étudier les propriétés thermophysiques des différents systèmes – masse volumique et viscosité - ces données étant nécessaires pour le dimensionnement des procédés. La viscosité, caractérisant la résistance du fluide au mouvement, est particulièrement importante, car les procédés ne fonctionnent que très rarement en mode statique. La connaissance de ces propriétés aide également à la compréhension de la structure et des interactions au niveau moléculaire en établissant des relations entre les propriétés macroscopiques et la structure moléculaire.

Les différents gaz à solubiliser - dioxyde de carbone, azote, protoxyde d'azote et éthane - choisis sont des GES ou des gaz utilisés dans le domaine industriel. Le dioxyde de carbone et l'azote sont deux gaz que l'on retrouve dans les fumées en sortie d'usine, le protoxyde d'azote est un GES d'origine industrielle listé dans le protocole de Kyoto tandis que l'éthane peut simuler le comportement du méthane, gaz

faisant également partie des principaux GES d'origine industrielle. Ces différents gaz présentent également un intérêt d'un point de vue fondamental du fait de leur nature et de leur structure moléculaire variable.

La sélection des systèmes liquides ioniques purs et liquides ioniques + eau a été influencée par la nature des interactions possibles avec les gaz préalablement choisis et plus particulièrement avec le dioxyde de carbone. Alors que la majorité des travaux actuels ou passés se sont pour le moment attardés sur les phénomènes de solubilité de dioxyde de carbone dans différents types de liquides ioniques, nous nous sommes penchés ici sur les liquides ioniques pouvant réagir chimiquement avec le dioxyde de carbone. L'avantage de travailler avec de tels liquides est d'obtenir une augmentation considérable (un ordre de grandeur) de l'absorption du dioxyde de carbone. L'étude de différentes familles de liquides ioniques purs et de mélanges binaires liquide ionique + eau a permis d'évaluer et d'optimiser les différentes propriétés de ces systèmes.

Une première partie du projet a porté sur les liquides ioniques avec un anion tris(pentafluoroethyl)trifluorophosphate (eFAP). Ces travaux font suite à l'étude de l'influence de la présence de chaines alkyles fluorées au niveau du cation sur l'absorption de gaz par les liquides ioniques.[16] Cette première partie s'intéresse cette fois à l'effet de la fluorination de l'anion. Il n'existe d'ailleurs à ce jour aucune explication définitive sur la nature des phénomènes entrant en jeu dans l'absorption du dioxyde de carbone par ces liquides ioniques, les informations trouvables dans la littérature révélant une controverse au sujet de l'existence ou non d'une réaction chimique possible entre ces liquides et le dioxyde de carbone. L'absorption de gaz - dioxyde de carbone, azote, protoxyde d'azote et éthane - a été mesurée dans trois liquides ioniques différents, le 1-butyl-3-methylimidazolium tris(pentafluoroethyl)trifluorophosphate $[C_1C_4Im][eFAP]$, le 1-butyl-1-methylpyrrolidinium tris(pentafluoroethyl)trifluorophosphate $[C_1C_4Pyrro][eFAP]$ et le trihexyl(tétradécyl)phosphonium tris(pentafluoroéthyl)trifluorophosphate $[P_{66614}][eFAP]$. La solubilité de l'eau dans ces liquides ioniques a également été étudiée afin de définir la gamme de composition applicable pour un procédé industriel. Les travaux concernant le liquide ionique avec le cation imidazolium sont regroupés dans le premier article disponible dans la partie 4 du présent manuscrit (*Absorption of carbon dioxide, nitrous oxide, ethane and nitrogen by 1-alkyl-3-methylimidazolium (C_nmIm, n=2,4,6) tris(pentafluoroethyl)trifluorophosphate ionic liquids (eFAP)*) tandis que les

travaux concernant les liquides ioniques basés sur les cations pyrrolidinium et phosphonium sont regroupés dans le second article (*Solubility of carbon dioxide, nitrous oxide, ethane and nitrogen in 1-butyl-1-methylpyrrolidinium and trihexyl(tetradecyl)phosphonium tris(pentafluoroethyl)trifluorophosphate (eFAP) ionic liquids.*).

La seconde partie du projet s'est intéressée à l'absorption de gaz dans les liquides ioniques avec un anion carboxylate et plus particulièrement avec l'anion acétate (OAc). Nous avons débuté ces mesures avec le 1-butyl-3-methylimidazolium acétate [C_1C_4Im][OAc] suite à la mise en évidence, dans la littérature, d'une réaction chimique possible entre ce liquide ionique et le dioxyde de carbone. Ensuite, nous avons travaillé avec le 1-ethyl-3-methylimidazolium acétate [C_1C_2Im][OAc] afin d'observer l'effet de la variation de la longueur de la chaine alkyle du cation sur les propriétés thermo-physiques et l'absorption de gaz. Enfin, l'effet, sur les propriétés thermo-physiques et sur l'absorption de dioxyde de carbone, de l'ajout d'eau dans les liquides a été étudié en réalisant différentes mesures dans les systèmes [C_1C_4Im][OAc] + H_2O et [C_1C_2Im][OAc] + H_2O. Les résultats relatifs à ces deux liquides ioniques sont rassemblés dans le troisième article (*Effect of water on the carbon dioxide absorption by 1-alkyl-3-methylimidazolium acetate ionic liquids*).

Le butylmethylpyrrolidinium acétate [C_1C_4Pyrro][OAc], du fait de son absence de proton labile et de cycle aromatique, a également été étudié afin de mieux comprendre les mécanismes qui contrôlent l'absorption du CO_2. Comme précédemment, différentes mesures dans les systèmes [C_1C_4Pyrro][OAc] + H_2O ont été réalisées afin d'observer l'effet de l'ajout d'eau les propriétés thermo-physiques et sur l'absorption de dioxyde de carbone. Pour mieux comprendre l'influence de l'anion sur l'absorption du CO_2, nous nous sommes également intéressés à des liquides ioniques possédant des anions carboxylates plus lourds et ne produisant ainsi pas de composés volatils. Les liquides ioniques pressentis pour cette étude étaient le 1-butyl-3-methylimidazolium isobutyrate [C_1C_4Im][ISB], le 1-butyl-3-methylimidazolium levulinate [C_1C_4Im][LEV] et le 1-butyl-3-methylimidazolium propionate [C_1C_4Im][PRO]. La synthèse du [C_1C_4Im][LEV] avec une pureté suffisamment importante a permis d'intégrer dans ce projet des mesures de propriétés thermophysiques ainsi que d'absorption de dioxyde de carbone dans ce liquide ionique pur. Les mesures concernant ces deux liquides ioniques sont présentes dans le quatrième article (*Absorption of carbon dioxide by ionic liquids with carboxylate anions*).

Les liquides ioniques utilisés au cours de ces travaux sont représentés dans le Tableau 1.

Tableau 1. Noms, formules moléculaires et abréviations des liquides ioniques utilisés.

Nom	Formule	Abréviation
1-ethyl-3-methylimidazolium acetate	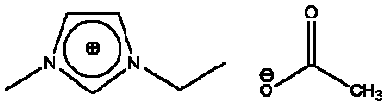	$[C_1C_2Im][OAc]$
1-butyl-3-methylimidazolium acetate	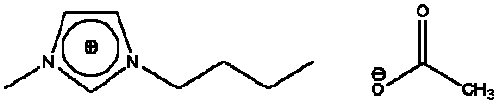	$[C_1C_4Im][OAc]$
1-butyl-1-methylpyrrolidinium acetate	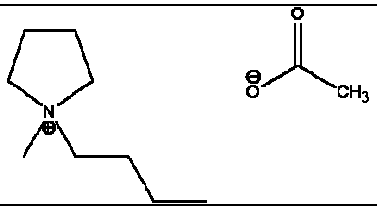	$[C_1C_4Pyrro][OAc]$
1-butyl-3-methylimidazolium levulinate	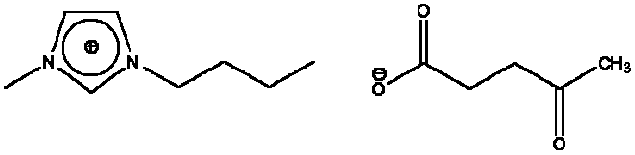	$[C_1C_4Im][LEV]$
1-butyl-3-methylimidazolium tris(pentafluoroethyl) trifluorophosphate	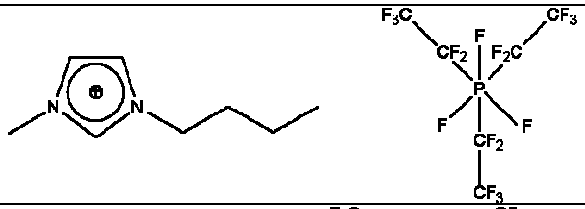	$[C_1C_4Im][eFAP]$
1-butyl-1-methylpyrrolidinium tris(pentafluoroethyl) trifluorophosphate	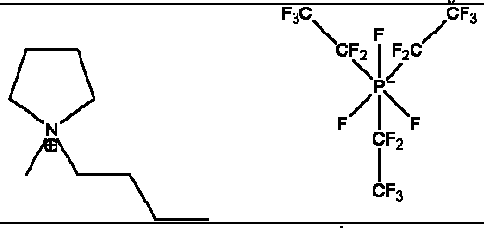	$[C_1C_4Pyrro][eFAP]$
trihexyl(tétradécyl)phosphonium tris(pentafluoroéthyl) trifluorophosphate	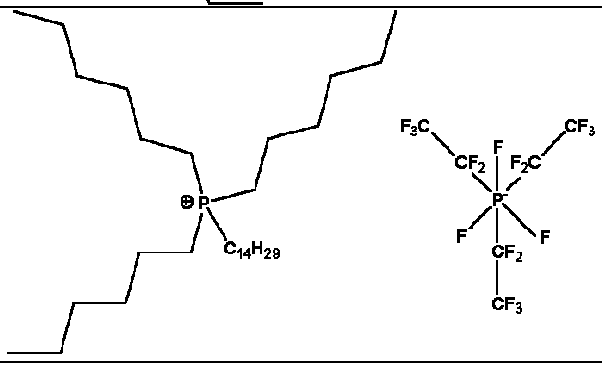	$[P_{66614}][eFAP]$

2. REVUE BIBLIOGRAPHIQUE

2.1 Captage de gaz dans les liquides ioniques

L'étude de l'absorption de gaz par des liquides ioniques débute en 1999 avec les travaux de Blanchard et al.[17] L'intérêt des liquides ioniques en tant que potentiels solvants dans les procédés industriels de captage et de séparation de gaz est mis en évidence trois ans plus tard, en 2002.[18] Dès lors, les recherches sur l'absorption de gaz et plus particulièrement de dioxyde de carbone par les liquides ioniques vont connaître un essor rapide, la grande variété de liquides ioniques allant de pair avec les nombreuses pistes de recherche développées. Ces différentes avancées ont fait l'objet de plusieurs reviews.[19,20] Selon ces travaux, les liquides ioniques présentent plusieurs avantages. L'absorption de dioxyde de carbone dans les liquides ioniques est plus importante (un ordre de grandeur au moins) comparée à celle d'autres gaz comme l'azote, l'oxygène, l'hydrogène et l'éthane. Le second intérêt des liquides ioniques réside dans le processus de régénération peu couteux d'un point de vue énergétique, les interactions entre le dioxyde de carbone et les liquides ioniques étant généralement de type physique. Les mesures d'absorption de dioxyde de carbone ont débuté avec des liquides ioniques avec un cation de type imidazolium et des anions hexafluorophosphate (PF_6), bis(trifluoromethylsulfonyl)imide (NTf_2) ou tetrafluoroborate (BF_4) avant de se tourner vers des liquides ioniques avec anion tris(pentafluoroalkyl)trifluorophosphate (FAP) ou acétate (OAc). L'ensemble des progrès et les axes de développement futurs pour trouver des liquides ioniques appropriés pour le captage de dioxyde de carbone ont également été discutés plus récemment.[21,22] Les propriétés des liquides ioniques sont comparées aux autres solvants commercialisés et si les capacités d'absorption de dioxyde de carbone et de sélectivité sont suffisamment intéressantes comparativement à ces autres solvants, le coût ainsi que le manque de données physicochimiques et thermodynamiques ou encore de données sur l'impact environnemental reste un frein en vue d'une application à l'échelle industrielle.

2.2 Liquides ioniques avec l'anion tris(pentafluoroethyl)trifluorophosphate

La synthèse des liquides ioniques avec un anion tris(pentafluoroalkyl)trifluorophosphate (FAP) est décrite pour la première fois en 2005.[23] Ces anions, de formule générale $[(C_nF_{2n+1})_3PF_3]^-$, sont une alternative aux anions $[PF_6]^-$, hydrolytiquement instables à haute température et ou certains

groupements fluors sont remplacés par des groupements perfluoroalkyl. Ils sont désignés sous les termes tris(pentafluoroethyl)trifluorophosphate (eFAP) $[(C_2F_5)_3PF_3]^-$, tris(heptafluoropropyl)trifluorophosphate (pFAP) $[(C_3F_7)_3PF_3]^-$ et tris(nonafluorobutyl)trifluorophosphate (bFAP) $[(C_4F_9)_3PF_3]^-$, etc en fonction de la longueur des chaines C_nF_{2n+1}. Ces anions peuvent être combinés avec des cations de type imidazolium, phosphonium, pyrrolidinium, pyridinium, ammonium, uronium, thiouronium ou encore guanidinium.[23] Ils possèdent des propriétés les démarquant des liquides ioniques avec un anion acétate. Parmi ces propriétés, on pense au caractère hydrophobe et par conséquent partiellement miscible avec l'eau, à la stabilité thermique plus importante (jusqu'à 300 °C) mais également à une viscosité moindre à cation équivalent.

Quelques mesures d'absorption de gaz dans cette famille de liquides ioniques sont décrites dans la littérature et concernent principalement le dioxyde de carbone. Les premières mesures expérimentales, effectuées par Maginn, sont des mesures d'absorption de dioxyde de carbone et d'oxygène dans le $[C_1C_3Im][pFAP]$ en fonction de la température.[24] D'autres valeurs expérimentales d'absorption de dioxyde de carbone ont été mesurées en fonction de la pression et de la température avec différents liquides en faisant varier la longueur de la chaine fluoroalkyle de l'anion par Muldoon et al.[25] Il ressort de cette étude que l'augmentation de la longueur de cette chaine fluoroalkyle est accompagnée d'une augmentation de l'absorption de dioxyde de carbone. L'absorption de dioxyde de carbone dans le $[C_1C_6Im][eFAP]$, à 298K et en fonction de la pression a également été mesurée par Yokozeki et al.[26] Récemment, Blath et al. ont mesuré l'absorption d'oxygène, d'azote et de dioxyde de carbone dans les liquides ioniques $[C_1C_6Im][eFAP]$ et $[P_{66614}][eFAP]$ à 333.15 K.[27]

D'autres résultats d'absorption de gaz ont également été obtenus par des méthodes prédictives. La méthode COSMO-RS a été utilisée afin de mesurer l'absorption de dioxyde de carbone en fonction de la température et de la pression dans différents liquides ioniques basés sur l'anion eFAP.[28] Des mesures expérimentales ont ensuite été réalisées sur trois liquides ioniques, le $[C_1C_6Im][eFAP]$, le $[C_1C_4Pyrro][eFAP]$ et le [ETT][eFAP] afin de pouvoir comparer les valeurs avec les résultats issus du modèle. Enfin, l'absorption de gaz a été déterminée par simulation moléculaire[29] dans le $[C_1C_6Im][eFAP]$. L'ensemble des constantes de Henry (K_H) de dioxyde de carbone dans les liquides ioniques avec l'anion nFAP, sont répertoriées dans le Tableau 2.

Tableau 2. Mesures de l'absorption de dioxyde de carbone à 0.1 MPa par méthode expérimentale (Maginn, 2005[24]; Muldoon et al., 2007[25];Yokozeki et al., 2007[26]; Blath et al., 2011[27]) et par différents modèles prédictifs (Zhang et al., 2008[28]; Zhang et al., 2009[29]).

Liquide ionique	T / K	K_H / 10^5Pa	Auteur	Référence
$[C_1C_6Im][pFAP]$	298.15	21.6	Muldoon et al., 2007	25
	333.15	36.0	Muldoon et al., 2007	25
$[C_1C_5Im][bFAP]$	298.15	20.2	Maginn, 2005	24
	333.15	32.9	Maginn, 2005	24
	298.15	20.2	Muldoon et al., 2007	25
	333.15	32.9	Muldoon et al., 2007	25
$[C_1C_6Im][eFAP]$	298.15	25.2	Muldoon et al., 2007	25
	333.15	42.0	Muldoon et al., 2007	25
	298.00	21.6	Yokozeki et al., 2008	26
	283.50	18.5	Zhang et al., 2008	28
	298.60	23.7	Zhang et al., 2008	28
	323.30	36.6	Zhang et al., 2008	28
	298.20	18.9	Zhang et al., 2009	29
	333.15	48.0	Blath et al., 2011	27
$[C_1C_4Pyrro][eFAP]$	283.50	20.3	Zhang et al., 2008	28
	298.60	28.5	Zhang et al., 2008	28
	323.30	44.5	Zhang et al., 2008	28
[ETT][eFAP]	283.50	20.8	Zhang et al., 2008	28
	298.60	29.4	Zhang et al., 2008	28
	323.30	48.4	Zhang et al., 2008	28
$[P_{66614}][eFAP]$	333.15	36.4	Blath et al., 2011	27

Si la majorité des auteurs s'accordent à dire que nous sommes ici en présence de phénomène de solubilité, la question reste toutefois actuellement ouverte. Le groupe de Yokozeki[26] notamment, à partir de leurs mesures expérimentales, a proposé un modèle d'équation d'état permettant d'étudier le comportement des systèmes dioxyde de carbone + liquide ionique. Il ressort de celui-ci que le comportement de l'absorption de dioxyde de carbone dans les liquides ioniques avec l'anion eFAP s'éloigne du domaine d'application de la loi de Raoult. Une importante déviation négative de l'absorption par rapport à la loi de Raoult suggère que l'absorption de dioxyde de carbone est contrôlée par l'existence de réaction chimique et non pas par des phénomènes de solubilité dans ce cas.

2.3 Liquides ioniques avec l'anion carboxylate

Les travaux s'attardant sur l'absorption de gaz et principalement de dioxyde de carbone dans les liquides ioniques avec l'anion carboxylate sont relativement importants.

Maginn a été le premier, en 2005, à publier des résultats expérimentaux d'absorption du dioxyde de carbone dans les liquides ioniques avec anion carboxylate et plus particulièrement dans le 1-butyl-3-methylimidazolium acetate [C_1C_4Im][OAc].[24] Ces premières mesures ont été réalisées par gravimétrie et en fonction de la température et de la pression. Parallèlement, l'origine de la forte absorption de dioxyde de carbone (un ordre de grandeur supérieure à ce qui avait été mesuré jusqu'ici dans d'autres liquides ioniques) a été expliquée par l'existence d'un mécanisme de réaction chimique entre le dioxyde de carbone et le liquide ionique. La formation d'acide acétique a été prouvée par RMN. Le mécanisme de réaction chimique, présenté sur la Figure 4 implique la déprotonation du noyau imidazolium en position C2 et aboutit à la formation d'un carbène et d'acide acétique. L'association entre le dioxyde de carbone et ce carbène entraine par la suite la formation d'une espèce de type sel de carboxylate.

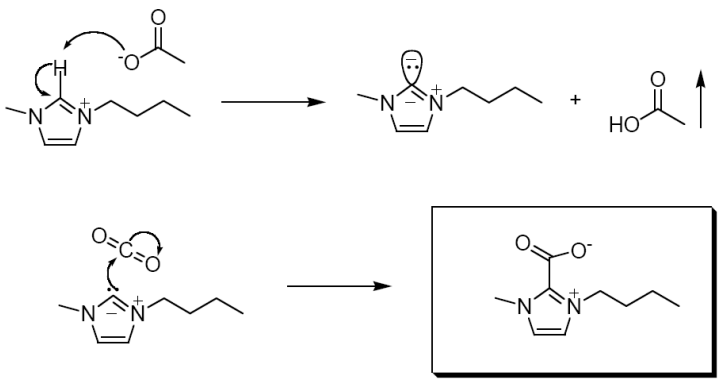

Figure 4. Mécanisme de réaction chimique entre le [C_1C_4Im][OAc] et le dioxyde de carbone proposée par Maginn.[24]

Le mécanisme proposé par Maginn n'a pas été confirmé ou infirmé jusqu'à très récemment. Les études qui ont fait suite à cette publication ont en effet proposé d'autres mécanismes pour expliquer le taux d'absorption important de dioxyde de carbone dans les liquides ioniques avec l'anion acétate. On trouve tout d'abord un article s'intéressant à l'absorption du dioxyde de carbone dans le [C_1C_4Im][OAc].[30] L'absorption est déterminée par une technique gravimétrique en fonction de la

température et jusqu'à une pression de 20 bar. Parallèlement, un modèle thermodynamique basé sur une équation d'état est développé et est destiné à prédire le comportement du système liquide ionique-dioxyde de carbone. La formation d'un complexe (réaction chimique) réversible a été révélée par l'intermédiaire de l'étude des propriétés thermodynamiques d'excès du système. La comparaison du $[C_1C_4Im][OAc]$ pur et du $[C_1C_4Im][OAc]$ en présence de dioxyde de carbone par analyse RMN au proton et analyse thermo gravimétrique couplée infra rouge n'a pas permis de détecter la formation de nouvelles espèces malgré l'odeur d'acide acétique présente après les mesures expérimentales d'absorption du dioxyde de carbone. Ceci laisse supposer que si réaction chimique il y a, celle-ci est mineure. De plus, l'analyse par infra rouge par réflexion totale atténuée et par spectroscopie infrarouge à transformée de Fourier laisse supposer la formation d'un sel de carboxylate. Enfin, l'analyse thermo gravimétrique couplée infra rouge et des mesures gravimétriques d'absorption/désorption ont montré que la formation du complexe est réversible.

La même équipe a étendu l'étude à l'absorption de dioxyde de carbone à 298K dans 18 liquides ioniques dont plusieurs avec un anion de type carboxylate.[26] Les mesures ont été corrélées avec un modèle d'équation d'état permettant d'étudier le comportement des systèmes dioxyde de carbone + liquide ionique et de déterminer l'énergie de Gibbs d'excès, l'enthalpie d'excès ainsi que l'entropie d'excès. La détermination de ces fonctions thermodynamiques d'excès a permis de mettre en évidence, au travers de valeurs d'énergie de Gibbs suffisamment négatives, l'existence d'absorption d'origine chimique dans plusieurs liquides ioniques. Celle-ci se traduit par la formation d'associations chimiques ou de complexes chimiques de type A + B = AB ou A + 2B = AB_2 ou A désigne le dioxyde de carbone et B désigne le liquide ionique. Les liquides ioniques avec anion carboxylate concernés par la formation d'un complexe de type A + 2B = AB_2 sont le 1-ethyl-3-methylimidazolium acetate $[C_1C_2Im][OAc]$, le 1-butyl-3-methylimidazolium levulinate $[C_1C_4Im][LEV]$, le 1-butyl-3-methylimidazolium acetate $[C_1C_4Im][OAc]$, le 1-butyl-3-methylimidazolium propionate $[C_1C_4Im][PRO]$, le 1-butyl-3-methylimidazolium isobutyrate $[C_1C_4Im][ISB]$, le bis(1-butyl-3 methylimidazolium) iminiodiacetate $[C_1C_4Im]_2[IDA]$ et le 1-butyl-3-methylimidazolium trimethylacetate $[C_1C_4Im][TMA]$.

Shiflett et al.[31] ont également publié d'autres travaux afin de comparer la capacité d'absorption du dioxyde de carbone pour des liquides ioniques basés sur l'anion acétate ou trifluoroacétate, $[C_1C_2Im][OAc]$ et $[C_1C_2Im][TFA]$, mettant en évidence une absorption chimique dans le premier cas et physique dans le second

cas. Les valeurs d'absorption de dioxyde de carbone plus importantes dans le $[C_1C_2Im][OAc]$ sont également expliquées par la formation réversible d'un complexe AB_2 lui même lié à une réaction acidobasique de Lewis.

Carvalho et al.[32] ont également travaillé avec le $[C_1C_4Im][OAc]$. Des mesures d'absorption sont réalisées dans une cellule pVT jusqu'à des pressions égales à 74 MPa. Leurs travaux indiquent que l'ion acétate réagit chimiquement avec le dioxyde de carbone pour les faibles fractions molaires de CO_2 (fraction molaire de gaz < 0.3). Les calculs ab initio ainsi que les spectres RMN au ^{13}C suggèrent la présence d'interactions de type acide base de Lewis entre le gaz et l'anion, les deux oxygènes de l'anion interagissant avec le dioxyde de carbone. Cependant, la mise en évidence d'acide acétique n'a pas été possible.

Shi et al.[33] ont mis en évidence par des calculs ab initio pour les liquides ioniques $[C_1C_2Im][OAc]$ et $[C_1C_4Pyrro][OAc]$ des interactions entre le cation et le dioxyde de carbone plus faibles que les interactions entre l'anion et le dioxyde de carbone et des interactions entre le dioxyde de carbone et l'anion plus fortes que les interactions entre l'hydrogène et l'anion. Enfin, les interactions entre le dioxyde de carbone et l'anion acétate dans le $[C_1C_2Im][OAc]$ sont de deux types, il existe à la fois des interactions suffisamment fortes entre le carbone du dioxyde de carbone et un oxygène de l'anion acétate pour former un complexe mais également des interactions faibles, le cation imidazolium interagissant avec l'anion et entrant ainsi en concurrence avec le dioxyde de carbone. En remplaçant le cation $[C_1C_2Im]^+$ par un cation de type pyrrolidinium $[C_nPyrro]^+$, le nombre d'atomes d'oxygènes libres pouvant interagir avec le dioxyde carbone est plus élevé, entraînant une augmentation de la capacité d'absorption du dioxyde de carbone.

Plus récemment, les mécanismes qui sont à la fois à l'origine de la formation d'acide acétique mais également à l'origine de la formation d'un carboxylate suite à la réaction des liquides ioniques avec le dioxyde de carbone ont été mis en évidence.

Tout d'abord, Tommasi et Sorrentino[34], ont démontré que la formation d'un 1,3-dialkylimidazolium-2-carboxylate était possible à partir de la carboxylation d'un sel 1,3-dialkylimidazolium chlorure avec un système CO_2/Na_2CO_3. La formation du carboxylate est caractérisée par RMN au proton et au carbone.

Wang et al[35] avaient également mis en évidence la possibilité de former des carboxylates en combinant une superbase de type 1,8-diazabicyclo[5.4.0]undec-7-ene (DBU) ou 1,3,4,6,7,8-hexahydro-1-methyl-2H-pyrimido[1,2-a]pyrimidine (MTBD) avec des liquides ioniques avec cation imidazolium, du fait de la faible acidité du proton du

cycle imidazolium situé en C2. La présence des différentes espèces est confirmé par RMN.

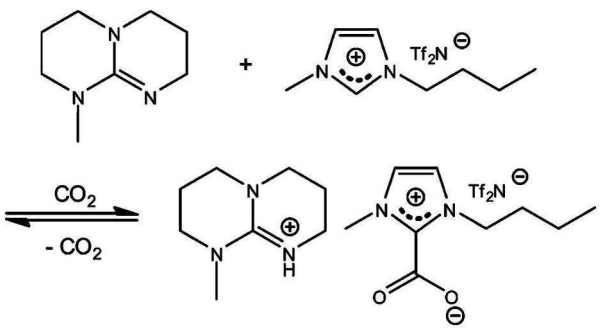

Figure 5. Mécanisme de réaction chimique entre le liquide ionique et une superbase proposé par Wang et al.[35]

Rodrigez et al[36] ont expliqué la formation d'un carbène accompagné de la présence d'acide acétique à l'état stable dans les liquides ioniques [C_1C_2Im][OAc] et [C_1C_4Im][OAc] purs.

Le liquide ionique réagit à la fois en tant que base et en tant que réactif pour la formation du carbène dans le cas de liquides ioniques possédant un anion suffisamment basique pour pouvoir réagir avec le proton situé en C2 sur le cation. Dans le cas des liquides ioniques [C_1C_2Im][OAc] et [C_1C_4Im][OAc], la formation de carbène est accompagnée de la formation d'acide acétique, l'anion étant suffisamment basique pour capter le proton en C2 du cation.

La volatilisation attendue de l'acide acétique formé qui serait synonyme de formation continue de carbène jusqu'a épuisement de la base n'est ici pas possible. En effet, l'acide carboxylique et le carboxylate forment un « complexe anionique » relativement stable. La stabilité d'un tel complexe a déjà été mise en évidence dans des travaux ultérieurs.[37,38] La formation d'acide acétique stable entraine ainsi un équilibre dans la réaction. Le mécanisme est résumé dans la Figure 6.

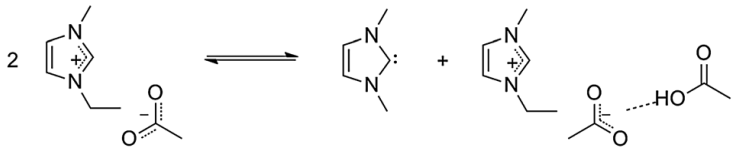

Figure 6. Mécanisme de stabilisation de l'acide acétique volatil proposée par Rodrigez et al.[36]

Le carbène formé peut ensuite réagir avec des molécules donneuses de proton, ici des chalcogènes, pour aboutir à la formation d'imidazolium-2-chalcogenones. Il est bien précisé que la formation d'imidazolium-2-chalciogenone ne peut se faire qu'après

formation de carbène et que cette réaction est par conséquent impossible avec des liquides ioniques possédant un anion pas suffisamment basique.

Les travaux suivants de Gurau et al.[39] ont cette fois cherché à confirmer le mécanisme de réaction proposé precedemment[36] ainsi que l'importance de la formation du « complexe anionique » par diffractométrie de rayons X. La mise en contact du dioxyde de carbone avec le 1-ethyl-3-methylimidazolium acétate, à pression atmosphérique et à température ambiante aboutit à la formation du 1-ethyl-3-methylimidazolium carboxylate. La présence du carboxylate est confirmée par analyse RMN.

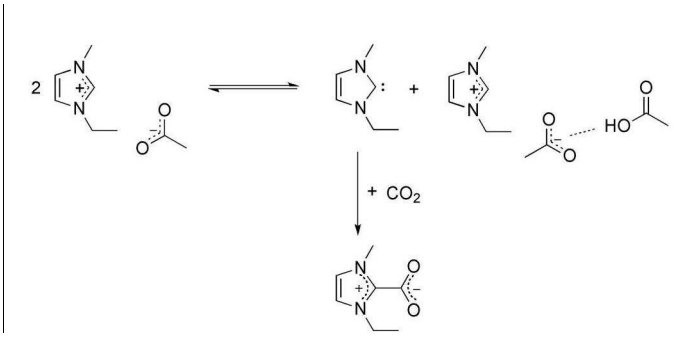

Figure 7. Mécanisme de réaction chimique entre le [C_1C_2Im][OAc] et le dioxyde de carbone proposée par Gurau et al.[39]

L'apparition de la phase solide est plus rapide lorsque la pression augmente. L'ajout d'eau, qui a pour effet d'inhiber la réaction de l'anion acétate avec le proton en C2, entraine une diminution du volume de la phase solide. L'étude par diffractométrie de rayons X est réalisée sur des mélanges [C_1C_2Im][OAc] : [C_1C_1Im][OAc] : [C_2C_2Im][OAc] + dioxyde de carbone. En absence d'eau la formation de carboxylate et de complexe entre l'acide acétique et l'acétate est confirmée, l'ajout de dioxyde de carbone dans le mélange aboutissant à la formation du [C_1C_2Im][$H(OAc)_2$] : [C_1C_2Im][OAc]. En présence d'eau, le dioxyde de carbone est largement libéré et s'accompagne de la formation de [C_1C_2Im][HCO_3].[39]

Coutinho et al.[40] ont également mis en évidence récemment, sous certaines conditions (298 K, 0.1 MPa), la formation du 1-butyl-3-methylimidazolium carboxylate lors de la mise en contact du 1-butyl-3-methylimidazolium acétate avec le dioxyde de carbone. La formation du carboxylate est mise en évidence par des calculs quantiques de type DFT, par spectroscopie Raman et IRTF et par RMN. La comparaison des spectres Raman et IRTF du [C_1C_4Im][OAc] pur et du mélange [C_1C_4Im][OAc] + CO_2 met en évidence l'apparition de trois nouvelles bandes pour ce dernier. Pour confirmer que ces nouvelles bandes obtenues par spectroscopie IR sont assignées au groupe –

COO^- de la molécule carboxylate, les valeurs ont été comparées avec les valeurs du 1-butyl-3-methylimidazolium carboxylate de Tommasi et Sorrentino.[34] De la même manière, la comparaison des spectres RMN au carbone du $[C_1C_4Im][OAc]$ pur et du mélange $[C_1C_4Im][OAc]$ + CO_2 montre l'apparition de nouveaux pics attribués à la formation d'un carboxylate. Enfin, l'étude RMN au proton a mis en évidence la formation d'acide acétique.

L'absorption de dioxyde de carbone a été mesurée par Blath et al. dans les liquides ioniques $[C_1C_2Im][OAc]$ et $[C_1C_2Im][pivalate]$[41]. Le mécanisme proposé pour l'absorption du dioxyde de carbone dans le $[C_1C_2Im][OAc]$ est celui de Maginn[24] et Tommassi et Sorrentino[34] mais adapté pour le $[C_1C_2Im][OAc]$.

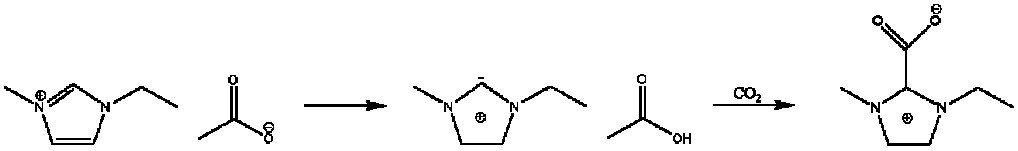

Figure 8. Mécanisme de réaction chimique proposé par Maginn[24] et adapté au $[C_1C_2Im][OAc]$ par Blath et al.[41]

La formation d'un carboxylate est mise en évidence par spectroscopie IRTF, confirmant les résultats de Tommasi et Sorrentino[34] ainsi que par analyse RMN au carbone, confirmant les résultats de Tommasi et Sorrentino[34], Wang et al.[35] et Gurau et al.[39]

Enfin, Shiflett et al.[42] se sont intéressés à l'absorption de dioxyde de carbone dans le 1-ethyl-3-ethylimidazolium acétate. Les fortes valeurs d'absorption de dioxyde de carbone sont expliquées par la formation réversible d'un complexe AB_2 identique à celui se formant dans le cas du $[C_1C_2Im][OAc]$.

Les résultats concernant l'absorption chimique de gaz par des liquides ioniques avec des anions de type carboxylate autres que l'acétate sont assez peu nombreux.

Cabaço et al.[43] ont mesuré l'absorption de dioxyde de carbone dans le $[C_1C_4Im][TFA]$. Les analyses par spectroscopie Raman et par des calculs quantiques de type DFT ont montré que l'absorption est principalement liée à des interactions entre l'atome de carbone du dioxyde de carbone (agissant comme un acide de Lewis) et l'atome d'oxygène du groupement $–COO^-$ du TFA (agissant comme une base de Lewis).

L'absorption de dioxyde de carbone dans le $[C_1C_2Im][TFA]$ a également été mesurée par Yokozeki et al. en précisant que l'absorption était ici uniquement de type physique.[31]

L'absorption de dioxyde de carbone dans le 1-butyl-3-methylimidazolium levulinate $[C_1C_4Im][LEV]$, le 1-butyl-3-methylimidazolium propionate $[C_1C_4Im][PRO]$ et le 1-butyl-3 methylimidazolium isobutyrate $[C_1C_4Im][ISB]$ a été mesurée par Shiflett et al.[26], la formation d'un complexe moléculaire réversible ayant été mis en évidence dans ce cas.

De la même manière, les travaux portant sur l'absorption de gaz ou sur les mécanismes réactionnels dans des liquides ioniques avec des cations qui ne sont pas des imidazoliums sont très rares.

Les quelques travaux portant sur le $[C_1C_4Pyrro][OAc]$[44] suggèrent l'existence d'une réaction chimique impliquant un proton du carbone de la chaine butyl avec l'azote du cycle pyrrolidinium, et aboutissant à la formation d'acide acétique, de methylpyrrolidine et de butène.

Les données concernant cette fois l'absorption de gaz dans les mélanges binaires (liquide ionique avec anion carboxylate + eau) sont plus rarement décrites dans la littérature par rapport à celles concernant les liquides ioniques purs.

Chinn et al.[45] sont les premiers à présenter des valeurs d'absorption de gaz, dioxyde de carbone et méthane, dans un système $[C_1C_4Im][OAc]$ + eau contenant 14 % d'eau en masse. Il ressort de cette étude que la présence d'eau facilite les liaisons entre le liquide ionique et le dioxyde de carbone, l'acétate interagissant avec l'eau pour former une liaison faible réversible avec le dioxyde de carbone.

L'absorption de dioxyde de carbone dans le mélange $[N_{2224}][OAc]$ + eau a également été étudiée.[46] L'absorption est ici décrite comme étant principalement d'origine chimique (réaction acide base de Lewis) lorsque la pression est inferieure à 3 bar et principalement physique pour des pressions comprises entre 3 bar et 30 bar. L'augmentation de la quantité d'eau entraine une diminution de l'absorption de dioxyde de carbone. Cette différence d'absorption dans le liquide ionique pur $[N_{2224}][OAc]$ et dans le mélange $[N_{2224}][OAc]$ + eau s'explique par le mécanisme d'absorption qui n'est pas le même dans les deux cas. Dans le premier cas, l'absorption est uniquement liée à une réaction acide base de Lewis. En présence d'eau, les analyses par spectroscopie IRTF et par étude RMN mettent en évidence une réaction chimique différente :

$$CH_3COO^- + nH_2O + CO_2 \leftrightarrow HCO_3^- + CH_3COOH + (n-1)\ H_2O \quad (1)$$

Dans ce second cas, la réaction chimique atteint l'équilibre lorsque l'anion acétate perd sa basicité, l'absorption de dioxyde de carbone devient alors physique. Quand la quantité d'eau dans le système binaire $[N_{2224}][OAc]$ + eau augmente, l'affinité de l'anion acétate avec le dioxyde de carbone est limitée, l'anion acétate réagissant préférentiellement avec les molécules d'eau. De plus, la réaction atteint la saturation en dioxyde de carbone plus rapidement, l'acide acétique étant plus stable lorsque la quantité d'eau augmente.

Plus récemment, les travaux de Gurau[39] ont montré que l'ajout d'eau avait pour effet d'inhiber la réaction de l'anion acétate avec le proton en C2 lors de la réaction entre le 1-ethyl-3-methylimidazolium acétate et le dioxyde de carbone. Dans des systèmes constitués à la fois de $[C_1C_2Im][OAc]$, de $[C_1C_1Im][OAc]$, de $[C_2C_2Im][OAc]$ et de dioxyde de carbone, l'ajout d'eau s'accompagne de la formation de $[C_1C_2Im][HCO_3]$.

Enfin, Shiflett et al.[42] ont mesuré l'absorption du dioxyde de carbone dans les mélanges $[C_2C_2Im][OAc]$ + eau à différentes compositions. Ils en ont conclu que l'ajout d'eau entraine à la fois une diminution de l'absorption de gaz mais également la formation de bicarbonate limitant ainsi le processus de désorption de gaz.

3. PARTIE EXPERIMENTALE

3.1 Préparation et caractérisation des systèmes

3.1.1 Matériaux

Les liquides ioniques utilisés au cours de cette étude sont reportés dans le Tableau 3.

Tableau 3. Masses molaires, quantité d'eau, pureté et provenance des liquides ioniques étudiés.

Liquide ionique	Masse molaire / $g \cdot mol^{-1}$	Quantité d'eau / pourcentage	Pureté / pourcentage	Fournisseur
$[C_1C_2Im][OAc]$	170.21	< 1[a]	98[a]	Solvionic, France
$[C_1C_4Im][OAc]$	198.26	< 1[a]	> 98[a]	Solvionic, France
$[C_1C_4Pyrro][OAc]$	201.30	< 1[a]	> 98[a]	Solvionic, France
$[C_1C_4Im][LEV]$	257.35			Synthétisé, LCOMS, Villeurbanne, France
$[C_1C_4Im][eFAP]$	584.23	< 1[a]	> 98[a]	Merck, Allemagne
$[C_1C_4Pyrro][eFAP]$	587.27	< 1[a]	> 98[a]	Merck, Allemagne
$[P_{66614}][eFAP]$	928.88	< 1[a]	> 98[a]	Merck, Allemagne

a : communiquée par les fournisseurs

Avant toute mesure, les liquides ioniques sont conditionnés sous vide. Ceci permet d'éliminer toute trace d'impuretés volatiles souvent présentes dans les liquides ioniques et pouvant modifier certaines de leurs propriétés. La nature de ces impuretés peut être fonction de la façon dont les liquides ioniques ont été synthétisés ou encore de leur caractère plus ou moins hydrophobe.

Les halogénures et les cations alcalins sont des impuretés que l'on retrouve fréquemment, toutefois, l'eau reste l'impureté que l'on retrouve en plus grande quantité dans les liquides ioniques[47]. Par conséquent, lorsque l'on veut éviter la présence de traces d'eau dans les liquides ioniques, leur mise en contact avec l'atmosphère est à proscrire notamment pour les plus hydrophiles d'entre eux.

Chaque liquide est introduit dans un Schlenk (SCH) avant d'être raccordé à une ligne de vide (Figure 9) puis soumis à une agitation magnétique. Le liquide est dégazé et séché pendant au moins 48 heures à température ambiante. Si besoin est, dans le cas de liquides très visqueux et/ou hydrophiles, le liquide peut être chauffé afin de diminuer la viscosité et d'augmenter la pression de vapeur de l'eau et donc faciliter son élimination sous vide.

3.1.2 Conditionnement et préparation des échantillons

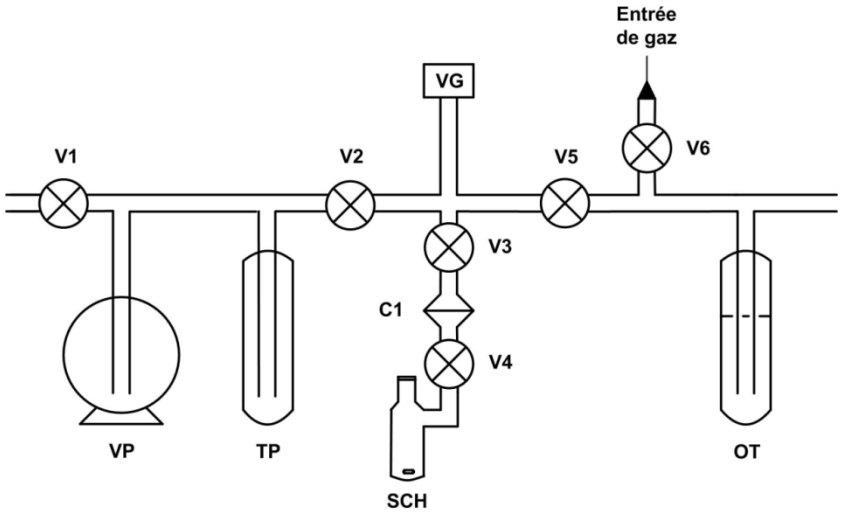

Figure 9. Ligne de conditionnement des liquides ioniques. VP : pompe à vide, TP : piège froid, SCH : Schlenk, VG : jauge de la pression (Pirani), OT : bulleur, C1 : connexion mobile, Vi : Vannes à piston.

Après avoir été séché, le liquide ionique pur peut être placé sous atmosphère inerte selon l'utilisation souhaitée. Le gaz utilisé pour conditionner les liquides ioniques est l'azote, l'hypothèse est faite que la solubilité de l'azote dans les liquides ioniques est négligeable et ne modifie pas leurs propriétés. La mise en contact avec l'azote peut se faire directement via l'entrée de gaz disponible sur la ligne de vide en fermant la vanne V1 puis en ouvrant les vannes V6 puis V5. La deuxième méthode consiste à retirer le Sclenk de la ligne de vide puis à le placer dans une boite à gants étanche dans laquelle on introduit l'azote.

Dans le cas de la préparation des mélanges liquide ionique – eau, l'eau utilisée est de l'eau tridistillée qui est ensuite dégazée sous vide par des cycles successifs de congélation et de décongélation en utilisant de l'azote liquide.

La pesée de tous les échantillons se fait à l'aide d'une balance de marque Mettler modèle AE240 (incertitude de 1×10^{-4} g).

3.1.3 Teneur en eau

Certains des liquides ioniques étudiés ici étant particulièrement hydrophiles, il est parfois impossible d'enlever complètement l'eau qu'ils contiennent, notamment lorsqu'ils sont en contact avec l'atmosphère. C'est pourquoi il est nécessaire, afin de caractériser au mieux la composition exacte de nos échantillons, de connaitre la

quantité d'eau présente dans les liquides ioniques avant et après leur conditionnement. L'analyse de la teneur en eau est faite par titrage Karl Fisher à l'aide d'un titreur coulométrique de Karl Fischer de modèle Mettler Toledo DL32 (précision ± 1 ppm).

3.2 Stabilité thermique

La stabilité thermique des liquides ioniques est déterminée par calorimétrie différentielle à balayage (DSC). L'appareil utilisé est un DSC 2920 de marque TA Instruments (précision calorimétrique de 1 %, précision de température de ±0.1 °C, plage de température comprise entre 213 K et 1073 K).

Le principe consiste à mesurer la différence calorifique entre l'échantillon de liquide ionique et une référence alors que ces deux derniers sont soumis à une variation contrôlée de la température.

Les échantillons sont placés dans des creusets en aluminium puis chauffés de 298.15 K à 673.15 K avec des rampes de montée en température allant de 1 à 10 K/min, sous azote.

Les résultats peuvent être représentés sous forme de thermogramme ou le flux de chaleur, exprimé en $W.g^{-1}$ est fonction de la température. La température de décomposition est égale à la température 'onset' qui elle-même correspond à l'intersection de la tangente à la ligne de base du flux thermique avec la tangente du pic du flux thermique.

3.3 Masse volumique

Les masses volumiques des liquides ioniques purs ont été déterminées dans une gamme de température comprise entre 293 K et 343 K et dans une gamme de pression comprise entre 0.1 MPa et 25 MPa.

Les masses volumiques des mélanges liquide ionique + eau ont également été mesurées en fonction de la pression et de la température pour différentes compositions. Ces données permettent d'accéder aux volumes molaires d'excès pour chacun des mélanges et ainsi de quantifier la non-idéalité des systèmes.

Les masses volumiques ont été obtenues à partir d'un densimètre à tube vibrant Anton Paar modèle DMA 512 opérant en mode statique.

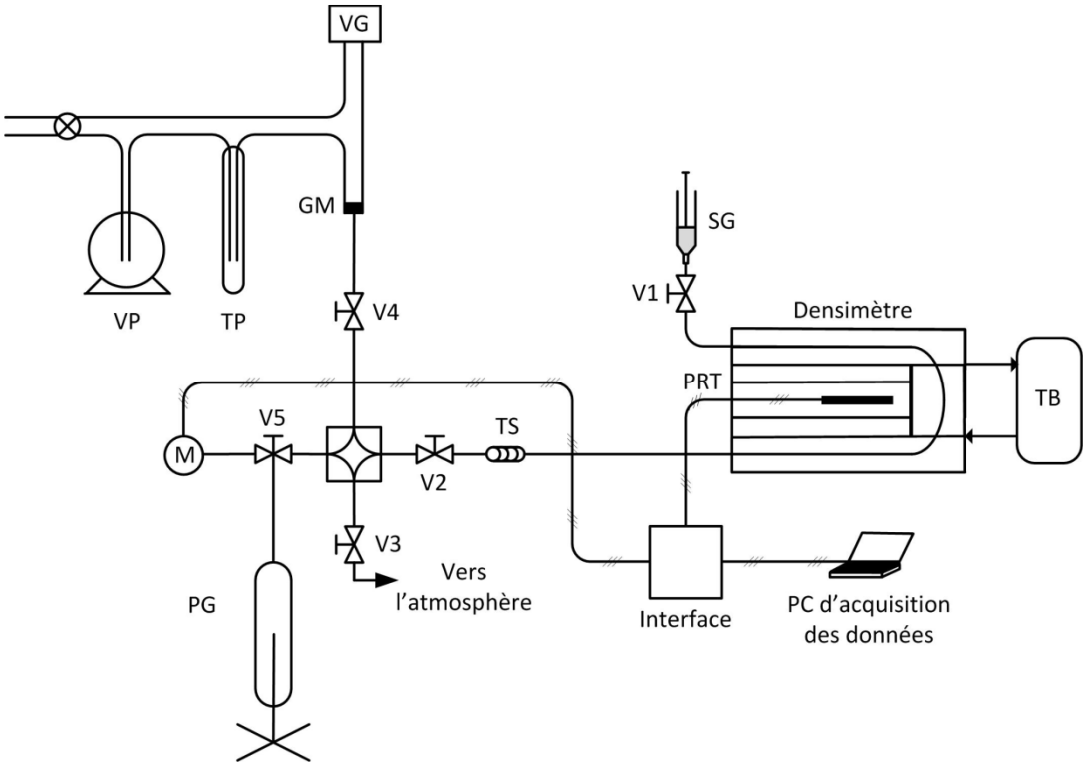

Figure 10. Représentation schématique du densimètre Anton Paar DMA 512 P. VP : pompe à vide; TP : piège froid; VG : jauge de pression (Pirani); GM : connexion métal – verre; V1, V2, V3, V4 et V5 : vannes haute pression; M : manomètre; TS : tube enroulé sous forme de spirale; PRT : sonde de température; SG : seringue en verre étanche aux gaz; PG : générateur de pression; TB : thermorégulateur.

Ce type d'appareillage permet d'effectuer des mesures jusqu'à des pressions pouvant atteindre 70 MPa et dans une gamme de température comprise entre 263 K et 423 K. La pression est mesurée par un manomètre Druck (PTX 610, 0-700 bar abs, précision ± 0.08 % pleine échelle) et la température par une sonde à résistance de platine à quatre fils de 100 Ω (précision ± 0.01 K, justesse 0.04 K). La température est maintenue constante au niveau du tube vibrant à l'aide d'un thermostat à circulation (Julabo FP40-HE). Une interface traduit la période d'oscillation (τ) issue du tube vibrant en signal électrique. L'acquisition de la période, de la température et de la pression est effectuée par un PC via un programme HP VEE.

Le principe de cet appareillage repose sur la mesure de la période de vibration propre d'un tube métallique rempli de liquide ionique. Ce tube est placé dans un champ électromagnétique provoquant des oscillations (mouvement sinusoïdal harmonique) d'amplitude constante et de fréquence dépendant de la masse du tube. Par

conséquent, il est possible de relier la période de vibration (τ) à la masse volumique (ρ) du liquide selon d'équation suivante :

$$\rho = A\tau^2 + B \quad (2)$$

Ou A et B désignent des constantes déterminées par étalonnage en fonction de la température et de la pression à l'aide de plusieurs fluides de référence.

Avant toute mesure, le densimètre est étalonné à l'aide de différents fluides de référence de masses volumiques parfaitement connues sur de larges gammes de température et de pressions selon la méthode de Lagourette.[48] Ces fluides sont choisis de façon à ce que la gamme de masses volumiques des liquides ioniques étudiés soit incluse dans la gamme de masses volumiques de ces fluides étalons. Les fluides utilisés sont le n-heptane (CAS Number 142-82-5, > 99.5 %, Fluka), le bromobenzene (CAS Number 86845-27-4, > 99.5 %, Fluka) et le 2,4-dichlorotoluène (CAS Number 95-73-8, 99 %, Sigma Aldrich), ces fluides ayant la particularité de couvrir une large gamme de masses volumiques (de 683.97 $kg \cdot m^{-3}$ jusqu'à 1493.4 $kg \cdot m^{-3}$, à 293 K et 0.1 MPa)[49]. L'étalonnage est réalisé dans une gamme de températures comprises entre 293 K et 413 K et une gamme de pression comprise entre 0.1 et 40 MPa. L'étalonnage en lui-même consiste à enregistrer les périodes d'oscillations (τ) du tube vibrant correspondantes aux fluides étalons employés, permettant ainsi de déterminer les constantes A et B de l'équation (2).

Lorsque la viscosité des liquides ioniques étudiés est supérieure à 100 mPa.s, un facteur de correction peut être apporté afin d'éliminer l'influence de la viscosité du fluide sur la vibration du tube. L'équation utilisée pour cette correction est fournie par le fabricant du densimètre à tube vibrant Anton Paar[50] :

$$\frac{\Delta\rho}{\rho} = \left(-0.5 + 0.45\sqrt{\eta}\right) \times 10^{-4} \quad (3)$$

Ou ρ est la masse volumique mesurée expérimentalement par le densimètre calibré, $\Delta\rho$ est la différence entre cette valeur et la valeur de masse volumique "corrigée" avec la viscosité et η est la viscosité dynamique de l'échantillon exprimée en mPa.s.

L'imprécision sur la masse volumique, dépendante à la fois des constantes A et B et de la période de vibration du tube vibrant (τ) est calculée à l'aide de l'équation suivante :

$$\sigma_\rho = \left[\left(\frac{\partial \rho}{\partial \tau}\right)^2 \cdot \sigma_\tau^2 + \left(\frac{\partial \rho}{\partial A}\right)^2 \cdot \sigma_A^2 + \left(\frac{\partial \rho}{\partial B}\right)^2 \cdot \sigma_B^2\right]^{1/2} \quad (4)$$

où σ_ρ est l'écart type sur la masse volumique, σ_τ désigne l'écart type obtenu directement par les mesures expérimentales et σ_A et σ_B sont les écarts types associées aux constantes de calibration du densimètre.

L'écart type sur la masse volumique est égal à 1×10^{-4} g·cm^{-3}. A noter que cette expression fait abstraction des fluctuations de température et de pressions, déjà prises en compte indirectement lors de la mesure de la période de vibration.

Les mesures de masses volumiques suivent une procédure préalablement testée.[51,52] Avant toute injection de liquide, le densimètre est mis sous vide puis la partie constituée par la ligne de vide est ensuite isolée en fermant la vanne V4. Une première mesure est effectuée sous vide et à 273.15 K afin de vérifier la période de vibration du tube. Le liquide est alors injecté dans le densimètre à l'aide d'une seringue en verre au niveau de la vanne V1. Le volume de liquide, délimité par les vannes V1 et V2, est de l'ordre de 3.5 mL. La pression du système est ajustée à l'aide d'un générateur de pression rempli d'un fluide hydraulique (dans le présent cas le décane CAS Number 124-18-5, > 99.5 %, Fluka).

Les volumes molaires des liquides ioniques purs peuvent être calculés en fonction de la température à partir des masses molaires M_i et des mesures de masse volumique des liquides ioniques purs ρ_i :

$$V_{m,i} = \frac{M_i}{\rho_i} \quad (5)$$

Dans le cas des systèmes binaires (liquide ionique + eau), les volumes molaires des mélanges peuvent également être calculés à l'aide de la relation suivante :

$$V_m^{mix} = \frac{1}{\rho_m} \sum_i x_i M_i \quad (6)$$

ou ρ_m et x_i désignent la masse volumique du mélange et la fraction molaire du constituant i, respectivement.

La connaissance du volume molaire des deux composés purs, $V_{m,i}$, et du mélange, V_m^{mix} permet alors d'accéder aux volume d'excès, V_m^E, en fonction de la composition :

$$V_m^E = V_m^{mix} - \sum_i x_i V_{m,i} \quad (7)$$

Cette grandeur, correspondant à l'écart entre le volume molaire réel du mélange et son volume idéal, permet de quantifier la non-idéalité des systèmes étudiés.

3.4 Viscosité

Les viscosités des liquides ioniques purs et des systèmes binaires liquides ioniques + eau ont été déterminées dans une gamme de températures comprises entre 293 K et 343 K et à pression atmosphérique. De même que pour les masses volumiques, les viscosités des mélanges liquide ionique + eau ont été mesurées pour différentes compositions.

La viscosité dynamique, η, des composés purs et des mélanges est mesurée à l'aide d'un viscosimètre automatique AMVn de la société Anton Paar. Le principe de mesure repose sur la loi de Stokes [53] et consiste à déterminer la viscosité à partir du temps de chute d'une bille à l'intérieur d'un capillaire. Le diamètre de la bille et du capillaire est choisi en fonction de la viscosité du liquide. Le temps de chute t_1 est mesuré par deux capteurs lasers et est relié, pour une masse volumique connue, à la viscosité dynamique (mPa·s) par l'équation suivante :

$$\eta = k(\rho_b - \rho_N)t_1 \quad (8)$$

avec : η la viscosité dynamique du fluide, k la constante de calibration, ρ_b la densité de la bille, ρ_N la masse volumique du fluide et t_1 le temps de chute de la bille.

Le viscosimètre AMVn de la société Anton Paar permet de travailler dans une gamme de températures comprises entre +5 ℃ et +135 ℃, avec une résolution de 0.01 ℃ et une précision < 0.05 ℃. La gamme de mes ure de viscosité dynamique est comprise entre 0.3 et 2500 mPa·s, avec une précision inferieure à 0.1 % et l'incertitude relative sur la mesure de la viscosité est inferieure à 0.1%.

Deux capillaires de diamètres différents, 1.8 mm et 3.0 mm sont utilisés en fonction de la gamme de viscosité souhaitée. Afin d'obtenir la constante k de l'équation (8), ces capillaires sont préalablement étalonnés en fonction de la température (entre 293 K et 373 K) et de l'angle du capillaire (entre 20° et 80°) à l'aide d'huile de références. Ces dernières, choisies de façon à ce que leur gamme de viscosités englobe celle des liquides ioniques étudiés, sont la N-35, N-100, N-350 et S-60 de la 'Cannon Instrument Company'.

Les composés sont ensuite introduits dans le capillaire correspondant. La température et l'angle du capillaire souhaités sont sélectionnés puis l'appareil effectue une série de douze mesures successives. Afin de vérifier la précision des résultats, un deuxième angle est sélectionné et une nouvelle série de douze mesures sont faites. Ce protocole est répété pour chaque température.

3.5 Miscibilité liquide ionique - eau

La solubilité de l'eau dans les liquides ioniques étudiés a été déterminée en fonction de la température. L'objectif est de connaitre la gamme de composition dans laquelle les mélanges sont constitués d'une seule phase liquide.

Les mesures de miscibilité liquide ionique - eau sont effectuées à l'aide d'un appareil basé sur une méthode pVT[54] (Figure 11).

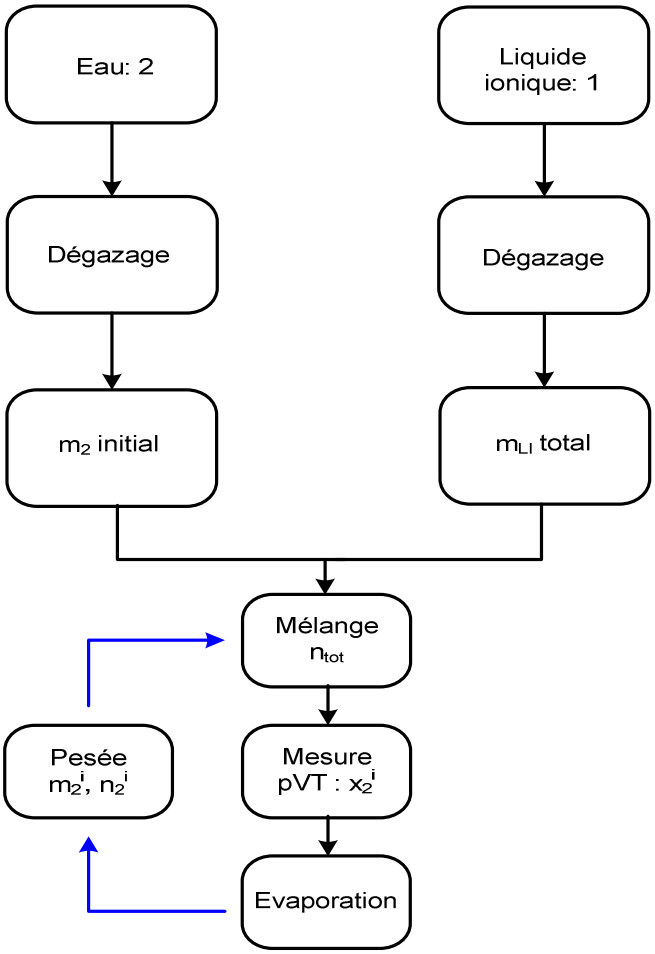

Figure 11. Schéma du principe de mesure de miscibilité la liquide ionique-eau.

La méthode repose sur la mise en contact, à une température donnée, de quantités connues de liquide ionique et d'eau à l'intérieur d'une cellule d'équilibre de volume connu. La pression de vapeur d'équilibre est enregistrée pour une composition bien définie. La composition du mélange est ensuite modifiée en éliminant progressivement l'eau et les pressions résultantes sont ensuite obtenues pour différentes compositions données. Tant que la pression est constante, celle-ci correspond à la pression de vapeur de l'eau et les deux liquides ne sont pas miscibles. La limite de miscibilité est atteinte lorsque la pression de vapeur d'équilibre est inferieure à la pression de vapeur de l'eau. La pression d'équilibre correspond alors à la pression du mélange et les deux liquides sont miscibles.

Le dispositif expérimental est constitué de deux parties, une première partie thermostatée à l'intérieure de laquelle les deux liquides sont mis en contact et une deuxième partie permettant la mise de l'ensemble de l'installation sous vide, les deux parties étant délimitées par la vanne V3 (Figure 12).

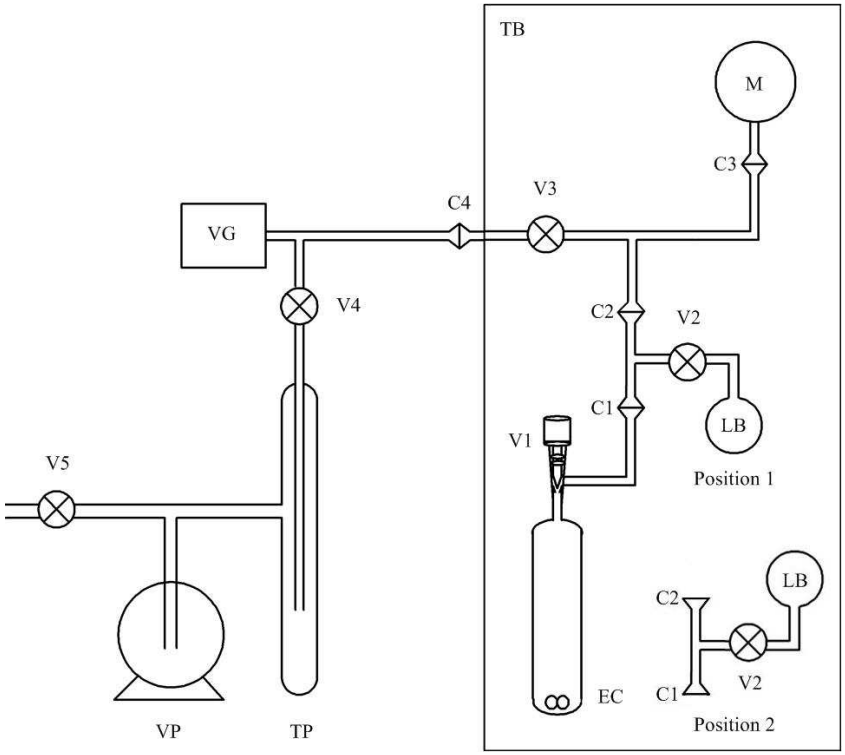

Figure 12. Schéma de l'appareil de mesure de miscibilité liquide-liquide. EC : cellule d'équilibre ; Vi : vannes ; Ci : connexions rotulex ; LB : ballons de gaz ; M : manomètre ; VP : pompe à vide.

La partie mesure est constituée d'une cellule d'équilibre liquide-liquide-vapeur (EC), d'un manomètre (M) (Druck DPI 262, 35-1400 mbar, incertitude de ± 0.1 %, pleine échelle), d'une vanne V1 et d'une connexion C1. La fermeture de la vanne V1 permet l'isolation de la cellule d'équilibre du reste de la partie mesure. La connexion C1 permet, d'une part, de déplacer la cellule d'équilibre et d'autre part de mettre en place le ballon contenant l'eau (LB).

L'ensemble de cette partie est maintenu à température constante dans un bain d'air (BT). La température est contrôlée à l'aide d'un contrôleur PID (Hart Scientific modèle 2200, résolution ± 0.01 K) et est mesurée à l'aide d'un thermomètre à résistance de platine (Modèle Leeds and Northrup 25 Ohm, précision 4×10^{-3} K). Cette résistance est mesurée à l'aide d'un multimètre Fluke 8840A (résolution de résistance $5^{1/2}$).

Le volume de la cellule d'équilibre (V_{EC}) est préalablement étalonné par pesée avec de l'eau tridistillée en fonction de la température, afin de prendre en considération les corrections dues à l'expansion thermique. Le volume total (V^{M}_{tot}) limité par la cellule

d'équilibre, la vanne V2 et le manomètre M est ensuite déterminé par expansion volumique de gaz (azote).

Premièrement, la cellule d'équilibre est mise sous vide puis pesée. Une quantité de liquide ionique est introduite dans la cellule. Cette dernière est ensuite connectée au dispositif et mise sous vide afin de sécher et de dégazez le liquide. La cellule d'équilibre est finalement isolée afin de déterminer la quantité exacte de liquide ionique par double pesée.

Dans un deuxième temps, le ballon (LB) contenant l'eau tridistillée est connecté au niveau de la vanne C1 dans la position 1. L'eau tridistillée est dégazée sous vide par des cycles successifs de congélation à l'aide d'azote liquide et de décongélation. Le ballon est ensuite fermé puis reconnecté dans la position 2 pour faciliter l'introduction de liquide moléculaire. Après avoir fait le vide dans l'ensemble du système, la partie mesure est isolée en fermant la vanne V3 et l'eau est alors introduite dans la cellule d'équilibre par gravité en ouvrant les vannes V1 et V2.

La cellule d'équilibre est de nouveau isolée en fermant la vanne V1 et pesée afin de connaitre précisément la composition du mélange liquide ionique + eau. Ensuite, la cellule d'équilibre est reconnectée au système et après avoir refait le vide dans l'installation, la vanne V2 est fermée tandis que la vanne V1 est ouverte. La pression de vapeur du mélange et la température sont alors enregistrées jusqu'à obtention de l'équilibre thermodynamique, pour une composition bien définie.

Afin d'obtenir une large gamme de résultats, cette dernière étape est répétée plusieurs fois. Il en résulte une diminution progressive, par évacuation, de la quantité d'eau dans la cellule d'équilibre.

Les résultats sont présentés sous la forme d'un graphique ou la fraction molaire d'eau (x_{H2O}) est représentée en fonction de la pression d'équilibre (p_{eq}) pour une température donnée (Figure 13).

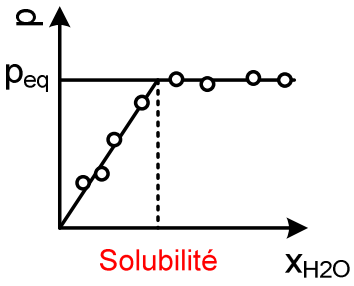

Figure 13. Pression de vapeur d'un mélange liquide ionique + eau en fonction de la fraction molaire d'eau.

L’observation du graphique permet de mettre en évidence deux stades distincts. La partie de droite correspond à la zone ou le liquide ionique est saturé en eau. Les deux liquides ne sont ici pas miscibles. La pression de vapeur saturante mesurée ici correspond à celle du mélange liquide ionique + eau et est proche de la pression de vapeur de l’eau pure, la pression de vapeur des liquides ioniques purs et la solubilité de l’eau dans les liquides ioniques étant négligeable. Dans la partie gauche du graphique, la pression de vapeur diminue avec la fraction molaire d’eau et les deux liquides deviennent miscibles. L’intersection des deux droites correspondantes aux deux états permet alors de déterminer la solubilité de l’eau dans le liquide ionique.

3.6 Absorption de gaz dans les liquides ioniques purs

L’absorption de gaz dans les liquides ioniques purs se fait par une méthode de saturation à volume constant qui permet de mesurer précisément l’absorption de gaz à une pression proche de l’atmosphérique et en fonction de la température.[55,56]

Le principe de mesure repose sur la mise en contact, à une température donnée, d’une quantité connue de liquide ionique avec une quantité connue de gaz. La différence entre la pression initiale de gaz et la pression à l’équilibre thermodynamique permet d’accéder à la quantité de gaz absorbé dans le liquide ionique. Ce principe est illustré par la Figure 14.

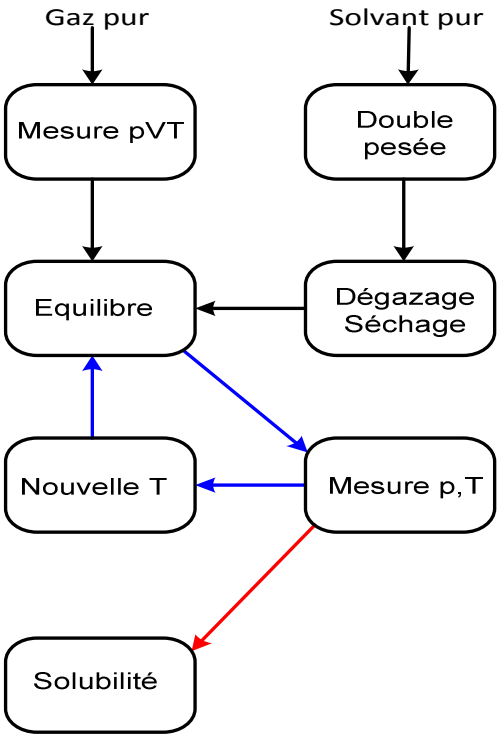

Figure 14. Schéma de la méthode expérimentale de mesure de solubilité de gaz dans les liquides ioniques purs.

Le dispositif expérimental, entièrement constitué de verre, est représenté par la Figure 15. Il est constitué de deux parties distinctes. La première partie est la cellule d'équilibre (EC), thermostatée et à l'intérieur de laquelle se fait le contact entre le solvant et le soluté et la seconde partie permet la mise sous vide de l'ensemble de l'installation ainsi que l'introduction du gaz. La cellule d'équilibre (EC) est constituée d'un manomètre (M) (Druck RPT 350, 35-3500 mbar, précision ± 0.01 %, pleine échelle) et de deux ballons en verre (BG_1 et BG_2) délimités par les vannes V2 et V3. La cellule d'équilibre a été construite de façon à pouvoir travailler avec des volumes de liquide ionique compris entre 2.5 mL et 5 mL et de manière à assurer le meilleur contact possible entre le gaz et le liquide ionique, ceci à l'aide notamment d'une agitation magnétique par un barreau en verre.

La cellule d'équilibre est placée dans une enceinte thermostatée constituée d'un bain d'eau (BT) de volume variable suivant l'installation. La température est maintenue constante en utilisant un contrôleur PID (Hart Scientific model 2200, résolution ± 0.01 K) et est mesurée précisément par une sonde de platine de 100 Ω (Hart Scientific model 1502A, USA ; calibrée au NIST, USA, exactitude de ± 0.018 K à 273.15 K).

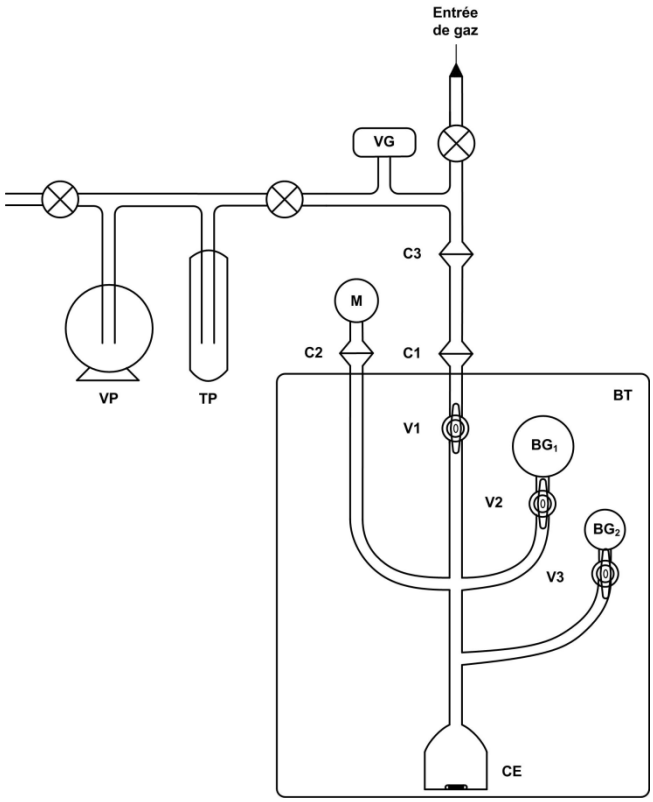

Figure 15. Dispositif expérimental pour la mesure de l'absorption de gaz dans les liquides ioniques purs. TB : Bain thermostaté; VP : pompe à vide; TP : piège froid; VG : jauge Pirani; M : manomètre; BGi : ballons de gaz; EC : cellule d'équilibre; Vi : vannes à volume constant; Ci : connexions mobiles.

Avant toute utilisation, les volumes des ballons BG_1 et BG_2 sont étalonnés par pesée avec de l'eau dégazée à plusieurs températures. Une fois le volume des différents ballons parfaitement connu, ils sont montés sur le reste de la cellule d'équilibre. Celle-ci est à son tour étalonnée à plusieurs températures par expansions volumiques de gaz successives ce qui nous donne le volume total de la cellule d'équilibre.

Plusieurs cellules d'équilibre sont disponibles, avec des ballons et des volumes totaux différents. L'avantage de posséder différents volumes de ballons, pouvant aller de 20 cm^3 à 70 cm^3, est de pouvoir travailler avec des quantités variables de soluté et de solvant, quantités dépendantes principalement de la valeur d'absorption attendue.

La première étape consiste à introduire puis à isoler en fermant la vanne V2 ou V3 une quantité parfaitement connue de gaz dans un ballon à une température donnée.

Dans un second temps, une quantité précise de liquide ionique (1) est placée dans la cellule d'équilibre au niveau de la connexion C2 à l'aide d'une seringue. La

masse de liquide ionique (m_1) introduite est déterminée par double pesée. La connaissance de la masse molaire (M_1) et de la masse volumique (ρ_1) permet d'accéder à la quantité (n_1) ainsi qu'au volume (V_1) de liquide ionique à une température donnée. Ce liquide ionique est alors séché et dégazé sous vide typiquement pendant une demi-journée.

Finalement, la vanne V1 est fermée, isolant la cellule d'équilibre. L'ouverture de la vanne V2 ou V3 permet la mise en contact du gaz avec le liquide ionique. Les valeurs de pression et de température sont enregistrées jusqu'à l'atteinte de l'équilibre thermodynamique. La représentation graphique de la pression en fonction du temps fait apparaitre deux étapes successives. La première est une diminution plus ou moins rapide et plus ou moins longue de la pression, suivie par une stabilisation correspondant à la saturation du liquide ionique en gaz. La durée de ces deux phases est dépendante de la nature ainsi que de la quantité de gaz et de liquide utilisés.

Le changement de température du système et l'obtention d'un nouvel équilibre thermodynamique permet de mesurer l'absorption de gaz dans une gamme de température comprise entre 303.15 K et 363.15 K.

La vérification des résultats passe par le remplissage indépendant de gaz et de liquide ionique. Typiquement, les mesures, pour un système donné, sont répétées au moins trois fois.

La quantité de gaz (n_2^{tot}) dans le ballon, déterminée à partir de la première mesure pVT est exprimée par la relation suivante :

$$n_2^{tot} = \frac{p_{ini} V_{ini}}{[Z_2(p_{ini}, T_{ini}) R T_{ini}]} \tag{9}$$

avec p_{ini} la pression initiale de gaz dans le ballon, V_{ini} le volume du ballon, T_{ini} la température dans le ballon, R la constante universelle des gaz parfaits et $Z_2(p_{ini}, T_{ini})$ le coefficient de compressibilité du soluté pur. Ce dernier est déterminé à partir du second coefficient du viriel :

$$z_2(p_{ini}, T_{ini}) = 1 + \frac{p_{ini} B_{22}}{R T_{ini}} \tag{10}$$

où B_{22} désigne le second coefficient du viriel du soluté pur [57].

La quantité de solvant introduite dans la cellule d'équilibre est donnée par :

$$n_1^{tot} = \frac{m_1^{tot}}{M_1^{tot}} \tag{11}$$

ou m_1^{tot} correspond à la masse de solvant obtenue gravimétriquement.

Les liquides ioniques étant considérés comme non-volatils, la totalité du solvant est présente sous forme liquide et par conséquent le nombre de moles de solvant est égal à :

$$n_1^{tot} = n_1^{liq} \tag{12}$$

L'hypothèse est faite que la masse de solvant reste la même avant et après dégazage.

La seconde mesure pVT a lieu lors de la mise en contact du solvant et du soluté. A l'équilibre thermodynamique $\left(p_{eq}, T_{eq}\right)$ le nombre de mole de gaz $\left(n_2^{vap}\right)$ restant dans la phase gazeuse est égal à :

$$n_2^{vap} = \frac{p_{eq}\left(V_{tot} - V_{liq}\right)}{\left[Z_2\left(p_{eq}, T_{eq}\right)RT_{eq}\right]} \tag{13}$$

avec p_{eq} la pression de gaz à l'équilibre, V_{tot} le volume total de la cellule d'équilibre, V_{liq} le volume occupé par la solution, T_{eq} la température à l'équilibre thermodynamique et $Z_2\left(p_{eq}, T_{eq}\right)$ le coefficient de compressibilité de la solution, calculé par la relation suivante :

$$z_2(p_{eq}, T_{eq}) = 1 + \frac{p_{eq}B_{22}}{RT_{eq}}\left[y_1B_1 + y_2B_{22} + y_1y_2(2B_{12} - B_{11} - B_{22})\right] \tag{14}$$

où y_1 et y_2 correspondent respectivement aux fractions molaires du solvant et du soluté dans la phase vapeur, B_{11} et B_{22} aux coefficients du viriel du solvant et du soluté et B_{12} au second coefficient du viriel croisé. Le solvant étant ici non volatil, $y_1 = 0$ et l'équation (14) peut être simplifiée de la manière suivante :

$$z_2(p_{eq},T_{eq}) = 1 + \frac{p_{eq}}{RT_{eq}}(y_2 B_{22}) \tag{15}$$

La quantité de gaz présente dans la phase liquide n_2^{liq} est alors définie de la manière suivante :

$$n_2^{liq} = n_2^{tot} - n_2^{vap} = \frac{p_{ini}V_{ini}}{[Z_2(p_{ini},T_{ini})RT_{ini}]} - \frac{p_{eq}(V_{tot} - V_{liq})}{[Z_2(p_{eq},T_{eq})RT_{eq}]} \tag{16}$$

L'absorption de gaz dans la phase liquide peut alors être exprimée en terme de fraction molaire de gaz x_2^{exp} de la manière suivante :

$$x_2^{exp} = \frac{n_2^{liq}}{n_1^{liq} + n_2^{liq}} \tag{17}$$

Pour les cas ou la loi de Henry est applicable, la fraction molaire de gaz peut être reliée à la constante de Henry K_H [58] :

$$K_H(T,p) \equiv \lim_{x_2 \to 0}\left(\frac{f_2^{liq}}{x_2}\right) \tag{18}$$

Dans le cas des solvants non-volatils, la fraction molaire du soluté dans la phase gazeuse (y_2) est égale à 1 et la fugacité du solvant et du soluté est égale[58] ce qui permet d'écrire :

$$f_i^{liq} = f_i^{vap} = \phi_2(p_{eq},T_{eq},y_2)y_2 p_{eq} = \Phi_2(p_{eq},T_{eq})p_{eq} \tag{19}$$

où $\phi_2\left(p_{eq},T_{eq}\right)$ est le coefficient de fugacité du soluté, qui peut être calculé par :

$$\phi_2(p_{eq}, T_{eq}) = \exp\left[\frac{p_{eq} B_{22}(T_{eq})}{R T_{eq}}\right] \quad (20)$$

Il est donc possible d'exprimer la constante de Henry de la manière suivante :

$$K_H(T,p) \cong \left(\frac{\phi_2(p_{eq}, T_{eq}) p_{eq}}{x_2^{exp}}\right) \quad (21)$$

La variation de la constante de Henry avec la pression étant considérée comme négligeable dans les conditions expérimentales étudiées, l'évolution de la constante de Henry avec la température peut être corrélée à l'aide de l'équation empirique suivante :

$$\ln\left[K_H(T)/10^5 Pa\right] = \sum_{i=0}^{n}\left[A_i (T/K)^i\right] \quad (22)$$

où K_H et A_i correspondent respectivement aux constantes de Henry calculées à partir des données expérimentales et aux paramètres ajustables de l'équation.

La connaissance de la constante de Henry en fonction de la température permet également d'accéder aux différentes propriétés thermodynamiques de solvatation des gaz dans des liquides ioniques, à savoir l'énergie de Gibbs de solvatation, l'enthalpie de solvatation et l'entropie de solvatation.

L'énergie de Gibbs de solvatation ($\Delta_{sol}G$) correspond à la différence d'énergie de Gibbs du soluté à la température T et à la pression p entre un état de gaz parfait et une solution infiniment diluée dans le solvant.[59] Dans le cas de solutés gazeux à basse pression, l'énergie libre de solvatation est considérée comme une approximation raisonnable de l'énergie de Gibbs de solution.[60,61,62]

L'énergie de Gibbs de solvatation fait intervenir un terme enthalpique $\Delta_{sol}H$ et un terme entropique $\Delta_{sol}S$ de la manière suivante[58] :

$$\Delta_{sol}G = (\Delta_{sol}H - T\Delta_{sol}S) \quad (23)$$

Le terme enthalpique est en relation avec les interactions soluté-solvant tandis que le terme entropique est en relation avec la structuration des molécules de solvant autour du soluté.

La constante de Henry est reliée à l'énergie de Gibbs de solvatation selon :

$$\Delta_{sol}G = RT\ln(K_H / p^0) \tag{24}$$

avec p^0 la pression à l'état standard (1 bar).

L'enthalpie et l'entropie de solvatation peuvent être alors exprimées en fonction de la constante de Henry de la manière suivante :

$$\Delta_{sol}H = -T^2\left[\frac{\partial(\Delta_{sol}G/T)}{\partial T}\right]_p = -RT^2\left[\frac{\partial \ln(K_H/p^0)}{\partial T}\right]_p \tag{25}$$

$$\Delta_{sol}S = \frac{\Delta_{sol}H - \Delta_{sol}G}{T} = -RT\left[\frac{\partial \ln(K_H/p^0)}{\partial T}\right]_p - R\ln\left(\frac{K_H}{p^0}\right) \tag{26}$$

3.7 Absorption de gaz dans les mélanges liquide ionique + eau

L'absorption de gaz dans les mélanges binaires liquide ionique + eau se fait également par une méthode de saturation à volume constant qui suit le même principe que précédemment mais avec quelques ajustements spécifiques.

Le principe repose cette fois sur la mise en contact, à une température donnée, d'un mélange constitué d'une quantité connue de liquide ionique et d'eau avec une quantité connue de gaz. La différence entre la pression initiale de gaz et la pression à l'équilibre thermodynamique dans le volume occupé par le gaz et le liquide ionique permet d'accéder à la quantité de gaz absorbé dans le liquide ionique. Ce principe est illustré par la Figure 16.

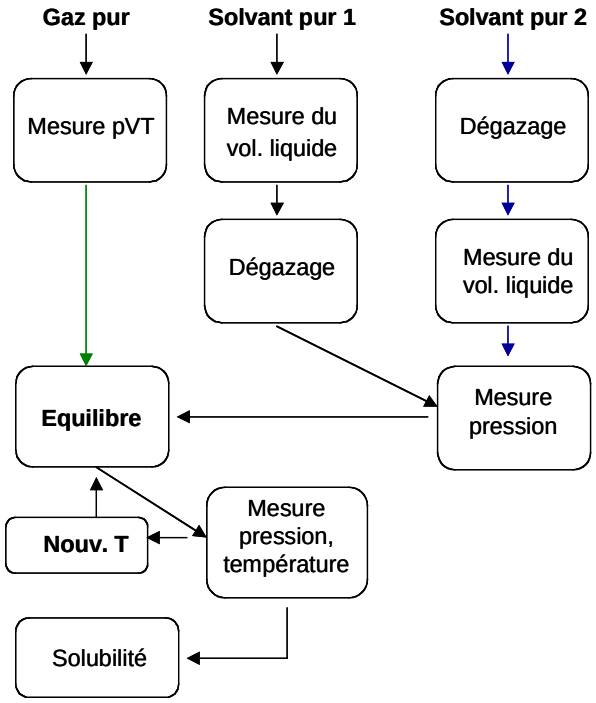

Figure 16. Schéma de la méthode expérimentale de mesure de l'absorption de gaz dans les mélanges binaires liquides ioniques + eau.

Le dispositif expérimental, représenté par la Figure 17, est constitué des deux parties décrites précédemment. La cellule d'équilibre (EC), contient une partie supplémentaire permettant l'introduction de l'eau et délimité par la connexion C3.

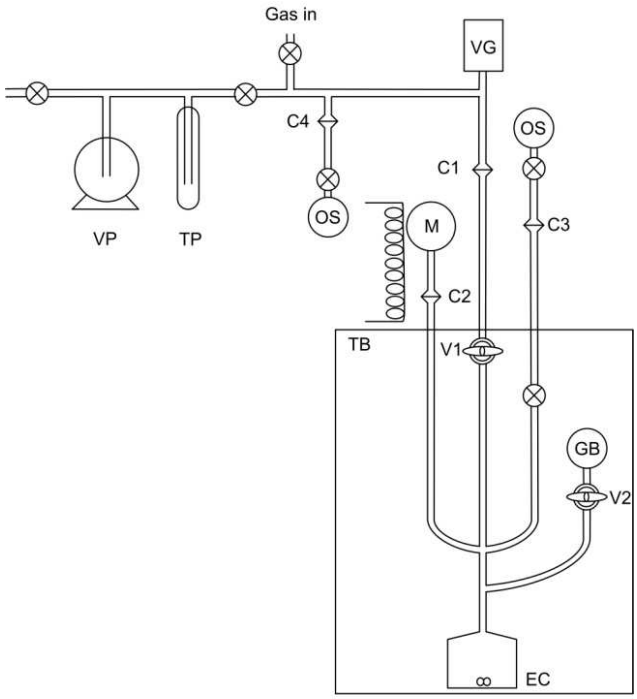

Figure 17. Dispositif expérimental pour la mesure de l'absorption de gaz dans les mélanges binaires liquide ionique + eau. TB : Bain thermostaté; VP : pompe à vide; TP : piège froid; VG : jauge Pirani; M : monomètre; BGi : ballons de gaz; EC : cellule d'équilibre; Vi : vannes à volume constant; Ci : connexions mobiles.

Le début de la procédure est identique à celle utilisée pour les mesures d'absorption de gaz dans les liquides ioniques purs. Après les deux premières étapes consistant à remplir de gaz et de liquide ionique, une troisième étape consistant au remplissage d'eau a lieu. De la même manière que pour les mesures de miscibilité, le ballon (OS) contenant l'eau tridistillée est connecté au niveau de la vanne C4 (Figure 17) afin que l'eau tridistillée soit dégazée sous vide par des cycles successifs de congélation en utilisant de l'azote liquide et de décongélation. Le ballon est ensuite isolé puis connecté au niveau de la vanne C3. Après avoir fait le vide dans la partie située entre la connexion C3 et la cellule d'équilibre, l'eau est introduite dans la cellule par gravité. Une fois cette étape réalisée, le mélange binaire n'est pas tout de suite mis en contact avec le gaz comme précédemment. Une première acquisition de pressions et de températures est faite afin de mesurer la pression de vapeur saturante du mélange à une température donnée. Cette valeur, entrant en compte dans le calcul de l'absorption de gaz, quantifie la quantité de solvant présente dans la phase vapeur. Une fois cette valeur mesurée, le gaz est mis en contact avec le mélange en ouvrant la

vanne V2 et comme précédemment, les valeurs de pression et de température sont enregistrées jusqu'à l'obtention de l'équilibre thermodynamique.

De la même manière, le changement de température du système et l'obtention d'un nouvel équilibre thermodynamique permet de mesurer l'absorption de gaz dans les mélanges binaires dans une gamme de température comprise entre 303.15 K et 363.15 K.

De la même manière que pour les mesures d'absorption de gaz dans les liquides ioniques purs, le nombre de moles de gaz n_2^{tot} dans le ballon est exprimé par la relation suivante :

$$n_2^{tot} = \frac{p_{ini} V_{ini}}{[Z_2(p_{ini}, T_{ini}) R T_{ini}]} \tag{9}$$

avec p_{ini} la pression dans le ballon, V_{ini} le volume du ballon, T_{ini} la température dans le ballon, R la constante universelle des gaz parfaits et $Z_2(p_{ini}, T_{ini})$ le coefficient de compressibilité du soluté pur.

La quantité de liquide ionique introduite dans la cellule d'équilibre est exprimée également sous la forme suivante :

$$n_1^{tot} = \frac{m_1^{tot}}{M_1^{tot}} \tag{11}$$

avec m_1^{tot} correspondant à la masse de solvant obtenue gravimétriquement.

Et le nombre de moles de solvant est égal à :

$$n_1^{tot} = n_1^{liq} \tag{12}$$

la pression de vapeur des liquides ioniques étant considérée comme nulle.

La quantité d'eau introduite dans la cellule d'équilibre est égale à :

$$n_3^{tot} = \frac{m_3^{tot}}{M_3^{tot}} \tag{11}$$

ou m_3^{tot} correspond à la masse d'eau obtenue gravimétriquement.

Le nombre total de moles d'eau (n_3^{tot}) se décompose de la manière suivante :

$$n_3^{tot} = n_3^{liq} + n_3^{vap} \tag{27}$$

Avec la quantité d'eau sous forme vapeur égal à :

$$n_3^{tot} = \frac{p_{vap} V_{vap}}{[Z_3(p_{ini}, T_{ini}) R T_{ini}]} \tag{9}$$

ou p_{vap} désigne la pression de vapeur de l'eau, V_{vap} le volume occupé par la phase vapeur, T_{ini} la température initiale, R la constante universelle des gaz parfaits et $Z_3(p_{ini}, T_{ini})$ le coefficient de compressibilité de l'eau.
Ce dernier est défini par l'équation suivante :

$$z_3(p_{ini}, T_{ini}) = 1 + \frac{p_{ini} B_{33}}{R T_{ini}} \tag{15}$$

où B_{33} désigne le second coefficient du viriel de l'eau. Le volume d'eau sous forme vapeur est, quand à lui, égal à :

$$V_{vap} = V_{tot} - V_{liq} \tag{28}$$

Avec le volume de solution liquide:

$$V_{liq} = V_{idéal} - V^E \tag{29}$$

Avec $V_{idéal}$ le volume de la solution supposée idéale et V^E le volume d'excès. On accède alors à la quantité de solvant dans la phase liquide :

$$n_{solv}^{liq} = n_1^{liq} + n_3^{liq} \tag{30}$$

La seconde mesure pVT a lieu lors de la mise en contact du solvant et du soluté. A l'équilibre thermodynamique $\left(p_{eq}, T_{eq}\right)$ le nombre de mole de gaz $\left(n_2^{vap}\right)$ restant dans la phase gazeuse est égal à :

$$n_2^{vap} = \frac{p_{eq} - x_{solv} p_{solv}^{sat} \left(V_{tot} - V_{liq}\right)}{\left[Z_{23}\left(p_{eq}, T_{eq}\right) RT_{eq}\right]} \tag{31}$$

avec p_{eq} est la pression à l'équilibre, V_{tot} le volume total de la cellule d'équilibre, V_{liq} le volume occupé par le solvant pur, T_{eq} est la température à l'équilibre thermodynamique, p_{solv}^{sat} la pression de vapeur saturante du mélange, x_{solv} la fraction molaire de soluté dans le solvant et $Z_{23}\left(p_{eq}, T_{eq}\right)$ le coefficient de compressibilité de la phase vapeur en équilibre avec la solution, calculé par la relation suivante :

$$z_{23}(p_{eq}, T_{eq}) = 1 + \frac{p_{eq}}{RT_{eq}} \left[y_2 B_{22} + y_3 B_{33} + y_2 y_3 \delta_{23}\right] \tag{32}$$

où y_1 et y_2 correspondent respectivement aux fractions molaires du solvant et du soluté dans la phase vapeur, B_{22} et B_{33} aux coefficients du viriel du gaz pur et de l'eau et $\delta_{23} = 2B_{23} - B_{22} - B_{33}$ avec B_{23} le coefficient croisé du viriel considéré comme la moyenne entre B_{22} and B_{33}.

La quantité de gaz présent dans la phase liquide n_2^{liq} est alors définie de la manière suivante :

$$n_2^{liq} = n_2^{tot} - n_2^{vap} = \frac{p_{ini} V_{ini}}{\left[Z_2\left(p_{ini}, T_{ini}\right) R T_{ini}\right]} - \frac{p_{eq} - x_{solv} p_{solv}^{sat}\left(V_{tot} - V_{liq}\right)}{\left[Z_2\left(p_{eq}, T_{eq}\right) R T_{eq}\right]} \quad (33)$$

L'absorption de gaz dans la phase liquide s'exprime cette fois en terme de fraction molaire de gaz x_2^{exp} de la manière suivante :

$$x_2^{exp} = \frac{n_2^{liq}}{n_{solv}^{liq} + n_2^{liq}} \quad (34)$$

4. COLLECTION D'ARTICLES

THE JOURNAL OF PHYSICAL CHEMISTRY B

Article

pubs.acs.org/JPCB

Absorption of Carbon Dioxide, Nitrous Oxide, Ethane and Nitrogen by 1-Alkyl-3-methylimidazolium ($C_n$mim, n = 2,4,6) Tris(pentafluoroethyl)trifluorophosphate Ionic Liquids (eFAP)

D. Almantariotis, S. Stevanovic, O. Fandiño, A. S. Pensado, A. A. H. Padua, J.-Y. Coxam, and M. F. Costa Gomes*

Institut de Chimie de Clermont-Ferrand, Equipe Thermodynamique et Interactions Moléculaires, Clermont Université, Université Blaise Pascal, BP 80026, 63171 Aubiere, France

CNRS, UMR6296 ICCF, BP 80026, 63171 Aubiere, France

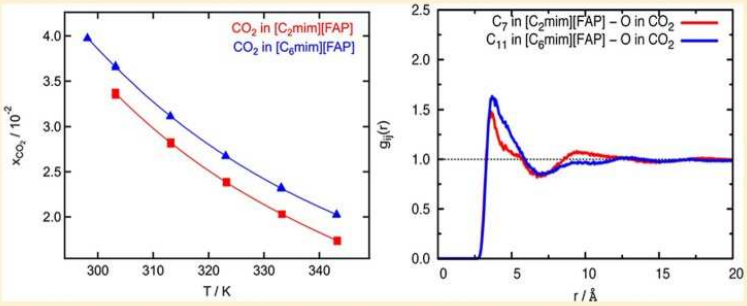

ABSTRACT: We measured the densities of 1-alkyl-3-methylimidazolium ($C_n$mim, n = 2,4,6) tris(pentafluoroethyl)-trifluorophosphate ionic liquids (eFAP) as a function of temperature and pressure and their viscosities as a function of temperature. These ionic liquids are less viscous than those based in the same cations but with other anions such as bis(trifluoromethylsulfonyl)imide. The ionic liquids studied are only partially miscible with water, their solubility increasing with the size of the alkyl side-chain of the cation and with temperature (from x_{H_2O} = 0.20 ± 0.03 for [C_4mim][eFAP] at 303.10 K to x_{H_2O} = 0.49 ± 0.07 for [C_6mim][eFAP] at 315.10 K). The solubility of carbon dioxide, nitrous oxide, ethane, and nitrogen in the three ionic liquids was measured as a function of temperature and at pressures close to atmospheric. Carbon dioxide and nitrous oxide are the more soluble gases with mole fraction solubilities of the order of 3×10^{-2} at 303 K. The solubility of these gases does not increase linearly with the size of the alkyl-side chain of the cation. The solubilities of ethane and nitrogen are much lower than those of carbon dioxide and nitrous oxide (mole fractions 60% and 90% lower, respectively). The higher solubility of CO_2 and N_2O can be explained by more favorable interactions between the solutes and the polar region of the ionic liquids as shown by the enthalpies of solvation determined experimentally and by the calculation of the site−site solute−solvent radial distribution functions using molecular simulation.

■ INTRODUCTION

Ionic liquids are considered promising media for gas separations[1] as they can selectively and efficiently absorb one gas in a mixture. In particular, they have been indicated as possible alternatives for carbon dioxide removal from flue-gas streams by chemical[2] or physical absorption.[3] Several properties are significant for the evaluation of ionic liquids as liquid absorbers for gaseous solutes—the absorption capacity, the selectivity, and the mass transfer—as they will determine the design and cost of possible industrial processes.[4]

We have studied the absorption of gases—carbon dioxide, nitrous oxide, ethane, and nitrogen—in ionic liquids based on the anion tris(pentafluoroethyl)trifluorophosphate and on a series of cations of the family of 1-alkyl-3-methylimidazolium ([$C_n$mim][eFAP] with n = 2,4,6). This new class of ionic liquids containing fluorinated anions was first synthesized by Ignat'ev et al.[5] as replacements for ionic liquids containing other fluorous groups in the anion, namely, hexafluorophosphate, that might be hydrolytically unstable, especially at elevated temperature.

Other authors have previously studied gas absorption in eFAP-based ionic liquids. Both Muldoon et al.[6] and Yokozeki et al.[7] have measured the absorption of carbon dioxide in [C_6mim]-[eFAP] at temperatures from 298 to 333 K and at pressures up to 15 MPa and at 298 K and up to 2 MPa, respectively. Blath et al.[8] also studied the carbon dioxide absorption in the same ionic liquid and have compared it with that of nitrogen at 333.15 K.

Received: May 9, 2012
Revised: June 7, 2012
Published: June 8, 2012

ACS Publications © 2012 American Chemical Society

Different predictive models have been used to assess gas absorption in these ionic liquids. Zhang et al.[9] have used COSMO-RS to predict the solubility of carbon dioxide in [C_6mim][eFAP] at 298 K, the values obtained being compared with experimental data obtained by the same authors at temperatures from 283 to 323 K. Finally, Zhang et al.[10] have used Monte Carlo simulation methods to study the same system between 298 and 323 K and at pressures of gas from 0.25 to 2.0 MPa.

This work is the continuation of a previous effort to explain the influence of fluoro-moieties in ionic liquids on the gas absorption by ionic liquids.[11] After concluding that the presence of fluorinated alkyl-side chains in imidazolium cations significantly influenced the absorption of carbon dioxide, we have decided to study the effect of the fluorination in the anion. We expect to clarify the mechanisms of gas solvation in these media by associating experimental determinations of the solubility of apolar gases such as nitrogen and ethane, a quadrupolar gas such as carbon dioxide, and a polar gas as nitrous oxide with molecular simulations, capable of providing insights into the structure of the solutions. The present study will also contribute to the choice of promising liquid absorbents for gases having an important environmental impact such as carbon dioxide and nitrous oxide by evaluating both the absorption capacity and the selectivity of different ionic liquids.

■ EXPERIMENTAL SECTION

Materials. The samples of ionic liquids used were purchased from Merck with mole fraction purities of 0.995. Their decomposition temperatures were determined using a modulated DSC 2920 from TA Instruments and were found to be 580 and 583 K for [C_4mim][eFAP] and [C_6mim][eFAP], respectively.

The ionic liquids were kept under vacuum for 15 h at 303 K before each measurement. The water contents of each degassed sample were determined, with a precision of ±5 ppm, using a coulometric Karl Fisher titrator (Mettler Toledo DL32). The water content of the degassed samples was found be 7 ppm for [C_2mim][eFAP], 11 ppm for [C_4mim][eFAP], and 23 ppm for [C_6mim][eFAP].

The gases were used as received from the manufacturer. Carbon dioxide was obtained from AGA/Linde Gas with a mole fraction purity of 0.99995; nitrous oxide was obtained from Linde with a mole fraction purity of 0.995; ethane was purchased at AGA/Linde GAZ with a mole fraction purity of 0.995, and nitrogen was obtained from SAGA with a mole fraction purity of 0.998.

Density Measurements. Densities were measured using a U-shape vibrating-tube densimeter (Anton Paar, model DMA 512) operating in a static mode, following the procedure described in previous publications.[12,13] Measurements for [C_2mim][eFAP], [C_4mim][eFAP], and [C_6mim][eFAP] were performed for pressures up to 25 MPa and at temperatures from 293 to 353 K.

The temperature in the densimeter was maintained constant to within ±0.01 K by means of a recirculating bath equipped with a PID temperature controller (Julabo FP40-HP). For measuring the temperature, a 100 Ohm platinum resistance thermometer (precision of ±0.02 K and accuracy of ±0.04 K) was used. Its calibration was performed by verifying a water triple point (triple point cell by Hart Scientific) and by comparison against a 100 Ohm platinum resistance Hart Scientific model 1502A. The pressure was measured using a precision pressure transmitter Druck, model PTX 610, working in a range from 0 to 70 MPa with an uncertainty of 0.08% full scale.

The measured period of vibration (τ) of a U tube is related to the density (ρ) according to: $\rho = A\tau^2 + B$, where A and B are parameters that are function of temperature and pressure determined by calibration between temperatures of 293 and 343 K (and pressures of 0.1 and 25 MPa), using as calibration fluids *n*-heptane, bromobenzene and 2,4-dichlorotoluene following the recommendations by Schilling et al.[14] Density measurements were performed in steps of 10 K. The uncertainty of the density measurements is estimated as 10^{-4} g cm^{-3}.

Viscosity Measurements. The dynamic viscosities of the three ionic liquids [C_2mim][eFAP], [C_4mim][eFAP], and [C_6mim][eFAP], previously dried under vacuum, were measured using an Anton Paar AMVn rolling ball viscosimeter, as a function of the temperature from 293.15 to 373.15 K (controlled to within 0.01 K and measured with an accuracy better than 0.05 K) and at atmospheric pressure. Before starting the measurements, the 3 mm diameter capillary tube was calibrated as a function of temperature and angle of measurement using a standard viscosity oil from Cannon (N35). The overall uncertainty on the viscosity is estimated as ±1.5%.

Gas-Solubility Measurements. The experimental method used for the gas solubility measurements is based on an isochoric saturation technique and has been described in previous publications.[15,16] In this technique, a known quantity of gaseous solute is put in contact with a precisely determined quantity of degassed solvent at a constant temperature inside an accurately known volume. When thermodynamic equilibrium is attained, the pressure above the liquid solution is constant and is directly related to the solubility of the gas in the liquid.

The quantity of ionic liquid introduced in the equilibration cell is determined gravimetrically. This quantity is equal to the amount of solvent present in the liquid solution, n_1^{liq}, as the ionic liquid does not present a measurable vapor pressure. The amount of solute present in the liquid solution, n_2^{liq} (subscripts 1 and 2 stand for solvent and solute, respectively), is calculated by the difference between two *pVT* measurements: first when the gas is introduced in a calibrated bulb with volume V_{GB}, and second after thermodynamic equilibrium is reached:

$$n_2^{liq} = \frac{p_{ini} V_{GB}}{[Z_2(p_{ini}, T_{ini})RT_{ini}]} - \frac{p_{eq}(V_{tot} - V_{liq})}{[Z_2(p_{eq}, T_{eq})RT_{eq}]} \quad (1)$$

where p_{ini} and T_{ini} are the pressure and temperature in the first *pVT* determination and p_{eq} and T_{eq} are the pressure and temperature at the equilibrium. V_{tot} is the total volume of the equilibration cell, V_{liq} is the volume of the liquid solution, and Z_2 is the compression factor for the pure gas. The solubility can then be expressed in mole fraction, or as Henry's law constant:

$$K_H = \lim_{x_2 \to 0} \frac{f_2(p, T, x_2)}{x_2} \cong \frac{\phi_2(p_{eq}, T_{eq})p_{eq}}{x_2} \quad (2)$$

where f_2 is the fugacity of the solute and ϕ_2 its fugacity coefficient.

We consider that the volume of the ionic liquid does not change when the gas is solubilized, and so the volume of the liquid solution is equal to the molar volume of the pure ionic liquid.

Water-Miscibility Measurements. The miscibility gap of [C_4mim][eFAP] with water and [C_6mim][eFAP] with water was determined at different temperatures using a *pVT* method that has been described in a previous publication.[17] An equilibrium cell equipped with precision manometers and placed in an air thermostat was used. Precisely known quantities of ionic liquid

Table 1. Experimental Densities, ρ, of the Ionic Liquids [C_2mim][eFAP], [C_6mim][eFAP], and [C_4mim][eFAP] between 293 and 353 K and up to 25 MPa

T/K	$p/10^5$ Pa	ρ/(kg·m^{-3})	T/K	$p/10^5$ Pa	ρ/(kg·m^{-3})
		[C_2mim][eFAP]			
293.14	1.01	1713.4	323.16	1.01	1677.5
293.13	5.00	1713.7	323.14	5.00	1678.1
293.13	10.0	1714.2	323.13	10.0	1678.6
293.14	25.0	1715.4	323.15	25.0	1680.1
293.14	50.0	1717.7	323.14	50.0	1682.6
293.14	100	1722.0	323.13	100	1687.4
293.13	150	1726.3	323.14	150	1692.1
293.13	200	1730.4	323.13	200	1696.7
293.13	250	1734.5	323.13	250	1701.1
303.16	1.01	1701.3	333.18	1.01	1665.6
303.17	5.00	1701.7	333.17	5.00	1666.2
303.18	10.0	1702.2	333.18	10.0	1666.7
303.18	25.0	1703.4	333.18	25.0	1668.2
303.19	50.0	1705.7	333.18	50.0	1670.8
303.22	100	1710.2	333.18	100	1675.8
303.19	150	1714.7	333.19	150	1680.7
303.18	200	1719.0	333.17	200	1685.5
303.19	250	1723.1	333.18	250	1690.0
313.15	1.01	1689.4	343.18	1.01	1653.9
313.17	5.00	1689.8	343.13	5.00	1654.7
313.18	10.0	1690.3	343.14	10.0	1655.2
313.18	25.0	1691.7	343.16	25.0	1656.8
313.17	50.0	1694.1	343.13	50.0	1659.5
313.18	100	1698.7	343.14	100	1664.7
313.17	150	1703.3	343.13	150	1669.8
313.16	200	1707.7	343.13	200	1674.6
313.17	250	1712.0	343.13	250	1679.4
		[C_6mim][eFAP]			
293.16	1.03	1556.1	323.17	1.03	1523.1
293.17	2.53	1556.3	323.16	2.53	1523.2
293.16	5.00	1556.6	323.14	5.00	1523.5
293.17	10.0	1557.0	323.15	10.0	1524.1
293.18	25.0	1558.1	323.15	25.0	1525.6
293.16	50.0	1560.6	323.19	50.0	1528.0
293.16	100	1564.8	323.19	100	1532.8
293.16	150	1569.0	323.19	150	1537.4
293.16	200	1573.1	323.19	200	1541.9
293.16	250	1577.0	323.19	250	1546.2
303.18	1.03	1544.9	333.19	1.03	1512.6
303.18	2.53	1545.1	333.19	2.53	1512.8
303.17	5.00	1545.3	333.19	5.00	1513.0
303.18	10.0	1545.8	333.19	10.0	1513.5
303.18	25.0	1547.2	333.19	25.0	1515.1
303.18	50.0	1549.5	333.19	50.0	1517.7
303.18	100	1554.0	333.19	100	1522.6
303.18	150	1558.3	333.19	150	1527.4
303.18	200	1562.5	333.19	200	1532.1
303.19	250	1566.5	333.18	250	1536.6
313.17	1.03	1534.1	343.19	1.03	1502.0
313.18	2.53	1534.2	343.18	2.53	1502.2
313.19	5.00	1534.4	343.18	5.00	1502.4
313.19	10.0	1535.0	343.18	10.0	1503.0
313.19	25.0	1536.4	343.18	25.0	1504.7
313.19	50.0	1538.8	343.16	50.0	1507.4
313.19	100	1543.3	343.15	100	1512.6
313.19	150	1547.8	343.14	150	1517.6
313.19	200	1552.2	343.13	200	1522.4
313.18	250	1556.4	343.13	250	1527.0
		[C_4mim][eFAP]			
293.18	1.05	1629.1	333.14	1.01	1584.0
293.18	5.00	1639.4	333.11	4.99	1584.4
293.18	10.0	1629.9	333.08	10.0	1585.0
293.18	25.0	1631.2	333.08	25.0	1586.6
293.18	50.0	1633.5	333.05	50.0	1589.3
293.18	100	1637.9	333.04	100	1594.3
293.18	150	1642.2	333.04	150	1599.2
293.18	200	1646.3	333.03	200	1603.9
293.18	250	1650.3	333.02	250	1608.5
303.21	1.02	1617.6	343.14	1.01	1573.1
303.22	4.98	1618.0	343.14	4.99	1573.5
303.23	10.0	1618.5	343.14	10.0	1574.1
303.26	25.0	1619.8	343.14	25.0	1575.8
303.26	50.0	1622.1	343.13	50.0	1578.5
303.26	100	1626.7	343.13	100	1583.7
303.26	150	1631.1	343.14	150	1588.8
303.27	200	1635.4	343.14	200	1593.7
303.28	250	1639.5	343.14	250	1598.4
313.15	1.01	1606.4	353.05	1.00	1562.5
313.14	5.00	1606.8	353.04	5.00	1562.9
313.16	10.0	1607.3	353.05	10.0	1563.5
313.18	25.0	1608.7	353.04	25.0	1565.3
313.18	50.0	1611.2	353.04	50.0	1568.1
313.18	100	1615.9	353.03	100	1573.5
313.18	150	1620.4	353.03	150	1578.7
313.19	200	1624.8	353.02	200	1583.8
313.20	250	1629.1	353.02	250	1588.6
323.19	1.01	1594.9			
323.21	5.00	1595.3			
323.21	10.0	1595.8			
323.20	25.0	1597.4			
323.20	50.0	1599.9			
323.20	100	1604.8			
323.20	150	1609.5			
323.22	200	1614.1			
323.23	250	1618.4			

and water, previously degassed under vacuum and by successive melting and freezing cycles, respectively, are put in contact, under their own vapor pressure, inside the equilibrium cell. The two components are mixed at constant temperature and in the constant and accurately known volumes of the apparatus. When thermodynamic equilibrium is reached, the vapor pressure is recorded. The composition of the liquid mixture is modified by evacuating the molecular compound, the new composition of the mixture being calculated gravimetrically. The temperature of the equilibrium cell and of the manometer was controlled to

Table 2. Tait Parameters C, B_0, B_1, and B_2 Used to Smooth the Experimental Densities as a Function of Pressure (to 25 MPa) and Temperature (from 293 to 353K) along with the Standard Deviation of the Fit, s

ionic liquid	$10^2 \cdot C$	B_0/ MPa	B_1/ MPa·K^{-1}	$10^3 \cdot B_2$/ MPa·K^{-2}	s
[C_2mim][eFAP]	+7.713	+413.748	−1.182	+0.912	0.01
[C_4mim][eFAP]	+6.922	+325.658	−0.871	+0.597	0.01
[C_6mim][eFAP]	+6.997	+289.715	−0.655	+0.253	0.01

dx.doi.org/10.1021/jp304501p | J. Phys. Chem. B 2012, 116, 7728−7738

Table 3. Experimental Dynamic Viscosities, η, of the Ionic Liquids [C_2mim][eFAP], [C_4mim][eFAP], and [C_6mim][eFAP] as a Function of Temperature at Atmospheric Pressure

	η/mPa s		
T/K	[C_2mim][eFAP]	[C_4mim][eFAP]	[C_6mim][eFAP]
293.15	74.71	100.3	118.8
303.15	48.34	62.36	70.75
313.15	33.36	42.04	45.57
323.15	24.38	29.24	31.64
333.15	18.10	20.84	22.15
343.15	14.01	15.50	16.38
353.15	11.18	11.88	12.49
363.15	9.041	9.337	9.754
373.15	7.447	7.527	7.878

Table 4. Experimental values of the vapour pressures $p_{mix}^{H_2O}$ of the [C_4mim][eFAP] + water and [C_6mim][eFAP] + water mixtures as a function of the composition, expressed in water mole fraction, x_{H_2O}

[C_4mim][eFAP] + H_2O T = 303.08 K		[C_6mim][eFAP] + H_2O T = 303.40 K		[C_6mim][eFAP] + H_2O T = 315.10 K	
x_{H_2O}	$p_{mix}^{H_2O}/10^2$ Pa	x_{H_2O}	$p_{mix}^{H_2O}/10^2$ Pa	x_{H_2O}	$p_{mix}^{H_2O}/10^2$ Pa
0.0519	15	0.072	18	0.068	16
0.0782	21	0.083	14	0.077	20
0.0817	23	0.098	18	0.103	33
0.0839	21	0.101	9	0.134	44
0.1050	23	0.161	20	0.139	39
0.2090	32	0.260	29	0.430	68
0.2830	38	0.386	36	0.564	75
0.4123	39	0.486	38	0.631	77
0.4797	39	0.530	39	0.668	77
0.4925	39	0.571	39	0.734	76
0.4935	39	0.611	39	0.777	77
0.5514	38	0.698	40	0.781	77
0.5874	39	0.715	40	0.820	77
0.6102	39	0.733	40	0.843	77
0.6615	39	0.751	40	0.853	77
0.7090	39	0.789	40	0.878	80
0.8299	39	0.815	40	0.883	77
		0.827	40	0.926	77
		0.832	41		
		0.840	40		
		0.858	40		
		0.875	41		
		0.881	40		
		0.884	40		
		0.898	40		
		0.899	40		
		0.914	41		

within ±0.01 K, in the temperature range of 288 to 313 K, and measured with a calibrated 100 Ohm platinum resistance thermometer from Hart Scientific (Secondary Reference Temperature Standard, model 1502A, accuracy of ±0.018 at 273 K). The pressure was measured using a quartz spiral manometer from Ruska (model 2465, uncertainty $\pm 10^{-5}$ bar) for [C_4mim][eFAP] and a precision manometer from Druck DPI 262 (3.5−140 kPa, uncertainty ±0.1% full scale) for [C_6mim][eFAP].

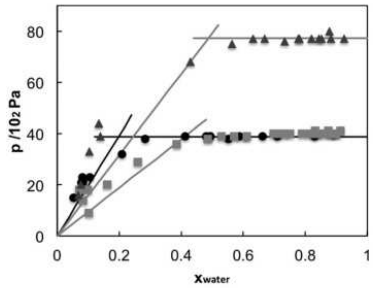

Figure 1. Vapor pressures of the [C_4mim][eFAP] + water and [C_6mim][eFAP] + water mixtures as a function of the composition: ●, [C_4mim][eFAP] + water at 303.10 K; ■, [C_6mim][eFAP] + water at 303.40 K; ▲, [C_6mim][eFAP] + water at 315.10 K.

Table 5. Experimental Values of Gases (CO_2, N_2O) in [C_2mim][eFAP] Expressed Both as Henry's Law Constants, K_H and as CO_2 Mole Fraction, x_2, Corrected for a Partial Pressure of Solute of 0.1 MPa[a]

T /K	p /10^2 Pa	K_H /10^5 Pa	x_2 /10^{-2}	dev %
		CO_2		
303.18	643.97	29.7	3.35	+ 0.6
303.18	536.22	29.4	3.38	− 0.4
303.18	625.41	29.4	3.38	− 0.4
313.16	672.57	35.5	2.81	+ 0.6
313.17	559.80	35.2	2.83	− 0.2
323.18	700.35	41.9	2.38	+ 0.2
323.21	679.96	41.8	2.38	− 0.1
323.22	582.84	41.7	2.39	− 0.3
333.20	727.51	49.2	2.03	+ 0.1
333.24	605.37	49.1	2.03	− 0.2
343.18	753.91	57.1	1.74	− 0.4
343.20	731.78	57.4	1.74	+ 0.1
343.23	627.50	57.6	1.73	+ 0.4
		N_2O		
303.15	546.68	28.7	3.47	− 0.1
303.16	496.96	28.9	3.45	+ 0.6
303.19	529.59	28.5	3.49	− 0.8
313.16	571.19	34.3	2.91	+ 0.2
313.17	518.65	34.6	2.87	+ 1.1
313.19	552.82	34.0	2.93	− 0.7
323.16	594.95	40.5	2.46	− 0.6
323.16	539.72	41.2	2.42	+ 1.2
323.19	575.66	40.5	2.46	− 0.6
333.14	618.11	47.6	2.09	− 1.5
333.20	560.49	48.8	2.04	+ 0.9
343.13	641.14	56.1	1.78	− 1.9
343.14	620.82	58.5	1.70	+ 2.2
343.23	580.80	57.3	1.74	+ 0.0

[a] p is the experimental equilibrium pressure and the percent deviation is relative to the correlations of the data reported in Table 8.

Molecular Simulation. The ionic liquids [C_2mim][eFAP] and [C_6mim][eFAP] were represented by an all-atom force field[18−20] based on the OPLS_AA framework[21,22] but developed specifically for ionic liquids. The force-field model contains the parameters required to simulate the [eFAP]$^-$ anion and the 1-alkyl-3-methylimidazolium cations. The functional form of the force field contains four kinds of potential energy: stretching of covalent bonds, bending of valence angles, torsion around dihedral angles, and nonbonded interactions. Nonbonded interactions are

Table 6. Experimental Values of Gases (CO_2, N_2O, C_2H_6, and N_2) in [C_4mim][eFAP] Expressed Both as Henry's Law Constants, K_H and as CO_2 Mole Fraction, x_2, Corrected for a Partial Pressure of Solute of 0.1 MPa[a]

T /K	p /10^2 Pa	K_H /10^5 Pa	x_2 /10^{-2}	dev %	T /K	p /10^2 Pa	K_H /10^5 Pa	x_2 /10^{-2}	dev %
		CO_2					C_2H_6		
303.16	658.5	25.0	3.99	+ 0.1	303.57	954.9	59.2	1.68	+ 1.2
303.16	655.1	25.0	3.98	+ 0.2	313.24	977.5	66.7	1.49	+ 0.5
303.18	665.0	24.8	4.01	− 0.4	313.25	975.6	65.7	1.51	− 1.0
313.15	686.0	29.3	3.40	+ 0.1	313.27	986.5	66.6	1.49	+ 0.4
313.17	691.7	29.3	3.40	− 0.1	323.21	1009.4	76.2	1.31	+ 1.3
313.18	684.3	29.4	3.39	+ 0.2	323.22	1007.3	75.0	1.33	− 0.2
323.20	717.9	34.1	2.92	+ 0.0	323.28	1018.9	74.6	1.33	− 0.8
323.20	712.9	34.0	2.93	− 0.1	333.16	1041.1	85.6	1.16	+ 0.8
323.23	712.5	34.1	2.93	+ 0.0	333.17	1050.8	83.4	1.19	− 1.7
333.21	743.6	39.3	2.53	+ 0.5	333.32	1039.4	85.5	1.16	+ 0.6
333.23	739.2	39.1	2.55	− 0.3	343.15	1083.0	93.1	1.07	− 2.5
333.24	739.9	39.0	2.55	− 0.3	343.15	1072.8	95.9	1.04	+ 0.6
343.24	766.8	44.4	2.24	− 0.5	343.33	1071.1	97.5	1.02	+ 1.9
343.24	764.9	44.4	2.24	− 0.5			N_2		
343.27	769.1	45.1	2.21	+ 1.1	303.17	910.4	241.9	0.413	+ 2.4
		N_2O			303.17	911.1	236.3	0.423	+ 0.1
303.15	651.0	23.7	4.20	+ 0.1	303.17	911.05	234.7	0.426	− 0.6
303.16	851.7	23.6	4.21	− 0.2	303.18	915.9	231.6	0.432	− 1.9
303.17	860.0	23.8	4.19	+ 0.3	313.16	940.8	247.9	0.403	+ 0.5
313.16	886.1	27.7	3.59	+ 1.6	313.18	940.1	252.6	0.396	+ 2.3
313.17	675.4	26.4	3.77	− 3.3	313.19	940.75	246.2	0.406	− 0.2
313.18	894.6	27.7	3.60	+ 1.4	313.19	945.7	240.1	0.417	− 2.8
323.16	919.4	32.0	3.11	+ 2.9	323.15	970.3	257.1	0.389	− 0.3
323.17	701.0	30.4	3.27	− 2.3	323.19	975.6	254.4	0.393	− 1.4
323.19	926.6	30.8	3.24	− 1.2	323.20	969.7	262.5	0.381	+ 1.7
333.15	952.1	36.6	2.73	+ 3.6	323.20	970.4	257.4	0.389	− 0.3
333.17	726.1	34.7	2.87	− 1.7	333.14	999.8	266.3	0.376	− 1.4
333.20	959.6	34.9	2.86	− 1.1	333.20	1000	269.2	0.372	− 0.3
343.06	983.8	41.2	2.42	+ 3.9	333.20	999.4	279.3	0.358	+ 3.4
343.17	750.3	38.6	2.58	− 2.7	333.20	1005.4	266.5	0.375	− 1.3
343.21	991.9	39.0	2.56	− 1.7	343.13	1028.8	297.2	0.337	+ 5.0
		C_2H_6			343.16	1029.4	279.3	0.358	− 1.1
303.26	943.7	57.5	1.73	− 1.4	343.20	1029.5	278.0	0.360	− 1.6
303.56	946.4	58.6	1.69	+ 0.2	343.22	1035.2	275.0	0.364	− 2.7

[a] p is the experimental equilibrium pressure, and the percent deviation is relative to the correlations of the data reported in Table 8.

active between atoms of the same molecule separated by more than three bonds and between atoms of different molecules. The potential energy associated with bonds and angles is described by harmonic terms, dihedral torsion energy is represented by a series of cosines, and nonbonded interactions are given by the Lennard-Jones sites and by Coulomb interactions (calculated using the Ewald summation method) between partial point charges placed on the atomic sites. The two ionic liquids considered were simulated in periodic cubic boxes containing 400 and 320 ion pairs for [C_2mim][eFAP] and [C_6mim][eFAP], respectively, using the molecular dynamics method implemented in the DL_POLY package.[23] The initial configurations were lattices with low density. Equilibrations starting from the low density arrangement of ions took 2 ns, at constant NpT and T = 423 K, with a time step of 2 fs (covalent bonds involving H atoms were considered rigid constraints). Once the equilibrium density was attained, simulation runs of 1 ns were performed. At the final densities of the ionic liquid state, the length of the side of the simulation boxes is approximately 60 Å for both ionic liquids. Additionally, simulation boxes containing 400 ion pairs of [C_2mim][eFAP] and eight CO_2 or N_2O molecules, and 320 ion pairs of [C_6mim][eFAP] and eight molecules of gas were prepared, to calculate solute−solvent radial distribution functions (RDFs) between the gas and the ionic liquid. We consider this reduced number of solute molecules in order to minimize solute−solute interactions, but still yielding good sampling of the liquid phase structure. The potential model of Harris and Yung[24] was used for CO_2, whereas the parameters for N_2O were those proposed by Costa Gomes et al.[25]

The chemical potentials of CO_2 and N_2O at 373 K in the two ionic liquids were calculated in a two-step procedure, similar to that used in previous works.[11,26] First, for both CO_2 and N_2O, a reduced-size version of the molecule was produced by subtracting 0.8 Å from the C−O, N−N, and N−O bond length and also from the Lennard-Jones diameters σ_O, σ_C (CO_2), and σ_N, σ_O (N_2O). The resulting molecules are small enough so that their chemical potentials can be calculated using the Widom test-particle insertion method[27] with efficient statistics.[26] For this calculation, we performed simulation runs of 600 ps at 373 K, from which 3000 configurations were stored. Then, 10^5 insertions were attempted in each of the 3000 stored configurations of the pure ionic liquids. Second, a stepwise finite-difference thermodynamic integration procedure[28] was used to calculate the free-energy difference between the initial, reduced versions of the

dx.doi.org/10.1021/jp304501p | J. Phys. Chem. B 2012, 116, 7728−7738

Table 7. Experimental Values of Gases (CO_2, N_2O, and C_2H_6) in [C_6mim][eFAP] Expressed Both as Henry's Law Constants, K_H, and as CO_2 Mole Fraction, x_2, Corrected for a Partial Pressure of Solute of 0.1 MPa[a]

T /K	p /10^2 Pa	K_H /10^5 Pa	x_2 /10^{-3}	dev %
		CO_2		
298.13	613.0	25.1	3.97	− 0.2
298.13	587.4	25.1	3.98	− 0.1
303.18	601.6	27.2	3.67	+ 0.4
303.22	627.2	27.3	3.65	+ 0.1
313.10	629.5	32.0	3.12	+ 0.1
313.10	654.6	32.1	3.11	− 0.3
323.07	681.2	37.3	2.67	− 0.2
323.08	656.7	37.3	2.68	+ 0.1
333.05	707.4	43.1	2.31	− 0.3
333.08	683.0	42.9	2.33	+ 0.3
343.06	733.0	49.3	2.02	− 0.1
343.08	709.1	49.2	2.03	+ 0.1
		N_2O		
303.16	500.4	23.4	4.26	+ 0.8
303.18	589.4	23.8	4.18	− 0.9
303.18	532.8	23.6	4.23	+ 0.3
313.15	557.2	28.1	3.55	+ 0.1
313.15	522.5	28.0	3.56	+ 0.5
313.18	615.2	28.4	3.51	− 0.9
323.15	580.8	33.2	3.00	+ 0.2
323.15	544.0	33.1	3.01	+ 0.5
323.21	640.5	33.6	2.97	− 0.8
333.13	565.1	39.1	2.54	+ 0.3
333.16	603.8	39.0	2.56	+ 0.6
333.24	665.1	39.4	2.53	− 0.5
343.16	585.9	45.9	2.17	− 0.2
343.17	626.4	45.4	2.20	+ 1.0
343.26	689.3	46.3	2.15	− 0.9
		C_2H_6		
303.14	520.4	59.8	1.67	+ 0.6
303.14	580.6	60.2	1.65	− 0.1
303.15	528.7	60.8	1.64	− 1.1
313.12	539.3	68.5	1.45	+ 1.0
313.12	547.6	69.0	1.45	+ 0.3
323.12	558.4	79.1	1.26	+ 1.4
323.12	623.2	80.9	0.911	− 0.9
323.13	567.1	81.1	1.23	− 1.1
333.12	577.6	93.3	1.07	+ 0.3
333.16	586.4	94.4	1.06	− 0.8
343.12	596.6	109	0.917	+ 0.7
343.13	665.6	110	0.911	+ 0.1
343.14	605.5	110	0.907	− 0.3

[a] p is the experimental equilibrium pressure, and the percent deviation is relative to the correlations of the data reported in Table 8.

carbon dioxide and nitrous oxide molecules and the full-size model. The free-energy calculation was performed over 10 intermediate steps along a linear path connecting the intermolecular parameters (bonds and diameters) of the reduced-size molecules to those of the full-size molecules. We selected this number of intermediate steps because the starting point and the final state of the thermodynamic integration route are not too far. A large number of intermediate steps would be required if we intended to calculate the chemical potential of CO_2 or N_2O by thermodynamic integration starting from the pure solvent. In the finite-difference thermodynamic integration scheme, derivatives (finite differences) of the total energy of the system with respect to the activation parameter were evaluated by a free-energy perturbation expression in the NpT ensemble using a three-point formula with increments of 2×10^{-3} in the activation parameter. We have selected the temperature of 373 K to avoid sampling problems related to the slow dynamics of the ionic liquids.[29]

Table 8. Parameters of Eq 11 Used to Smooth the Experimental Results on K_H from Tables 5− 7 along with the Percent Standard Deviation of the Fit (s)

gas	A_0	A_1	A_2	s
		[C_2mim][eFAP]		
CO_2	+ 10.14	− 2.413 × 10^3	+ 1.104 × 10^5	0.4
N_2O	+ 13.66	− 4.631 × 10^3	+ 4.568 × 10^5	1.1
		[C_4mim][eFAP]		
CO_2	+ 7.649	− 1.253 × 10^3	− 5.784 × 10^4	0.4
N_2O	+ 7.623	− 1.366 × 10^3	+ 4.288 × 10^3	2.3
C_2H_6	+ 10.07	− 2.429 × 10^3	+ 1.842 × 10^5	1.2
N_2	+ 8.597	− 1.497 × 10^3	+ 1.659 × 10^5	2.0
		[C_6mim][eFAP]		
CO_2	+ 8.703	− 1.744 × 10^3	+ 3.286 × 10^4	0.2
N_2O	+ 11.06	− 3.154 × 10^3	+ 2.298 × 10^5	0.7
C_2H_6	+ 17.22	− 6.719 × 10^3	+ 8.306 × 10^5	0.7

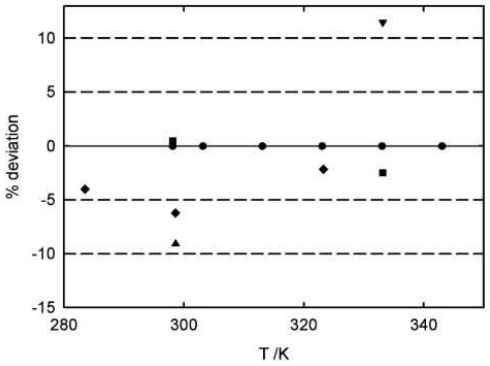

Figure 2. Percent deviations from the literature values to the correlation of the Henry's law constants obtained in this work for carbon dioxide in [C_6mim][eFAP]: (●) this work; (■) Muldoon et al.; (▲) Yokozeki et al.; (♦) Zhang et al.; (▼) Blath et al.

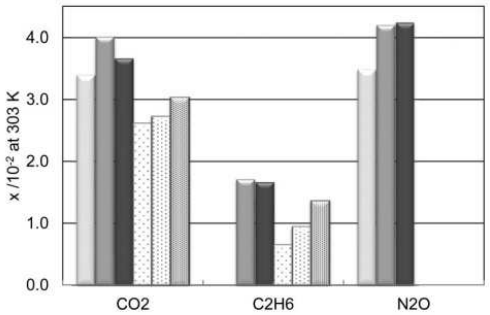

Figure 3. Mole fraction solubility of carbon dioxide, ethane, and nitrous oxide in the ionic liquids studied herein, [$C_n$mim][eFAP], at 303 K. Also represented are the solubilities of the same gases in ionic liquids including the NTf_2^- anion, [$C_n$mim][NTf_2], also at 303 K: light gray, [C_2mim][eFAP]; dark gray, [C_4mim][eFAP]; black, [C_6mim][eFAP]; and dotted, [C_2mim][NTf_2]; 2× dotted, [C_4mim][NTf_2]; 4× dotted, [C_6mim][NTf_2].

RESULTS AND DISCUSSION

The experimental values obtained for the density of [C_2mim][eFAP], [C_4mim][eFAP], and [C_6mim][eFAP] as a function of pressure and at temperatures from 293 to 353 K are reported in Table 1. The values of density at atmospheric pressure (necessary for the calculation of the gas solubility) were adjusted to linear functions of temperature:

$$\rho_{[C_2mim][eFAP]}/kgm^{-3} = 2060.0 - 1.1897 \times (T/K) \quad (3)$$

$$\rho_{[C_4mim][eFAP]}/kgm^{-3} = 1955.4 - 1.1140 \times (T/K) \quad (4)$$

$$\rho_{[C_6mim][eFAP]}/kgm^{-3} = 1869.5 - 1.0720 \times (T/K) \quad (5)$$

The standard deviation of the fits is always better than 0.1%.

The values determined for [C_2mim][eFAP] and [C_4mim][eFAP] are 0.2% and 0.1% higher than those claimed by the manufacturer at 293 K, respectively. For [C_6mim][eFAP], our values are 0.3% lower than those of Ignat'ev et al.[5] at 293 K and 0.1% lower than those reported by Yao et al.[30] at the same temperature. The values published by Yokozeki et al.[7] at 298 K are 1.4% above those measured herein.

The densities as a function of pressure were correlated using the Tait equation:

$$\rho(T,p) = \left[\frac{\rho^0(T,p^0)}{1 - C\ln\left(\frac{B(T)+p}{B(T)+p^0}\right)}\right] \quad (6)$$

where $\rho^0(T,p^0)$ is the density value at a reference temperature T and at the pressure $p^0 = 0.1$ MPa; C is an adjustable parameter, and $B(T)$ a polynomial defined by

$$B(T) = \sum_{i=0}^{2} B_i(T)^i \quad (7)$$

The parameters found for the present data are listed in Table 2.

The dynamic viscosity was measured for the three ionic liquids, previously dried, and are listed in Table 3 as a function of temperature from 293 to 373 K. The Vogel−Fulcher−Tammann (VFT) equation was used to correlate the experimental viscosities as a function of temperature of [C_2mim][eFAP], [C_4mim][eFAP], and [C_6mim][eFAP] with a standard deviation of 0.2, 1.0, and 0.3%, respectively:

$$\eta_{[C_2mim][eFAP]}/mPas = (6.90 \times 10^{-3}) \times (T/K)^{1/2} \exp\left[\frac{865}{(T/K) - 159}\right] \quad (8)$$

$$\eta_{[C_4mim][eFAP]}/mPas = (0.60 \times 10^{-3}) \times (T/K)^{1/2} \exp\left[\frac{1214}{(T/K) - 139}\right] \quad (9)$$

$$\eta_{[C_6mim][eFAP]}/mPas = (4.40 \times 10^{-3}) \times (T/K)^{1/2} \exp\left[\frac{949}{(T/K) - 164}\right] \quad (10)$$

The values measured in this work for [C_6mim][eFAP] agree, to within the experimental error, with those reported by Yao et al.[30] at 293 K. The viscosities measured for the three ionic liquids are only slightly higher than those reported for ionic liquids based on the [NTf_2] anion and much lower than those based on the hexafluorophosphate or octylsulfate anions.

Table 9. Thermodynamic Properties of Solvation of Carbon Dioxide, Nitrous Oxide, Ethane, and Nitrogen in the Ionic Liquids [$C_n$mim][eFAP], n = 2,4,6, in the Temperature Range Studied

ionic liquid	$-\Delta_{solv}H^\infty$/kJ mol^{-1}	$-\Delta_{solv}S^\infty$/J mol^{-1} K^{-1}
	CO_2	
[C_2mim][eFAP]	14 ± 2	75 ± 2
[C_4mim][eFAP]	12.5 ± 0.1	68.0 ± 0.5
[C_6mim][eFAP]	12.7 ± 0.2	69 ± 1
	N_2O	
[C_2mim][eFAP]	14 ± 2	75 ± 5
[C_4mim][eFAP]	11 ± 4	63 ± 9
[C_6mim][eFAP]	14 ± 1	72 ± 3
	C_2H_6	
[C_4mim][eFAP]	10 ± 1	68 ± 2
[C_6mim][eFAP]	12 ± 3	73 ± 8
	N_2	
[C_4mim][eFAP]	4 ± 1	58 ± 4

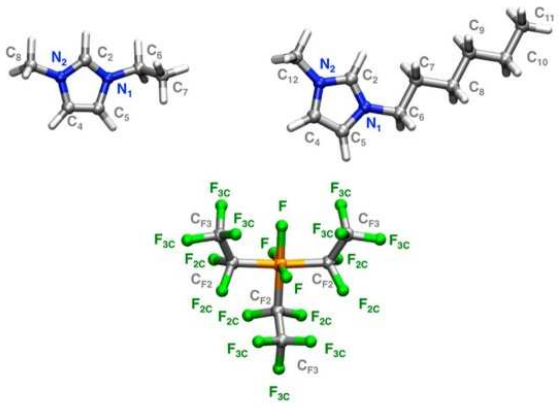

Figure 4. Nomenclature for the sites of the ionic liquids 1-ethyl-3-methyimidazolium tris(pentafluoroethyl)trifluorophosphate and 1-hexyl-3-methylimidazolium tris(pentafluoroethyl)trifluorophosphate used in molecular simulation.

As expected, the viscosity of the [$C_n$mim][eFAP] ionic liquids depend on the length of the alkyl side chain. The viscosities, at 293.15 K, of [C_6mim][eFAP] (118.8 mPa s) and [C_4mim][eFAP] (100.3 mPa s) are 59% and 34% higher than that of [C_2mim][eFAP], respectively. These differences decrease with temperature and are equal to 6% and 1% at 373.15 K, respectively.

In order to determine the miscibility gap in the water + ionic liquid mixtures, the vapor pressure was measured for [C_4mim][eFAP] + water at 303.10 K and for [C_6mim][eFAP] + water at 303.40 and 313.10 K. The results obtained are presented in Table 4 and depicted in Figure 1. Phase separation is determined from the discontinuity of the pressure curves as a function of the composition and, in the present case, phase separation occurs at $x_{H_2O} = 0.20 \pm 0.03$ for [C_4mim][eFAP] at 303.10 K, at $x_{H_2O} = 0.43 \pm 0.05$ for [C_6mim][eFAP] at 303.40 K, and at $x_{H_2O} = 0.49 \pm 0.07$ for [C_6mim][eFAP] at 315.10 K. The water solubility in the ionic liquids increases for larger alkyl side chains of the cation and also increases with temperature. The solubility of the ionic liquid in water appears as negligible as the values of the pressure measured above the biphasic mixtures are very close to those of pure water at the same temperature.

dx.doi.org/10.1021/jp304501p | J. Phys. Chem. B 2012, 116, 7728−7738

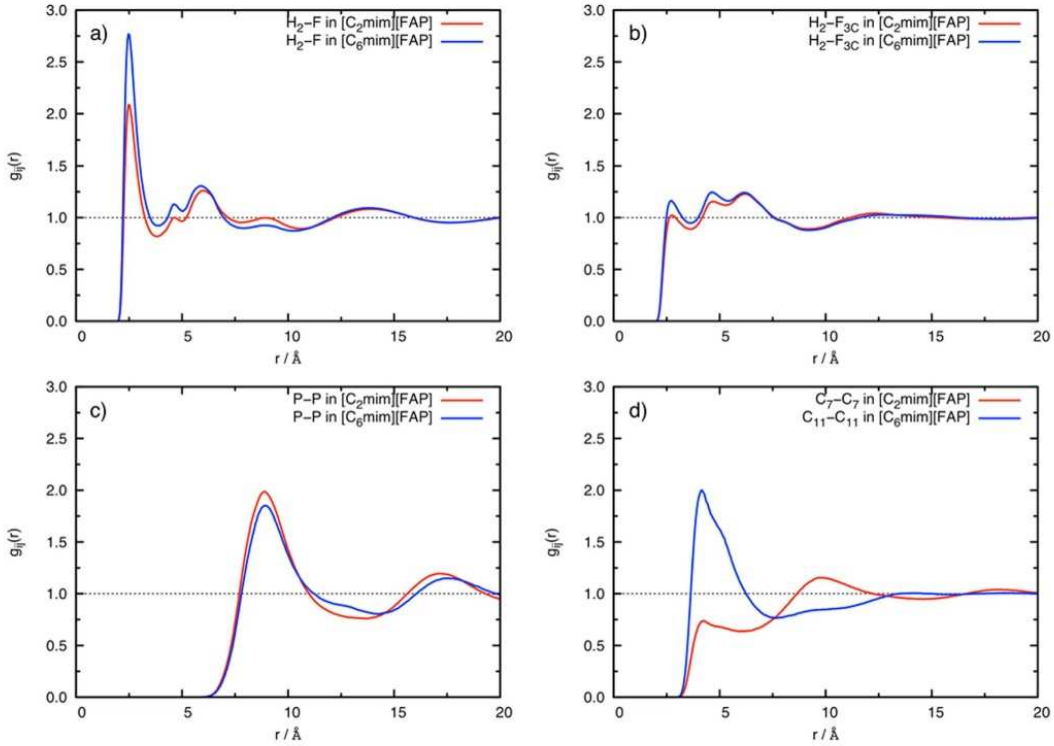

Figure 5. Selected cation−anion site−site RDFs.

For each (gas + ionic liquid) system studied, multiple experimental data points were obtained in the temperature interval between 303 and 343 K in steps of approximately 10 K. The experimental mole fraction solubilities of CO_2 and N_2O in [C_2mim][eFAP], of CO_2, C_2H_6, N_2O, and N_2 in [C_4mim]-[eFAP] and of CO_2, C_2H_6, and N_2O in [C_6mim][eFAP] are reported in Tables 5−7, respectively. Henry's law constants can be calculated from the experimental values and are used to determine the mole fraction solubility assuming a partial pressure of the gaseous solute equal to 0.1 MPa. The second virial coefficients for the gases, necessary for the calculation of the compressibility factor, were taken from the compilation by Dymond and Smith.[31]

The Henry's law constants have been adjusted to an empirical equation of the form

$$\ln[K_H/10^5\ \text{Pa}] = \sum_{i=0}^{n} A_i (T/K)^{-i} \qquad (11)$$

The coefficients A_i as well as the standard deviations of the fits, considered as a measure of the precision of the experimental solubility data for the different gases in the three ionic liquids are listed in Table 8. The Henry's law constants, calculated from the solubility measurements, are in general considered to be precise to within less than 1%. In the present work, the data for nitrous oxide and nitrogen in [C_4mim][eFAP] seem less precise with a standard deviation of fit around 2%. In order to estimate the accuracy of the solubilities reported, we have represented in Figure 2, the comparison between the Henry's law constants for carbon dioxide in [C_6mim][eFAP] herein and those obtained by other authors. For the temperature range covered, the Henry's law constants agree to within ±5% with those reported by Muldoon et al.[6] and by Zhang et al.[10] and to within ±10% with those reported by Yokozeki et al.[7] and Blath et al.[8]

In Figure 3 are depicted the values for the solubility of the different gases in the three ionic liquids at 303 K. It is observed that the solubilities of carbon dioxide, ethane, and nitrous oxide are higher in the ionic liquids studied herein, [$C_n$mim][eFAP], than in similar ionic liquids having the bis(trifluorosulfonyl)-amide anion, [$C_n$mim][NTf_2]. Also, the variation of the solubility of the different gases with the length of the alkyl side-chain in the cation of the ionic liquids is different in the two families. For the [$C_n$mim][NTf_2] family, the gas solubility increases when the alkyl side chains of the imidazolium cations increase from 2 to 6 carbon atoms. For the [$C_n$mim][eFAP] ionic liquids, the solubility of the three gases studied increases from $n = 2$ to $n = 4$ but then remains constant (to within the mutual experimental uncertainty) when the alkyl side chain increases from 4 to 6 carbon atoms in the imidazolium cation.

In order to try to elucidate the reasons for the behaviors found for the absorption of the different gases by the ionic liquids, we have calculated their thermodynamic properties of solvation.[32] The average values, calculated for the temperature range covered in this work, are listed in Table 9. Both in the case of carbon dioxide and nitrous oxide, the lower solubilities in the ionic liquid [C_2mim][eFAP] are explained by the more negative entropic contributions to the Gibbs energy of solvation, and no differences in the mechanisms of solvation were found in the case of the two other ionic liquids. For ethane, the situation seems slightly different as the enthalpy of solvation is, as expected, slightly more favorable for [C_6mim][eFAP], but it is

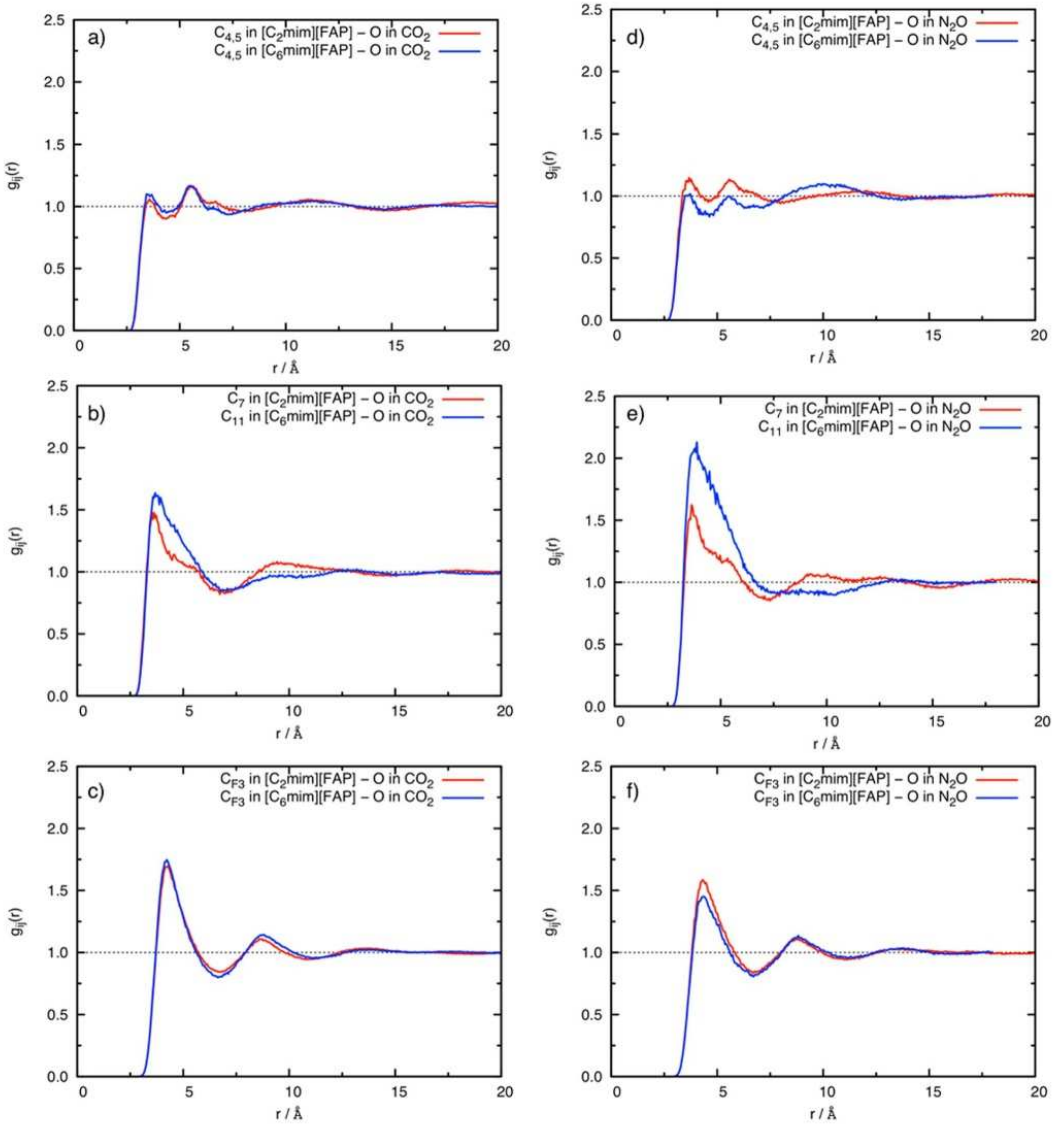

Figure 6. Solute–solvent site–site RDFs of carbon dioxide (left-hand side) and nitrous oxide (right-hand side) in two ionic liquids [C_2mim][eFAP] (in red) and [C_6mim][eFAP] (in blue).

balanced by a more negative entropy of solvation, leading to similar values for the Gibbs energies of solvation.

Molecular simulation was used in order to explain the molecular mechanisms of solvation in these systems. Two gases were chosen, CO_2 and N_2O, in two ionic liquids, [C_2mim][eFAP] and [C_6mim][eFAP]. The nomenclature adopted for the atomic sites of the ionic liquids studied is indicated in Figure 4.

Calculations of the free energy of solvation of CO_2 and N_2O in the ionic liquids [C_2mim][eFAP] and [C_1mim][eFAP] at 373 K allow the calculation of the Henry's law constants, K_H, and of the gas solubility. The calculation of the free energy of solvation of CO_2 in both ionic liquids at 373 K yielded values of $K_H = (132 \pm 13) \times 10^5$ Pa and $K_H = (86.5 \pm 8.6) \times 10^5$ Pa, which correspond to $x_{CO2} = (0.8 \pm 0.1) \times 10^{-2}$ and $x_{CO2} = (1.2 \pm 0.1) \times 10^{-2}$ at a partial pressure $p_{CO2} = 10^5$ Pa for [C_2mim][eFAP] and [C_6mim][eFAP], respectively. Although the calculated solubility values are slightly underestimated, they are sufficiently close to the extrapolated experimental values to validate the force field models used to describe CO_2–ionic liquid interactions.

For N_2O, the values calculated at 373 K are $K_H = (1524 \pm 153) \times 10^5$ Pa and $K_H = (1066 \pm 106) \times 10^5$ Pa, which correspond to $x_{N2O} = (0.7 \pm 0.1) \times 10^{-3}$ and $x_{N2O} = (0.9 \pm 0.1) \times 10^{-3}$ at a partial pressure $p_{N2O} = 10^5$ Pa for [C_2mim][eFAP] and [C_6mim][eFAP], respectively. The values obtained for the gas solubility of N_2O in the two ionic liquids are much lower that the ones obtained experimentally. It is possible that the force field model used to describe the interactions between N_2O and the ionic liquid is not accurate enough. Costa Gomes et al.[25] have observed that, in order to obtain a good agreement between the N_2O solubilities in fluorinated alkanes obtained experimentally

dx.doi.org/10.1021/jp304501p | J. Phys. Chem. B 2012, 116, 7728–7738

and those calculated by molecular simulation, it is necessary to include an unlike interaction parameter, k_{ij} = 0.92, in the Lorentz−Berthelot mixing rules for the Lennard-Jones well-depths $\varepsilon_{ij} = k_{ij}(\varepsilon_{ii}\varepsilon_{jj})^{1/2}$. The parameter k_{ij} could eventually be adjusted to reproduce correctly by molecular simulation the gas solubility values, but a drastic change on the structure of the solutions is not expected.

In Figure 5 are represented the site−site RDFs of representative atoms of the anion and cation of both ionic liquids, showing several features in the liquid-phase structures in the pure ionic liquids. It is observed in panels a and b of Figure 5 that the fluorine atoms of the [eFAP] anion are more probably found close to the hydrogen atom in position C_2 of the imidazolium ring. A more intense peak is observed in the ionic liquid [C_6mim][eFAP], reflecting a stronger structure of this ionic liquid when compared to [C_2mim][eFAP]. This is also reflected, as expected, in the RDFs between the terminal atoms of the alkyl chains of both cations, in agreement with previous experimental[33−35] and molecular simulation[36,37] studies (panel d) of Figure 5). This aspect is no longer present in the [C_2mim][eFAP], the large and voluminous [eFAP]$^-$ anion dominating the structure of the ionic liquid when the side chain of the cation is short.[38] Panel c of Figure 5 shows the RDF between the phosphorus atoms of the anions where a strong peak at a distance around 9 Å can be observed. This peak reflects the strong structure of the anions, an observation compatible with the more important role of larger anions like [eFAP] on the nanoscale organization of the ionic liquid. The different microscopic structures of the liquid phase of these two, relatively similar, ionic liquids can influence the solvation of different species.[11,39,40] One can also expect, as proven before, that even relatively minor differences on the solutes lead to completely different solvation properties, anticipating interesting performances of ionic liquids as reaction or separation media.[41]

Both anions and cations can play an important role on the solubility of different gases on ionic liquids as demonstrated recently by Almantariotis et al.[11] that through partial fluorination of the alkyl chain in an octylimidazolium-based ionic liquid increased the solubility of CO_2 by 20%. We explored the structure of the solutions of CO_2 and N_2O in [C_2mim][eFAP] and [C_6mim][eFAP] in order to gain insights on the molecular mechanisms of solvation in the two gases. Panels a−c of Figure 6 present the RDFs between the oxygen atoms of CO_2 and several representative atoms of the cation and anion of the two ionic liquids. Panels d−f present the RDFs between the oxygen atom of the N_2O molecules and different sites of the ionic liquids.

The RDFs show that CO_2 and N_2O are solvated in similar ways in the ionic liquids [C_2mim][eFAP] and [C_6mim][eFAP], a result compatible with the relatively close experimental solubilities. Both gases interact preferentially with the [eFAP]$^-$ anion, but also with the charged part of the cation. The increase of gas solubility for cations with larger alkyl side-chains is demonstrated by the strong peak observed in panels b and e of Figure 6, more important in the case of [C_6mim][eFAP].

■ CONCLUSIONS

This work presents an original study of the physicochemical properties of the [$C_n$mim][eFAP] ionic liquids with n = 2, 4, and 6 carbons. Our aim is to study the solvation mechanisms of different gases, relevant for carbon dioxide capture processes, in these ionic liquids with large fluorinated moieties in the anions.

We have observed that the ionic liquids studied are, as expected, more dense than those based on the bis(trifluoromethylsulfonyl) imide anion but present viscosities that are lower which can constitute an advantage for industrial used needing high fluidities.

The [$C_n$mim][eFAP] ionic liquids are only partially miscible with water, the solubility increasing with temperature and with the length of the alkyl side chain in the cation. This result is unexpected as, in other families of ionic liquid, the water immiscibility increases with the increasing length of the alkyl side-chain of the cation. The presence of large fluorinated anions seems to contradict this tendency.

We have also observed that carbon dioxide and nitrous oxide have a high solubility in the [$C_n$mim][eFAP] ionic liquids, its increase not being very significant when the length of the alkyl side-chain of the cation increases. The slightly higher solubility of nitrous oxide can be explained by the more favorable interaction of this gas with the charged part of the ionic liquid, as proven by molecular simulation calculations and by a slightly more negative enthalpy of solvation determined from the experimental data. It is also noteworthy that the solubility of carbon dioxide in [eFAP] based ionic liquids is larger than that in [NTf_2] based ionic liquids with the same cation − at 303.15 K $x_{CO2} = 2.62 \times 10^{-2}$, 2.73×10^{-2} and 3.01×10^{-2} for [C_2mim][NTf_2], [C_4mim]-[NTf_2], and [C_6mim][NTf_2], respectively; compared with $x_{CO2} = 3.35 \times 10^{-2}$, 3.99×10^{-2} and 3.97×10^{-2} for [C_2mim][eFAP], [C_4mim][eFAP], and [C_6mim][eFAP], respectively. This fact is probably explained by the presence of larger fluorinated moieties in the [$C_n$mim][eFAP] ionic liquids.

Ethane is three times less soluble in the [$C_n$mim][eFAP] ionic liquids and nitrogen is 1 order of magnitude less soluble in the temperature range studied. The solubility of all the gases studied decreases with temperature thus corresponding to exothermic processes of solvation.

■ AUTHOR INFORMATION

Corresponding Author

*E-mail: margarida.c.gomes@univ-bpclermont.fr.

Notes

The authors declare no competing financial interest.

■ ACKNOWLEDGMENTS

D.A. thanks the ADEME (Agence de l'Environnement et de la Maîtrise de l'Energie) for financing his Ph.D. O.F. thanks the Université Blaise Pascal for a postdoctoral grant. The FUI ACACIA project is also acknowledged for financing part of this work and the Ph.D. grant of S.S.

■ REFERENCES

(1) Costa Gomes, M. F.; Husson, P. *ACS Symp. Ser.* **2010**, *1030* (16), 223.

(2) Bates, E. D.; Mayton, R. D.; Ntai, I.; Davis, J. H. J. *J. Am. Chem. Soc.* **2002**, *124*, 926.

(3) Shiflett, M.; Drew, D. W.; Cantini, R. A.; Yokozeki, A. *Energy Fuels* **2010**, *24*, 5781.

(4) Henley, E. J. ; Seader, J. D. ; Roper, D. K. *Separation Process Principles*, 3rd ed.; John Wiley & Sons: New York, 2011.

(5) Ignat'ev, N. V.; Welz-Biermann, U.; Kucheryna, A.; Bissky, G.; Willner, H. *J. Fluorine Chem.* **2005**, *126*, 1150.

(6) Muldoon, M. J.; Aki, S. N. V. K.; Anderson, J. L.; Dixon, J. K.; Brennecke, J. F. *J. Phys. Chem. B* **2007**, *111*, 9001.

(7) Yokozeki, A.; Shiflett, M. B.; Junk, C. P.; Grieco, L. M.; Foo, T. *J. Phys. Chem. B* **2008**, *112*, 16654.

(8) Blath, J.; Christ, J.; Deubler, N.; Hirth, T.; Schiestel, T. *Chem. Eng. J.* **2011**, *172*, 167.

(9) Zhang, X.; Liu, Z.; Wang, W. *AIChE J.* **2008**, *54*, 2717.
(10) Zhang, X.; Huo, F.; Liu, Z.; Wang, W.; Shi, W.; Maginn, E. J. *J. Phys. Chem. B* **2009**, *113*, 7591.
(11) Almantariotis, D.; Gefflaut, T.; Pádua, A. A. H.; Coxam, J.-Y.; Costa Gomes, M. F. *J. Phys. Chem. B* **2010**, *114*, 3608.
(12) Jacquemin, J.; Husson, P.; Padua, A. A. H.; Majer, V. *Green Chem.* **2006**, *8*, 172.
(13) Jacquemin, J.; Husson, P.; Majer, V.; Cibulka, I. *J. Chem. Eng. Data* **2007**, *52*, 2204.
(14) Schilling, G.; Kleinrahm, R.; Wagner, W. *J. Chem. Thermodyn.* **2008**, *40*, 1095.
(15) Jacquemin, J.; Costa Gomes, M. F.; Husson, P.; Majer, V *J. Chem. Thermodyn.* **2006**, *38*, 490.
(16) Jacquemin, J.; Husson, P.; Majer, V.; Costa Gomes, M. F. *Fluid Phase Equilib.* **2006**, *240*, 87.
(17) Husson, P.; Pison, L.; Jacquemin, J.; Costa Gomes, M. F. *Fluid Phase Equilib.* **2010**, *294*, 98.
(18) Canongia Lopes, J. N.; Deschamps, J.; Padua, A. A. H. *J. Phys. Chem. B* **2004**, *108*, 2038.
(19) Canongia Lopes, J. N.; Pádua, A. A. H. *J. Phys. Chem. B* **2004**, *108*, 16893.
(20) Shimizu, K.; Almantariotis, D.; Costa Gomes, M. F.; Pádua, A. A. H.; Canongia Lopes, J. N. *J. Phys. Chem. B* **2010**, *114*, 3592.
(21) Cornell, W. D.; Cieplak, P.; Bayly, C. I.; Gould, I. R.; Merz, K. M.; Fergusin, D. M.; Spellmeyer, D. C.; Fox, T.; Caldwell, J. W.; Kollman, P. A. *J. Am. Chem. Soc.* **1995**, *117*, 5179.
(22) Jorgensen, W. L.; Maxwell, D. S.; Tirado-Rives, J. *J. Am. Chem. Soc.* **1996**, *118*, 11225.
(23) Smith, W.; Forester, T. R. *DL_POLY Molecular Simulation Package*, 2007
(24) Harris, J. G.; Yung, K. H. *J. Phys. Chem.* **1995**, *99*, 12021.
(25) Costa Gomes, M. F.; Deschamps, J.; A.A.H., P. *J. Phys. Chem. B* **2006**, *110*, 18566.
(26) Pensado, A. S.; Costa Gomes, M. F.; Padua, A. A. H. *J. Phys. Chem. B* **2011**, *115*, 3942.
(27) Widom, B. *J. Chem. Phys.* **1963**, *39*, 2808.
(28) Mezei, M. *J. Chem. Phys.* **1987**, *86*, 7084.
(29) Del Pópolo, M. G.; Voth, G. A. *J. Phys. Chem. B* **2004**, *108*, 1744.
(30) Yao, C.; Pitner W., R.; Anderson, L. *J. Anal. Chem.* **2009**, *81*, 5054.
(31) Dymond, J. H.; Smith, E. B. *The Virial Coefficients of Pure Gases and Mixtures*; Clarendon Press: Oxford, 1980.
(32) D. Almantariotis, D.; Fandino, O.; Coxam, J. Y.; Costa Gomes, M. F. *Int. J. Greenhouse Gas Control* **2012**, accepted for publication.
(33) Triolo, A.; Russina, O.; Bleif, H.-J.; Di Cola, E. *J. Phys. Chem. B* **2007**, *111*, 4641.
(34) Triolo, A.; Russina, O.; Fazio, B.; Triolo, R.; Di Cola, E. *Chem. Phys. Lett.* **2008**, *457*, 362.
(35) Russina, O.; Triolo, A.; Gontrani, L.; Caminiti, R.; Xiao, D.; Hines, L. G., Jr; Bartsch, R. A.; Quitevis, E. L.; Plechkova, N.; Seddon, K. R. *J. Phys.: Condens. Matter* **2009**, *21*, 424121.
(36) Wang, Y.; Voth, G. A. *J. Am. Chem. Soc.* **2005**, *127*, 12192.
(37) Canongia Lopes, J. N.; Pádua, A. A. H. *J. Phys. Chem. B* **2006**, *110*, 3330.
(38) Pensado, A. S.; Costa Gomes, M. F.; Canongia Lopes, J. N.; Malfreyt, P.; Padua, A. A. H. *Phys. Chem. Chem. Phys.* **2011**, *13*, 13518.
(39) Jacquemin, J.; Costa Gomes, M .F.; Husson, P.; Majer, V.; Pádua, A. A. H. *Green Chem.* **2008**, *10*, 944.
(40) Costa Gomes, M. F.; Pison, L.; Pensado, A. S.; Padua, A. A. H. *Faraday Disc.* **2012**, *154*, 41.
(41) Pison, L.; Canongia Lopes, J. N.; Rebelo, L. P. N.; Padua, A. A. H.; Costa Gomes, M. F. *J. Phys. Chem. B* **2008**, *112*, 12394.

Solubility of carbon dioxide, nitrous oxide, ethane and nitrogen in 1-butyl-1-methylpyrrolidinium and trihexyl(tetradecyl)phosphonium tris(pentafluoroethyl)trifluorophosphate (eFAP) ionic liquids

S. Stevanovic, M.F. Costa Gomes*

Institut de Chimie de Clermont-Ferrand, Equipe Thermodynamique et Interactions Moléculaires, Clermont Université, Université Blaise Pascal, BP 80026, 63171 Aubière, France and CNRS, UMR6296 ICCF, BP 80026, 63171 Aubière, France

Abstract

The density and viscosity of the ionic liquids 1-butyl-1-methylpyrrolidinium tris(pentafluoroethyl)trifluorophosphate [C_1C_4Pyrro][eFAP] and trihexyl(tetradecyl)phosphonium tris(pentafluoroethyl)trifluorophosphate [P_{66614}][eFAP] were measured as a function of temperature and pressure and as a function of temperature, respectively. These two ionic liquids are more viscous than those based in the same anion associated to imidazolium cations. The effect of the addition of water on the density and viscosity of [P_{66614}][eFAP] was studied at pressures close to atmospheric and as a function of the temperature. This ionic liquid is only partially miscible with water, its solubility being of around $x_{H_2O} = 0.2$ in the range of 303 K to 315 K. Experimental values of the solubility of carbon dioxide, nitrous oxide, ethane and nitrogen were obtained as a function of temperature and at pressures close to atmospheric. Carbon dioxide and nitrous oxide are the more soluble gases with mole fraction solubilities up to 7×10^{-2}. Ethane is four times and 1.3 times less soluble than carbon dioxide in [C_1C_4Pyrro][eFAP] and [P_{66614}][eFAP], respectively. Nitrogen is one order of magnitude less soluble than the others gases in the two ionic liquids studied. In order to understand behavior of the different gases with these ionic liquids, the thermodynamic functions of solvation such as enthalpy and entropy were calculated from the variation of the Henry's law constant with temperature. It is shown that the more favorable interactions of the gases with the ionic liquid explain the larger solubility of carbon dioxide and nitrous oxide in [C_1C_4Pyrro][eFAP]. In the case of [P_{66614}][eFAP], it is the less favorable entropic contribution that explains the lower solubility of ethane in this ionic liquid.

* Corresponding author. E-mail: margarida.c.gomes@univ-bpclermont.fr

Introduction

Ionic liquids are considered as attractive solvents for gas separations[1] as they can be able to selectively and efficiently absorb one gas in a mixture. In particular, they have been indicated as possible alternatives for carbon dioxide removal from flue-gas streams by chemical[2] or physical absorption[3]. Several properties are significant for the evaluation of ionic liquids as liquid absorbers for gaseous solutes – the absorption capacity, the selectivity and the mass transfer – as they will determine the design and cost of possible industrial processes[4].

We are interested in the measurement of the solubility of gases – carbon dioxide, nitrous oxide, ethane and nitrogen – in ionic liquids based on the anion tris(pentafluoroethyl)trifluorophosphate coupled to the 1-butyl-1-methylpyrrolidinium or the trihexyl(tetradecyl)phosphonium cation. This new class of ionic liquids containing fluorinated anions was first synthesized in 2005 by Ignat'ev et al.[5] and have been proposed as replacements for ionic liquids containing other fluorinated anions that might be hydrolytically unstable, especially at elevated temperature.

The solubility of different gases in tris(pentafluoroethyl)trifluorophosphate based ionic liquids has already been reported in the literature but mainly for those containing imidazolium cations. Solubility of carbon dioxide in $[C_1C_6Im][eFAP]$ was measured experimentally by Muldoon et al.[6] and Yokozeki et al.[7]. Blath et al.[8] also studied the solubility of different gases in this same ionic liquid. Recently, Almantariotis et al.[9] have measured experimentally the solubility of carbon dioxide, nitrogen, ethane and nitrous oxide in $[C_1C_2Im][eFAP]$, $[C_1C_4Im][eFAP]$ and $[C_1C_6Im][eFAP]$. Results for the solubility of carbon dioxide in $[C_1C_6Im][eFAP]$, expressed in Henry's law constant, agree to within 2.5% between the different authors except for the values reported by Blath et al.[8], that show deviations of up to 12% from the other sets of values.

Different predictive models have also been used to assess gas solubility in these ionic liquids. The solubility of carbon dioxide in $[C_1C_2Im][eFAP]$, $[C_1C_4Im][eFAP]$ and $[C_1C_6Im][eFAP]$ was predicted by Zhang et al.[10] using

COSMO-RS and Zhang et al.[11] studied the solubility of carbon dioxide in [C_1C_6Im][eFAP] using Monte Carlo simulation.

It was observed that the length of the alkyl chain of the cations does not affect significantly the solubility of carbon dioxide in the tris(pentafluoroethyl)trifluorophosphate based ionic liquids. On the contrary, the nature of the anion has a very significant effect on the solubility of carbon dioxide, the tris(pentafluoroethyl)trifluorophosphate based ionic liquids showing higher solubilities of carbon dioxide when compared to ionic liquids with other anions. For carbon dioxide in [C_1C_4Im][eFAP], an Henry's law constant of 25.0 bar was found at 303.15 K[9], compared with 36.4[12] bar, 57.1[13] bar and 61.6[14] bar in [C_1C_4Im][NTf_2], [C_1C_4Im][PF_6] and [C_1C_4Im][BF_4], respectively.

The solubility of gases in tris(pentafluoroethyl)trifluorophosphate based ionic liquids with cations different from alkylimidazolium are rare. Blath et al.[8] have reported values of solubility of carbon dioxide, nitrogen, carbon monoxide and methane in [P_{66614}][eFAP]. Zhang et al.[10] have used COSMO-RS to predict also the solubility of carbon dioxide in [C_1C_4Pyrro][eFAP] at 298 K, and have compared these values with experimental data they obtained at temperatures from 283 to 323 K. The work of Blath et al. showed that the solubility of carbon dioxide is higher in [C_1C_6Im][eFAP] than in [P_{66614}][eFAP] when expressed in mass fraction. Zhang et al. have measured an higher solubility of carbon dioxide in [C_1C_6Im][eFAP] than in [C_1C_4Pyrro][eFAP] with values of Henry's law constants equal to 23.7 and 28.5, respectively, at 298.6 K.

This work follows previous studies aiming to explain the influence of fluoro-moieties in ionic liquids in the gas absorption by these liquids[15,9]. It has been concluded before that the presence of fluorinated alkyl-side chains in imidazolium cations significantly influences the solubility of carbon dioxide[15]. The effect of the fluorination in the anion was assessed by studying gas solubility in ionic liquids containing the tris(pentafluoroethyl)trifluorophosphate anion coupled with imidazolium based cations[9]. The presence of this anion influences the solubility of gases and such ionic liquids were found to be good absorbents for carbon dioxide,

the Henry's law constant for CO_2 in $[C_1C_4Im][eFAP]$ being as low as 25.0 at 303.15 K[9]. To complete these results, we have decided to study the effect of changing the cation in the ionic liquids with the tris(pentafluoroethyl)trifluorophosphate anion.

In the present work, experimental solubilities of carbon dioxide, nitrous oxide, ethane and nitrogen in $[C_1C_4Pyrro][eFAP]$ and $[P_{66614}][eFAP]$ are determined as a function of the temperature from 303.15 K to 343.15 K and at pressure close to atmospheric, using an isochoric saturation method. From the solubility data, the Henry's law constants and the thermodynamic properties of solvation were calculated.

Experimental

Materials

The two samples of ionic liquids used were purchased from Merck with mole fraction purities of 0.995. Their decomposition temperatures were determined using a modulated DSC 2920 from TA Instruments and were found to be 503 K for $[C_1C_4Pyrro][eFAP]$ and 473 K for $[P_{66614}][eFAP]$, respectively.

The ionic liquids were kept under vacuum for 15 h at 303 K before each measurement. The water contents of each degassed sample was determined, with a precision of ± 5 ppm, using a coulometric Karl Fisher titrator (Mettler Toledo DL31). The water content of the degassed samples was found to be 15 ppm for $[C_1C_4Pyrro][eFAP]$ and less than 5 ppm for $[P_{66614}][eFAP]$.

The gases used have the following specifications: carbon dioxide from AGA/Linde Gas has a mole fraction purity of 0.99995; nitrous oxide from Linde has a mole fraction purity of 0.995; ethane from AGA/Linde GAZ has a mole fraction purity of 0.995 and nitrogen from SAGA has a mole fraction purity of 0.998. The gases were used as received from the manufacturer.

Density measurements

Densities were measured using a U-shape vibrating-tube densimeter (Anton Paar, model DMA 512) operating in a static mode, following the procedure

described in previous publications[16,17]. Measurements for [C_1C_4Pyrro][eFAP] and [P_{666614}][eFAP] were performed for pressures up to 25 MPa and at temperatures from 293 to 343 K.

The temperature in the densimeter was maintained constant to within ±0.01K by means of a recirculating bath equipped with a PID temperature controller (Julabo FP40-HP). For measuring the temperature, a 100 Ohm platinum resistance thermometer (precision of ±0.02 K and accuracy of ±0.04 K) was used. Its calibration was performed by verifying a water triple point (triple point cell by Hart Scientific) and by comparison against a 100 Ohm platinum resistance Hart Scientific model 1502A.

The measured period of vibration (τ) of a U tube is related to the density (ρ) according to: $\rho = A\tau^2 + B$ where *A* and *B* are parameters that are function of temperature and pressure determined by calibration between temperatures of 293 and 343 K (and pressures of 0.1 and 25 MPa), using as calibration fluids n-heptane, bromobenzene and 2,4-dichlorotoluène following the recommendations by Schilling *et al.*[18]. Density measurements were performed in steps of 10 K. The uncertainty of the density measurements is estimated as 10^{-4} g cm^{-3}.

Viscosity measurements

The dynamic viscosities of the two ionic liquids [C_1C_4Pyrro][eFAP] and [P_{666614}][eFAP] previously dried under vacuum were measured using an Anton Paar AMVn rolling ball viscosimeter, as a function of the temperature from 293.15 K to 363.15 K (controlled to within 0.01 K and measured with an accuracy better than 0.05 K) and at atmospheric pressure. Before starting the measurements, the 3 mm diameter capillary tube was calibrated as a function of temperature and angle of measurement using a standard viscosity oil from Cannon (N35). The overall uncertainty on the viscosity is estimated as ±1.5%.

Gas-solubility measurements

The experimental method used for the gas solubility measurements is based on an isochoric saturation technique that has been described in

previous publications[13,14]. In this technique, a known quantity of gaseous solute is placed in contact with a precisely determined quantity of degassed solvent at a constant temperature inside an accurately known volume. When thermodynamic equilibrium is attained, the pressure above the liquid solution is constant and is directly related to the solubility of the gas in the liquid.

The quantity of ionic liquid introduced in the equilibration cell is determined gravimetrically. This quantity is equal to the amount of solvent present in the liquid solution, n_1^{liq}, as the ionic liquid does not present a measurable vapour pressure. The amount of solute present in the liquid solution, n_2^{liq} (subscripts 1 and 2 stand for solvent and solute, respectively), is calculated by the difference between two *pVT* measurements: first when the gas is introduced in a calibrated bulb with volume V_{GB} and second after thermodynamic equilibrium is reached:

$$n_2^{liq} = \frac{p_{ini} V_{GB}}{\left[Z_2\left(p_{ini}, T_{ini}\right) R T_{ini}\right]} - \frac{p_{eq}\left(V_{tot} - V_{liq}\right)}{\left[Z_2\left(p_{eq}, T_{eq}\right) R T_{eq}\right]} \qquad (1)$$

where p_{ini} and T_{ini} are the pressure and temperature in the first *pVT* determination and p_{eq} and T_{eq} the pressure and temperature at the equilibrium. V_{tot} is the total volume of the equilibration cell, V_{liq} is the volume of the liquid solution and Z_2 is the compression factor for the pure gas. The solubility can then be expressed in mole fraction, or as Henry's law constant:

$$K_H = \lim_{x_2 \to 0} \frac{f_2\left(p, T, x_2\right)}{x_2} \cong \frac{\phi_2\left(p_{eq}, T_{eq}\right) p_{eq}}{x_2} \qquad (2)$$

where f_2 is the fugacity of the solute and ϕ_2 its fugacity coefficient.

We consider that the volume of the ionic liquid does not change when the gas is dissolved and so the volume of the liquid solution is equal to the volume of the pure ionic liquid.

Water-miscibility measurements

The miscibility gap of $[P_{466614}]$[eFAP] with water was determined at different temperatures using a pVT method which has been described in a previous

publication[19]. An equilibrium cell equipped with precision manometers and placed in an air thermostat was used. Precisely known quantities of ionic liquid and water, previously degassed under vacuum and by successive melting and freezing cycles, respectively, are put in contact, under their own vapour pressure, inside the equilibrium cell. The two components are mixed at constant temperature and in the constant and accurately known volume of the apparatus. When thermodynamic equilibrium is reached, the vapour pressure is recorded. The liquid mixtures of different compositions were prepared gravimetrically after a controlled evaporation of the molecular compound. The temperature of the equilibrium cell and of the manometer was maintained to within ± 0.01 K, in the temperature range of 288 to 313 K, and measured with a calibrated 100 Ohm platinum resistance thermometer from Hart Scientific (Secondary Reference Temperature Standard, model 1502A, accuracy of ±0.018 K at 273 K). The pressure was measured using a quartz spiral manometer from Ruska (model 2465, uncertainty ± 10^{-5} bar).

Results and discussion

The experimental values obtained for the density of $[C_1C_4Pyrro][eFAP]$ and $[P_{66614}][eFAP]$ as a function of pressure and at temperatures from 293 to 353 K are reported in Table 1. The values of density at atmospheric pressure (necessary for the calculation of the gas solubility) were adjusted to linear functions of temperature:

$$\rho_{[C_1C_4Pyrro][eFAP]} / \mathrm{kg \cdot m^{-3}} = 1917.8 - 1.0721\left(T / \mathrm{K}\right) \quad (3)$$

$$\rho_{[P_{66614}][eFAP]} / \mathrm{kg \cdot m^{-3}} = 1426.2 - 0.8209\left(T / \mathrm{K}\right) \quad (4)$$

the standard deviation of the fits is always better than 0.1%.

The values determined for $[C_1C_4Pyrro][eFAP]$ and $[P_{66614}][eFAP]$ are 0.8% and 0.5% higher than those claimed by the manufacturer at 293 K, respectively.

The densities as a function of pressure were correlated using the Tait equation:

$$\rho(T,P) = \left[\frac{\rho^0(T,p^0)}{1 - C \ln\left(\frac{B(T)+p}{B(T)+p^0} \right)} \right] \quad (5)$$

where $\rho^0(T,p^0)$ is the density value at a reference temperature T and at the pressure p^0 = 0.1 MPa; C is an adjustable parameter and $B(T)$ a polynomial defined by:

$$B(T) = \sum_{i=0}^{2} B_i (T)^i \quad (6)$$

The parameters found for the present data are listed in Table 2.

The values for the dynamic viscosity, measured for the two ionic liquids previously dried, are listed in Table 3 as a function of temperature from 293 to 363 K. The Vogel–Fulcher–Tammann (VFT) equation was used to correlate the experimental viscosities as a function of temperature of $[C_1C_4Pyrro][eFAP]$ and $[P_{66614}][eFAP]$ with a standard deviation of 0.5 and 1.2%, respectively:

$$\rho_{[C_1C_4Pyrro][eFAP]} / \text{mPas} = \left(5.07 \times 10^{-3}\right)\left(T/K\right)^{\frac{1}{2}} \exp\left[\frac{992}{\left(T/K\right) - 173} \right] \quad (7)$$

$$\rho_{[P_{66614}][eFAP]} / \text{mPas} = \left(1.12 \times 10^{-3}\right)\left(T/K\right)^{\frac{1}{2}} \exp\left[\frac{1569}{\left(T/K\right) - 138} \right] \quad (8)$$

In Figure 1 are compared the values for the viscosity of these two ionic liquids studied and the tris(pentafluoroethyl)trifluorophosphate based ionic liquids with imidazolium cations studied previously.[9] As expected, the viscosities of the ionic liquids depend on the nature of the cation. We showed in our previous work that the viscosity of the ionic liquid depends on the length of the alkyl side chain in the imidazolium based ionic liquids. Furthermore, $[C_1C_4Pyrro][eFAP]$ and $[P_{66614}][eFAP]$ present viscosities higher than these of the imidazolium based ionic liquids. The viscosity, at 293.15 K, of $[P_{66614}][eFAP]$ (470.8 mPa s) is 1.4, 4.0, 4.7 and 6.3 times larger than that of $[C_1C_4Pyrro][eFAP]$, $[C_1C_6Im][eFAP]$, $[C_1C_4Im][eFAP]$ and

[C_1C_2Im][eFAP], respectively. These differences decrease with temperature and are equal to 1.3, 2.2, 2.3 and 2.4 times at 373.15 K, respectively. These results are in good agreement with the values of viscosity of [C_1C_4Pyrro][eFAP] and [P_{66614}][eFAP] that can be found in literature[20,21,22].

In order to determine the miscibility gap in the water + ionic liquid mixtures, the vapour pressure was measured for the mixture [P_{66614}][eFAP] + water at 303.30 K and 315.10 K. The results obtained are presented in Table 4 and depicted in Figure 2. Phase separation is determined from the discontinuity of the pressure curves as a function of the composition (intercept of the two lines that fit the data at each temperature) and, in the present case, phase separation occurs at $x_{H_2O} = 0.21$ for [P_{66614}][eFAP] at 303.30 K and at $x_{H_2O} = 0.22$ at 315.10 K. The water solubility in [P_{66614}][eFAP] is similar to the one measured in [C_1C_4Im][eFAP] and reported in our previous work but it does not increase with temperature as was observed for the [C_1C_6Im][eFAP].[9] The solubility of the ionic liquid in water appears as negligible as the values of the pressure measured above the biphasic mixtures are very close to those of pure water at the same temperature.

The solubility of the different gases was measured in the temperature interval between 303 K and 343 K in steps of approximately 10 K. Multiple experimental data points were obtained at each temperature. The experimental mole fraction solubilities of CO_2, N_2O, C_2H_6, and N_2 in [C_1C_4Pyrro][eFAP] and [P_{66614}][eFAP] are reported in Tables 5 to 8, respectively. Henry's law constants can be calculated from the experimental values and are used to determine the mole fraction solubility assuming a partial pressure of the gaseous solute equal to 0.1 MPa. The second virial coefficients for the gases, necessary for the calculation of the compressibility factor, were taken from the compilation by Dymond and Smith[23].

The Henry's law constants have been adjusted to an empirical equation of the form:

$$\ln\left(K_H / 10^5 Pa\right) = \sum_{i=0}^{n}\left[A_i \left(T / K\right)^{-i}\right] \qquad (9)$$

The coefficients A_i as well as the standard deviations of the fits, considered as a measure of the precision of the experimental solubility data for the different gases in the three ionic liquids are listed in Table 9. The Henry's law constants, calculated from the solubility measurements, are in general considered to be precise to within less than 1%. In the present work, the data for nitrous oxide, ethane and nitrogen in $[C_1C_4Pyrro][eFAP]$ and carbon dioxide, ethane and nitrogen in $[P_{66614}][eFAP]$ seem less precise with a standard deviation of the fit of up to 5%.

It is observed that $[P_{66614}][eFAP]$ presents a higher mole fraction solubility of all four gases than $[C_1C_4Pyrro][eFAP]$. Solubility of gases in this one seems to be comparable to the imidazolium based ionic liquids. In Figure 3 are depicted the values for the solubility of the different gases in the two ionic liquids studied and the imidazolium based ionic liquid studied before[9], at 303 K, expressed both in mole fraction (upper plot) and in mass fraction of gas (lower plot). The large differences in the mole fraction gas solubilities in $[P_{66614}][eFAP]$ and the other ionic liquids are less pronounced when the solubility is expressed in mass fraction.

Nitrous oxide is the most soluble gas in all studied ionic liquids followed by carbon dioxide, ethane and nitrogen. The solubility of ethane is two times lower and that of nitrogen is one order of magnitude lower than that of CO_2 or N_2O. For $[P_{66614}][eFAP]$, the ideal selectivity (calculated as the ratio of Henry's law constants) for carbon dioxide absorption is much less favorable than in the other ionic liquids, the selectivity for CO_2/N_2O and for CO_2/C_2H_6 being equal to 0.7 and 0.9, at 303.15 K, respectively.

In order to try to elucidate the reasons for the behavior found for the solubility of the different gases in the two ionic liquids studied, we have calculated their thermodynamic properties of solvation[24] and we have compared them to those of the eFAP based ionic liquids with imidazolium cations previously measured.[9] The average values, calculated for the temperature range covered in this work, are listed in Table 10. For the two

ionic liquids studied here, the higher solubility of carbon dioxide and nitrous oxide can be explained by more favorable solute-solvent interactions as shown by the more negative enthalpies of solvation of these two gases in both ionic liquids. The two gases – CO_2 and N_2O – are more soluble in the phosphonium based ionic liquids because the entropy of solvation is more favorable in this case, probably corresponding to a higher mobility of the solute in the ionic liquid with larger non-polar domains[25]. It can also be concluded from the analysis of the thermodynamic properties of solvation that it is the more favorable interaction between the gas and the ionic liquid that explains the relatively high solubility of ethane in $[P_{66614}][eFAP]$. This result is in agreement with our previous work[25] in which it is shown that the solubility of ethane is higher for ionic liquids with longer alkyl chains. The solubility of nitrogen is controlled by the entropic contributions, $[P_{66614}][eFAP]$ presenting a less negative entropy value, compared to $[C_1C_4Pyrro][eFAP]$.

Conclusions

This work presents an original study of the physico-chemical properties of the ionic liquids $[C_1C_4Pyrro][eFAP]$ and $[P_{66614}][eFAP]$ with the aim of studying the solvation mechanisms of different gases, relevant for carbon dioxide capture processes, in these media.

We have observed that $[P_{66614}][eFAP]$ is, as expected, less dense than $[C_1C_4Pyrro][eFAP]$ and than ionic liquids based on the same anion and on the imidazolium cation. $[P_{66614}][eFAP]$ and $[C_1C_4Pyrro][eFAP]$ present higher viscosities than the imidazolium based ionic liquids, which can constitute an disadvantage for industries needing low viscosities.

The $[P_{66614}][eFAP]$ ionic liquid is only partially miscible with water, the solubility being the same with the increase of the temperature, with molar fraction of water between 0.21 and 0.22 at 303.30 K and 315.10 K, respectively.

Carbon dioxide and nitrous oxide are the more soluble gases in the two ionic liquids $[C_1C_4Pyrro][eFAP]$ and $[P_{66614}][eFAP]$. Ethane is 4 times and 1.3 times less soluble than carbon dioxide in $[C_1C_4Pyrro][eFAP]$ and $[P_{66614}][eFAP]$, respectively; and nitrogen is one order of magnitude less soluble than the three

others gases in the two ionic liquids. [C_1C_4Pyrro][eFAP] and [P_{66614}][eFAP] present values of solubility of gases in the same order of magnitude than imidazolium based ionic liquids with the same anion. The behavior of [P_{66614}][eFAP] as a solvent for the gases studied is slightly different, this ionic liquid presenting a better affinity for ethane when compared with [C_1C_4Pyrro][eFAP] or [C_1C_nIm][eFAP] ionic liquids. This feature, resulting in different ideal selectivities, was explained by calculating the thermodynamic properties of solvation, both enthalpic and entropic terms influencing differently the solubility of the different gases in the ionic liquids.

Acknowledgements

The FUI ACACIA project is acknowledged for financing part of this work and the PhD grant of S.S. The authors thank Mrs. L. Pison for the calibration of the vibrating tube densimeter.

Table 1

Experimental Densities, ρ, of the ionic liquids $[C_1C_4Pyrro][eFAP]$ and $[P_{66614}][eFAP]$ between 293 K and 353 K and up to 25 MPa.

T / K	ρ^{exp} / kg·m^{-3}	T / K	ρ^{exp} / kg·m^{-3}
$[C_1C_4Pyrro][eFAP]$			
p = 0.10 ± 0.01 MPa		p = 0.50 ± 0.01 MPa	
293.19	1603.7 (1602.5)	293.19	1604.0
303.18	1592.8 (1591.9)	303.20	1593.1
313.20	1581.9 (1581.3)	313.20	1582.3
323.14	1571.0 (1570.5)	323.14	1571.4
333.17	1560.4 (1560.0)	333.17	1560.8
343.16	1549.9 (1549.5)	343.17	1550.4
353.17	1539.5 (1539.2)	353.17	1540.1
p = 1.00 ± 0.01 MPa		p = 2.50 ± 0.01 MPa	
293.19	1603.9	293.18	1604.9
303.19	1593.1	303.26	1593.9
313.20	1582.3	313.21	1583.3
323.15	1571.5	323.14	1572.5
333.17	1560.9	333.18	1562.0
343.18	1550.5	343.19	1551.6
353.18	1540.3	353.18	1541.4
p = 5.00 ± 0.01 MPa		p = 10.00 ± 0.01 MPa	
293.17	1606.7	293.17	1610.2
303.26	1595.8	303.25	1599.5
313.20	1585.3	313.19	1589.1
323.15	1574.6	323.14	1578.5
333.17	1564.2	333.18	1568.2
343.20	1553.9	343.20	1558.1
353.17	1543.8	353.19	1548.2

p = 15.00 ± 0.01 MPa		p = 20.00 ± 0.01 MPa	
293.17	1614.1	293.17	1618.0
303.26	1603.6	303.25	1607.6
313.21	1593.3	313.20	1597.4
323.14	1582.9	323.14	1587.2
333.18	1572.7	333.18	1577.2
343.20	1562.8	343.20	1567.4
353.18	1553.0	353.19	1557.7
p = 25.00 ± 0.01 MPa			
293.17	1621.7		
303.25	1611.4		
313.21	1601.4		
323.14	1591.3		
333.18	1581.4		
343.21	1571.7		
353.19	1562.2		
293.17	1621.7		

$[P_{66614}][eFAP]$

p = 0.10 ± 0.01 MPa		p = 0.50 ± 0.01 MPa	
293.20	1185.7 (1184.6)	293.21	1185.9
303.19	1177.4 (1176.6)	303.19	1177.7
313.15	1169.1 (1168.5)	313.17	1169.4
323.16	1160.6 (1160.2)	323.15	1161.0
333.11	1152.6 (1152.2)	333.12	1152.9
343.13	1144.5 (1144.2)	343.07	1145.0
353.20	1136.5 (1136.3)	353.22	1137.0
p = 1.00 ± 0.01 MPa		p = 2.50 ± 0.01 MPa	
293.22	1185.9	293.22	1186.7
303.19	1177.7	303.21	1178.5

313.17	1169.4	313.17	1170.3
323.15	1161.1	323.16	1162.0
333.12	1153.0	333.12	1154.0
343.07	1145.1	343.08	1146.1
353.23	1137.1	353.22	1138.2
p = 5.00 ± 0.01 MPa		p = 10.00 ± 0.01 MPa	
293.22	1188.3	293.22	1191.3
303.22	1180.1	303.22	1183.3
313.17	1172.0	313.17	1175.4
323.15	1163.8	323.15	1167.3
333.13	1156.8	333.12	1159.5
343.09	1148.1	343.08	1151.9
353.22	1140.2	353.23	1144.2
p = 15.00 ± 0.01 MPa		p = 20.00 ± 0.01 MPa	
293.23	1194.7	293.23	1198.0
303.23	1186.8	303.23	1190.2
313.17	1179.1	313.17	1182.6
323.14	1171.1	323.15	1174.7
333.13	1163.4	333.14	1167.2
343.08	1156.0	343.10	1159.9
353.23	1148.4	353.25	1152.5
p = 25.00 ± 0.01 MPa			
293.22	1201.2		
303.25	1193.5		
313.17	1186.0		
323.16	1178.3		
333.13	1171.0		
343.09	1163.7		
353.25	1156.4		

Table 2

Tait parameters C, B_0, B_1 and B_2 used to smooth the experimental densities as a function of pressure (to 25 MPa) and temperature (from 293 to 353K) along with the standard deviation of the fit, s.

Ionic liquid	$10^2 \cdot C$	B_0 / MPa	B_1 /MPa·K^{-1}	$10^3 \cdot B_2$ /MPa·K^{-2}	s
[C_1C_4Pyrro][eFAP]	-10.533	-708.007	2.152	-1.954	0.01
[P_{66614}][eFAP]	-20.957	-1578.329	5.909	-6.592	0.01

Table 3

Experimental dynamic viscosities, η, of the ionic liquids $[C_1C_4Pyrro][eFAP]$ and $[P_{66614}][eFAP]$ as a function of temperature at atmospheric pressure.

T / K	η^{exp} / mPa·s	T / K	η^{exp} / mPa·s
$[C_1C_4Pyrro][eFAP]$		$[P_{66614}][eFAP]$	
293.15	333.789	293.15	470.83
303.15	179.864	303.15	259.01
313.15	105.999	313.15	155.29
323.15	68.082	323.15	94.33
333.15	45.368	333.15	65.00
343.15	31.900	343.15	42.67
353.15	23.423	353.15	30.35
363.15	17.581	363.15	22.81
373.15	13.714	373.15	17.53

Table 4

Experimental values of the vapour pressures $p_{mix}^{H_2O}$ of the $[P_{66614}][eFAP]$ + water mixture as a function of the composition, expressed in water mole fraction, x_{H_2O}.

$[P_{66614}][eFAP]$ T = 303.32 K		$[P_{66614}][eFAP]$ T = 313.08 K	
x_{H_2O}	$p_{mix}^{H_2O}/10^2$Pa	x_{H_2O}	$p_{mix}^{H_2O}/10^2$Pa
0.0374	11	0.0243	19
0.0748	13	0.0245	25
0.0757	12	0.2126	65
0.1699	33	0.2267	67
0.1728	35	0.4111	69
0.2851	40	0.5580	70
0.3727	40	0.7965	69
0.4847	40	0.8386	67
0.5687	40	0.9311	66
0.6953	40		
0.7098	40		
0.7840	40		
0.8580	40		
0.9019	40		

Table 5

Experimental values of the solubility of CO_2 in $[C_1C_4Pyrro][eFAP]$ and $[P_{66614}][eFAP]$ expressed both as Henry's law constants, K_H (calculated from the experimental mole fractions, x_2^{exp}) and as CO_2 mole fraction, x_2, corrected for a partial pressure of solute of 0.1 MPa. p is the experimental equilibrium pressure and the per cent deviation is relative to the correlations of the data reported in Table 9.

T / K	p / 10^2Pa	x_2^{exp}	K_H / 10^5Pa	x_2 / 10^{-2}	dev / %
		$[C_1C_4Pyrro][eFAP]$			
303.16	641.11	2.49	25.7	3.88	0.3
303.16	635.00	2.46	25.7	3.87	-0.1
303.18	637.05	2.47	25.7	3.87	0.0
313.15	665.06	2.18	30.4	3.28	-0.4
313.19	670.76	2.22	30.1	3.31	0.4
313.22	666.50	2.19	30.4	3.29	-0.3
323.12	699.13	2.00	34.9	2.86	0.5
323.22	693.90	1.96	35.3	2.83	-0.4
323.33	694.95	1.97	35.1	2.83	0.0
333.13	721.73	1.78	40.5	2.46	-0.6
333.21	726.94	1.82	39.9	2.5	0.9
333.33	722.46	1.79	40.4	2.47	-0.1
343.09	748.93	1.62	46.1	2.16	-0.9
343.23	754.14	1.66	45.4	2.2	0.9
343.38	749.40	1.63	45.9	2.17	-0.2
		$[P_{66614}][eFAP]$			
303.17	678.39	3.55	19.1	5.22	0.2
303.18	677.00	3.51	19.2	5.17	-0.6
303.18	682.70	3.58	19.0	5.24	0.6

313.19	705.00	3.25	21.6	4.61	0.2
313.19	709.55	3.29	21.6	4.64	0.2
313.25	703.96	3.21	21.9	4.55	-0.9
323.23	731.08	3.01	24.2	4.12	0.6
323.23	736.03	3.06	24.0	4.15	1.4
323.25	730.63	2.93	24.8	4.01	-1.9
333.23	756.92	2.70	28.0	3.37	-2.8
333.26	756.84	2.81	26.9	3.71	1.2
333.26	762.07	2.85	26.7	3.74	2.0
343.25	782.96	2.49	31.3	3.18	-3.7
343.30	782.44	2.62	29.7	3.35	1.5
343.30	788.07	2.66	29.6	3.37	2.1

Table 6

Experimental values of the solubility of N_2O in $[C_1C_4Pyrro][eFAP]$ and $[P_{66614}][eFAP]$ expressed both as Henry's law constants, K_H (calculated from the experimental mole fractions, x_2^{exp}) and as N_2O mole fraction, x_2, corrected for a partial pressure of solute of 0.1 MPa. p is the experimental equilibrium pressure and the per cent deviation is relative to the correlations of the data reported in Table 9.

T / K	p / 10^2Pa	x_2^{exp}	K_H / 10^5Pa	x_2 / 10^{-2}	dev / %
		$[C_1C_4Pyrro][eFAP]$			
303.15	655.60	2.78	23.5	4.23	2.6
303.15	604.93	2.49	24.2	4.11	-0.1
303.17	647.08	2.61	24.7	4.03	-2.2
313.17	677.42	2.32	29.1	3.42	-3.1
313.18	633.00	2.23	28.3	3.52	-0.3
313.18	685.83	2.50	27.4	3.63	3.0
323.22	659.73	2.03	32.5	3.07	0.3
323.23	706.45	2.09	33.7	2.96	-3.3
323.29	715.38	2.26	31.6	3.15	3.2
333.18	743.52	2.06	35.9	2.77	3.4
333.21	685.84	1.85	36.9	2.70	0.6
333.24	734.65	1.90	38.6	2.58	-3.6
343.17	711.22	1.70	41.6	2.39	1.0
343.19	771.73	1.88	40.9	2.44	2.9
343.22	762.22	1.73	43.9	2.27	-4.1
		$[P_{66614}][eFAP]$			
303.15	653.79	4.56	14.3	6.96	-0.1
303.18	585.48	4.11	14.2	7.00	0.5

303.18	670.02	4.67	14.3	6.95	-0.2
313.18	610.42	3.73	16.3	6.09	0.1
313.19	698.02	4.25	16.4	6.07	-0.3
313.20	681.61	4.15	16.4	6.07	-0.2
323.21	725.43	3.89	18.6	5.36	-0.2
323.23	634.76	3.41	18.6	5.37	0.1
323.24	708.67	3.81	18.6	5.37	0.1
333.18	752.35	3.58	21.0	4.75	-0.2
333.25	735.19	3.52	20.8	4.78	0.4
333.26	658.62	3.15	20.9	4.77	0.2
343.15	761.50	3.24	23.4	4.25	-0.1
343.20	778.97	3.31	23.4	4.25	-0.1
343.23	682.19	2.90	23.4	4.25	0.0

Table 7

Experimental values of the solubility of C_2H_6 in $[C_1C_4Pyrro][eFAP]$ and $[P_{66614}][eFAP]$ expressed both as Henry's law constants, K_H (calculated from the experimental mole fractions, x_2^{exp}) and as C_2H_6 mole fraction, x_2, corrected for a partial pressure of solute of 0.1 MPa. p is the experimental equilibrium pressure and the per cent deviation is relative to the correlations of the data reported in Table 9.

T / K	p / 10^2Pa	x_2^{exp}	K_H / 10^5Pa	x_2 / 10^{-2}	dev / %
		$[C_1C_4Pyrro][eFAP]$			
303.16	706.14	1.06	66.1	1.50	3.7
303.27	746.06	1.07	69.4	1.43	-1.3
303.27	920.00	1.30	70.5	1.42	-2.8
313.19	731.73	0.97	74.6	1.33	1.1
323.22	756.97	0.91	83.1	1.19	0.2
333.23	782.28	0.83	93.1	1.07	-1.4
343.25	807.58	0.80	100.4	0.99	0.7
		$[P_{66614}][eFAP]$			
303.16	687.16	4.01	17.1	5.82	-1.3
303.17	683.77	4.05	16.8	5.92	0.4
303.17	694.78	4.14	16.7	5.94	0.9
313.16	721.80	3.72	19.3	5.14	1.0
313.18	713.83	3.57	19.9	5.00	-1.9
313.18	711.26	3.66	19.3	5.14	1.0
323.19	748.83	3.33	22.4	4.44	0.7
323.24	738.75	3.30	22.3	4.46	1.2
323.24	740.34	3.19	23.1	4.30	-2.5

333.19	775.22	3.02	25.6	3.89	1.3
333.23	765.15	3.03	25.2	3.95	3.0
333.27	766.60	2.84	26.9	3.70	-3.5
343.20	801.87	2.69	29.6	3.36	0.3
343.22	791.53	2.77	28.5	3.49	4.4
343.29	792.61	2.53	31.2	3.19	-4.6

Table 8

Experimental values of the solubility of N_2 in $[C_1C_4Pyrro][eFAP]$ and $[P_{66614}][eFAP]$ expressed both as Henry's law constants, K_H (calculated from the experimental mole fractions, x_2^{exp}) and as N_2 mole fraction, x_2, corrected for a partial pressure of solute of 0.1 MPa. p is the experimental equilibrium pressure and the per cent deviation is relative to the correlations of the data reported in Table 9.

T / K	p / 10^2Pa	x_2^{exp}	K_H / 10^5Pa	x_2 / 10^{-2}	dev / %
		$[C_1C_4Pyrro][eFAP]$			
303.16	924.85	0.389	237.5	0.421	-2.0
303.17	923.67	0.401	230.4	0.434	1.0
303.17	924.30	0.402	229.8	0.435	1.3
313.16	954.89	0.390	244.7	0.409	-1.5
313.17	953.75	0.397	239.9	0.417	0.5
313.18	954.37	0.400	238.3	0.420	1.2
323.17	984.54	0.388	253.9	0.394	-1.2
323.18	985.00	0.386	255.0	0.392	-1.6
323.20	983.80	0.397	247.9	0.403	1.2
333.15	1014.47	0.386	262.7	0.381	-0.4
333.18	1014.88	0.394	257.8	0.388	1.5
333.19	1013.83	0.392	258.8	0.386	1.1
343.14	1043.86	0.375	278.2	0.360	-1.7
343.14	1044.39	0.385	271.0	0.369	0.9
		$[P_{66614}][eFAP]$			
303.16	732.12	0.70	104.7	0.96	-3.5
303.17	733.68	0.74	99.4	1.01	1.7
303.19	723.70	0.73	98.6	1.01	2.4
313.18	756.09	0.70	108.3	0.92	-2.6

313.20	757.71	0.74	102.3	0.98	3.1
313.23	747.90	0.70	107.2	0.93	-1.6
323.22	781.90	0.73	107.7	0.93	3.7
323.23	780.35	0.68	114.6	0.87	-2.5
323.28	771.79	0.69	112.4	0.89	-0.6
333.21	806.25	0.69	116.3	0.86	2.8
333.24	804.58	0.66	122.4	0.82	-2.3
333.27	795.69	0.67	119.4	0.84	0.2
343.20	830.41	0.68	122.7	0.82	5.3
343.24	829.20	0.60	137.7	0.73	-6.2
343.28	819.72	0.64	128.4	0.78	0.7

Table 9

Parameters of equation (9) used to smooth the experimental results on K_H from Tables along with the per cent standard deviation of the fit (s).

Gas	A_0	A_1	A_2	s
		[C_1C_4Pyrro][eFAP]		
CO_2	+ 6.916	-6.771×10^2	-1.319×10^5	0.2
N_2O	+ 7.036	-8.576×10^2	-9.395×10^3	0.9
C_2H_6	+ 10.69	-3.034×10^3	$+3.254 \times 10^5$	0.9
N_2	+ 9.600	-2.207×10^3	$+2.876 \times 10^5$	3.1
		[P_{66614}][eFAP]		
CO_2	+ 6.886	-1.202×10^3	-2.828×10^4	0.5
N_2O	+ 7.149	-1.446×10^3	$+2.586 \times 10^3$	0.1
C_2H_6	+ 10.52	-3.307×10^3	$+2.951 \times 10^5$	0.6
N_2	+ 14.73	-5.815×10^3	$+8.331 \times 10^5$	3.7

Table 10

Thermodynamic properties of solvation of carbon dioxide, nitrous oxide, ethane and nitrogen in the ionic liquids $[C_1C_4Pyrro][eFAP]$ and $[P_{66614}][eFAP]$ in the temperature range studied.

Gas	$-\Delta_{sol}H$ / kJ·mol^{-1}	$-\Delta_{sol}S$ / J·mol^{-1}·K^{-1}
	$[C_1C_4Pyrro][eFAP]$	
CO_2	12.5 ± 0.3	68.1 ± 0.9
N_2O	12.0 ± 0.2	66.0 ± 0.6
C_2H_6	8 ± 1	61 ± 3
N_2	4 ± 1	58 ± 3
	$[P_{66614}][eFAP]$	
CO_2	9.7 ± 0.2	56.7 ± 0.6
N_2O	10.5 ± 0.2	56.9 ± 0.8
C_2H_6	12 ± 1	62 ± 3
N_2	4 ± 3	52 ± 8

Figure 1

Viscosity of the ionic liquids studied herein, and the imidazolium based ionic liquid: (◊); $[C_1C_2Im][eFAP]$, (○); $[C_1C_4Im][eFAP]$, (□); $[C_1C_6Im][eFAP]$, (▼); $[C_1C_4Pyrro][eFAP]$ and (●); $[P_{66614}][eFAP]$ at 0.1 MPa and as a function of the temperature.

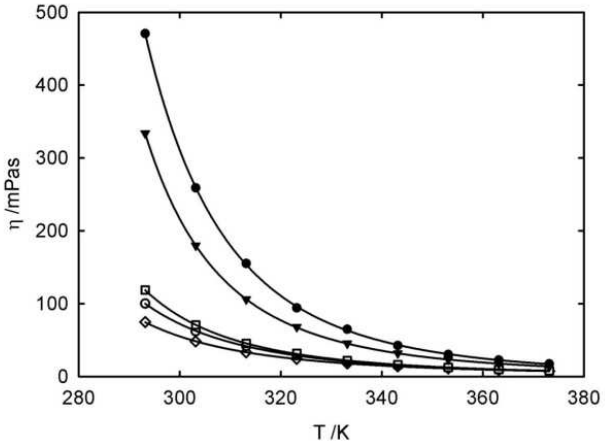

Figure 2

Vapour pressures of $[P_{66614}][eFAP]$ + water as a function of the composition: ●, 303.15 K; ■, 313.15 K.

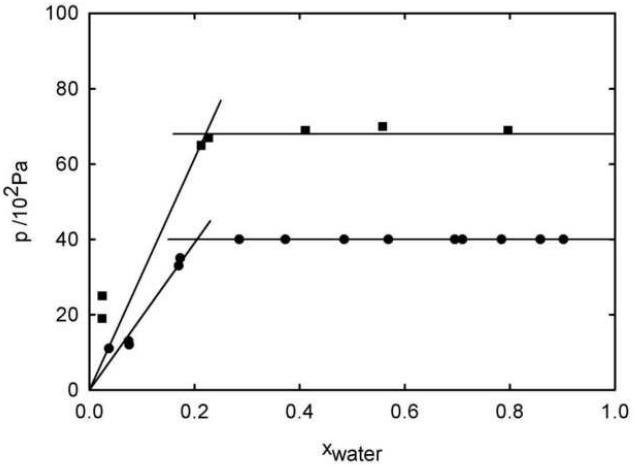

Figure 3

Mole fraction solubility (a) and mass fraction solubility (b) of carbon dioxide, nitrous oxide, ethane and nitrogen in the ionic liquids studied herein, and the imidazolium based ionic liquid, at 303 K: ▫, $[C_1C_2Im][eFAP]$; ▫, $[C_1C_4Im][eFAP]$; ▫, $[C_1C_6Im][eFAP]$; ▫, $[C_1C_4Pyrro][eFAP]$; ■, $[P_{66614}][eFAP]$.

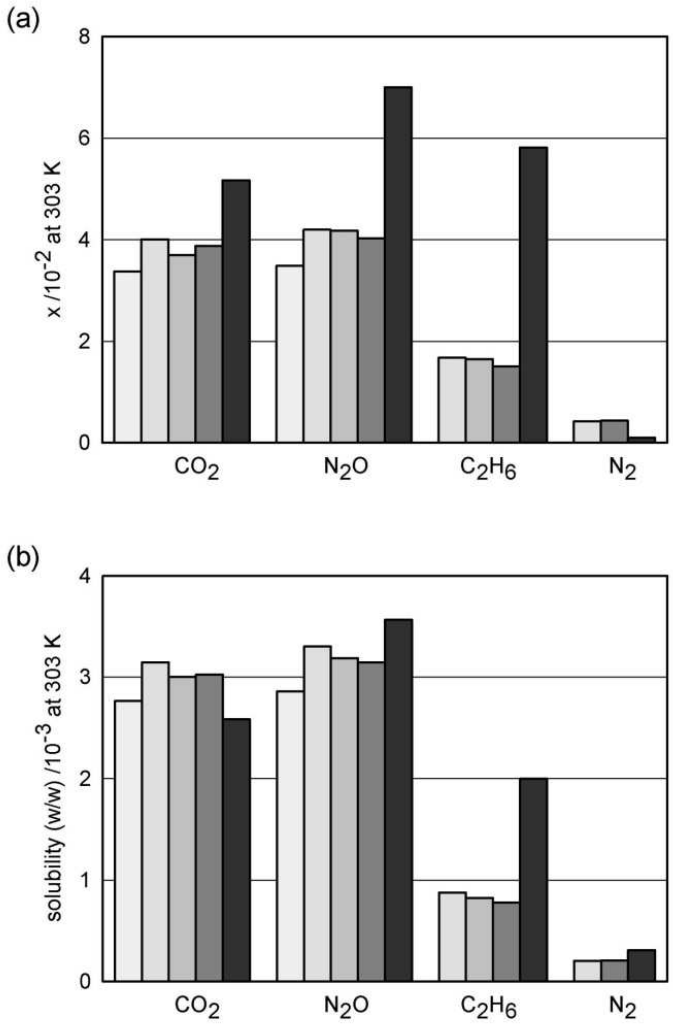

References

1 Costa Gomes, M. F.; Husson, P. *ACS Symposium Series* 1030 (16) (2010) 223.

2 Bates, E. D.; Mayton, R. D.; Ntai, I.; Davis, J. H. J. *J. Am. Chem. Soc.* **2002**, *124*, 926.

3 Shiflett, M.; Drew, D.W.; Cantini, R.A.; Yokozeki, A. *Energy Fuels* **2010**, *24*, 5781.

4 Henley, E.J.; Seader, J.D.; Roper, D.K. Separation Process Principles, 3rd Ed., John Wiley & Sons, 2011.

5 Ignat'ev, N. V.; Welz-Biermann, U.; Kucheryna, A.; Bissky, G.; Willner, H. *J. Fluorine Chem.* **2005**, *126*, 1150.

6 Muldoon, M. J.; Aki, S. N. V. K.; Anderson, J. L.; Dixon, J. K.; Brennecke, J. F. *J. Phys. Chem. B* **2007**, *111*, 9001.

7 Yokozeki, A.; Shiflett, M. B.; Junk, C. P.; Grieco, L. M.; Foo, T. *J.Phys.Chem. B* **2008**, *112*, 16654.

8 Blath, J.; Christ, J.; Deubler, N.; Hirth, T.; Schiestel, T. *Chem. Eng. J.* **2011**, *172*, 167.

9 Almantariotis, D.; Stevanovic, S.; Fandino, O.; Pensado. A.; Padua. A.; Costa Gomes. M. F. *J. Phys. Chem. B.* **2012**, 116, 7728-7738.

10 Zhang, X.; Liu, Z.; Wang, W. *AIChE J.* **2008**, *54*, 2717.

11 Zhang, X.; Huo, F. ; Liu, Z.; Wang, W.; Shi, W.; Maginn, E. J. *J. Phys. Chem. B* **2009**, *113*, 7591.

12 Jacquemin, J.; Husson, P.; Majer, V.; Costa Gomes, M.F, I. *J. Solution. Chem.* **2007**, *36*, 967.

13 Jacquemin, J.; Husson, P.; Majer V.; Costa Gomes, M.F. *Fluid Phase Equilibr.* **2006**, *240*, 87.

14 Jacquemin, J.; Costa Gomes, M.F.; Husson P.; Majer V., *J. Chem. Thermodyn.* **2006**, *38*, 490.

15 Almantariotis, D.; Gefflaut, T.; Pádua, A. A. H.; Coxam, J.-Y.; Costa Gomes, M. F. *J. Phys. Chem. B* **2010**, *114*, 3608.

16 Jacquemin, J.; Husson, P.; Padua, A. A. H.; Majer, V. *Green Chemistry* **2006**, *8*, 172.

17 Jacquemin, J.; Husson, P.; Majer, V.; Cibulka, I. *J. Chem. Eng. Data* **2007**, *52*, 2204.

18 Schilling, G.; Kleinrahm, R.; Wagner, W. *J. Chem. Thermodyn*. **2008**, *40*, 1095.

19 Husson, P.; Pison, L.; Jacquemin, J.; Costa Gomes, M. F. *Fluid Phase Equilibr.* **2010**, *294*, 98.

20 Fletcher, S.; Sillars, F.; Hudson, N.; Hall, P. J. *Chem. Eng. Data* **2010**, *55*, 778.

21 Gacino, F.; Regueira, T.; Lugo, L.; Comunas, M.; Fernandez, J. *Chem. Eng. Data* **2011**, *56*, 4984.

22 Ferreira, C.; Talavera-Prieto, N.; Fonseca, I.; Portugal, A.; Ferreira, A. *J. Chem. Thermodynamics* **2012**, *47*, 183.

23 Dymond, J. H.; Smith, E. B. *The virial coefficients of pure gases and mixtures*; Clarendon Press: Oxford, 1980.

24 Almantariotis, D.; Fandino, O.; Coxam, J.Y.; Costa Gomes, M. F. *Int. J. Greenhouse Gas Control* **2012**, DOI: 10.1016/j.ijggc.2012.06.018.

25 Costa Gomes, M.F. ; Pison, L. ; Pensado, A.S. ; Padua, A.A.H. *Faraday Disc.* **2012**, 154, 41-52.

THE JOURNAL OF PHYSICAL CHEMISTRY B

Article

pubs.acs.org/JPCB

Effect of Water on the Carbon Dioxide Absorption by 1-Alkyl-3-methylimidazolium Acetate Ionic Liquids

Stéphane Stevanovic, Ajda Podgoršek, Agilio A. H. Pádua, and Margarida F. Costa Gomes*

Institut de Chimie de Clermont-Ferrand, Thermodynamique et Interactions Moléculaires, Clermont Université, Université Blaise Pascal, BP 80026, 63171 Aubiere, France, and CNRS, UMR6296 ICCF, BP 80026, 63171 Aubiere, France

Supporting Information

ABSTRACT: The absorption of carbon dioxide by the pure ionic liquids 1-ethyl-3-methylimidazolium acetate ([C_1C_2Im][OAc]) and 1-butyl-3-methylimidazolium acetate ([C_1C_4Im][OAc]) was studied experimentally from 303 to 343 K. As expected, the mole fraction of absorbed carbon dioxide is high (0.16 at 303 K and 5.5 kPa and 0.19 at 303 and 9.6 KPa for [C_1C_2Im][OAc] and [C_1C_4Im][OAc], respectively), does not obey Henry's law, and is compatible with the chemisorption of the gas by the liquid. Evidence of a chemical reaction between the gas and the liquid was found both by NMR and by molecular simulation. In the presence of water, the properties of the liquid absorber significantly change, especially the viscosity that decreases by as much as 25% (to 78 mPa s) and 30% (to 262 mPa s) in the presence of 0.2 mol fraction of water for [C_1C_2Im][OAc] and [C_1C_2Im][OAc] at 303 K, respectively. The absorption of carbon dioxide decreases when the water concentration increases: a decrease of 83% in CO_2 absorption is found for [C_1C_4Im][OAc] with 0.6 mol fraction of water at 303 K. It is proved in this work, by combining experimental data with molecular simulation, that the presence of water not only renders the chemical reaction between the gas and the ionic liquid less favorable but also lowers the (physical) solubility of the gas as it competes by the same solvation sites of the ionic liquid. The lowering of the viscosity of the liquid absorbent largely compensates these apparent drawbacks and the mixtures of [C_1C_2Im][OAc] and [C_1C_2Im][OAc] with water seem promising to be used for carbon dioxide capture.

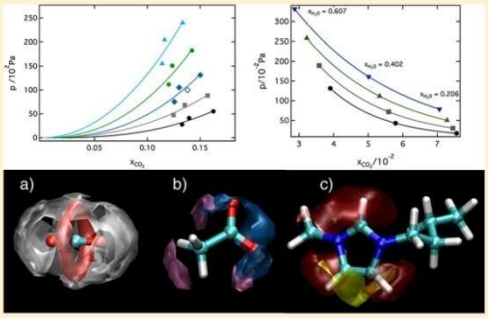

1. INTRODUCTION

It has recently been shown that alkylimidazolium acetate ionic liquids can chemically absorb carbon dioxide,[1−3] leading to solutions of almost 30 mol % CO_2 at atmospheric pressure.[4] These ionic liquids are considered as potential absorbents for carbon dioxide and have even been studied as potential substitutes of amine-based solutions,[5] as they associate selective absorption capabilities to negligible vapor pressures, low melting temperatures and good thermal stabilities.

The absorption of carbon dioxide in ionic liquids based on the acetate anion has been reported by several authors. Maginn et al.[6] first studied the absorption of CO_2 in the [C_1C_4Im]-[OAc] and proposed a mechanism for the chemical reaction of the gas with the ionic liquid based on NMR results. They proposed a first step of deprotonation of the imidazolium cation at the C2 position of the ring by the acetate anion followed by the association between the formed carbene and carbon dioxide. This simple mechanism was refuted by subsequent studies[4,7,8] and, more recently, it has been shown that the mechanism of reaction between carbon dioxide and acetate based alkylimidazolium ionic liquids is more elaborate[1−3] and also involves the formation of a complex anion.

Shiflett et al. reported experimental measurements of the absorption of carbon dioxide in [C_1C_2Im][OAc],[9,10] [C_1C_4Im][OAc],[10] and [C_2C_2Im][OAc][11] and have mentioned the reversible formation of a chemical complex due to a Lewis acid base interaction. More recently, they have proved that the mechanisms proposed by Gurau et al.[2] and Besnard et al.[3] using NMR spectroscopy and X-ray diffraction analysis and IR, Raman, and NMR spectroscopy, respectively, are compatible with the equilibrium measurements and models developed.[11]

To improve the properties of gas absorbent including its selectivity for carbon dioxide, the research is focused on the addition of a molecular cosolvent, such as water, to the ionic liquid. The presence of water in ionic liquid affects the physicochemical properties of the liquid mixture, i.e., lowering the viscosity of the mixture,[12] an advantage for industrial applications. Contrary to many studies on the solubility of gases in pure ionic liquids, at both low and high pressures, very few data are available on ternary systems [C_1C_4Im][OAc] + water + CO_2[2,11] even if they are more representative of real mixtures. Gurau et al.[2] have observed a fast release of the absorbed CO_2 upon the addition of water to [C_1C_2Im][OAc], leading to the formation of [C_1C_2Im][HCO_3]. Shiflett et al.[11] observe that the addition

Received: October 10, 2012
Revised: November 12, 2012
Published: November 13, 2012

ACS Publications © 2012 American Chemical Society

of water to a solution of CO_2 in $[C_2C_2Im][OAc]$ may lead to the formation of a bicarbonate salt that can prevent the regeneration of the ionic liquid upon the desorption of the gas. As far as the authors are aware, no research group has quantified the effect of water on the absorption of carbon dioxide by alkylimidazolium acetate ionic liquids as a function of the composition in water, temperature and pressure of the gas. Even if Chinn et al.[13] report the carbon dioxide absorption by a mixture of $[C_1C_4Im]$-$[OAc] + H_2O$ (14 wt %), again, no study of the effect of different concentrations of water is reported.

The aim of this work is to obtain a consistent and precise set of experimental data on the absorption of CO_2 by imidazolium acetate ionic liquids and to study the influence of water on the solubility of carbon dioxide in $[C_1C_2Im][OAc]$ and $[C_1C_4Im]$-$[OAc]$ at temperatures between 303 and 343 K. Moreover, the solvation of CO_2 and its solubility in the studied ionic liquids was investigated by molecular dynamic simulations. The analysis of the data enabled the access to the molecular mechanism of the carbon dioxide absorption in these ionic liquids. ^1H and ^{13}C NMR spectroscopy provided further experimental evidence for the solvation mechanism proposed with or without the presence of water.

2. EXPERIMENTAL SECTION

Materials. The ionic liquids 1-ethyl-3-methylimidazolium acetate (98%), $[C_1C_2Im][OAc]$, 1-butyl-3-methylimidazolium acetate, $[C_1C_4Im][OAc]$ (98%) were supplied by SOLVIONIC. The carbon dioxide (AGA/Linde Gaz, with purity >0.99995 mol fraction) and the nitrogen (AGA/Linde Gaz, with purity >0.99995 mol fraction) were used as received. Water was distilled three times and degassed using melting−freezing cycles before use.

The water content of the ionic liquid sample was determined by coulometric Karl Fisher Titration using a Mettler Toledo DL31 titrator. Before each measurement the sample of ionic liquid was degassed and dried under vacuum at 303 K at least for 72 h. The quantity of water was determined to be 500 and 600 ppm for $[C_1C_2Im][OAc]$ and $[C_1C_4Im][OAc]$, respectively.

The temperature of decomposition of the ionic liquids was determined by a modulated DSC 2920 from TA Instruments. The value determined was 423 and 433 K for $[C_1C_2Im][OAc]$ and $[C_1C_4Im][OAc]$, respectively.

Mixtures of ionic liquids with different water contents were prepared gravimetrically. The ionic liquid was first introduced in a glass vial, and then the appropriate amount of water was added and the glass vial was sealed. The vial was completely filled with the liquid mixture to minimize the volume of the vapor phase in equilibrium with the liquid solution and so reduce the error in composition due to differential evaporation. The uncertainty of the mole fraction is estimated as ±0.0001.

Density Measurements. Densities were measured using a U-shaped vibrating-tube densimeter (Anton Paar, model DMA 512) operating in a static mode, following the procedure described in previous publications.[8,14] Measurements of the pure ionic liquids and the mixtures ionic liquid + water were performed at pressures up to 25 MPa and in the temperature range from 293 to 353 K. The temperature was maintained constant within ±0.01 K by means of a recirculating bath equipped with a PID temperature controller (Julabo FP40-HP). For measuring the temperature, a 100 Ohm platinum resistance thermometer (precision of ±0.02 K and accuracy of ±0.04 K) was used. Its calibration was performed by verifying a water triple point (triple point cell by Hart Scientific) and by comparison against a 100 Ohm platinum resistance Hart Scientific model 1502A. The pressure was measured using a precision pressure transmitter Druck, model PTX 610, working in a range from 0 to 70 MPa with an uncertainty 0.08% full scale. The uncertainty of the density measurement is estimated as 10^{-4} g cm^{-3}.[14]

Viscosity Measurements. The dynamic viscosities of pure ionic liquids and mixtures of ionic liquid + water were measured using an Anton Paar AMVn rolling ball viscosimeter at atmospheric pressure and temperatures between 293.15 and 363.15 K. The temperature was controlled to within 0.01 K and measured with accuracy better than 0.05 K. Before the measurements the 1.8 and 3 mm diameter capillary tubes were calibrated as a function of temperature and angle of measurement using a standard viscosity oil from Cannon (N35). The overall uncertainty on the viscosity is estimated as ±1.5%.

Gas-Absorption Measurements. The experimental apparatus used for the gas absorption measurements in pure ionic liquids was based on an isochoric saturation technique and has been described in previous publications.[15−17] In this technique a known quantity of gaseous solute is put in contact with a precisely determined quantity of degassed solvent at a constant temperature inside an accurately known volume. When thermodynamic equilibrium is attained, the pressure above the liquid solution is directly related to the absorption of the gas by the liquid. Absorption of CO_2 was determined in the temperature range from 303.15 to 353.15 K. The method of data reduction was reported in previous publications.[15,16]

A second cell was used to determine the absorption of carbon dioxide in the mixtures of ionic liquid + water. This cell is also a pVT constant volume cell and the experimental apparatus used for the present gas solubility measurements was based on an isochoric saturation method that has been described in a previous publication.[18,19] In this technique a known quantity of gaseous solute is put into contact with a precisely determined quantity of degassed solvent at constant temperature inside an accurately known volume. As previously, when thermodynamic equilibrium is attained, the pressure above the liquid solution is constant and directly related to the solubility of the gas in the liquid. Details of the data reduction are given in our previous publications.[18,19]

Molecular Simulations. Ionic liquids were represented by an all-atom force field, which is based on the AMBER/OPLS_AA framework.[20,21] For the imidazolium cation, force field parameters were developed specifically.[22] Acetate[21,23] was represented with the potential models existing in the literature, whereas the potential model of Mallet et al.[24] was used for carbon dioxide.

The ionic liquid $[C_1C_4Im][OAc]$ was simulated in periodic cubic boxes containing 127 ion pairs, using the molecular dynamics method implemented in the DL_POLY package.[20] Initial low-density configurations, with ions placed at random in periodic cubic boxes, were equilibrated to attain liquid-like densities and structures at 373 K and 1 bar. Temperature and pressure were maintained using a Nosé−Hoover thermostat and barostat, respectively. Once the equilibrium density was attained, simulation runs of 1 ns were performed, with an explicit cutoff distance of 16 Å for nonbonded interactions, from which 5000 configurations were stored. Structural quantities such as radial and spatial distribution functions were calculated from configurations generated during the production runs. Additionally, simulation boxes containing 200 ion pairs and 12 CO_2 molecules were prepared in the same manner, to calculate solute−solvent radial distribution functions between the gas and the

ionic liquid and the cation−anion interaction energy in the presence of CO_2.

The chemical potentials of CO_2 at 373 K in the two ionic liquids were calculated in a two-step procedure, as already described by Almantariotis et al.[25] First, for CO_2, a reduced-size version of the molecule was made by subtracting 0.8 Å from the C−O bond length and also from the Lennard-Jones diameters σ_O and σ_C. The resulting molecule is small enough so that its chemical potential can be calculated using the Widom test-particle insertion method[26] with efficient statistics (100 000 insertions into each of 5000 stored configurations of pure ionic liquids). Second, a stepwise finite difference thermodynamic integration procedure[27] was followed to calculate the free-energy difference between the initial, reduced versions of the carbon dioxide molecule and the final full-size model. The free energy calculation was performed on six intermediate steps along a linear path connecting the intermolecular parameters (bonds and diameters) of the reduced-size to those of the full-size molecule. This relatively modest number of intermediate steps is adequate because the starting point of the thermodynamic integration route is not too far from the final state. In the finite-difference thermodynamic integration scheme, derivatives (finite differences) of the total energy of the system with respect to the activation parameter were evaluated by a free-energy perturbation expression in the NpT ensemble using a three-point formula with increments of 2×10^{-3}.

NMR Measurements. ^{1}H and ^{13}C NMR data were collected at 25 or 40 °C on a Bruker AC 300 MHz spectrometer with the resonance frequency at 300.130 MHz for the ^{1}H nucleus. Samples of $[C_1C_4Im][OAc]$ were recorded in solution using acetone-d_6 as a solvent. The deuterium in DMSO-d_6 was used for the external lock of the NMR magnetic field, and the residual proton in DMSO-d_6 was used as the ^{1}H NMR external reference at 2.5 ppm.

3. RESULTS AND DISCUSSION

Densities of the pure ionic liquids and of the mixtures of ionic liquid + water were obtained as a function of temperature from 293 to 353 K and of pressure from 0.1 to 25 MPa. The experimental data are presented in Table S-1 in the Supporting Information. The values of the density at atmospheric pressure (necessary for the calculation of the gas solubility) were adjusted to linear functions of temperature. The coefficients of the fits are listed in Table 1 together with the standard deviation, which is always better than 0.1%.

The densities as a function of pressure were correlated using the Tait equation:

$$\rho(T,p) = \left[\frac{\rho^0(T,p^0)}{1 - C\ln\left(\frac{B(T)+p}{B(T)+p^0}\right)}\right] \quad (1)$$

where $\rho^0(T,p^0)$ is the density value at a reference temperature T and at the pressure p^0 = 0.1 MPa; C is an adjustable parameter and $B(T)$ is a polynomial defined by

$$B(T) = \sum_{i=0}^{2} B_i(T)^i \quad (2)$$

The parameters found for the present experimental data are listed in Table 2.

The volumetric data measured were used to calculate the excess molar volume of the mixtures of the ionic liquids $[C_1C_2Im]$-[OAc] and [C1C4Im][OAc] with water using the relation:

$$V^E = V_m^{mix} - \sum_i x_i \frac{M_i}{\rho_i} \quad (3)$$

where V_m^{mix} is the molar volume of the mixture, x_i the mole fraction of component i with molar mass M_i and density ρ_i. The values calculated are listed in Table S-2 of the Supporting Information. The uncertainty of the excess molar volumes, evaluated by propagation of the errors, is estimated to be ±0.1 cm^3 mol^{-1}.

Table 1. Parameters A_0 and A_1 of Linear Functions[a] Used To Smooth the Experimental Densities at 0.1 MPa as a Function of Temperature

IL	A_0/kg·m^{-3}	A_1/kg·m^{-3}·K^{-1}	S/%
$[C_1C_2Im][OAc]$	1281.0	−0.6064	0.02
$[C_1C_2Im][OAc]$ + water (x_{water} = 0.2000)	1278.3	−0.5862	0.02
$[C_1C_2Im][OAc]$ + water (x_{water} = 0.4040)	1282.6	−0.5912	0.01
$[C_1C_2Im][OAc]$ + water (x_{water} = 0.6028)	1290.2	−0.6089	0.01
$[C_1C_2Im][OAc]$ + water (x_{water} = 0.8020)	1295.4	−0.6541	0.03
$[C_1C_4Im][OAc]$	1230.7	−0.5927	0.01
$[C_1C_4Im][OAc]$ + water (x_{water} = 0.1966)	1231.3	−0.5888	0.01
$[C_1C_4Im][OAc]$ + water (x_{water} = 0.3958)	1236.3	−0.5846	0.06
$[C_1C_4Im][OAc]$ + water (x_{water} = 0.6002)	1249.1	−0.6230	0.01
$[C_1C_4Im][OAc]$ + water (x_{water} = 0.7992)	1267.0	−0.6765	0.01

[a] $\rho_{IL\,phase} = A_1 + A_1 \times T$.

Table 2. Tait Parameters C, B_0, B_1, and B_2 Used To Smooth the Experimental Densities as a Function of Pressure (to 25 MPa) and Temperature (from 293 to 453 K) along with the Percent Average Absolute Deviations of the Fit (AAD)

IL	10^2C	B_0/MPa	B_1/MPa·K^{-1}	10^3B_2/MPa·K^{-2}	AAD/%
$[C_1C_2Im][OAc]$	−1.578	+103.666	+0.093	+0.090	0.013
$[C_1C_2Im][OAc]$ + water (x_{water} = 0.2000)	+8.505	+255.188	+0.554	−1.872	0.005
$[C_1C_2Im][OAc]$ + water (x_{water} = 0.4040)	+9.260	+471.050	−0.467	−0.463	0.005
$[C_1C_2Im][OAc]$ + water (x_{water} = 0.6028)	+11.743	+1305.881	−4.581	+5.228	0.013
$[C_1C_2Im][OAc]$ + water (x_{water} = 0.8020)	+7.618	−106.151	+2.913	−5.582	0.014
$[C_1C_4Im][OAc]$	+6.659	−213.387	+2.764	−5.067	0.006
$[C_1C_4Im][OAc]$ + water (x_{water} = 0.1966)	+9.835	+272.040	+0.573	−2.104	0.005
$[C_1C_4Im][OAc]$ + water (x_{water} = 0.3958)	+31.131	−2763.812	+24.953	−0.043	0.047
$[C_1C_4Im][OAc]$ + water (x_{water} = 0.6002)	+3.908	−553.792	+4.486	−7.639	0.008
$[C_1C_4Im][OAc]$ + water (x_{water} = 0.7992)	+3.823	+336.813	−0.957	+0.719	0.009

dx.doi.org/10.1021/jp3100377 | J. Phys. Chem. B 2012, 116, 14416−14425

As can be observed in Figure 1, the excess molar volumes are negative (with a minimum value around -2 cm^3 mol^{-1}) for all the mixtures studied in the range of temperature and pressure covered. The minimum of the excess molar volumes is found for mole fractions of water of around 0.7 for the two ionic liquids studied at all the temperatures and pressures. The variation of the excess molar volume with temperature or with pressure is represented in Figure 1 (plots a and b) for the example of $[C_1C_4Im][OAc]$. V^E becomes less negative when the temperature increases, the variation with pressure being negligible for the ionic liquids studied. Furthermore, it is observed that the excess molar volume does not vary significantly with the size of the alkyl side-chain of the cation (Figure 1, plot c).

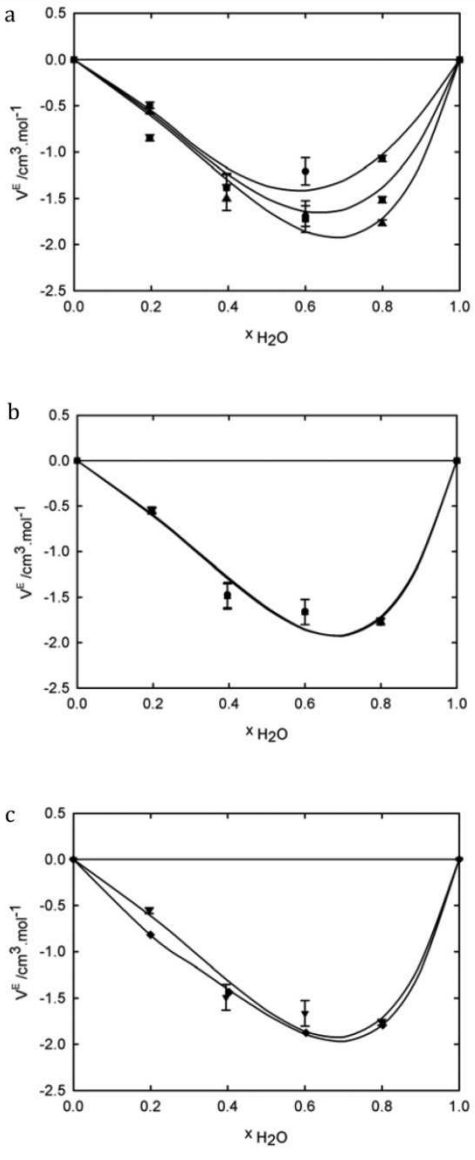

Figure 1. Excess molar volumes of the mixtures $[C_1C_4Im][OAc]$ + water. (a) At atmospheric pressure as a function of the water mole fraction and as a function of the temperature: ▲, 293.15 K; ■, 323.15 K; ●, 353.15 K. (b) At 293.15 K as a function of the water mole fraction and as a function of pressure: ●, 1 bar; ▼, 10 bar; ◆, 100 bar. (c) Water at 293.15 K and at atmospheric pressure for ▲, $[C_1C_2Im][OAc]$; ■, $[C_1C_4Im][OAc]$.

Experimental values of the viscosity of the pure ionic liquids and of the mixtures of ionic liquids + water are reported in Table S-3 in the Supporting Information. From the comparison of the viscosities of $[C_1C_2Im][OAc]$ and $[C_1C_4Im][OAc]$ it can be concluded that it diminishes when the length of the alkyl side chain decreases in the cation, as observed in other families of ionic liquids based on the imidazolium cation. It was noted that the high viscosity of ionic liquids with anion acetate significantly decreases by increasing the temperature from 293 to 363 K. The dependence of the viscosity with the temperature for the pure ionic liquids and for their mixtures with water is represented by Vogel–Fulcher–Tammann (VFT) equations of the form

$$\eta = A \times T^{1/2} \exp\left(\frac{k}{T - T_0}\right) \quad (4)$$

The parameters obtained for the fit of the viscosity data measured herein are listed in Table 3.

Table 3. Correlation Parameters of the VFT Equation (k, A, and T_0) with the Percent Average Absolute Deviation of the Fit (AAD) for the Viscosity of ILs as a Function of Temperature Determined from Measurements between 293 and 373 K

IL	k/K	$10^{-3}A$/ mPa·s·K$^{-1/2}$	T_0/K	AAD/%
$[C_1C_2Im][OAc]$	663	10.33	199	0.3
$[C_1C_2Im][OAc]$ + water (x_{water} = 0.2088)	1042	1.99	164	0.6
$[C_1C_2Im][OAc]$ + water (x_{water} = 0.4000)	890	3.96	169	0.3
$[C_1C_2Im][OAc]$ + water (x_{water} = 0.6014)	1078	1.83	148	0.3
$[C_1C_2Im][OAc]$ + water (x_{water} = 0.8023)	1279	0.57	126	0.7
$[C_1C_4Im][OAc]$	1081	2.45	185	1.2
$[C_1C_4Im][OAc]$ + water (x_{water} = 0.1843)	1128	1.95	177	0.3
$[C_1C_4Im][OAc]$ + water (x_{water} = 0.3889)	927	3.86	183	0.5
$[C_1C_4Im][OAc]$ + water (x_{water} = 0.5951)	1021	2.07	168	0.3
$[C_1C_4Im][OAc]$ + water (x_{water} = 0.8004)	751	3.08	175	0.3

The addition of water also significantly lowers the viscosity of the liquid. For example, the addition of 0.2 mol fraction of water leads to a decrease of the viscosity of more than 25% (to 77.9 mPa s) and 30% (to 262.3 mPa s) for $[C_1C_2Im][OAc]$ and $[C_1C_4Im][OAc]$ at 303 K, respectively. The viscosity also significantly lowers with temperature and the same mixtures exhibit viscosities of 20.8 mPa s and 48.7 mPa s at 333 K for $[C_1C_2Im][OAc]$ + H_2O (x_{H_2O} = 0.2) and $[C_1C_4Im][OAc]$ + H_2O (x_{H_2O} = 0.2), respectively. These facts can constitute a significant advantage for using these liquid mixtures as absorbents for carbon dioxide capture, provided that the absorption capacity is maintained.

As stressed in a previous work,[28] simple exponential representations are not sufficient to correlate the viscosity of mixtures

of ionic liquids with molecular compounds in the entire composition range and equations normally used to describe the viscosity of electrolyte solutions can not be applied to the mixtures studied here. We have used the empirical Grunberg–Nissan equation[29] to describe the viscosity of the studied mixtures, η_{mix}:

$$\ln \eta_{mix} = x_1 \ln \eta_1 + x_2 \ln \eta_2 + \ln(\eta_{mix}/\eta^{id}) \quad (5)$$

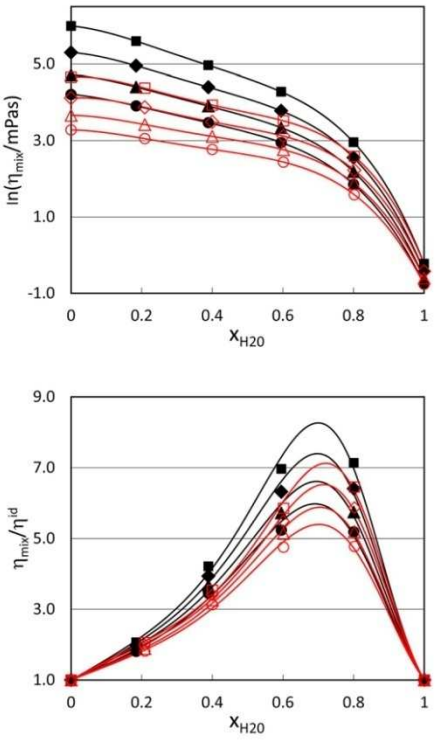

Figure 2. Logarithm of the viscosity (upper plot) and real to ideal ratio of (ionic liquid + water) mixtures (lower plot) as a function of mole fraction composition of water and at different temperatures: ■, {[C_1C_4Im][OAc] + H_2O} at 303 K; ◆, {[C_1C_4Im][OAc] + H_2O} at 313 K; ▲, {[C_1C_4Im][OAc] + H_2O} at 323 K; ●, {[C_1C_4Im][OAc] + H_2O} at 333 K; □, {[C_1C_2Im][OAc] + H_2O} at 303 K; ◇, {[C_1C_2Im][OAc] + H_2O} at 313 K; △, {[C_1C_2Im][OAc] + H_2O} at 323 K; ○, {[C_1C_2Im][OAc] + H_2O} at 333 K.

Table 4. Parameters *A*, *B*, and *C* of the Redlich–Kister-Type Fittings, Eq 6, Used To Fit the Experimental Viscosity Deviations Calculated from the Data of Table 4 along with the Standard Error of the Estimation

T/K	*A*	*B*	*C*	std dev
		[C_1C_2Im][OAc]		
303	6.0850	−5.9222	5.4257	0.03
313	5.8974	−5.6094	4.8395	0.04
323	5.7138	−5.2878	3.8018	0.03
333	5.4774	−5.0017	3.4375	0.04
		[C_1C_4Im][OAc]		
303	4.5035	−5.9547	6.9542	0.05
313	6.6192	−5.6196	4.1411	0.05
323	6.2792	−5.2901	3.7429	0.05
333	5.9831	−5.0228	3.2402	0.05

where x_i and η_i are the mole fraction and the viscosity of component *i*, respectively and (η_{mix}/η^{id}) is the ratio between the real and ideal viscosities of the mixture. This last term is calculated by a Redlich–Kister type equation:

$$\ln(\eta_{mix}/\eta^{id}) = x_1x_2[A + B(x_1 - x_2) + C(x_1 - x_2)^2] \quad (6)$$

where η^{id} is calculated here by the composition-weighted geometrical mean of the viscosities of the pure components, $\eta^{id} = \eta_1^{x_1}\eta_2^{x_1}$. The $\ln \eta_{mix}$ values and the corresponding ration (η_{mix}/η^{id}) are plotted in Figure 2 as a function of the water mole fraction at different temperatures studied for [C_1C_2Im][OAc] and [C_1C_4Im][OAc]; the parameters *A*, *B*, and *C* of eq 5 at the

Table 5. Experimental Values of CO_2 in ILs Expressed as CO_2 Mole Fraction x_2 and the Experimental Equilibrium Pressure *p*

T/K	$10^{-2}p$/Pa	x_2	*T*/K	$10^{-2}p$/Pa	x_2
[C_1C_2Im][OAc]			[C_1C_4Im][OAc]		
303.34	27.96	0.1415	303.54	96.26	0.1904
303.30	41.36	0.1485	303.54	206.49	0.2188
303.34	55.44	0.1624	303.54	99.40	0.1932
313.36	47.70	0.1383	303.53	176.61	0.2155
313.31	68.45	0.1443	313.54	265.72	0.2069
313.34	88.55	0.1570	313.53	144.58	0.1851
323.37	75.52	0.1339	313.51	231.30	0.2043
323.30	105.20	0.1387	323.58	191.61	0.1730
323.37	131.48	0.1501	323.55	329.27	0.1945
333.38	111.68	0.1283	323.50	197.16	0.1759
333.29	150.99	0.1319	333.45	255.55	0.1659
333.37	182.75	0.1421	333.51	354.35	0.1676
343.41	155.51	0.1217	343.50	309.06	0.1527
343.25	204.60	0.1241	343.57	463.78	0.1690
343.23	239.86	0.1334	343.52	255.55	0.1659
			343.15	418.30	0.1676
[C_1C_2Im][OAc] + H_2O (x_{H_2O} = 0.2059)			[C_1C_4Im][OAc] + H_2O (x_{H_2O} = 0.2045)		
303.33	17.49	0.0756	303.33	58.60	0.1205
313.34	30.68	0.0745	313.34	92.57	0.1160
323.37	50.62	0.0728	323.35	136.00	0.1104
333.35	78.74	0.0706	333.37	187.52	0.1040
			343.39	244.97	0.0971
[C_1C_2Im][OAc] + H_2O (x_{H_2O} = 0.4016)			[C_1C_4Im][OAc] + H_2O (x_{H_2O} = 0.4054)		
303.33	43.25	0.0579	303.28	45.50	0.0656
313.36	72.23	0.0559	313.29	72.23	0.0635
323.37	111.56	0.0533	323.20	112.07	0.0606
333.40	161.49	0.0501	333.0	159.95	0.0572
			342.99	216.16	0.0534
[C_1C_2Im][OAc] + H_2O (x_{H_2O} = 0.6066)			[C_1C_4Im][OAc] + H_2O (x_{H_2O} = 0.6462)		
303.34	131.75	0.0390	303.35	133.88	0.0320
313.35	189.64	0.0358	313.35	190.29	0.0294
323.40	258.14	0.0322	323.36	256.25	0.0264
333.47	331.86	0.0287	333.30	331.28	0.0233
			343.19	410.94	0.0205
			[C_1C_4Im][OAc] + H_2O (x_{H_2O} = 0.8015)		
			303.35	378.6	0.0146
			313.37	452.91	0.0129
			323.41	533.51	0.0114
			333.48	620.21	0.0101
			343.55	716.36	0.0091

dx.doi.org/10.1021/jp3100377 | J. Phys. Chem. B 2012, 116, 14416–14425

different temperatures for the two ionic liquids are listed in Table 4.

According to eq 6, used previously to correlate the viscosity of liquid mixtures containing ionic liquids,[28] the viscosity ratio (η_{mix}/η^{id}) is 1 for the pure components and mixtures with ideal viscosity. For real mixtures with a water mole fraction composition between 0.6 and 0.8, the real to ideal ratio can reach values larger than 7 for {[C_1C_4Im][OAc] + H_2O} at 303 K, the mixture that shows a larger deviation from the ideal viscosity. As seen in Figure 2, the behaviors, in terms of the viscosity, of the two ionic liquids when mixed with water are similar in the temperature range covered.

The quantities of carbon dioxide absorbed by the pure ionic liquids and by the mixtures of the ionic liquids + water are listed in Table 5 at different temperatures (from 303 to 343 K) and equilibrium pressures (varying from 2.50 to 24.0 kPa for [C_1C_2Im][OAc] and from 9.50 to 47 kPa for [C_1C_4Im]-[OAc]). The results are depicted in Figure 3 for the two ionic

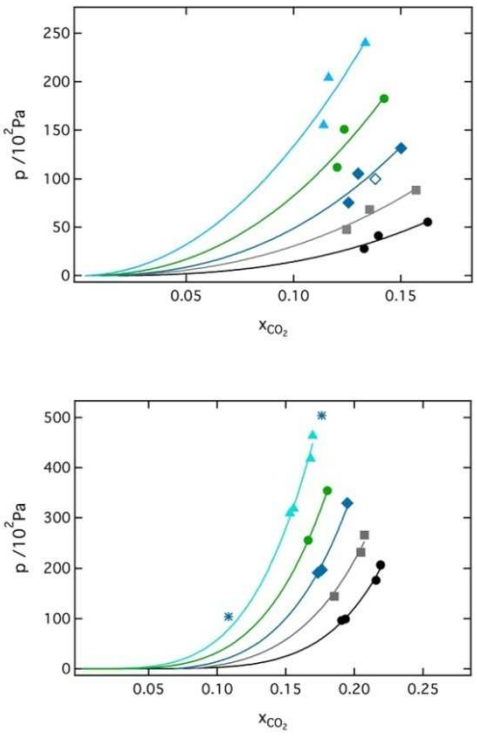

Figure 3. Absorption of carbon dioxide by [C_1C_2Im][OAc] (upper plot) and [C_1C_4Im][OAc] (bottom plot) at different temperatures. This work: ●, 303 K; ■, 313 K; ◆, 323 K; ●, 333 K; ▲, 343 K. ◇: Shiflett and Yokozeki, 2009, 323 K. *, Shiflett et al., 2008, 323 K.

liquids at the different temperatures and as a function of the pressure. It is observed that the solubility decreases when the alkyl side chain of the cation decreases and when the temperature increases. The variation of the solubility with the pressure does not obey Henry's law, as previously demonstrated by other authors, the variation of the mole fraction with pressure being compatible with the chemical absorption of the gas by the ionic liquid.

As can be seen in the upper plot of Figure 4, the addition of water to the ionic liquids causes a decrease on the absorption of

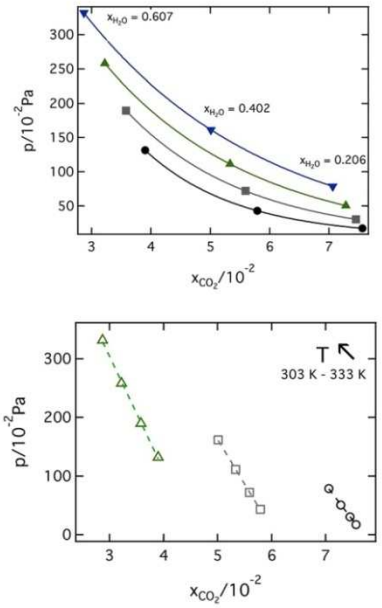

Figure 4. Absorption of carbon dioxide by mixtures of [C_1C_2Im]-[OAc] + H_2O at different compositions at different temperatures. Upper plot: representation as a function of composition for set temperatures: ●, 303 K; ■, 313 K; ▲, 323 K; ▼, 333 K. Lower plot: representation as a function of temperature for set compositions of water in the ionic liquid: △, x_{H_2O} = 0.6; □, x_{H_2O} = 0.6; ○, x_{H_2O} = 0.6.

carbon dioxide. The lower plot of Figure 4 illustrates the fact that, for each composition studied, the carbon dioxide absorption decreases with temperature. Furthermore, the variations of the solubility with the temperature seem quite similar for all the solutions of absorbent (ionic liquid + water), which means that the energetics of absorption of the gas does not significantly change with the quantity of water present in the system. Wang et al.[30] have studied the dissolution behavior of CO_2 in the ionic liquid triethylbutylammonium acetate [N_{2224}][OAc]. They found evidence of the formation of a complex between the ionic liquid and water and a conservation of the carbon dioxide absorption capacity of the liquid.

Although we did not specifically quantify the recyclability of the liquid absorbents (pure ionic liquids or mixtures of ionic liquids with water), we have used repeatedly the ionic liquid after desorption of the gas by putting the solution under primary vacuum. No difference in the absorption capacity of the ionic liquid was found even if the composition of water, for the mixtures studied, was modified by differential evaporation of the molecular liquid.

In Figure 5 are depicted the ^{1}H and ^{13}C NMR spectra of pure [C_1C_4Im][OAc] and of [C_1C_4Im][OAc] saturated with carbon dioxide, with and without addition of water. The exact chemical shifts for each system are reported in the Supporting Information. The NMR spectra show that, in the absence of water, CO_2 causes the formation of a new species, structurally very similar with the pure ionic liquid. The signals corresponding to this new species formed are marked with * and ◆ in Figure 5, upper plot b and lower plot b, respectively. The fact that all the signals corresponding to the ionic liquid remain intact (no observable change in the chemical shifts of the protons and carbons in the sample of the pure ionic liquids and in the mixture)

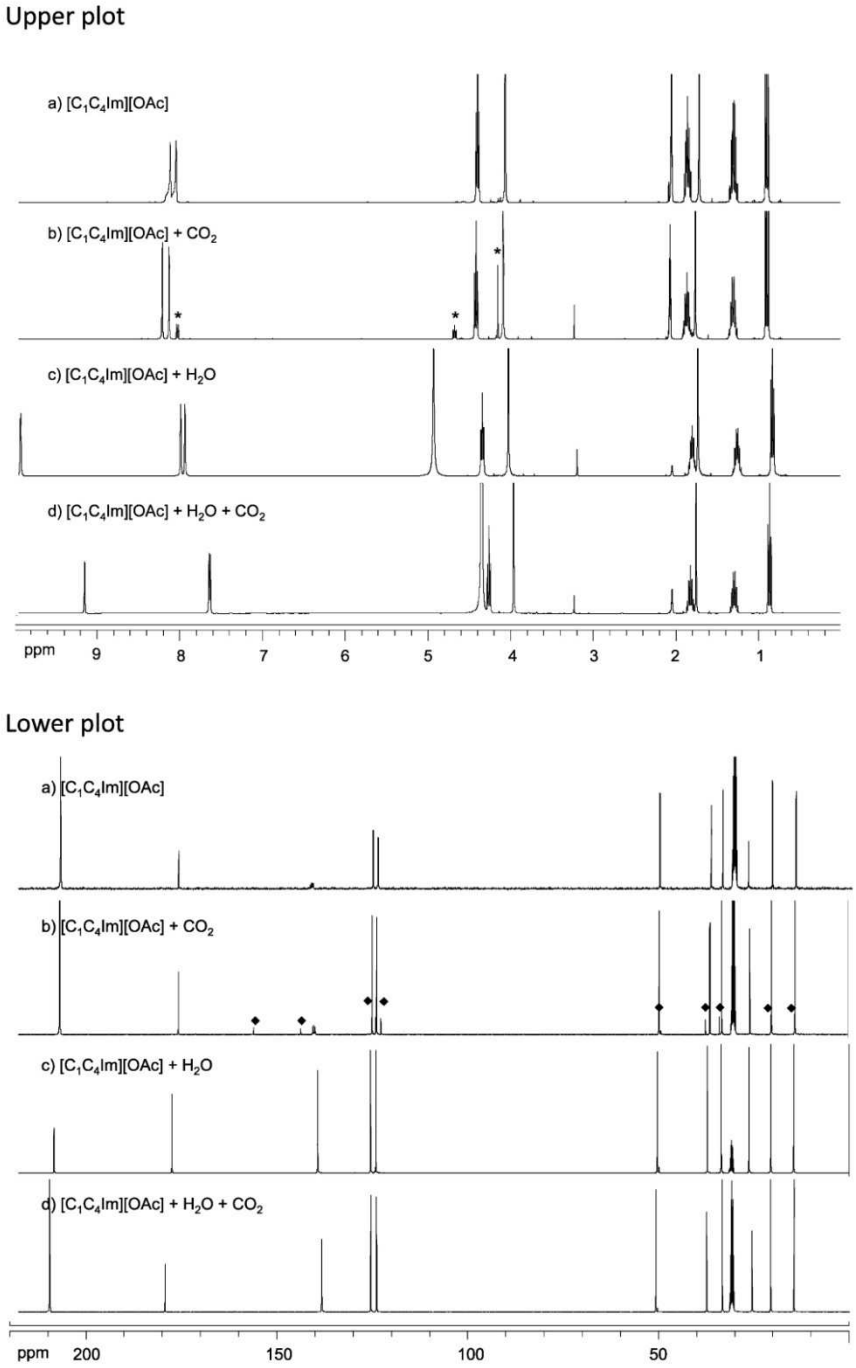

Figure 5. ^{1}H NMR spectra of various samples of 1-butyl-3-methylimidazolium acetate (upper plot) and ^{13}C NMR spectra of various samples of 1-butyl-3-methylimidazolium acetate (lower plot).

indicates that the observed high gas absorption is a consequence of the chemical reaction (or at least of the strong complexation) with the imidazolium cation, leading to the formation of a new chemical species. This species could not be clearly identified but a mechanism of formation through the abstraction of H_2 of the imidazolium cation, as suggested by Maginn,[6] cannot be excluded.

Recently, several authors[1−3] have also independently reported experimental data that lead to the conclusion that there is a chemical reaction between carbon dioxide and acetate based ionic liquids. Contrary to these conclusions, Shiflett et al.[9] had reported that their ^{1}H NMR spectra of pure $[C_1C_4Im][OAc]$ and $[C_1C_4Im][OAc] + CO_2$ are the same, within the experimental

uncertainty, leading to the conclusion that any mechanism involving chemical reaction is minor. This observation was further supported by Carvalho et al.,[7] who ascribed high CO_2 absorption only to strong interactions in the system evidenced by ^{13}C NMR. However, we proved that high CO_2 absorption in pure $[C_1C_4Im][OAc]$ is not only the consequence of strong interaction. Moreover, chemical reaction is the major pathway, because 12% molar could be ascribed to the new chemical species formed, the remaining 8% molar (the gas solubility being around 20% molar) can be attributed to the physical solubility of the gas.

In the presence of water ($[C_1C_4Im][OAc] + H_2O + CO_2$), the formation of a new ionic liquid form was not detected (Figure 5 upper plot d and lower plot d), indicating a different solubility mechanism of CO_2 in imidazolium acetate ionic liquids in the presence of water. The comparison between the two spectra, Figure 5 lower plot c and lower plot d, shows a slight downfield shift of the carbonyl carbon of the acetate anion (C═O, from 177.5 to 179.4 ppm), due to CO_2, indicating the presence of a Lewis acid/base interaction. Furthermore, a minor upfield shift is observed also for the methyl carbon of the acetate (CH_3, from 26.3 to 25.6 ppm). Also the position of C2 of the imidazolium cation is shifted slightly upfield (from 139.2 to 138.3 ppm) due to interactions of CO_2 with the cation. For comparison, to the sample of pure $[C_1C_4Im][OAc]$ was added acetic acid, which resulted in an additional signal of H(OAc) at 11.5 ppm. Because this peak is seen in none of the spectra in the upper plot of Figure 5, we have concluded that either there is no formation of AcOH or it is formed in such a lower amount that it cannot be detected by NMR. Furthermore, CO_2 is seen in none of the ^{13}C NMR spectra (possibly at about 120−130 ppm), which could be attributed to the high mobility of this molecule in solution. Here we can conclude that in the presence of water, both paths (chemical reaction involving cation and interaction of CO_2 and acetate) are disfavored, because there is competition between water and CO_2 for the same interaction site (OAc).

To get further insight on the mechanisms responsible for the difference in carbon dioxide absorption in the ionic liquid $[C_1C_4Im][OAc]$ and the effect of water on the microscopic structure of the pure ionic liquid and on the CO_2 solutions, these systems were investigated using molecular dynamic simulations. Molecular dynamics simulations were done in a condensed phase and took into account all the two-body interactions from the environment of each molecule or ion, labeled as depicted in Figure 6. The radial distribution functions presented in Figure 6 (solid lines refer to the pure ionic liquid and dotted lines to the mixture CO_2 + IL) indicate that the presence of CO_2 does not affect the structure of the ionic liquid. Carbon dioxide is solvated preferentially in the vicinity of the anion and in the nonpolar region of imidazolium ionic liquids.

The structural features of the mixture of CO_2 + IL can be perceived and confirmed in the 3-dimensional spatial distribution functions depicted in Figure 7. In Figure 7a is represented the distribution of the local density of the cationic and the anionic atomic sites around CO_2 in $[C_1C_4Im][OAc]$. As already deduced from the radial distribution functions, the spatial distribution function shows that CO_2 is mainly solvated by the anion and the terminal carbon atoms of CT_{Im}. Looking at the distribution of atomic density around acetate (Figure 7b) it is found that both carbon dioxide and the cation (position $C2_{Im}$) interact with the oxygen atoms of the anion. Figure 7c confirms these observations.

Calculations of the free energy of solvation of CO_2 in $[C_1C_4Im][OAc]$ at 373 K following a procedure described and tested elsewhere[25] give access to the Henry's law constants constants, K_H, that allow us to calculate the gas solubility at a partial pressure of gas, p_{gas} = 1 bar. The results obtained show a great disparity between the experimentally determined solubility (0.13 mol fraction solubility of carbon dioxide extrapolated to 373 K using the values in Table 5 compared with 0.002 ± 0.001 calculated here). This disparity constitutes another evidence of

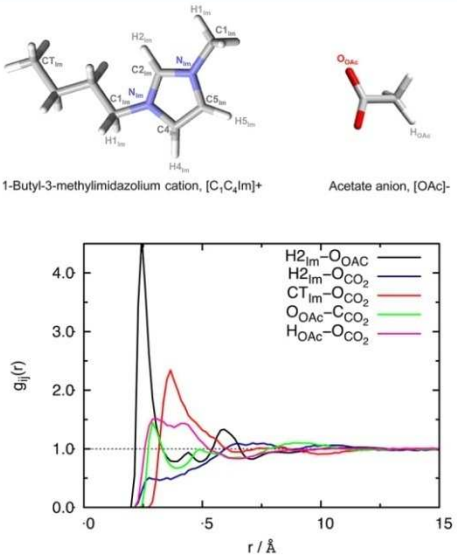

Figure 6. Preferential interaction sites between CO_2 and $[C_1C_4Im][OAc]$.

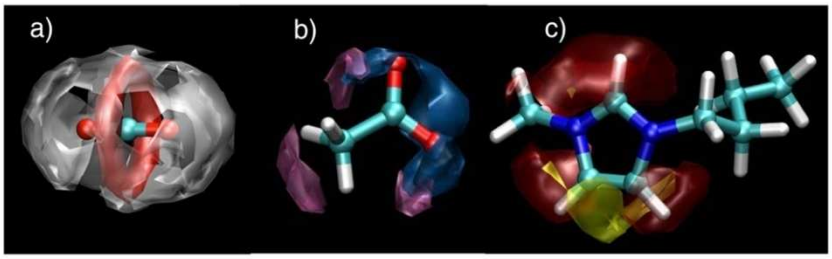

Figure 7. Spatial distribution functions between selected atomic sites in $[C_1C_4Im][OAc]$, and CO_2. (a) Iso-surface corresponding to a local density of twice the average density of the CT_{Im} (gray) and of the O_{OAc} (red), (b) Iso-surface corresponding to a local density of 3-times the average density of the $H2_{Im}$ (blue) and C_{CO_2} (purple), (c) Iso-surface around $C_1C_4Im^+$ corresponding to a local density of twice the average density of the O_{CO_2} (yellow) and of twice of the O_{OAc} (red).

the chemical nature of the absorption of carbon dioxide by the ionic liquid rich mixtures. To evaluate the physical interactions present in solution, the overall system configuration energy of the mixtures CO_2 + IL was decomposed, as represented in Figure 8. It can be observed that the presence of CO_2 increases

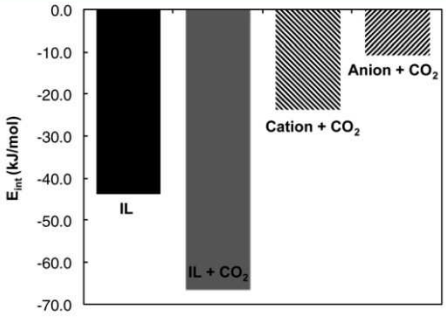

Figure 8. (a) Comparison of the cation−anion interaction energies in pure ionic liquids and in the mixtures with CO_2. The values are normalized by a number of the amount of substance of IL in moles. (b) Anion−CO_2 and cation−CO_2 interaction energies in the mixtures IL + CO_2 (normalized by the number of CO_2 molecules). Exact values are reported in Table S-4 on the Supporting Information.

the cation−anion interactions, which causes stronger ion pair association. Surprisingly, CO_2 was found to interact stronger with the cation than with the anion constituting the ionic liquid.

4. CONCLUSION

The chemical absorption of carbon dioxide by the pure ionic liquids 1-ethyl-3-methylimidazolium acetate ($[C_1C_2Im][OAc]$) and 1-butyl-3-methylimidazolium acetate ($[C_1C_4Im][OAc]$) was evidenced by the measurement of the quantities of gas absorbed from 303 to 343 K, by the NMR study of the solutions and by molecular simulation calculations.

The study of the influence of the presence of water on the capability of the ionic liquid to absorb carbon dioxide was studied herein as a function of the concentration of water and as a function of temperature. The properties of the liquid absorber significantly change particularly the viscosity that decreases by as much as 25% and 30% in the presence of 0.2 mol fraction of water for $[C_1C_2Im][OAc]$ and $[C_1C_2Im][OAc]$ at 303 K, respectively. The absorption of carbon dioxide also decreases when the water concentration increases: a decrease of 83% in CO_2 absorption is found for $[C_1C_4Im][OAc]$ with 0.6 mol fraction of water at 303 K. Because for low concentrations of water (p.e. 0.2 mol fraction) the viscosity decreases very significantly and the carbon dioxide absorption capacity only slightly, we consider that the mixtures of acetate based ionic liquids with water can be considered as promising absorbents for CO_2 capture.

By combining experimental data with molecular simulation, we have proved that the presence of water not only renders the chemical reaction between the gas and the ionic liquid less favorable but also lowers the (physical) solubility of the gas as it competes by the same solvation sites of the ionic liquid.

Only one other study of the effect of water on the carbon dioxide absorption capacity of acetate based ionic liquids was found in the literature. Wang et al.[30] have reported the reversible CO_2 absorption in triethylbutylammonium acetate and its mixtures with water. Although the presence of water affects the viscosity of the ionic liquid, it does not seem to affect the carbon dioxide absorption capacity in their case.

■ ASSOCIATED CONTENT

Supporting Information

Tables of the experimental densities (ρ) of the pure ILs and of the ILs + water between 293 and 353 K and up to 25 MPa; values of the calculated excess molar volumes V_m^E for $[C_1C_2Im]$-$[OAc]$ + water and $[C_1C_4Im][OAc]$ + water as a function of the composition, expressed in mole fraction of water, x_{water}, and as a function of temperature; experimental viscosities (η) of the pure ILs and of the mixtures (IL + water) as a function of the temperature at atmospheric pressure; calculated values of the cation−anion interaction energies for pure ionic liquids and in the mixture with CO_2 and cation−CO_2 and anion−CO_2 interactions energies; NMR chemical shifts of the different samples of ionic liquids. This material is available free of charge via the Internet at http://pubs.acs.org.

■ AUTHOR INFORMATION

Corresponding Author

*E-mail: margarida.c.gomes@univ-bpclermont.fr.

Notes

The authors declare no competing financial interest.

■ ACKNOWLEDGMENTS

S.S. Ph.D. grant was financed by the FUI project ACACIA. A.P. is financed by the *Contrat d'Objectifs Partagés*, CNRS-UBP, Région Auvergne, France. The authors thank Mrs. L. Pison for her participation in the preliminary experimental studies.

■ REFERENCES

(1) Stevanovic, S.; Podgoršek, A.; Pádua, A. A. H.; Costa Gomes, M. F. *Absorption of CO_2 by acetate ionic liquids*; 4th Congress on Ionic Liquids, COIL4, Washington DC, U.S.A., June 2011; poster

(2) Gurau, G.; Rodriguez, H.; Kelley, S. P.; Janiczek, P.; Kalb, R. S.; Rogers, R. D. *Angew. Chem., Int. Ed.* **2011**, *123*, 12230−12232.

(3) Besnard, M.; Cabaço, M. I.; Chavez, F. V.; Pinaud, N.; Sebastiao, P. J.; Coutinho, J. A. P.; Danten, Y. *Chem. Commun.* **2012**, *48*, 1245−1247.

(4) Shiflett, M. B.; Kasprzak, D. J.; Junk, C. P.; Yokozeki, A. *J. Chem. Thermodyn.* **2008**, *40*, 25−31.

(5) Shiflett, M. B.; Drew, D. W.; Cantini, R. A.; Yokozeki, A. *Energy Fuels* **2010**, *24*, 5781−5789.

(6) Maginn, E. J. Quaterly Technical Report to U.S. DOE, 2005.

(7) Carvalho, P. J.; Alvarez, V. H.; Schroder, B.; Gil, A. M.; Marrucho, I. M.; Aznar, M.; Santos, L. M. N. B. F.; Coutinho, J. A. P. *J. Phys. Chem. B* **2009**, *113*, 6803−6812.

(8) Barrosse-Antle, L. E.; Compton, R. G. *Chem Comm* **2009**, 3744−3746.

(9) Shiflett, M. B.; Yokozeki, A. *J. Chem. Eng. Data* **2009**, *54*, 108−114.

(10) Yokozeki, A.; Shiflett, M. B.; Junk, C. P.; et al. *J. Phys. Chem. B.* **2008**, *112*, 16654−16663.

(11) Shiflett, M. B.; Elliott, B. A.; Lustig, S. R.; Sabesan, S.; Kelkar, M. S.; Yokozeki, A. *ChemPhysChem* **2012**, *13*, 1806−1817.

(12) Jacquemin, J.; Husson, P.; Padua, A. A. H.; Majer, V. *Green Chem.* **2006**, *8*, 172−180.

(13) Chinn, D.; Vu, D. Q.; Driver, M. S.; Boudreau., L. C. U.S. Patent 0251558 A1, 2006.

(14) Jacquemin, J.; Husson, P.; Majer, V.; Cibulka, I. *J. Chem. Eng. Data* **2007**, *52*, 2204−2211.

(15) Jacquemin, J.; Costa Gomes, M. F.; Husson, P.; Majer, V. *J. Chem.Thermodyn* **2006**, *38*, 490−502.

(16) Jacquemin, J.; Husson, P.; Majer, V.; Costa Gomes, M. F. *Fluid Phase Equilib.* **2006**, *240*, 87−95.
(17) Costa Gomes., M. F. *J. Chem. Eng. Data* **2007**, *52*, 472−475.
(18) Hong, G.; Jacquemin, J.; Husson, P.; Costa Gomes, M. F.; Deetlefs, M.; Nieuwenhuyzen, M.; Sheppard, O.; Hardacre, C. *Ind. Eng. Chem. Res.* **2006**, *45*, 8180−8188.
(19) Husson, P.; Pison, L.; Jacquemin, J.; Costa Gomes, M. F. *Fluid Phase Equilib.* **2010**, *294*, 98−104.
(20) Smith, W. F.; Todorov, T. R. *The DL_POLY molecular simulation package*, 2.20; STFC Daresbury Laboratorys: Warrington, U.K., 2007.
(21) Jorgensen, W. L.; Maxwell, D. S.; TiradoRives, J. *J. Am. Chem. Soc.* **1996**, *118*, 11225−11236.
(22) Canongia Lopes, J. N.; Deschamps, J.; Padua, A. A. H. *J. Phys. Chem. B* **2004**, *108*, 2038−2047.
(23) Yu, Z. Y.; Jacobson, M. P.; Josovitz, J.; Rapp, C. S.; Friesner, R. A. *J. Phys. Chem. B* **2004**, *108*, 6643−6654.
(24) Mallet, J.; Molinari, M.; Martineau, F.; Delavoie, F.; Fricoteaux, P.; Troyon, M. *Nano Lett.* **2008**, *8*, 3468−3474.
(25) Almantariotis, D.; Gefflaut, T.; Padua, A. A. H.; Coxam, J. Y.; Costa Gomes, M. F. *J. Phys. Chem. B* **2010**, *114*, 3608−3617.
(26) Widom, B. J. *J. Chem. Phys.* **1963**, *39*, 2908−2911.
(27) Mezei, M. *J. Chem. Phys.* **1987**, *86* (12), 7084−7088.
(28) Canongia Lopes, J. N.; Costa Gomes, M. F.; Husson, P.; Padua, A. A. H.; Rebelo, L. P. N.; Sarraute, S.; Tariq, M. *J. Chem. Phys. B* **2011**, *115*, 6088−6099.
(29) Grunberg, L.; Nissan, A. H. *Nature (London)* **1949**, *164*, 799−801.
(30) Wang, G.; Hou, W.; Xiao, F.; Geng, J.; Wu, Y.; Zhang, Z. J. *Chem. Eng. Data* **2011**, *56*, 1125−1133.

Effect of water on the carbon dioxide absorption by 1-alkyl-3-methylimidazolium acetate ionic liquids

S. Stevanovic, A. Podgoršek, A.A.H. Pádua, M.F. Costa Gomes[1]

Institut de Chimie de Clermont-Ferrand, Equipe Thermodynamique et Interactions Moléculaires, Clermont Université, Université Blaise Pascal, BP 80026, 63171 Aubiere, France and CNRS, UMR6296 ICCF, BP 80026, 63171 Aubiere, France

SUPPORTING INFORMATION

[1] To whom correspondence should be addressed. E-mail: margarida.costa-gomes@univ-bpclermont.fr.

Table 1 Experimental densities (ρ) of the pure ILs and of the ILs + water between 293 K and 353 K and up to 25 MPa.

T / K	ρ / kg·m^{-3}	δ / %	T / K	ρ / kg·m^{-3}	δ / %
		[C_1C_2Im][OAc]			
	p = 0.10 ± 0.01 MPa			p = 0.50 ± 0.01 MPa	
293.17	1103.4	-0.017	293.15	1103.6	-0.020
303.19	1097.2	-0.008	303.19	1097.4	-0.006
313.17	1091.1	0.000	313.18	1091.2	0.003
323.18	1084.7	0.033	323.17	1084.9	0.030
333.15	1078.7	0.024	333.16	1078.9	0.024
343.14	1072.9	-0.001	343.16	1073.1	-0.003
353.16	1067.2	-0.030	353.16	1067.4	-0.029
	p = 1.00 ± 0.01 MPa			p = 2.50 ± 0.01 MPa	
293.16	1103.4	-0.020	293.15	1103.7	-0.022
303.19	1097.2	-0.006	303.18	1097.5	-0.005
313.18	1091.1	0.005	313.19	1091.3	0.006
323.16	1084.8	0.029	323.17	1085.0	0.031
333.17	1078.8	0.025	333.16	1079.1	0.023
343.16	1073.0	-0.004	343.18	1073.3	-0.002
353.17	1067.2	-0.029	353.17	1067.6	-0.030
	p = 5.00 ± 0.01 MPa			p = 10.00 ± 0.01 MPa	
293.14	1104.5	-0.023	293.17	1105.8	-0.023
303.19	1098.2	-0.005	303.20	1099.6	-0.004
313.21	1092.0	0.008	313.21	1093.5	0.006
323.18	1085.8	0.031	323.18	1087.3	0.030
333.16	1079.9	0.022	333.16	1081.4	0.023
343.19	1074.1	-0.002	343.18	1075.7	-0.002
353.17	1068.4	-0.031	353.16	1070.1	-0.031
	p = 15.00 ± 0.01 MPa			p = 20.00 ± 0.01 MPa	
293.17	1107.6	-0.023	293.16	1109.4	-0.023
303.17	1101.5	-0.007	303.17	1103.3	-0.007
313.21	1095.4	0.008	313.21	1097.2	0.009

323.19	1089.2	0.033	323.17	1091.1	0.032
333.16	1083.4	0.023	333.17	1085.3	0.023
343.19	1077.7	-0.001	343.18	1079.7	-0.001
353.17	1072.1	-0.032	353.18	1074.1	-0.033
	p = 25.00 ± 0.01 MPa				
293.17	1111.1	-0.023			
303.17	1105.1	-0.006			
313.21	1099.1	0.009			
323.18	1093.0	0.032			
333.14	1087.3	0.022			
343.17	1081.7	-0.003			
353.20	1076.1	-0.031			
293.17	1111.1	-0.023			
	$[C_1C_2Im][OAc]$ + water (x_{water}=0.2000)				
	p = 0.10 ± 0.01 MPa			p = 0.50 ± 0.01 MPa	
293.19	1106.8	-0.025	293.16	1107.0	-0.026
302.80	1100.9	-0.004	302.81	1101.1	-0.004
312.97	1094.6	0.022	312.99	1094.8	0.028
323.19	1088.7	0.016	323.18	1088.9	0.019
333.12	1082.9	0.015	333.12	1083.3	-0.001
343.13	1077.1	0.007	343.13	1077.3	0.015
353.17	1071.7	-0.030	353.15	1071.9	-0.030
	p = 1.00 ± 0.01 MPa			p = 2.50 ± 0.01 MPa	
293.16	1107.2	-0.027	293.16	1107.7	-0.028
302.80	1101.3	-0.006	302.82	1101.8	-0.005
313.00	1095.0	0.024	313.00	1095.6	0.021
323.19	1089.1	0.016	323.21	1089.6	0.019
333.13	1083.2	0.021	333.12	1083.8	0.021
343.13	1077.5	0.008	343.13	1078.1	0.011
353.17	1072.1	-0.036	353.17	1072.8	-0.040
	p = 5.00 ± 0.01 MPa			p = 10.00 ± 0.01 MPa	
293.20	1108.6	-0.026	293.21	1110.3	-0.026

302.83	1102.8	-0.011	302.83	1104.6	-0.012
313.03	1096.5	0.024	313.05	1098.3	0.025
323.23	1090.6	0.022	323.24	1092.4	0.022
333.13	1084.8	0.021	333.13	1086.7	0.021
343.15	1079.1	0.012	343.16	1081.0	0.013
353.16	1073.8	-0.042	353.15	1075.9	-0.043
	p = 15.00 ± 0.01 MPa			p = 20.00 ± 0.01 MPa	
293.20	1112.1	-0.028	293.22	1113.8	-0.024
302.84	1106.4	-0.012	302.84	1108.2	-0.013
313.05	1100.1	0.026	313.06	1101.9	0.026
323.25	1094.3	0.023	323.24	1096.2	0.019
333.13	1088.7	0.021	333.12	1090.6	0.018
343.15	1083.0	0.013	343.15	1084.9	0.012
353.16	1077.9	-0.044	353.17	1079.8	-0.039
	p = 25.00 ± 0.01 MPa				
293.21	1115.5	-0.025			
302.85	1109.9	-0.011			
313.06	1103.7	0.026			
323.24	1098.0	0.020			
333.13	1092.4	0.019			
343.15	1086.8	0.011			
353.16	1081.7	-0.039			
	$[C_1C_2Im][OAc]$ + water (x_{water}=0.4040)				
	p = 0.10 ± 0.01 MPa			p = 0.50 ± 0.01 MPa	
293.12	1109.5	-0.013	293.13	1109.6	-0.012
303.14	1103.5	-0.007	303.14	1103.6	-0.008
313.22	1097.4	0.006	313.22	1097.5	0.005
323.25	1091.3	0.019	323.24	1091.5	0.018
333.00	1085.5	0.021	332.99	1085.7	0.021
343.19	1079.8	-0.003	343.19	1079.9	-0.002
353.23	1074.0	-0.022	353.23	1074.2	-0.022
	p = 1.00 ± 0.01 MPa			p = 2.50 ± 0.01 MPa	

293.14	1109.8	-0.014	293.14	1110.3	-0.013
303.14	1103.8	-0.007	303.14	1104.4	-0.008
313.22	1097.7	0.005	313.24	1098.3	0.006
323.24	1091.7	0.017	323.24	1092.2	0.017
332.99	1085.9	0.022	333.00	1086.4	0.024
343.20	1080.1	-0.001	343.20	1080.6	-0.003
353.23	1074.4	-0.023	353.26	1074.9	-0.023
	p = 5.00 ± 0.01 MPa			p = 10.00 ± 0.01 MPa	
293.14	1111.2	-0.015	293.14	1112.9	-0.017
303.14	1105.2	-0.005	303.15	1107.0	-0.006
313.23	1099.2	0.005	313.25	1100.9	0.009
323.25	1093.1	0.018	323.25	1095.0	0.019
332.99	1087.3	0.026	332.97	1089.2	0.022
343.20	1081.6	-0.004	343.21	1083.5	-0.004
353.26	1075.9	-0.024	353.26	1077.9	-0.023
	p = 15.00 ± 0.01 MPa			p = 20.00 ± 0.01 MPa	
293.15	1114.6	-0.016	293.16	1116.2	-0.016
303.14	1108.7	-0.006	303.15	1110.4	-0.006
313.25	1102.7	0.008	313.25	1104.4	0.007
323.25	1096.7	0.019	323.26	1098.5	0.020
332.96	1091.1	0.022	332.96	1092.9	0.023
343.20	1085.4	-0.005	343.20	1087.3	-0.004
353.28	1079.8	-0.022	353.27	1081.7	-0.023
	p = 25.00 ± 0.01 MPa				
293.16	1117.9	-0.016			
303.14	1112.1	-0.006			
313.25	1106.1	0.005			
323.26	1100.2	0.021			
332.96	1094.7	0.022			
343.20	1089.1	-0.005			
353.29	1083.5	-0.022			
	$[C_1C_2Im][OAc]$ + water (x_{water}=0.6028)				

p = 0.10 ± 0.01 MPa			p = 0.50 ± 0.01 MPa		
293.14	1111.7	0.002	293.12	1111.8	0.002
303.20	1105.6	-0.004	303.21	1105.8	-0.002
313.26	1099.5	-0.004	313.17	1099.7	-0.006
323.20	1093.5	-0.009	323.20	1093.7	-0.010
332.99	1087.3	0.015	332.99	1087.4	0.017
343.20	1081.0	0.021	343.19	1081.2	0.018
353.13	1075.4	-0.021	353.16	1075.5	-0.019
p = 1.00 ± 0.01 MPa			p = 2.50 ± 0.01 MPa		
293.09	1112.1	-0.013	293.07	1113.8	-0.063
303.21	1105.9	-0.005	303.23	1106.4	0.041
313.20	1099.9	-0.002	313.21	1100.3	0.025
323.20	1093.8	0.000	323.21	1094.3	0.009
332.99	1087.6	0.033	332.98	1088.1	0.020
343.19	1081.4	0.042	343.19	1081.9	0.011
353.16	1076.4	-0.057	353.16	1076.2	-0.042
p = 5.00 ± 0.01 MPa			p = 10.00 ± 0.01 MPa		
293.16	1113.3	-0.003	293.16	1115.0	-0.006
303.23	1107.2	0.002	303.24	1108.8	0.003
313.20	1101.2	-0.006	313.19	1102.9	-0.006
323.22	1095.2	-0.006	323.24	1096.9	-0.003
332.98	1089.0	0.017	332.97	1090.8	0.017
343.19	1082.8	0.022	343.20	1084.6	0.020
353.16	1077.2	-0.025	353.17	1079.1	-0.025
p = 15.00 ± 0.01 MPa			p = 20.00 ± 0.01 MPa		
293.16	1116.5	-0.007	293.16	1118.1	-0.008
303.24	1110.4	0.003	303.24	1112.0	0.003
313.21	1104.5	-0.006	313.21	1106.2	-0.005
323.26	1098.5	0.000	323.26	1100.2	-0.002
332.97	1092.5	0.017	332.96	1094.2	0.019
343.20	1086.4	0.019	343.20	1088.2	0.017
353.18	1080.9	-0.026	353.18	1082.7	-0.025

	p = 25.00 ± 0.01 MPa	
293.17	1119.6	-0.008
303.24	1113.6	0.003
313.21	1107.8	-0.005
323.25	1101.8	-0.001
332.96	1095.9	0.021
343.20	1089.9	0.018
353.18	1084.5	-0.027

$[C_1C_2Im][OAc]$ + water (x_{water}=0.8020)

	p = 0.10 ± 0.01 MPa			p = 0.50 ± 0.01 MPa	
293.15	1103.0	0.057	293.14	1103.9	0.029
303.22	1097.2	-0.008	303.20	1097.5	0.002
313.12	1091.1	-0.044	313.12	1091.2	-0.024
323.20	1084.4	-0.036	323.24	1084.5	-0.023
333.12	1077.7	-0.017	333.13	1077.8	-0.012
343.11	1070.9	0.008	343.11	1071.0	0.003
353.20	1064.0	0.039	353.21	1064.1	0.025
	p = 1.00 ± 0.01 MPa			p = 2.50 ± 0.01 MPa	
293.15	1104.1	0.026	293.15	1104.6	0.024
303.20	1097.7	0.003	303.24	1098.1	0.004
313.14	1091.4	-0.022	313.13	1091.9	-0.023
323.24	1084.6	-0.021	323.26	1085.1	-0.020
333.13	1078.0	-0.012	333.13	1078.5	-0.011
343.11	1071.2	0.002	343.11	1071.7	0.001
353.22	1064.3	0.024	353.22	1064.8	0.023
	p = 5.00 ± 0.01 MPa			p = 10.00 ± 0.01 MPa	
293.15	1105.4	0.025	293.14	1106.8	0.024
303.23	1098.9	0.006	303.23	1100.4	0.005
313.13	1092.6	-0.023	313.14	1094.2	-0.021
323.26	1085.9	-0.022	323.26	1087.5	-0.022
333.14	1079.3	-0.012	333.12	1080.9	-0.012
343.11	1072.5	0.001	343.11	1074.2	0.002

353.23	1065.6	0.025	353.23	1067.3	0.024
	p = 15.00 ± 0.01 MPa			p = 20.00 ± 0.01 MPa	
293.15	1108.3	0.023	293.15	1109.7	0.022
303.23	1101.9	0.004	303.25	1103.3	0.007
313.15	1095.7	-0.020	313.15	1097.2	-0.020
323.26	1089.1	-0.019	323.25	1090.7	-0.020
333.12	1082.6	-0.014	333.12	1084.2	-0.013
343.12	1075.9	0.001	343.12	1077.6	0.001
353.23	1069.0	0.024	353.22	1070.8	0.024
	p = 25.00 ± 0.01 MPa				
293.14	1111.1	0.022			
303.24	1104.8	0.005			
313.14	1098.7	-0.020			
323.26	1092.2	-0.017			
333.11	1085.8	-0.013			
343.12	1079.2	-0.001			
353.23	1072.4	0.024			
		[C_1C_4Im][OAc]			
	p = 0.10 ± 0.01 MPa			p = 0.50 ± 0.01 MPa	
298.12	1054.0	-0.004	298.12	1054.2	-0.009
302.87	1051.1	0.003	302.88	1051.2	0.010
312.55	1045.4	0.004	312.57	1045.6	0.001
322.44	1039.7	-0.008	322.45	1039.8	-0.007
332.16	1033.8	0.003	332.18	1033.9	0.002
343.26	1027.1	0.011	343.26	1027.3	0.011
353.06	1021.5	-0.008	353.06	1021.7	-0.009
	p = 1.00 ± 0.01 MPa			p = 2.50 ± 0.01 MPa	
298.10	1054.5	-0.007	298.11	1055.1	-0.004
302.88	1051.5	0.007	302.89	1052.3	-0.003
312.59	1045.8	0.002	312.62	1046.4	0.008
322.45	1040.0	-0.005	322.45	1040.7	-0.002
332.19	1034.2	0.002	332.21	1034.9	-0.002

343.26	1027.5	0.013	343.26	1028.2	0.018
353.06	1021.9	-0.010	353.06	1022.7	-0.015
	p = 5.00 ± 0.01 MPa			p = 10.00 ± 0.01 MPa	
298.10	1056.2	-0.008	298.12	1058.1	-0.007
302.90	1053.3	-0.004	302.91	1055.4	-0.007
312.63	1047.5	0.009	312.64	1049.6	0.008
322.45	1041.8	0.003	322.45	1043.9	0.003
332.16	1036.1	-0.002	332.19	1038.3	0.002
343.26	1029.4	0.024	343.26	1031.7	0.027
353.03	1024.1	-0.022	353.01	1026.5	-0.026
	p = 15.00 ± 0.01 MPa			p = 20.00 ± 0.01 MPa	
298.11	1060.2	-0.008	298.09	1062.2	-0.013
302.91	1057.4	-0.008	302.93	1059.4	-0.004
312.65	1051.6	0.010	312.65	1053.7	0.010
322.45	1046.1	0.003	322.45	1048.2	0.005
332.21	1040.5	0.004	332.22	1042.6	0.006
343.26	1033.9	0.026	343.26	1036.1	0.027
353.01	1028.9	-0.028	353.00	1031.2	-0.030
	p = 25.00 ± 0.01 MPa				
298.09	1064.1	-0.014			
302.93	1061.3	-0.004			
312.65	1055.7	0.011			
322.45	1050.2	0.006			
332.22	1044.7	0.005			
343.26	1038.3	0.026			
353.00	1033.4	-0.031			
	$[C_1C_4Im][OAc]$ + water (x_{water}=0.1966)				
	p = 0.10 ± 0.01 MPa			p = 0.50 ± 0.01 MPa	
293.14	1058.9	-0.014	293.14	1059.1	-0.015
303.21	1052.9	-0.007	303.24	1053.0	-0.007
312.92	1047.0	0.008	312.95	1047.1	0.010
323.17	1040.8	0.021	323.16	1041.0	0.021

333.18	1035.0	0.011	333.18	1035.2	0.012
343.08	1029.3	0.004	343.05	1029.5	0.002
353.17	1023.6	-0.022	353.16	1023.8	-0.022
	p = 1.00 ± 0.01 MPa			p = 2.50 ± 0.01 MPa	
293.13	1059.3	-0.022	293.13	1059.9	-0.018
303.25	1053.2	-0.007	303.26	1053.8	-0.005
312.99	1047.3	0.015	312.98	1048.0	0.007
323.17	1041.2	0.034	323.18	1041.8	0.026
333.19	1035.4	0.029	333.15	1036.1	0.011
343.06	1030.5	-0.052	343.05	1030.4	0.005
353.18	1024.1	0.003	353.16	1024.8	-0.027
	p = 5.00 ± 0.01 MPa			p = 10.00 ± 0.01 MPa	
293.13	1060.9	-0.018	293.13	1062.8	-0.020
303.26	1054.9	-0.005	303.29	1056.8	-0.003
313.01	1049.0	0.008	313.00	1051.1	0.003
323.16	1043.0	0.023	323.17	1045.0	0.026
333.16	1037.2	0.015	333.18	1039.3	0.019
343.06	1031.5	0.006	343.04	1033.8	0.005
353.18	1026.0	-0.029	353.19	1028.3	-0.031
	p = 15.00 ± 0.01 MPa			p = 20.00 ± 0.01 MPa	
293.14	1064.8	-0.020	293.13	1066.7	-0.021
303.30	1058.8	-0.005	303.31	1060.7	-0.005
313.03	1053.1	0.009	313.05	1055.1	0.011
323.17	1047.1	0.027	323.17	1049.2	0.026
333.17	1041.6	0.012	333.19	1043.6	0.013
343.04	1036.0	0.007	343.05	1038.1	0.011
353.21	1030.5	-0.030	353.18	1032.8	-0.034
	p = 25.00 ± 0.01 MPa				
293.13	1068.5	-0.024			
303.35	1062.5	0.000			
313.04	1057.1	0.006			
323.18	1051.2	0.027			

333.18	1045.7	0.011
343.05	1040.2	0.015
353.18	1035.0	-0.036

$[C_1C_4Im][OAc]$ + water (x_{water}=0.3958)

p = 0.10 ± 0.01 MPa			p = 0.10 ± 0.01 MPa		
293.16	293.16	293.16	293.16	293.16	293.16
302.84	302.84	302.84	302.84	302.84	302.84
312.57	312.57	312.57	312.57	312.57	312.57
323.07	323.07	323.07	323.07	323.07	323.07
333.12	333.12	333.12	333.12	333.12	333.12
343.09	343.09	343.09	343.09	343.09	343.09
352.96	352.96	352.96	352.96	352.96	352.96
p = 1.01 ± 0.01 MPa			p = 1.01 ± 0.01 MPa		
293.16	293.16	293.16	293.16	293.16	293.16
302.84	302.84	302.84	302.84	302.84	302.84
312.56	312.56	312.56	312.56	312.56	312.56
323.08	323.08	323.08	323.08	323.08	323.08
333.13	333.13	333.13	333.13	333.13	333.13
343.08	343.08	343.08	343.08	343.08	343.08
352.96	352.96	352.96	352.96	352.96	352.96
p = 5.00 ± 0.01 MPa			p = 5.00 ± 0.01 MPa		
293.15	293.15	293.15	293.15	293.15	293.15
302.83	302.83	302.83	302.83	302.83	302.83
312.54	312.54	312.54	312.54	312.54	312.54
323.10	323.10	323.10	323.10	323.10	323.10
333.10	333.10	333.10	333.10	333.10	333.10
343.28	343.28	343.28	343.28	343.28	343.28
352.97	352.97	352.97	352.97	352.97	352.97
p = 15.00 ± 0.01 MPa			p = 15.00 ± 0.01 MPa		
293.15	293.15	293.15	293.15	293.15	293.15
302.77	302.77	302.77	302.77	302.77	302.77
312.59	312.59	312.59	312.59	312.59	312.59

323.10	323.10	323.10	323.10	323.10	323.10
333.09	333.09	333.09	333.09	333.09	333.09
343.11	343.11	343.11	343.11	343.11	343.11
352.96	352.96	352.96	352.96	352.96	352.96
	p = 25.00 ± 0.01 MPa			p = 25.00 ± 0.01 MPa	
293.16	293.16	293.16	293.16	293.16	293.16
302.81	302.81	302.81	302.81	302.81	302.81
312.62	312.62	312.62	312.62	312.62	312.62
323.10	323.10	323.10	323.10	323.10	323.10
333.11	333.11	333.11	333.11	333.11	333.11
343.09	343.09	343.09	343.09	343.09	343.09
352.96	352.96	352.96	352.96	352.96	352.96
	$[C_1C_4Im][OAc]$ + water (x_{water}=0.6002)				
	p = 0.10 ± 0.01 MPa			p = 0.50 ± 0.01 MPa	
293.22	1066.6	-0.008	293.21	1066.7	-0.018
302.84	1060.5	0.000	302.84	1060.6	-0.003
312.57	1054.4	0.004	312.58	1054.3	0.020
323.07	1047.7	0.014	323.08	1047.8	0.014
333.12	1041.6	-0.001	333.13	1041.7	0.004
343.09	1035.5	-0.011	343.08	1035.7	-0.006
353.06	1029.2	0.001	352.96	1029.6	-0.011
	p = 1.00 ± 0.01 MPa			p = 2.50 ± 0.01 MPa	
293.21	1066.9	-0.008	293.22	1067.5	-0.019
302.84	1060.8	0.006	302.84	1061.3	-0.004
312.56	1054.5	0.031	312.53	1055.1	0.020
323.08	1048.8	-0.047	323.11	1048.6	0.018
333.13	1042.0	0.014	333.11	1042.5	0.006
343.08	1035.9	0.004	343.08	1036.5	-0.007
352.96	1029.8	-0.001	352.96	1030.4	-0.013
	p = 5.00 ± 0.01 MPa			p = 10.00 ± 0.01 MPa	
293.21	1068.4	-0.020	293.22	1070.2	-0.018
302.83	1062.3	-0.005	302.83	1064.1	-0.003

312.54	1056.0	0.023	312.55	1058.0	0.012
323.10	1049.6	0.013	323.11	1051.6	0.015
333.10	1043.5	0.010	333.08	1045.4	0.024
343.08	1037.6	-0.010	343.10	1039.7	-0.015
352.97	1031.5	-0.012	352.98	1033.6	-0.015
	p = 15.00 ± 0.01 MPa			p = 20.00 ± 0.01 MPa	
293.23	1071.9	-0.013	293.23	1073.7	-0.016
302.77	1066.0	-0.006	302.80	1067.8	-0.003
312.59	1059.9	0.011	312.59	1061.8	0.009
323.10	1053.5	0.012	323.11	1055.4	0.016
333.09	1047.4	0.021	333.11	1049.4	0.020
343.11	1041.7	-0.012	343.10	1043.7	-0.011
352.96	1035.7	-0.012	352.96	1037.8	-0.015
	p = 25.00 ± 0.01 MPa				
293.23	1075.4	-0.018			
302.81	1069.5	-0.002			
312.62	1063.6	0.010			
323.10	1057.3	0.016			
333.11	1051.3	0.018			
343.09	1045.7	-0.010			
352.96	1039.9	-0.015			
	$[C_1C_4Im][OAc]$ + water (x_{water}=0.7992)				
	p = 0.10 ± 0.01 MPa			p = 0.50 ± 0.01 MPa	
293.16	1068.7	0.004	293.17	1068.8	0.006
302.88	1062.1	0.008	302.87	1062.2	0.007
312.54	1055.7	-0.007	312.54	1055.8	-0.007
323.02	1048.7	-0.013	323.02	1048.8	-0.015
333.03	1041.8	-0.002	333.00	1041.9	-0.003
343.05	1034.9	0.005	343.06	1035.0	0.007
352.85	1028.3	0.005	352.84	1028.4	0.004
	p = 1.00 ± 0.01 MPa			p = 2.50 ± 0.01 MPa	
293.17	1068.9	0.006	293.16	1069.5	0.004

302.87	1062.4	0.007	302.87	1062.9	0.008
312.54	1056.0	-0.007	312.51	1056.5	-0.007
323.02	1049.0	-0.016	323.09	1049.5	-0.014
333.00	1042.1	-0.002	333.00	1042.7	-0.003
343.05	1035.3	0.006	342.99	1035.8	0.007
352.84	1028.7	0.005	352.83	1029.2	0.004
	p = 5.00 ± 0.01 MPa			p = 10.00 ± 0.01 MPa	
293.14	1070.4	0.057	293.17	1072.0	0.012
302.85	1063.8	0.055	302.84	1065.5	0.022
312.52	1059.7	-0.182	312.55	1059.2	0.015
323.08	1050.4	0.018	323.02	1052.2	0.022
332.98	1043.7	0.020	333.02	1047.8	-0.183
342.99	1036.9	0.021	343.05	1038.8	0.052
352.82	1030.3	0.011	352.87	1032.2	0.060
	p = 15.00 ± 0.01 MPa			p = 20.00 ± 0.01 MPa	
293.17	1073.6	-0.071	293.17	1075.2	0.001
302.88	1064.9	0.153	302.89	1068.8	0.009
312.56	1060.9	-0.053	312.57	1062.7	-0.010
323.02	1054.0	-0.034	323.02	1055.7	-0.002
333.03	1047.3	-0.015	333.02	1049.2	-0.001
343.04	1040.7	0.003	343.05	1042.6	0.001
352.85	1034.2	0.017	352.87	1036.1	0.003
	p = 25.00 ± 0.01 MPa				
293.17	1076.8	-0.001			
302.87	1070.4	0.006			
312.58	1064.3	-0.005			
323.02	1057.4	0.000			
333.02	1051.0	-0.002			
343.05	1044.4	0.000			
352.88	1038.0	0.002			
293.17	1076.8	-0.001			

Table S-2. Excess molar volumes V_m^E for $[C_1C_2Im][OAc]$ + water and $[C_1C_4Im][OAc]$ + water as a function of the composition, expressed in mole fraction of water, x_{water} and as a function of temperature.

x_{water}	V_m^E ($cm^3\ mol^{-1}$)	x_{water}	V_m^E ($cm^3\ mol^{-1}$)	x_{water}	V_m^E ($cm^3\ mol^{-1}$)
$[C_1C_2Im][OAc]$ + water					
T = 293.15 K		T = 303.15 K		T = 313.15 K	
0.0000	0.000	0.0000	0.000	0.0000	0.000
0.2000	-0.817	0.2000	-0.827	0.2000	-0.836
0.4040	-1.434	0.4040	-1.417	0.4040	-1.400
0.6028	-1.874	0.6028	-1.824	0.6028	-1.774
0.8020	-1.792	0.8020	-1.701	0.8020	-1.608
1.0000	0.000	1.0000	0.000	1.0000	0.000
T = 323.15 K		T = 333.15 K		T = 343.15 K	
0.0000	0.000	0.0000	0.000	0.0000	0.000
0.2000	-0.846	0.2000	-0.857	0.2000	-0.868
0.4040	-1.383	0.4040	-1.366	0.4040	-1.349
0.6028	-1.723	0.6028	-1.671	0.6028	-1.619
0.8020	-1.514	0.8020	-1.419	0.8020	-1.323
1.0000	0.000	1.0000	0.000	1.0000	0.000
T = 353.15 K					
0.0000	0.000				
0.2000	-0.879				
0.4040	-1.333				
0.6028	-1.566				
0.8020	-1.225				
1.0000	0.000				
$[C_1C_4Im][OAc]$ + water					
T = 293.15 K		T = 303.15 K		T = 313.15 K	
0.0000	0.000	0.0000	0.000	0.0000	0.000
0.1966	-0.556	0.1966	-0.515	0.1966	-0.546
0.3958	-1.490	0.3958	-1.415	0.3958	-1.472

0.6002	-1.664	0.6002	-1.364	0.6002	-1.590
0.7992	-1.763	0.7992	-1.309	0.7992	-1.651
T = 323.15 K		T = 333.15 K		T = 343.15 K	
0.0000	0.000	0.0000	0.000	0.0000	0.000
0.1966	-0.505	0.1966	-0.536	0.1966	-0.494
0.3958	-1.396	0.3958	-1.453	0.3958	-1.377
0.6002	-1.286	0.6002	-1.516	0.6002	-1.207
0.7992	-1.191	0.7992	-1.539	0.7992	-1.071
T = 353.15 K					
0.0000	0.000				
0.1966	-0.525				
0.3958	-1.434				
0.6002	-1.441				
0.7992	-1.425				

Table S-3. Experimental viscosities (η) of the pure ILs and of the mixtures (IL + water) as a function of the temperature at atmospheric pressure

T / K	η^{exp} / mPa·s	δ / %	T / K	η^{exp} / mPa·s	δ / %
	$[C_1C_2Im][OAc]$			**$[C_1C_4Im][OAc]$**	
293.15	203.0	0.0	298.15	594.8	-0.1
303.15	104.8	0.1	303.15	399.6	0.3
313.15	61.13	-0.1	313.15	200.1	0.0
323.15	38.91	-0.2	323.15	111.7	-1.0
333.15	26.56	-0.3	333.15	67.25	-1.4
343.15	19.01	0.3	343.15	41.64	2.0
353.15	14.24	0.8	353.15	27.86	3.1
			363.15	19.87	2.3
			373.15	14.82	0.9
$[C_1C_2Im][OAc]$ + water (x_{water}=0.2088)			**$[C_1C_4Im][OAc]$ + water (x_{water}=0.1843)**		
293.15	138.9	0.0	293.15	558.7	0.0
303.15	77.91	-0.2	303.15	262.3	0.1
313.15	47.22	-0.1	313.15	138.2	-0.1
323.15	30.12	1.2	323.15	79.67	-0.3
333.15	20.80	-0.1	333.15	48.65	1.0
343.15	15.07	-1.7	343.15	32.37	-0.4
			353.15	22.25	-0.1
			363.15	15.93	0.2
			373.15	11.94	-0.5
$[C_1C_2Im][OAc]$ + water (x_{water}=0.4000)			**$[C_1C_4Im][OAc]$ + water (x_{water}=0.3889)**		
293.15	88.60	0.0	293.15	298.10	0.0
303.15	52.66	0.2	303.15	150.05	0.3
313.15	33.89	-0.2	313.15	84.98	-0.5
323.15	23.04	-0.1	323.15	51.83	-0.3
333.15	16.47	-0.3	333.15	33.58	0.5
343.15	12.24	-0.2	343.15	23.31	0.0
353.15	9.270	1.2	353.15	16.58	1.5

$[C_1C_2Im][OAc]$ + water (x_{water}=0.6014)			$[C_1C_4Im][OAc]$ + water (x_{water}=0.5951)		
293.15	51.81	0.0	293.15	124.3	0.0
303.15	32.63	0.2	303.15	68.85	0.3
313.15	21.88	-0.1	313.15	41.90	-0.5
323.15	15.40	-0.6	323.15	26.97	-0.3
333.15	11.09	0.6	333.15	18.26	0.3
343.15	8.394	0.2	343.15	13.00	0.5
			353.15	9.640	0.3
			363.15	7.370	0.2
$[C_1C_2Im][OAc]$ + water (x_{water}=0.8023)			$[C_1C_4Im][OAc]$ + water (x_{water}=0.8004)		
293.15	20.45	0.0	293.15	32.14	0.0
303.15	13.51	0.0	303.15	19.69	0.2
313.15	9.407	-0.8	313.15	13.12	-0.6
323.15	6.602	1.5	323.15	9.087	0.5
333.15	4.948	0.5			
343.15	3.801	-0.1			
353.15	3.021	-1.6			

Table S-4. Cation-anion interaction energy for pure ionic liquids and in the mixture with CO_2 and cation-CO_2 and anion-CO_2 interactions energies. Values are in kJ/mol and are normalized by a number of the amount of substance of IL in moles or by number of CO_2 molecules.

Ionic liquid	Cation−Anion	Cation−Anion (CO_2)	Cation−CO_2	Anion-CO_2
$[C_1C_4Im][OAc]$	-0.54±0.2	-0.33±0.1	-0.118±0.007	-0.053±0.009
$[C_1C_4Im][TFA]$	-0.50±0.2	-0.327±0.09	-0.116±0.007	-0.053±0.009
$[C_1C_4Pyrro][OAc]$	-0.36±0.2	-0.239±0.08	-0.116±0.007	-0.051±0.009

NMR chemical shifts of different samples of ionic liquids

1-butyl-3-methylimidazolium acetate, [C_1C_4Im][OAc]

^{1}H NMR (acetone-d_6, ppm): δ 0.90 (t, *J* = 7.4 Hz, 3H), 1.30 (sext, *J* = 7.6 Hz, 2H), 1.72 (s, 3H), 1.86 (pent, *J* = 7.4 Hz, 2H), 4.06 (s, 3H), 4.39 (t, *J* = 7.2 Hz, 2H), 8.04 (d, *J* = 1.8 Hz, 1H), 8.11 (d, *J* = 1.8 Hz, 1H). ^{13}C NMR (acetone-d_6, ppm): δ 14.7, 21.0, 27.2, 33.9, 37.0, 50.3, 124.2, 125.4, 141.5, 176.3.

1-butyl-3-methylimidazolium acetate saturated with carbon dioxide, [C_1C_4Im][OAc] + CO_2

^{1}H NMR (acetone-d_6, ppm): δ 0.89 (t, *J* = 7.4 Hz), 1.29 (sext, *J* = 7.6 Hz), 1.75 (s), 1.85 (*J* = 7.4 Hz, pent), 4.06 (s), **4.13 (s)**, 4.40 (t, *J* = 7.2 Hz), **4.65 (t, *J* = 7.3 Hz)**, **7.99 (d, *J* = 1.9 Hz)**, **8.01 (d, *J* = 1.9 Hz)**, 8.10 (d, *J* = 1.8 Hz, 1H), 8.19 (d, *J* = 1.80 Hz, 1H), **10.2 (s)**. ^{13}C NMR (acetone-d_6, ppm): δ 14.7, **14.2**, 20.9, **21.1**, 26.5, 33.9, **34.6**, 37.0, **38.2**, 50.3, **50.5**, **123.2**, 124.3, **124.6**, 125.5, 140.8, **144.4**, **156.6**, 176.3.

1-butyl-3-methylimidazolium acetate in the presence of water, [C_1C_4Im][OAc] + H_2O

^{1}H NMR (acetone-d_6, ppm): δ 0.83 (t, *J* = 7.4 Hz, 3H), 1.26 (sext, *J* = 7.6 Hz, 2H), 1.73 (s, 3H), 1.81 (pent, *J* = 7.4 Hz, 2H), 4.03 (s, 3H), 4.35 (t, *J* = 7.2 Hz, 2H), *4.94 (s, H(H_2O))*, 7.96 (d, *J* = 1.8 Hz, 1H), 8.01 (d, *J* = 1.8 Hz, 1H), 9.95 (s, 1H). ^{13}C NMR (acetone-d_6, ppm): δ 14.5, 20.6, 26.3, 33.5, 37.2, 50.3, 124.1, 125.4, 139.2, 177.5.

1-butyl-3-methylimidazolium acetate in the presence of water and saturated with carbon dioxide, [C_1C_4Im][OAc] + H_2O + CO_2

^{1}H NMR (acetone-d_6, ppm): δ 0.87 (t, *J* = 7.4 Hz, 3H), 1.30 (sext, *J* = 7.6 Hz, 2H), 1.76 (s, 3H), 1.83 (pent, *J* = 7.4 Hz, 2H), 3.97 (s, 3H), 4.27 (t, *J* = 7.2 Hz, 2H), 4.36 *(s, H(H_2O)),* 7.65 (d, *J* = 1.8 Hz, 1H), 7.67 (d, *J* = 1.8 Hz, 1H), 9.17 (s, 1H). ^{13}C NMR (acetone-d_6, ppm): δ 14.6, 20.7, 25.6, 33.4, 37.5, 50.7, 123.9, 125.5, 138.3, 179.4.

Absorption of carbon dioxide by ionic liquids with carboxylate anions

S. Stevanovic[1], A. Podgorsek[1], L. Moura[1,2], C.C. Santini[2], A.A.H. Padua[1], M.F. Costa Gomes[1*]

[1]*Institut de Chimie de Clermont-Ferrand, Equipe Thermodynamique et Interactions Moléculaires, Clermont Université, Université Blaise Pascal, BP 80026, 63171 Aubière, France and CNRS, UMR6296 ICCF, BP 80026, 63171 Aubière, France*

[2]*Université de Lyon, Institut de Chimie de Lyon, UMR 5265 CNRS-Université de Lyon 1-ESCPE Lyon, C2P2, Equipe Chimie Organométallique de Surface, ESCPE 43 Boulevard du 11 Novembre 1918, 69616 Villeurbanne, France*

Abstract

Experimental values of the absorption of carbon dioxide in two ionic liquids with carboxylate anions – the 1-butyl-3-methylimidazolium levulinate $[C_1C_4Im][LEV]$ and the 1-butyl-1-methylpyrrolidinium acetate $[C_1C_4Pyrro][OAc]$ – are reported as a function of temperature and at pressures close to atmospheric. Mole fraction absorption of carbon dioxide in $[C_1C_4Im][LEV]$ and $[C_1C_4Pyrro][OAc]$ are equal to 0.93×10^{-2} and 1.10×10^{-2} at 303.15 and 89.2 KPa and 353.15 K and 67.1 KPa, respectively. The effect of the presence of controlled amounts of water on the absorption of carbon dioxide was measured for $[C_1C_4Pyrro][OAc]$. The presence of a 0.35 mole fraction of water in $[C_1C_4Pyrro][OAc]$ decreases the viscosity of the ionic liquid phase and dramatically increases the amount of carbon dioxide absorbed, pointing towards a chemical reaction between the gas and the liquid absorbent. Increasing the amounts of water lowers the viscosity further but also the absorption capacity of the ionic liquid. Molecular dynamics simulations were used to interpret the molecular mechanism of solvation of carbon dioxide in $[C_1C_4Pyrro][OAc]$. Results show that carbon dioxide is solvated preferentially in the non-polar domain of the solvent, and that the CO_2−anion interactions dominate over the CO_2−cation interactions. Molecular simulations could reproduce the experimental solubility of CO_2 in $[C_1C_4Im][TFA]$ (known to be a physical process), but not in $[C_1C_4Pyrro][OAc]$ and reinforcing the conclusion that the higher solubility of carbon dioxide in the acetate based ionic liquid can be ascribed to a chemical reaction.

* Corresponding author : margarida.c.gomes@univ-bpclermont.fr

Introduction

Ionic liquids are considered as promising media for gas separations[1] as they are able to selectively and efficiently absorb one gas in a mixture. In particular, they have been indicated as possible alternatives for carbon dioxide removal from flue-gas streams[2] by chemical[3] or physical absorption[4]. Several properties are significant for the evaluation of ionic liquids as liquid absorbers for gaseous solutes – the absorption capacity, the selectivity and the mass transfer – as they will determine the design and cost of possible industrial processes[5].

We are interested in exploring the use of ionic liquids having carboxylate anions for the absorption of carbon dioxide, as they seem to be capable of chemically coordinating this gas hence showing a high absorption capacity[6,7]. This chemical reaction, evidenced by several authors for acetate based ionic liquids[8,9,10], seems to be reversible and so it is possible to recycle the absorbent at a relatively low energy cost. Nevertheless, ionic liquids based on the acetate anions and on the imidazolium cations have shown some drawbacks linked to the possibility of proton transfer between the anion and the cation (due to the acidity of the hydrogen in the position C_2 of the imidazolium ring). Although the equilibrium constant of this reaction seems relatively unimportant, submitting the ionic liquid to repeated pressure cycles displaces the equilibrium in the sense of the formation of acetic acid, a volatile product. This means that these ionic liquids can, to some extent, be considered as protic ionic liquids[11] and so they are in reality a liquid mixture of different molecular compounds and ions, the composition of the mixture depending on the conditions at which it has been kept.

In this work, we have studied the absorption of carbon dioxide by two ionic liquids having carboxylate anions. Firstly, we have considered the 1-butyl-1-methylpyrrolidinium acetate [C_1C_4Pyrro][OAc], an ionic liquid based on the acetate anion but having no acidic proton in the cation. Due to its low fluidity we have studied the absorption capacity of the mixtures of this ionic liquid with water. Secondly, we have studied an ionic liquid with a heavier carboxylic anion, the 1-butyl-3-methylimidazolium levulinate [C_1C_4Im][LEV], in order to check if the absorption mechanism was the same as in the case of the acetate-

based imidazolium ionic liquids. We predict a considerable advantage on the use of this ionic liquid linked to the fact that, if the cation-anion proton transfer occurs, a molecular species of low volatility is formed (as levulinic acid is much less volatile than acetic acid).

In order to contribute to the understanding of the mechanisms of solvation of carbon dioxide in this family of ionic liquids, the absorption of carbon dioxide in [C_1C_4Pyrro][OAc] was compared with the solvation of CO_2 by 1-butyl-3-methylimidazolium trifluoroacetate [C_1C_4Im][TFA]. In this last ionic liquid, the absorption of carbon dioxide is purely physical and so linked to the gas-liquid molecular interactions and to the molecular structure of the solution.

Absorption of carbon dioxide by [C_1C_4Im][LEV] was first studied by Yokozeki et al.[12] and the value of absorption was found to be equal to 0.245 at 298.1 K and at 100.2 KPa, when expressed in mole fraction of gas. Absorption of gas in [C_1C_4Pyrro][OAc] was not yet reported but a cation-anion proton transfer has been suggested (transfer of a proton from the butyl chain of the cation to the anion) with the release of acetic acid, methyl pyrrolidine and butane[13]. It seems then that the low acidity of the protons in the alkyl side-chain in the pyrrolidinium cation is sufficient to cause a cation-anion proton transfer.

Values of absorption of carbon dioxide in [C_1C_4Im][TFA] are available in the literature and were found to be significantly lower than in ionic liquids based on the acetate anion and an imidazolium cation[14,15,16]. Many explanations have been advanced to explain this difference in solubility mainly based on the stronger CO_2 – OAc^- interaction than CO_2 –TFA^- which can be attributed to the lower electron density, and therefore lower donor ability, of the trifluoroacetate anion when compared with the acetate anion. The exact mechanism of carbon dioxide absorption by these ionic liquids is, nevertheless, still not well understood.

We investigate the absorption of carbon dioxide and its solubility in the [C_1C_4Pyrro][OAc] and the [C_1C_4Im][TFA] by molecular dynamic simulations. The comparison of the systems ionic liquid + carbon dioxide (ionic liquid = [C_1C_4Im][TFA] and [C_1C_4Pyrro][OAc]) is expected to enabled the access to the molecular mechanism of the carbon dioxide absorption in these ionic

liquids. ^{1}H and ^{13}C NMR spectroscopy provided further evidence for solvation mechanism.

Materials

The $[C_1C_4Pyrro][OAc]$ was purchased from Solvionic with mole fraction purities of 0.995. The $[C_1C_4Im][LEV]$ samples were synthesized at the laboratory of Chemistry, Catalysis, Polymers and Processes of Lyon.

During the synthesis of 1-butyl-3-methylimidazolium levulinate, $[C_1C_4Im][LEV]$, all the operations were performed in absence of oxygen and of water and under a purified argon atmosphere using glove box (Jacomex or MBraun) or vacuum-line techniques. 1-Methylimidazole (> 99 %, Aldrich) was distilled prior to use. Chlorobutane (> 99 %, Aldrich) was used without further purification. Sodium levulinate was previously synthesized at the laboratory LMOPS, Lyon, France and was used without further purification.

For the synthesis of the 1-butyl-3-methylimidazolium chloride, $[C_1C_4Im][Cl]$, the first operation consisted on the slowly addition of 1-chlorobutane (106 mL, 1.01 mol) to 1-methylimidazole (50 mL, 0.63 mol) under strong stirring. The mixture was left stirring for 2 days at 343.15 K. The hot solution was then transferred drop wise via a cannula into dry toluene (200 mL) at 273.15 K under vigorous mechanical stirring. The white precipitate formed was then filtered and washed repeatedly with dry toluene (3 × 200 mL) and dried overnight under vacuum giving a white solid (95.6 g, 0.55 mol, 87%)[17].

To obtain the final product, 1-butyl-3-methylimidazolium levulinate, $[C_1C_4Im][LEV]$, sodium levulinate (32.9 g, 0.24 mol) was dissolved in water (60 mL). 1-butyl-3-methylimidazolium chloride, $[C_1C_4Im][Cl]$ (34.4 g, 0.20 mol), was dissolved in dichloromethane (170 mL). The aqueous phase was added drop wise to the organic phase under strong stirring, at 303.15 K. The mixture was left stirring during 60-70h at 303.15 K. After separating the two phases and drying the aqueous one, a dark viscous fluid was obtained (4.2 g, 0.08 mol, 41%).

The water contents of the degassed sample were determined, with a precision of ± 5 ppm, using a coulometric Karl Fisher titrator (Mettler Toledo DL31). The ionic liquids were kept under vacuum for 72 h at 303 K before each

measurement. The water content of the degassed samples was found to be 365 ppm for $[C_1C_4Im][LEV]$.

The temperature of decomposition of the ionic liquids used herein (represented in Figure 1) was determined using a modulated DSC 2920 from TA Instruments and was found to be 448 K for $[C_1C_4Im][LEV]$ and 518 K for $[C_1C_4Pyrro][OAc]$, respectively. The temperature of fusion for $[C_1C_4Pyrro][OAc]$, an ionic liquid which is solid at room temperature, was found to be 353 K.

Mixtures of $[C_1C_4Pyrro][OAc]$ and water of different compositions were prepared gravimetrically. The $[C_1C_4Pyrro][OAc]$ was first introduced in a glass vial and then the appropriate amount of water was added and the glass vial was sealed. The vial was completely filled with the liquid mixture in order to minimize the volume of the vapor phase in equilibrium with the liquid solution and so reduce the error in composition due to differential evaporation. The uncertainty of the mole fraction is estimated at ± 0.0001. The molar fraction of water in the prepared mixtures was 0.35 to 0.85.

The gases used for this study were used as received from the manufacturer. Carbon dioxide was obtained from AGA/Linde Gas with mole fraction purity of 0.99995.

Density measurements

Densities were measured using a U-shape vibrating-tube densimeter (Anton Paar, model DMA 512) operating in a static mode, following the procedure described in previous publications[18,19]. Measurements for $[C_1C_4Im][LEV]$ and $[C_1C_4Pyrro][OAc]$ + water were performed for pressures up to 25 MPa and at temperatures from 293 to 343 K.

The temperature in the densimeter was maintained constant to within ±0.01K by means of a recirculating bath equipped with a PID temperature controller (Julabo FP40-HP). For measuring the temperature, a 100 Ohm platinum resistance thermometer (precision of ±0.02 K and accuracy of ±0.04 K) was used. Its calibration was performed by verifying a water triple point (triple point cell by Hart Scientific) and by comparison against a 100 Ohm platinum resistance Hart Scientific model 1502A.

The measured period of vibration (τ) of a U tube is related to the density (ρ) according to: $\rho = A\tau^2 + B$ where A and B are parameters that are function of temperature and pressure determined by calibration between temperatures of 293 and 343 K (and pressures of 0.1 and 25 MPa), using as calibration fluids n-heptane, bromobenzene and 2,4-dichlorotoluene following the recommendations by Schilling *et al.*[20]. Density measurements were performed in steps of 10 K. The uncertainty of the density measurements is estimated as 10^{-4} g cm^{-3}.

The density of the pure $[C_1C_4Pyrro][OAc]$ was calculated using a group contribution model developed by Jacquemin et al[21,22].

Viscosity measurements

The dynamic viscosities of the two systems, $[C_1C_4Im][LEV]$ previously dried under vacuum and $[C_1C_4Pyrro][OAc]$ + water were measured using an Anton Paar AMVn rolling ball viscosimeter, as a function of the temperature from 293.15 K to 363.15 K (controlled to within 0.01 K and measured with an accuracy better than 0.05 K) and at atmospheric pressure. Before starting the measurements, the 3 mm diameter capillary tube was calibrated as a function of temperature and angle of measurement using a standard viscosity oil from Cannon (N35). The overall uncertainty on the viscosity is estimated as ±1.5%.

Gas-absorption measurements

The experimental method used for the gas absorption measurements in pure ionic liquids is based on an isochoric saturation technique and has been described in previous publications[23,24]. In this technique, a known quantity of gaseous solute is put in contact with a precisely determined quantity of degassed solvent at a constant temperature inside an accurately known volume. When thermodynamic equilibrium is attained, the pressure above the liquid solution is constant and is directly related to the absorption of the gas in the liquid.

The quantity of ionic liquid introduced in the equilibration cell is determined gravimetrically. This quantity is equal to the amount of solvent present in the

liquid solution, n_1^{liq}, as the ionic liquid does not present a measurable vapour pressure. The amount of solute present in the liquid solution, n_2^{liq} (subscripts 1 and 2 stand for solvent and solute, respectively), is calculated by the difference between two pVT measurements: first when the gas is introduced in a calibrated bulb with volume V_{GB} and second after thermodynamic equilibrium is reached:

$$n_2^{liq} = \frac{p_{ini} V_{GB}}{[Z_2(p_{ini}, T_{ini}) RT_{ini}]} - \frac{p_{eq}(V_{tot} - V_{liq})}{[Z_2(p_{eq}, T_{eq}) RT_{eq}]} \quad (1)$$

where p_{ini} and T_{ini} are the pressure and temperature in the first pVT determination and p_{eq} and T_{eq} the pressure and temperature at the equilibrium. V_{tot} is the total volume of the equilibration cell, V_{liq} is the volume of the liquid solution and Z_2 is the compression factor for the pure gas. The solubility can then be expressed in mole fraction, which is calculated from the following equation:

$$x_2 = \frac{n_{2}^{liq}}{n_{1}^{liq} + n_{2}^{liq}} \quad (2)$$

where n_2^{liq} is the amount of solute dissolved in the ionic liquid and $n_2^{liq} = n_1^{tot}$ is the total amount of ionic liquid.

We consider that the volume of the ionic liquid does not change when the gas is solubilised and so the volume of the liquid solution is equal to the molar volume of the pure ionic liquid.

A second experimental method is used for the gas absorption measurements in the mixtures ionic liquid + water. This one is also based on an isochoric saturation technique and has been described in previous publications[25,26].

In this technique a known quantity of gaseous solute is put into contact with a precisely determined quantity of degassed solvent at constant temperature inside an accurately known volume. As previously, when thermodynamic equilibrium is attained the pressure above the liquid solution is constant and directly related to the solubility of the gas in the liquid.

The gas absorption can be expressed as mole fraction of the gas in the liquid mixture, x_2 calculated through:

$$x_2 = \frac{n_2^{liq}}{n_{solv}^{liq} + n_2^{liq}} \quad (3)$$

where $n_{solv}^{liq} = n_1^{liq} + n_3^{liq}$ is the amount of solvent in the liquid phase with n_1^{liq} being the amount of ionic liquid which due to its negligible vapour pressure is equal to the total quantity of ionic liquid introduced in the equilibrium cell and n_3^{liq} the amount of water in the liquid solution.

Molecular simulations

The microscopic structures and interactions in the mixtures of ionic liquids ([C_1C_4Im][TFA] and [C_1C_4Pyrro][OAc]) and carbon dioxide were investigated by molecular dynamics simulations. Ionic liquids were represented by an all-atom force field, which is based on the AMBER/OPLS_AA framework[27,28]. For imidazolium cation force field parameters were developed specifically,[29] meanwhile for the pyrrolidinium cation they were retrieved from the force field for amines[30]. Acetate[28,31] and trifluoroacetate[32] were represented with the potential models existing in the literature, whereas the potential model of Harris and Yung[33] was used for carbon dioxide.

The ionic liquids [C_1C_4Im][TFA] and [C_1C_4Pyrro][OAc] were simulated in periodic cubic boxes containing 127 ion pairs, using the molecular dynamics method implemented in the DL_POLY package[34]. Initial low-density configurations, with ions placed at random in periodic cubic boxes, were equilibrated to attain liquid-like densities and structures at 373 K and 1 bar. Temperature and pressure were maintained using a Nosé-Hoover thermostat and barostat, respectively. Once the equilibrium density attained, simulations runs of 1 ns were performed, with an explicit cutoff distance of 16 Å for non-bonded interactions, from which 5000 configurations were stored. Structural quantities such as radial and spatial distribution functions were calculated from configurations generated during the production runs. Additionally, simulation boxes containing 200 ion pairs and 12 carbon dioxide molecules were prepared in the same manner, to calculate solute−solvent radial distribution functions between the gas and the ionic liquid and the cation−anion interaction energy in the presence of carbon dioxide.

The chemical potentials of carbon dioxide at 373 K in the two ionic liquids were calculated in a two-step procedure, as already described by Almantariotis et al.[35] First, for carbon dioxide, a reduced-size version of the molecule was made by subtracting 0.8 Å from the C-O bond length and also from the Lennard-Jones diameters σ_O and σ_C. The resulting molecule is small enough so that its chemical potential can be calculated using the Widom test-particle insertion method with efficient statistics (100000 insertions into each of 5000 stored configurations of pure ionic liquids). Second, a stepwise finite difference thermodynamic integration procedure was followed to calculate the free-energy difference between the initial, reduced versions of the carbon dioxide molecule and the final full-size model. The free energy calculation was performed on six intermediate steps along a linear path connecting the intermolecular parameters (bonds and diameters) of the reduced-size to those of the full-size molecule. This relatively modest number of intermediate steps is adequate because the starting point of the thermodynamic integration route is not too far from the final state. In the finite-difference thermodynamic integration scheme, derivatives (finite differences) of the total energy of the system with respect to the activation parameter were evaluated by a free-energy perturbation expression in the NpT ensemble using a three-point formula with increments of 2×10^{-3}.

NMR measurements

^{1}H and ^{13}C NMR data were collected at 298.15 K or 313.15 K on a Bruker AC 400 MHz spectrometer. Spectra of $[C_1C_4Im][LEV]$ and $[C_1C_4Pyrro][OAc]$ samples were recorded in solution using acetone-d_6 and $CDCl_3$ as solvents, respectively. A coaxial capillary tube loaded with DMSO-d_6 was inserted into the 5 mm NMR tube filled with the $[C_1C_4Pyrro][OAc]$ + water sample to avoid any contact between the deuterated solvent and the analysed mixture. The deuterium in DMSO-d_6 was used for the external lock of the NMR magnetic field and the residual proton in DMSO-d_6 was used as the ^{1}H NMR external reference at 2.5 ppm.

Results and discussion

The experimental values obtained for the density of $[C_1C_4Im][LEV]$ and $[C_1C_4Pyrro][OAc]$ + water as a function of pressure and at temperatures from 293 to 353 K are reported in Table S-2 of the supplementary information. The values of density at atmospheric pressure (necessary for the calculation of the gas solubility) were adjusted to linear functions of temperature:

$$\rho_{[C_1C_4Im][LEV]} \Big/ \mathrm{kg \cdot m^{-3}} = 1281.7 - 0.6112\left(T/\mathrm{K}\right) \quad (4)$$

$$\rho_{[C_1C_4Pyrro][OAc]+H_2O(x=0.4)} \Big/ \mathrm{kg \cdot m^{-3}} = 1186.3 - 0.5669\left(T/\mathrm{K}\right) \quad (5)$$

$$\rho_{[C_1C_4Pyrro][OAc]+H_2O(x=0.6)} \Big/ \mathrm{kg \cdot m^{-3}} = 1198.7 - 0.5858\left(T/\mathrm{K}\right) \quad (6)$$

$$\rho_{[C_1C_4Pyrro][OAc]+H_2O(x=0.8)} \Big/ \mathrm{kg \cdot m^{-3}} = 1233.0 - 0.6689\left(T/\mathrm{K}\right) \quad (7)$$

the standard deviation of the fits is always better than 0.1%.

The density of $[C_1C_4Im][LEV]$ was compared to both the acetate based ionic liquids with imidazolium cations studied in our previous work[8] and was found to be lower than $[C_1C_2Im][OAc]$ and higher than $[C_1C_4Im][OAc]$. Mixtures of $[C_1C_4Pyrro][OAc]$ + water present, as expected, lower densities than mixtures of $[C_1C_2Im][OAc]$ + water or $[C_1C_4Im][OAc]$ + water[8] for an equivalent mole fraction of water. The density increases when the quantity of water increases as it was observed previously for the systems $[C_1C_2Im][OAc]$ + water and $[C_1C_4Im][OAc]$ + water.

The densities measured herein as a function of pressure were correlated using the Tait equation:

$$\rho(T,P) = \left[\frac{\rho^0(T,p^0)}{1 - C\ln\left(\frac{B(T)+p}{B(T)+p^0}\right)} \right] \quad (8)$$

where $\rho^0(T,p^0)$ is the density value at a reference temperature T and at the pressure $p^0 = 0.1\text{MPa}$; C is an adjustable parameter and B(T) a polynomial defined by:

$$B(T) = \sum_{i=0}^{2} B_i (T)^i \quad (9)$$

The parameters found for the present data are listed in Table 1.

The dynamic viscosity was measured for the systems $[C_1C_4Im][LEV]$ and $[C_1C_4Pyrro][OAc]$ + water, and is listed in Table 2 as a function of temperature from 293 to 373 K. The Vogel–Fulcher–Tamman (VFT) equation was used to correlate the experimental viscosities as a function of temperature:

$$\eta_{[C_1C_4Im][LEV]} / \text{mPa}\cdot\text{s} = \left(2.07\times10^{-3}\right)\left(T/K\right)^{1/2} \exp\left[\frac{1197}{\left(T/K\right)-190}\right] \quad (10)$$

$$\eta_{[C_1C_4Pyrro][OAc]+H_2O(x=0.4)} / \text{mPa}\cdot\text{s} = \left(2.54\times10^{-3}\right)\left(T/K\right)^{1/2} \exp\left[\frac{985}{\left(T/K\right)-183}\right] \quad (11)$$

$$\eta_{[C_1C_4Pyrro][OAc]+H_2O(x=0.6)} / \text{mPa}\cdot\text{s} = \left(1.01\times10^{-3}\right)\left(T/K\right)^{1/2} \exp\left[\frac{1173}{\left(T/K\right)-164}\right] \quad (12)$$

$$\eta_{[C_1C_4Pyrro][OAc]+H_2O(x=0.8)} / \text{mPa}\cdot\text{s} = \left(1.97\times10^{-3}\right)\left(T/K\right)^{1/2} \exp\left[\frac{868}{\left(T/K\right)-177}\right] \quad (13)$$

As expected, the viscosities of the ionic liquids depend both on the nature of the anion and the cation. Values of viscosity, at 303.15 K, of $[C_1C_4Im][LEV]$ are equal to 1441 mPas, so 3.6 and 13.7 times higher than values of $[C_1C_4Im][OAc]$ and $[C_1C_2Im][OAc]$, respectively.[8] The system $[C_1C_4Pyrro][OAc]$ + water (for a mole fraction of water equal to 0.4) presents

a viscosity of 330.4 mPas at 293.15 K, a value 1.1 and 3.7 times higher than those of $[C_1C_4Im][OAc]$ + water and $[C_1C_2Im][OAc]$ + water. The viscosity of the mixture $[C_1C_4Pyrro][OAc]$ + water decreases with the addition of water, the viscosity, for a mole fraction of water equal to 0.8 being as low as 45.43 mPas at 293 K, 2.1 and 7.3 times lower than for mole fractions of water equal to 0.6 and 0.4, respectively.

For both $[C_1C_4Im][LEV]$, $[C_1C_4Pyrro][OAc]$ and for the mixtures of $[C_1C_4Pyrro][OAc]$ + water, multiple experimental data points on the absorption of carbon dioxide were obtained in the temperature interval between 303.15 K and 343.15 K in steps of approximately 10 K. The pure ionic liquid $[C_1C_4Pyrro][OAc]$ was only studied at 353 K. For the $[C_1C_4Pyrro][OAc]$ + water mixtures, measurements of the CO_2 absorption were made at 303.15 and 313.15 K for mole fractions of water equal to 0.35, 0.6 and 0.85. The experimental values are reported in Table 3.

The absorption of carbon dioxide in pure $[C_1C_4Im][LEV]$ is represented in Figure 2 as a function of pressure for the different temperatures studied. The gas is absorbed up to a 0.93×10^{-2} mole fraction at 303.15 K and 67.1 KPa. Absorption of carbon dioxide in $[C_1C_4Im][LEV]$ increases when the partial pressure of gas increases and when the temperature decreases. It is observed in Figure 2 that the carbon dioxide absorption progress linearly with the pressure for all temperatures studied, indicating that Henry's law is verified and that carbon dioxide is only physically dissolved in that case. Compared to the imidazolium acetate ionic liquids studied previously by our research group,[8] which are able to both chemically and physically absorb carbon dioxide, absorption in the $[C_1C_4Im][LEV]$ was found to be one order of magnitude lower.

The results presented herein on the absorption of CO_2 in the mixtures $[C_1C_4Pyrro][OAc]$ + water are presented in Figure 3. The absorption of carbon dioxide decreases when the mole fraction of water increases, the absorbed quantity of gas varying from 10.9×10^{-2} to 0.9×10^{-2} at 303.15 K and 9.4 KPa and 303.15 K and 63.8 KPa for water mole fractions equal to 0.35 and 0.85, respectively.

In order to compare the absorption of carbon dioxide in all studied systems,

experimental data were extrapolated linearly to 353.15 K for all systems except for [C_1C_4Pyrro][OAc]. In that case, it is assumed that the pressure differences do not affect significantly the values of absorption of carbon dioxide in the different systems studied. Results are presented in Figure 4. The absorption of carbon dioxide in the mixtures [C_1C_4Pyrro][OAc] + water for water mole fractions equal to 0.35 and 0.60 is one order of magnitude higher than in the three other systems. Values are comparable to these found for the systems [C_1C_2Im][OAc] + water and [C_1C_4Im][OAc] + water studied previously[8]. It implies that the system [C_1C_4Pyrro][OAc] + water can react chemically with carbon dioxide when the amount of water present is sufficient. Absorption of carbon dioxide in pure [C_1C_4Pyrro][OAc] was found to be lower than in mixtures of [C_1C_4Pyrro][OAc] + water for water mole fraction equal to 0.35 and 0.60. Absorption of carbon dioxide in pure [C_1C_4Pyrro][OAc] is also one order of magnitude lower than in [C_1C_2Im][OAc] and [C_1C_4Im][OAc]. It appears that pure [C_1C_4Pyrro][OAc] is only able to physically absorb carbon dioxide and the mechanism of chemical reaction between [C_1C_4Pyrro][OAc] + water and carbon dioxide is different from that of the systems with the ionic liquids [C_1C_2Im][OAc] and [C_1C_4Im][OAc], these two ionic liquids reacting chemically with carbon dioxide with and without water present.

Absorption of carbon dioxide in [C_1C_4Pyrro][LEV] is comparable to the absorption in pure [C_1C_4Pyrro][OAc] or in the mixture [C_1C_4Pyrro][OAc] + water for water molar fraction equal to 0.85.

In order to explain the difference in carbon dioxide absorption in the studied ionic liquids as well as the effect of water on the microscopic structure of the pure ionic liquids and in their mixtures with carbon dioxide, we have used molecular dynamics simulations. Two ionic liquids were considered, the 1-butyl-3-methyl trifluoroacetate [C_1C_4Im][TFA] and the [C_1C_4Pyrro][OAc]. In the first case, it is well known that the absorption of CO_2 is purely physical[15] and we expect that the comparison between the behavior of the two ionic liquids will contribute to the understanding of the mechanisms of gas absorption in [C_1C_4Pyrro][OAc].

Molecular dynamics simulations were done in all a condensed-phase and

took into account all the two-body interactions from the environment of each molecule or ion, labeled as depicted in Figure 5.

Initially, the microscopic structure of the pure ionic liquids [C_1C_4Im][TFA] and [C_1C_4Pyrro][OAc], was perceived by the analysis of the site-site radial distribution function − probability of finding two selected atomic sites at a certain distance is represented in Figure 6 for several representative atomic sites in the pure ILs. From the plots in Figure 6 it can be observed that in the imidazolium ionic liquid, the cation and the anion interact preferentially through the $H2_{Im}$ hydrogen of the $C_1C_4Im^+$ and the O_{TFA} oxygen of TFA^-, where negative charge is concentrated. The oxygen atom of the anion TFA^- is also found with significant probability in the vicinity of the nitrogen N_{Im} of imidazolium cation. This result was expected and is consistent with other imidazolium liquids reported in literature.

Likewise, in the pyrrolidinium ionic liquid the interaction between the partially positive NPyrro (as well as $C1_{Pyrro}$) and the oxygen of the OAc− are of the most importance. Whereas the other interactions sites between the cation and the anion are present, but less expressed. However, the distance between these cation and anion atomic sites are shorter for the imidazolium ionic liquid[8] than for the pyrrolidinium based one, in accordance with accessibility and acidity of imidazolim $H2_{Im}$ and therefore stronger acid-base interactions in the former case.

The molecular simulation results indicate that the presence of carbon dioxide does not affects the principle interaction sites present in the pure ionic liquids. This can be also deduced from the plots in Figure 6, where solid lines refer to the pure ionic liquid and dotted lines to the mixture CO_2+IL. In the [C_1C_4Im][TFA] both peaks, one corresponding to the interactions of the terminal carbon atoms of the alkyl chain of the cation CT_{Im} and the oxygen of CO_2 (O_{CO2}), and the other between the oxygen of the anion (O_{OAc}) and carbon of carbon dioxide (C_{CO2}) are of significant importance. This indicates that carbon dioxide is solvated preferentially in the vicinity of the anion and in the non-polar region of imidazolium ionic liquids. Carbon dioxide was found to be solvated similarly in [C_1C_4Im][TFA] than in [C_1C_4Im][OAc] as we can see in our previous work[8]. Analogously in

[C_1C_4Pyrro][OAc], there is a high probability of finding carbon dioxide near oxygen of OAc− and CT_{Pyrro}. No significant difference in solvation of carbon dioxide in both types of ionic liquid, imidazolium[8] and pyrrolidinium, was observed.

These structural features of the mixture of CO_2+IL can be perceived and confirmed also in 3 dimensional spatial distribution functions in Figure 7. In Figures 7a and 7d is represented the distribution of the local density of the cationic and the anionic atomic sites around carbon dioxide in [C_1C_4Im][TFA] and [C_1C_4Pyrro][OAc], respectively. As already deduced from the radial distribution functions, for the two ionic liquids studied the spatial distribution function shows that carbon dioxide is mainly solvated by the anion (O_{OAC} or O_{TFA}, red) and the terminal carbon atoms of CT_{Im} or CT_{Pyrro} (grey). Looking at distribution of atomic density around acetate or trifluoroacetate (Figures 7b and 7e) is expected to find C_{CO2} (cyan) and $C2_{Im}$ or N_{Pyrro} (blue) interacting with the oxygen atoms of the anion. From the Figures 7c and 7f we can observe that the presence of the oxygen of carbon dioxide around the cation is minor.

Calculations of the free energy of solvation of carbon dioxide in [C_1C_4Im][TFA] and [C_1C_4Pyrro][OAc] at 373 K give access to the Henry's law constants constants, K_H, that allow us to calculate the gas solubility at a partial pressure of gas p_{gas} = 1 bar. The results are summarized in Table 4, where a comparison with the experimental values is also reported. The results of the simulations agree with the experiments for [C_1C_4Im][TFA]. Whereas, simulations did not reproduce experimental trends. Solubilities calculated for [C_1C_4Im][TFA] were found to be the same than for [C_1C_4Im][OAc] studied previously[8], within the incertitude of simulations. This implies that the nature of the cation does not affect the solubility of carbon dioxide significantly.

The disparity in the solubility of carbon dioxide in the studied ionic liquids can be ascribed either to the structural difference in ionic liquids or/and different strength and nature of interactions. As the structural analysis showed no significant difference between [C_1C_4Im][TFA] and [C_1C_4Pyrro][OAc], the strength of interactions CO_2−solute must be of

significant importance.

In order to explain such a difference in the solubility of carbon dioxide the simulation results were examined in detail. The overall system configuration energy of the mixtures CO_2+IL was decomposed to the energy between each pair of species, represented in Figure 8. The overall cation−anion interactions are stronger for the pair $[C_1C_4Im]^+[TFA]^-$ than for $[C_1C_4Pyrro]^+[OAc]^-$. These observations were already made from the analysis of the site-site radial distribution functions in Figure 6. The presence of carbon dioxide increases the cation−anion interactions thus favoring the ion pair association. No significant difference in the interaction energy between carbon dioxide and cation/anion was observed for the two ionic liquids. Surprisingly, carbon dioxide was found to interact stronger with cation than with the anion.

Molecular simulation reproduces the correct carbon dioxide solubility in $[C_1C_4Im][TFA]$, but not in $[C_1C_4Pyrro][OAc]$, meaning that in the later case some mechanism of gas absorption other than physical absorption (the only implemented in the molecular simulations), prevails.

To obtain further information about the interaction of carbon dioxide and the ionic liquids, which could help to interpret the trends of the experimental values of carbon dioxide absorption, ^1H and ^{13}C NMR spectra of pure and carbon dioxide-saturated ionic liquids were recorded at atmospheric pressure. Figure 9 shows NMR spectra of pure $[C_1C_4Im][LEV]$ and $[C_1C_4Im][LEV]$ saturated with carbon dioxide. Comparison of the spectra a) and b) in the upper and lower plots of Figure 9 shows no noticeable changes neither in ^1H or in ^{13}C chemical shifts upon saturation of the ionic liquid with carbon dioxide. This observation proves that no chemical reaction is involved in the carbon dioxide absorption by $[C_1C_4Im][LEV]$, in agreement with the lower values of absorption found compared to the imidazolium acetate based ionic liquids[8]. Furthermore, the small peak in spectrum b) of the lower plot in Figure 9 at around 175 ppm is the clear signature of free CO_2 in solution.[36]

To obtain further insight into the mechanism of carbon dioxide absorption by

pyrrolidinium acetate, ^{1}H and ^{13}C NMR spectra of pure $[C_1C_4Pyrro][OAc]$, of the $[C_1C_4Pyrro][OAc]+H_2O$ mixtures and of the solutions containing CO_2 in these liquids were recorded and are depicted in Figure 10. Since $[C_1C_4Pyrro][OAc]$ is a solid at room conditions with a melting point at 353 K, the pure ionic liquid was dissolved in $CDCl_3$ before the NMR spectra of the solution were recorded. Comparison of the spectra a) and b) in the upper and lower plots of Figure 10 shows no noticeable changes, neither in ^{1}H or in ^{13}C chemical shifts upon saturation of the mixture with carbon dioxide. This indicates that, without the presence of water, the mechanism of absorption is different from the mechanism in $[C_1C_4Im][OAc]$ in which chemical reactions with acetate were observed previously[8]. Contrary to $[C_1C_4Im][OAc]$, solubility measurements showed that the presence of water in $[C_1C_4Pyrro][OAc]$ increases dramatically the absorption of gas when compared with that on the pure ionic liquid. This is another evidence that the mechanism of absorption of the gas is different in the two ionic liquids containing the acetate anion. An additional peak appears in the ^{13}C NMR spectrum at 158.5 ppm (• in the lower plot labeled d) in Figure 10) when the ionic liquid + water mixture is saturated with CO_2. Most probably, this peak corresponds to the formed HCO_3^-, as proved independently by dissolving $NaHCO_3$ in the ionic liquid (Figure S-1 in the supplementary information). This observation is in agreement with previously established results, which showed that solubility of carbon dioxide in triethylbutylammonium acetate is excluded by chemical reaction involving cation[37], but instead involves the acetate anion. Although the reaction is possible only in the presence of water, water displaces equilibrium towards the reactants and decreases the absorption, as proved by the experimental measurements herein.

Conclusions

This work presents an original study of the physico-chemical properties of the ionic liquids $[C_1C_4Im][LEV]$, $[C_1C_4Pyrro][OAc]$ and $[C_1C_4Pyrro][OAc]$ + water. Our aim is to study the absorption mechanisms of carbon dioxide, relevant for carbon dioxide capture processes, in these solvents.

We have observed that the ionic liquid $[C_1C_4Im][LEV]$ presents a higher viscosity than the imidazolium acetate based ionic liquids, which can constitute a disadvantage for industrial processes needing high fluidities. The mixtures $[C_1C_4Pyrro][OAc]$ + water present also higher values of absorption than $[C_1C_2Im][OAc]$ + water and $[C_1C_4Im][OAc]$ + water for the same water molar composition.

We have observed that absorption of carbon dioxide in the pure ionic liquids is of the order of 10^{-2} when expressed in mole fraction of gas, indicating that no chemical reaction between carbon dioxide and ionic liquids are involved unlike in the case of imidazolium acetate based ionic liquids. Absence of chemical reaction is confirmed by comparison between the NMR spectra of pure ionic liquids and those of carbon dioxide saturated ionic liquids.

The mixtures $[C_1C_4Pyrro][OAc]$ + water present values for the carbon dioxide absorption one order of magnitude higher than that in the pure ionic liquids. These values, comparable to those that can be found in the systems $[C_1C_2Im][OAc]$ + water and $[C_1C_4Im][OAc]$ + water, point towards the existence of chemical reaction between $[C_1C_4Pyrro][OAc]$ and carbon dioxide but only in the presence of water. The NMR study reported here proves that, in the case of $[C_1C_4Pyrro][OAc]$ + water, the mechanism of CO_2 absorption is different from that previously reported for $[C_1C_4Im][OAc]$ + water mixtures.

Acknowledgements

The FUI ACACIA project is acknowledged for financing part of this work and the PhD grant of S.S. The authors thank D. Pic from LMOPS, Lyon, France, for his help in the synthesis of one of the products used.

Table 1

Tait parameters C, B_0, B_1 and B_2 used to smooth the experimental densities as a function of pressure (to 25 MPa) and temperature (from 293 to 353K). AAD indicated the percent average absolute deviation of the fit.

Ionic liquid	$10^2 \cdot C$	B_0 / MPa	B_1 /MPa·K^{-1}	$10^3 \cdot B_2$ /MPa·K^{-2}	AAD/%
[C_1C_4Pyrro][OAc]+water (x_{water}=0.4077)	−2.137	+278.999	−2.339	+3.808	0.016
[C_1C_4Pyrro][OAc]+water (x_{water}=0.6028)	−1.527	−107.704	+0.136	+0.007	0.016
[C_1C_4Pyrro][OAc]+water (x_{water}=0.8027)	−2.005	−136.864	+0.230	−0.158	0.020

Table 2

Experimental dynamic viscosities, η, of the ionic liquids $[C_1C_4Im][LEV]$ and $[C_1C_4Pyrro][OAc]$ + water mixtures as a function of temperature at atmospheric pressure.

T / K	η^{exp} / mPa·s	δ / %	T / K	η^{exp} / mPa·s	δ / %
	$[C_1C_4Im][LEV]$			$[C_1C_4Pyrro][OAc]$+water (x_{water}=0.4077)	
303.15	1441	+ 0.0	293.15	330.4	+ 0.0
313.15	619.6	– 0.2	303.15	160.12	– 0.2
323.15	300.2	+ 0.7	313.15	86.23	+ 0.4
333.15	165.0	– 0.9	323.15	51.09	+ 0.4
			333.15	32.67	– 0.2
			343.15	22.10	– 0.5
			353.15	15.73	– 1.2
			363.15	11.52	– 0.8
			373.15	8.644	+ 0.6
	$[C_1C_4Pyrro][OAc]$+water (x_{water}=0.6028)			$[C_1C_4Pyrro][OAc]$+water (x_{water}=0.8027)	
293.15	152.7	+ 0.1	293.15	45.43	+ 0.0
303.15	81.31	– 0.6	303.15	26.05	+ 0.2
313.15	45.97	+ 1.5	313.15	16.32	– 0.2
323.15	29.13	– 0.7	323.15	10.90	– 0.3
333.15	18.89	+ 0.5	333.15	7.665	– 0.2
343.15	13.23	– 1.1			
353.15	9.512	– 1.3			

Table 3

Experimental values of carbon dioxide in $[C_1C_4Pyrro][LEV]$, $[C_1C_4Pyrro][OAc]$ and $[C_1C_4Pyrro][OAc]$ + water expressed as carbon dioxide mole fraction, x_2. p is the experimental equilibrium pressure.

T / K	p / 10^2Pa	x_2^{exp}	K_H / 10^5Pa	x_2 / 10^{-2}	dev / %
			$[C_1C_4Pyrro][LEV]$		
303.16	670.78	0.0093	72.2	1.38	– 0.1
313.28	633.60	0.0078	81.4	1.22	+ 1.9
313.28	691.26	0.0083	82.9	1.20	+ 0.1
313.31	696.99	0.0082	84.4	1.18	– 1.7
323.32	658.57	0.0066	99.5	1.00	+ 0.1
323.34	717.90	0.0073	97.4	1.02	+ 2.3
323.34	723.84	0.0070	102.5	0.97	– 2.7
333.35	683.20	0.0056	122.3	0.82	+ 1.4
333.36	750.17	0.0060	124.1	0.80	+ 0.0
333.41	747.00	0.0059	125.7	0.79	– 1.2
			$[C_1C_4Pyrro][OAc]$		
353.55	891.8	0.011	84.5	0.012	
353.18	434.26	0.005	88.8	0.011	
			$[C_1C_4Pyrro][OAc]$+water (x_{water}=0.35)		
303.34	94.00	0.109			
313.35	147.00	0.103			
			$[C_1C_4Pyrro][OAc]$+water (x_{water}=0.6)		
303.32	154.00	0.057			
313.72	221.00	0.053			
			$[C_1C_4Pyrro][OAc]$+water (x_{water}=0.85)		
303.35	638	0.009			
313.36	709	0.008			

Table 4

Comparison of experimental solubilities of carbon dioxide in ionic liquids and calculated by molecular dynamic simulations expressed in mole fraction: $[C_1C_4Im][TFA]$ and $[C_1C_4Pyrro][OAc]$.

Ionic liquid	[a]Calculated, x_{sim}	Experimental, x_{exp}
$[C_1C_4Im][TFA]$	0.004 ± 0.001	0.005[c]
$[C_1C_4Pyrro][OAc]$	0.002 ± 0.001	0.012[d]

[a]373 K. [b] Extrapolated to 373 K. [c] 298 K. [d] 353 K.

Figure 1

Ionic liquids used in this work. A. 1-butyl-3-methylimidazolium levulinate [C_1C_4Im][LEV]; B. 1-butyl-1-methylpyrrolidinium acetate [C_1C_4Pyrro][OAc].

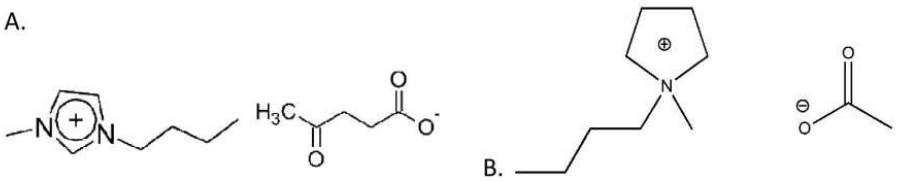

Figure 2

Mole fraction absorption of carbon dioxide in the $[C_1C_4Im][LEV]$ as a function of the temperature: (□), 303.15 K; (●), 313.15 K; (▽),323.15 K; (♦), 333.15 K.

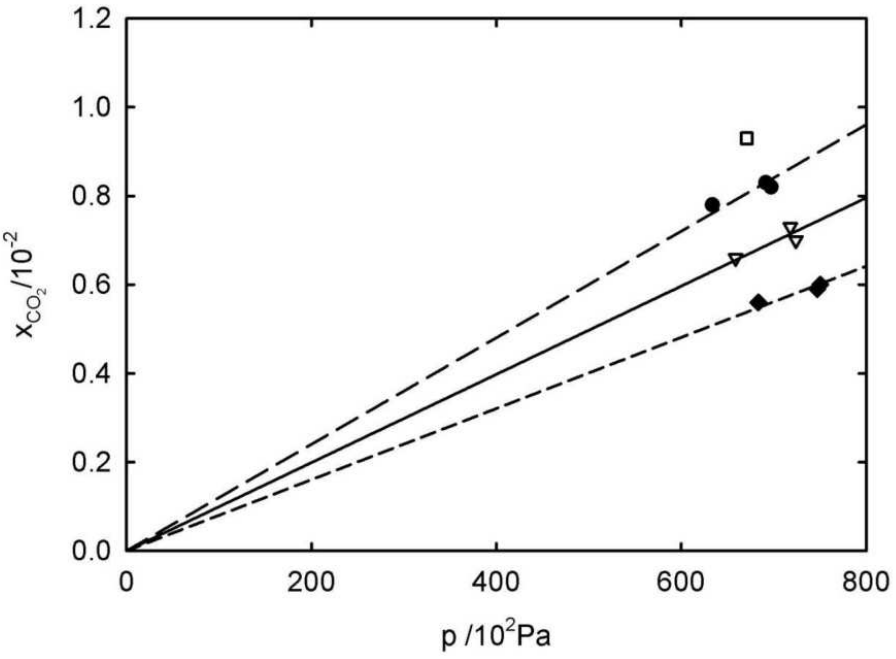

Figure 3

Mole fraction absorption of carbon dioxide in the systems $[C_1C_4Pyrro][OAc]$ + water as a function of the temperature: ■, 303.15 K; ■, 313.15 K. The number above each bar represents the equilibrium pressure in mbar.

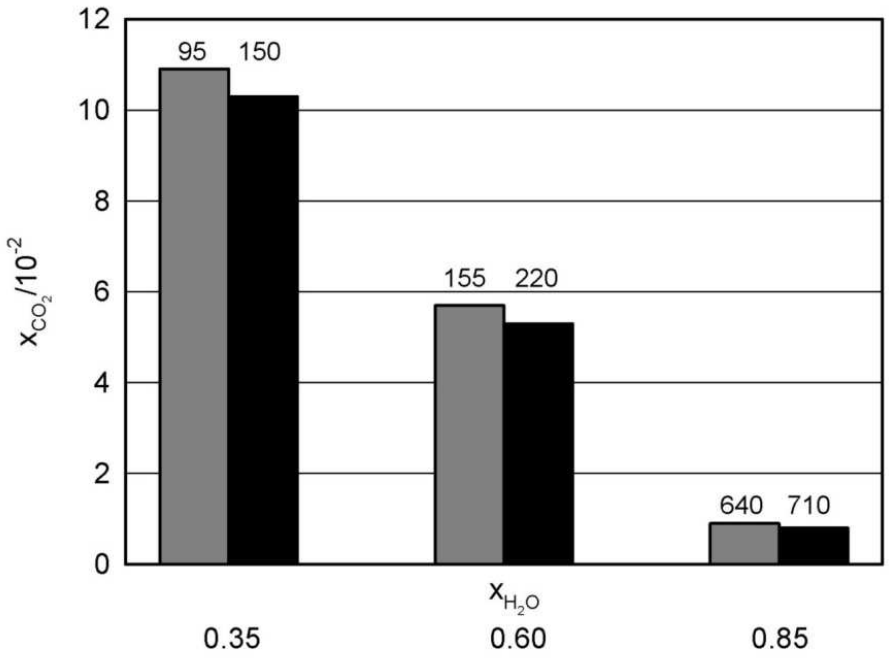

Figure 4

Mole fraction absorption of carbon dioxide in the ionic liquids and ionic liquids + water systems studied herein, at 353.15 K: ■, $[C_1C_4Pyrro][OAc]$; ■, $[C_1C_4Pyrro][OAc]$ + water (x_{H2O}=0.35); ■, $[C_1C_4Pyrro][OAc]$ + water (x_{H2O}=0.60); ■, $[C_1C_4Pyrro][OAc]$ + water (x_{H2O}=0.80); ■, $[C_1C_4Im][LEV]$. Values are obtain by extrapolating linearly experimental data to 353.15 K for all systems except for $[C_1C_4Pyrro][OAc]$.

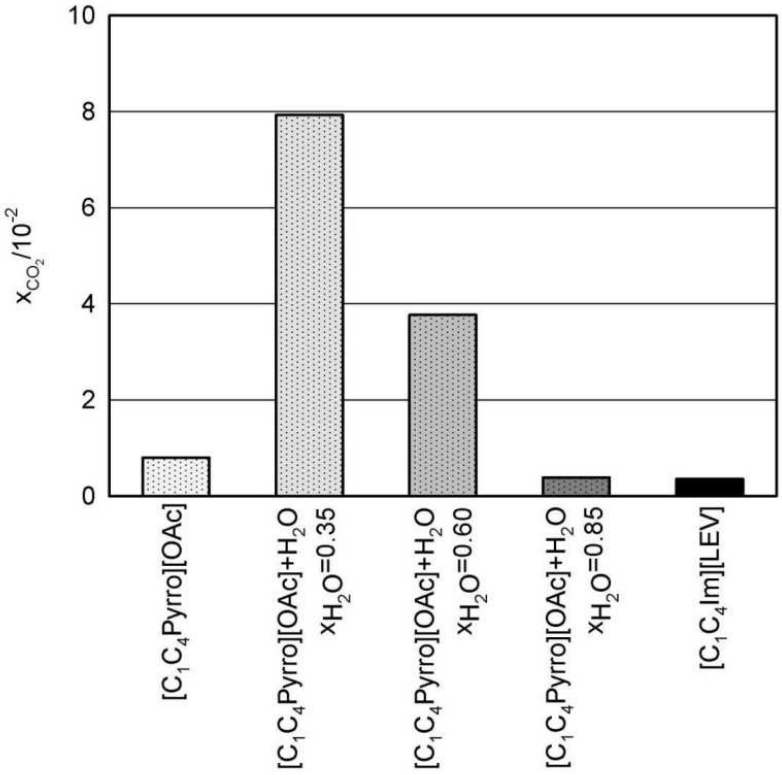

Figure 5

Atom labelling in 1-butyl-3-methylimidazolium and N-butyl-N-methylpyrrolidinium cations and acetate and trifluoroacetate anions.

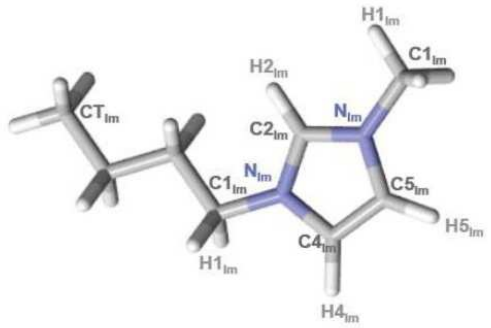

1-Butyl-3-methylimidazolium cation, $[C_1C_4Im]^+$

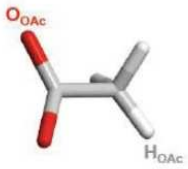

Acetate anion, $[OAc]^-$

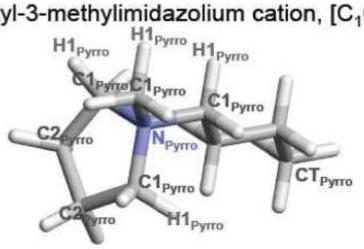

N-Butyl-*N*-methylpyrrolidinium cation, $[C_1C_4Pyrro]^+$

Trifluorocetate anion, $[TFA]^-$

Figure 6

Preferential interaction sites between ionic liquid and carbon dioxide. On the left-hand side: $[C_1C_4Im][TFA]$ and on the right-hand side: $[C_1C_4Pyrro][OAc]$.

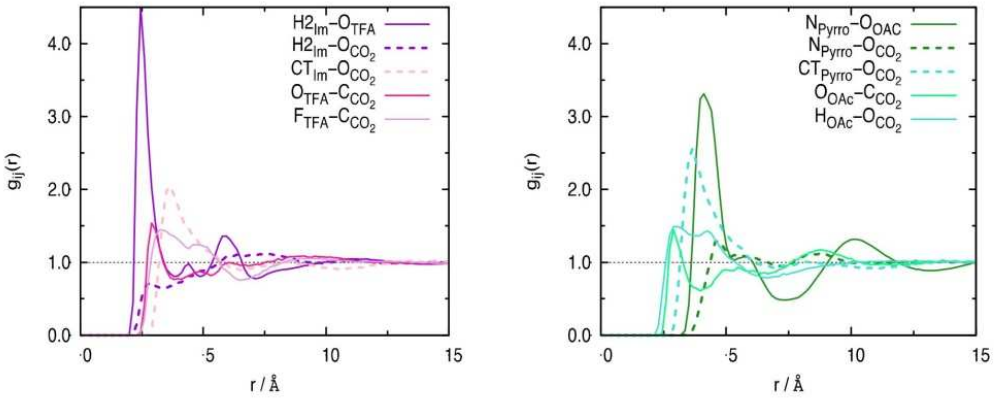

Figure 7

Spatial distribution functions between selected atomic sites in [C_1C_4Im][TFA], [C_1C_4Pyrro][OAc] and carbon dioxide.

Figure a and d: around carbon dioxide: Iso-surface corresponding to a local density of twice the average density of the CT_{Im} or CT_{Pyrro} (grey) and of the O_{OAc} or O_{TFA}(red).

Figure b and e: around OAc^- or TFA^-. Iso-surface corresponding to a local density of 3-times the average density of the $H2_{Im}$ (blue) and C_{CO2} (purple).

Figure c and f: around $C_1C_4Im^+$ or $C_1C_4Pyrro^+$. Iso-surface corresponding to a local density of twice the average density of the O_{CO2} (yellow) and of 4-times of the O_{OAc} or O_{TFA} (red).

[C_1C_4Im][TFA]

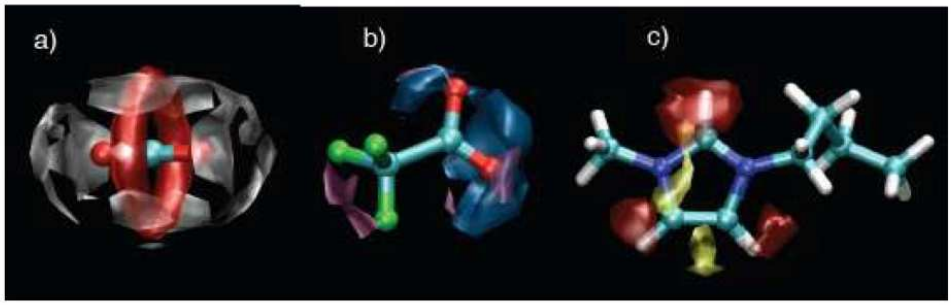

[C_1C_4Pyrro][OAc]

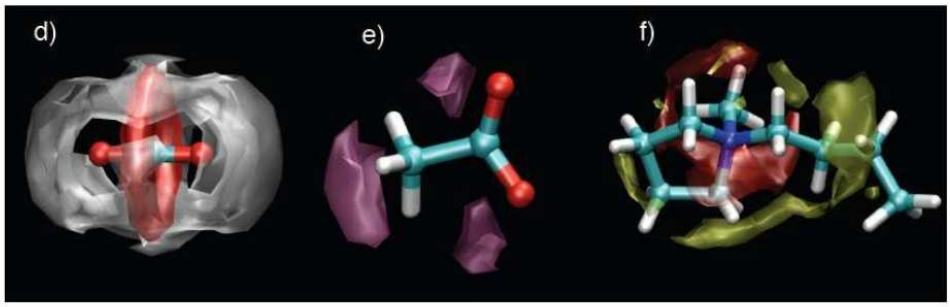

Figure 8

Comparison of the cation – anion, cation – CO_2 and anion – CO_2 interaction energies in pure ionic liquids and in the mixtures with carbon dioxide. The values are normalized by a number of the amount of substance of ionic liquid in moles. In the mixtures IL+CO_2 interaction energies are normalized by number of CO_2 molecules. Exact values are reported in Table S-1 (ESI).

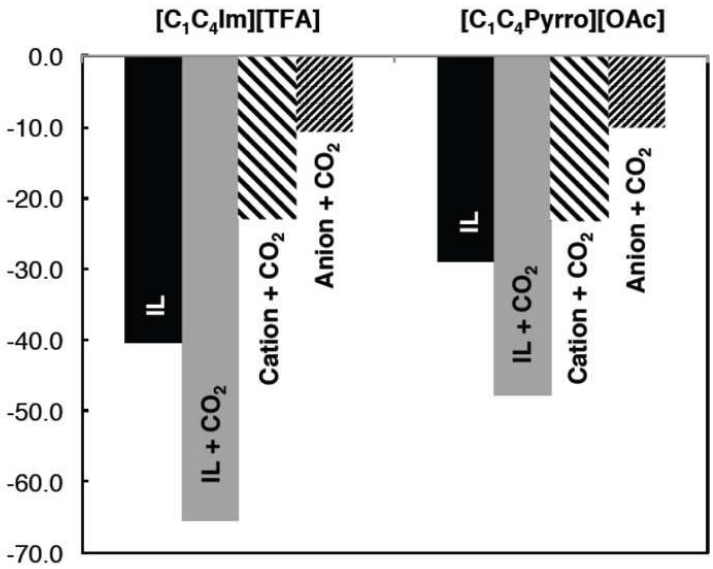

Figure 9

^{1}H NMR (upper plot) and ^{13}C NMR spectra (lower plot) of various samples of $[C_1C_4Im][LEV]$ in acetone-d_6.

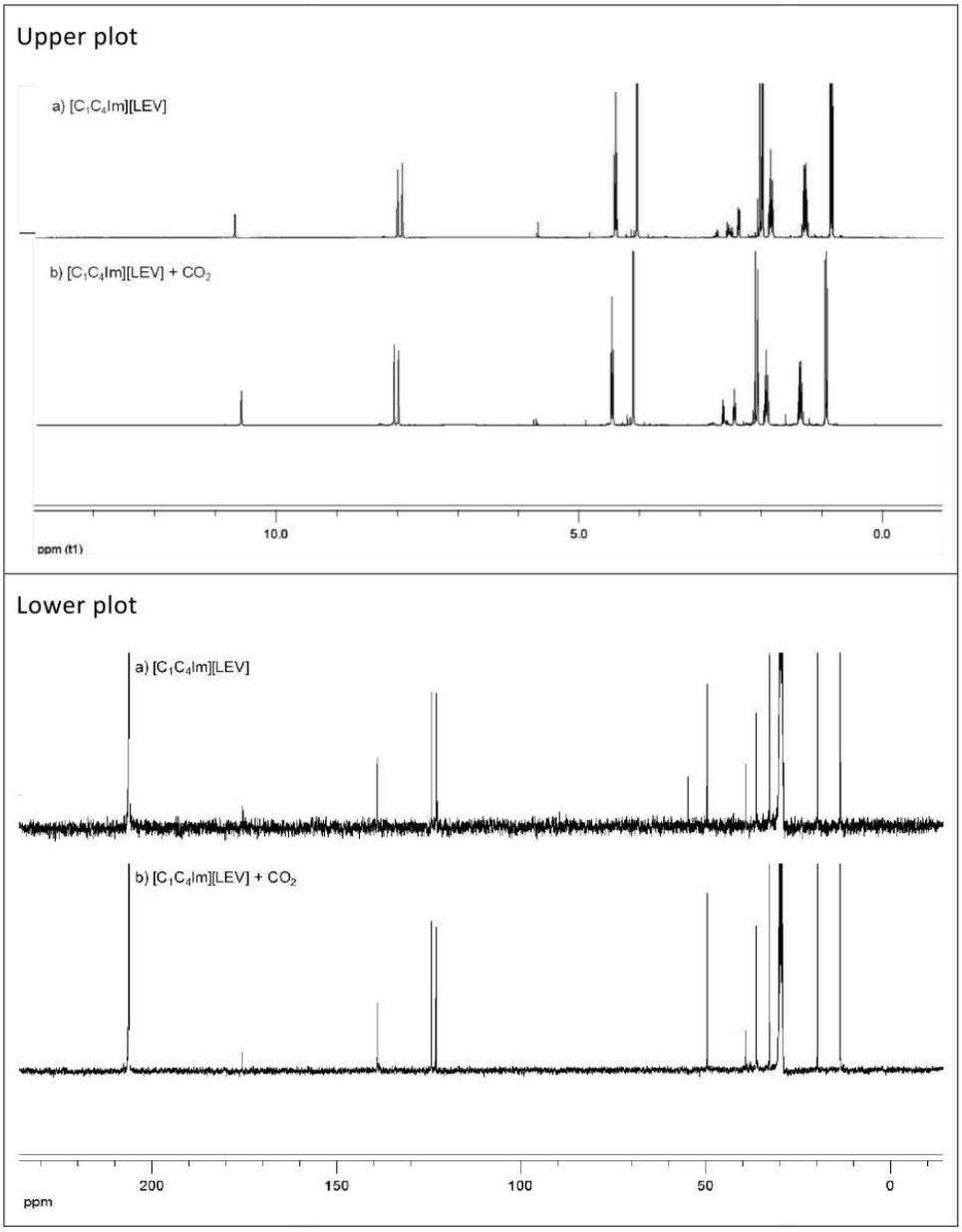

Figure 10

^{1}H NMR spectra (upper plot) and ^{13}C NMR spectra (lower plot) of various samples of $[C_1C_4Pyrro][OAc]$. Samples a) and b) were recorded in solution in $CDCl_3$ while samples c) and d) were recorded in a coaxial tube loaded with DMSO-d_6.

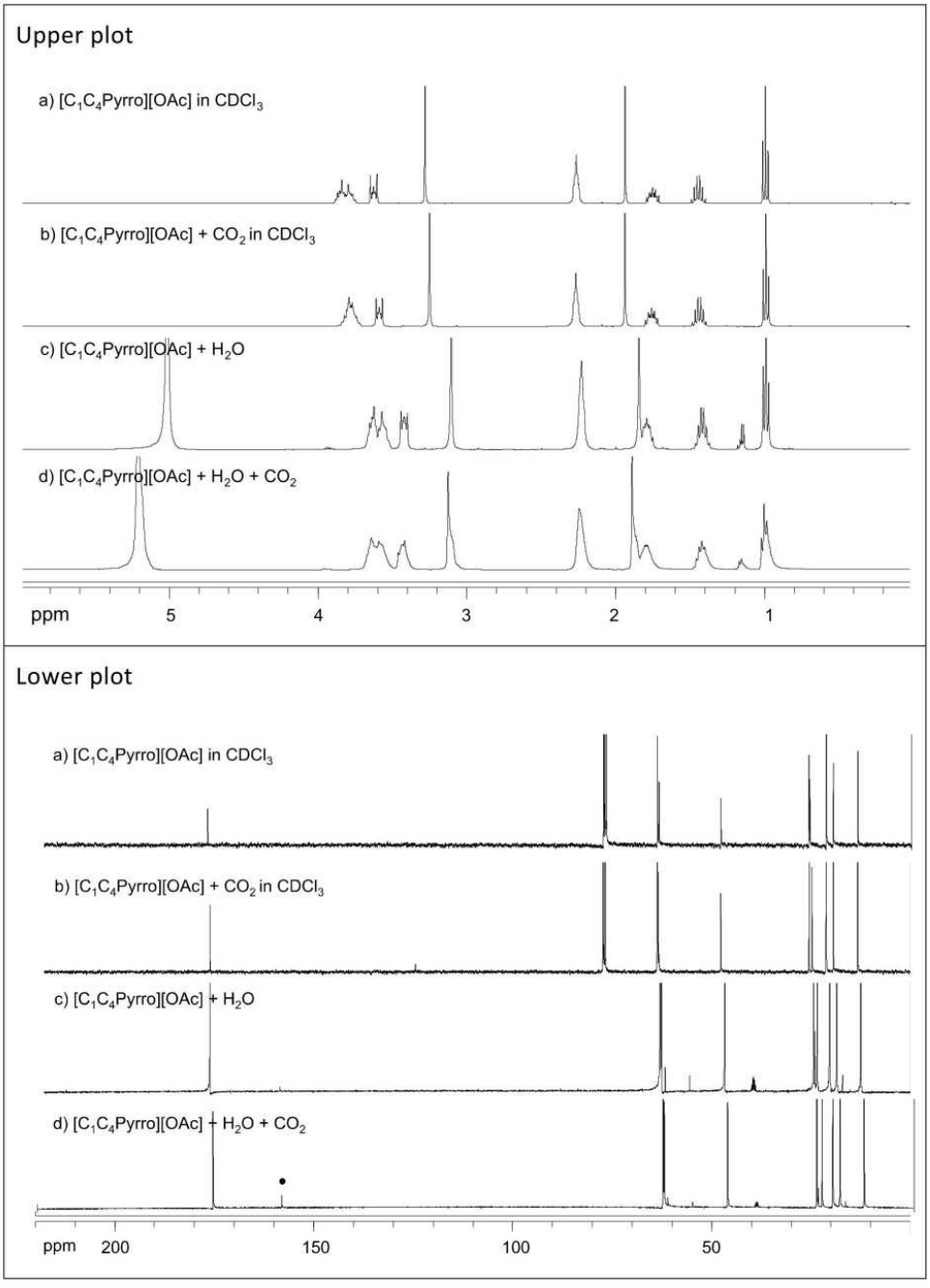

References

1 Costa Gomes, M. F.; Husson, P. *ACS Symposium Series* 1030 (16) (2010) 223.

2 Ramdin, M. ; de Loos, T.W. ; Vlugt, T.J.H. *Ind. Eng. Chem. Res.* **2012**, *51*, 8149-8177.

3 Bates, E. D.; Mayton, R. D.; Ntai, I.; Davis, J. H. J. *J. Am. Chem. Soc.* **2002**, *124*, 926.

4 Shiflett, M.; Drew, D.W.; Cantini, R.A.; Yokozeki, A. *Energy Fuels* **2010**, *24*, 5781.

5 Henley, E.J.; Seader, J.D.; Roper, D.K. Separation Process Principles, 3rd Ed., John Wiley & Sons, 2011.

6 Maginn, E.J., Quaterly Technical Report to DOE. USA., **2005**.

7 Shiflett, M.B; Kasprzak, D.J; Junk. C P. et al., *J. Chem. Thermodynamics* **2008**, *40*, 25.

8 Stevanovic, S.; Podgorsek, A.; Pádua, A. A. H.; Costa Gomes, M. F, submitted.

9 G. Gurau, H. Rodriguez, S.P. Kelley, P. Janiczek, R.S. Kalb, R.D. Rogers, *Angew. Chem. Int. Ed.* **2011**, 123, 12230-12232.

10 M. Besnard, M.I. Cabaço, F.V. Chavez, N. Pinaud, P.J. Sebastiao, J.A.P. Coutinho, Y. Danten, *Chem. Commun.* **2011**.

11 Greaves, T. L.; Brummond, C. J. *Chem. Rev.* **2008**, *108*, 206.

12 Yokozeki, A.; Shiflett, M.B.; Junk, C.P.; Grieco, L.M.; Foo, T. *J. Phys. Chem. B.* **2008**, *112*, 16654.

13 Yoshizawa-Fujita M. Johansson K. Newman P. MacFarlane D.R. Forsyth M., *Tetrahedron Lett.* **2006**, *47*, 2755-2758.

14 Shiflett, M. B.; Yokozeki, A.; Junk, C. P.; Grieco, L. M.; Foo, T. *J. Chem. Eng. Data* **2009**, *54*, 108.

15 Carvalho, P. J.; Alvarez, V. H.; Schroder, B.; Gil, A. M.; Marrucho, I.M.; Aznar, M.; Santos, L. M. N. B. F.; Coutinho, J. A. P. *J. Phys. Chem. B.* **2009**, *113*, 6803.

16 Cabaco, M.I.; Besnard, M.; Danten, Y.; Coutinho, J. A. P. CB, 2011, 115, 3538. *J. Phys. Chem. B.* **2011**, *115*, 3538.

17 Magna, L., Chauvin, Y., Niccolai, G.P. & Basset, J.-M. *Organometallics* **2003**, *22*, 4418.

18 Jacquemin, J.; Husson, P.; Padua, A. A. H.; Majer, V. *Green Chem.* **2006**, *8*, 172.

19 Jacquemin, J.; Husson, P.; Majer, V.; Cibulka, I. *J. Chem. Eng. Data* **2007**, *52*, 2204.

20 Schilling, G.; Kleinrahm, R.; Wagner, W. *J. Chem. Thermodyn.* **2008**, *40*, 1095.

21 Jacquemin, J.; Ge, R.; Nancarrow P.; Rooney, D. W.; Costa Gomes, M. F.; Padua, A. A. H.; Hardacre, C. *J. Chem. Eng. Data* **2008**, *53*, 716.

22 Jacquemin, J.; Nancarrow, P.; Rooney, D. W.; Costa Gomes, M. F.; Husson, Majer, V.; P.; Padua, A. A. H.; Hardacre, C. *J. Chem. Eng. Data* **2008**, *53*, 2133.

23 Jacquemin, J.; Costa Gomes, M.F.; Husson P.; Majer V., *J. Chem. Thermodyn.* **2006**, *38*, 490.

24 Jacquemin, J.; Husson, P.; Majer V.; Costa Gomes, M.F. *Fluid Phase Equilibr.* **2006**, *240*, 87.

25 G. Hong. J. Jacquemin. P. Husson. M.F. Costa Gomes. M. Deetlefs. M. Nieuwenhuyzen. O. Sheppard. C. Hardacre. *Ind. Eng. Chem. Res.*, 45, 8180-8188, **2006**.

26 P. Husson. L. Pison. J. Jacquemin. M.F. Costa Gomes. *Fluid Phase Equilib.* **2010**, *294*, 98.

27 W. F. Smith, T. R.; Todorov, I. T.; *The DL_POLY molecular simulation package*, 2.20; STFC Daresbury Laboratorys: Warrington, UK, 2007.

28 W. L. Jorgensen; D. S. Maxwell; J. TiradoRives, *J. Am. Chem. Soc.* **1996,** *118*, 11225.

29 J. N. C. Lopes; J. Deschamps; A. A. H. Padua, *J. Phys. Chem. B* **2004,** *108*, 2038.

30 R. C. Rizzo; W. L. Jorgensen, *J. Am. Chem. Soc.* **1999,** *121*, 4827.

31 Z. Y. Yu; M. P. Jacobson; J. Josovitz; C. S. Rapp; R. A. Friesner, *J. Phys. Chem. B* **2004,** *108*, 6643.

32 X. M. Liu; S. J. Zhang; G. H. Zhou; G. W. Wu; X. L. Yuan; X. Q. Yao, *J. Phys. Chem. B* **2006,** *110*, 12062.

33 J. Mallet; M. Molinari; F. Martineau; F. Delavoie; P. Fricoteaux; M. Troyon, *Nano Letters* **2008,** *8*, 3468.

34 W. F. Smith, T. R.; Todorov, I. T.; *The DL_POLY molecular simulation package*, 2.20; STFC Daresbury Laboratorys: Warrington, UK, 2007.

35 D. Almantariotis; T. Gefflaut; A. A. H. Padua; J. Y. Coxam; M. F. Costa Gomes, *J. Phys. Chem. B 114*, 3608.

36 K. Tomizaki, M. Kanakubo, H. Nanjo, S. Shimizu, M. Onoda, Y. Fujioka, *Ind. Eng. Chem. Res.* 2010, 49, 1222-1228.

37 G. Wang, W. Hou, F. Xiao, J. Geng, Y. Wu, Z. Zhang, *J. Chem. Eng. Data* 2011, 56, 1125-1133.

Absorption of carbon dioxide by ionic liquids with carboxylate anions

S. Stevanovic[1], A. Podgorsek[1], L. Moura[1,2], C.C. Santini[2], Agilio A. H. Padua[1], M.F. Costa Gomes[11]

[1]*Institut de Chimie de Clermont-Ferrand, Equipe Thermodynamique et Interactions Moléculaires, Clermont Université, Université Blaise Pascal, BP 80026, 63171 Aubière, France and CNRS, UMR6296 ICCF, BP 80026, 63171 Aubière, France*

[2]*Université de Lyon, Institut de Chimie de Lyon, UMR 5265 CNRS-Université de Lyon 1-ESCPE Lyon, C2P2, Equipe Chimie Organométallique de Surface, ESCPE 43 Boulevard du 11 Novembre 1918, 69616 Villeurbanne, France*

SUPPORTING INFORMATION

[1] Corresponding author : margarida.c.gomes@univ-bpclermont.fr

NMR chemical shifts of different samples of ionic liquids

1-butyl-3-methylimidazolium chloride, [C_1C_4Im][Cl]

^{1}H-NMR (400 MHz, CD_2Cl_2) δ (ppm): 10.76 (1H, s, CH-2), 7.64 (H, d, CH-4), 7.54 (H, d, CH-5), 4.31 (2H, t, N-CH_2), 4.07 (3H, s, N-CH_3), 1.88 (2H, m, N-CH_2-CH_2-), 1.37 (2H, m, N-CH_2-CH_2-CH_2-), 0.95 (3H, t, N-CH_2-CH_2-CH_2-CH_3)

^{13}C-NMR (400 MHz, CD_2Cl_2) δ (ppm): 138.2 (s, C-2), 123.4 (s, C-4), 121.9 (s, C-5), 49.5 (s, N-$CH_2(CH_2)_2CH_3$), 36.3 (s, N-CH_3), 32.0 (s, $NCH_2CH_2CH_2CH_3$), 19.4 (s, N-$(CH_2)_2CH_2CH_3$), 13.2 (s, $N(CH_2)_3CH_3$)

1-butyl-3-methylimidazolium levulinate, [C_1C_4Im][Lev]

^{1}H-NMR (400 MHz, CD_2Cl_2) δ (ppm): 8.62 (1H, s, CH-2), 7.38 (H, d, CH-4), 7.33 (H, d, CH-5), 4.09 (2H, t, N-CH_2), 3.76 (3H, s, N-CH_3), 2.67 (2H, t, CH_3-CO-CH_2-C**H**$_2$-COO), 2.30 (2H, t, CH_3-CO-C**H**$_2$-CH_2-COO), 2.11 (3H, s, C**H**$_3$-CO-CH_2-C**H**$_2$-COO), 1.74 (2H, m, N-CH_2-C**H**$_2$-), 1.22 (2H, m, N-CH_2-CH_2-C**H**$_2$-), 0.81 (3H, t, N-CH_2-CH_2-CH_2-C**H**$_3$)

^{13}C-NMR (400 MHz, CD_2Cl_2) δ: 214.8 (s, CH_3-**C**O-CH_2-CH_2-COO), 180.7 (s, CH_3-CO-CH_2-CH_2-**C**OO), 135.8 (s, C-2), 123.5 (s, C-4), 122.2 (s, C-5), 49.3 (s, N-**C**H$_2$$(CH_2)_2CH_3$), 39.4 (s, **C**H$_3$-CO-$CH_2$-$CH_2$-COO), 35.7 (s, N-$CH_3$), 31.2 (s, NCH_2**C**H$_2$$CH_2CH_3$), 31.0 (s, CH_3-CO-**C**H$_2$-CH_2-COO), 29.3 (s, CH_3-CO-CH_2-**C**H$_2$-COO), 18.8 (s, N-$(CH_2)_2$**C**H$_2$$CH_3$), 12.7 (s, $N(CH_2)_3$**C**H$_3$)

m/z (Fab+): 139 (100%) $[C_4C_1Im]^+$, 393 (20%) $[(C_4C_1Im)_2[LEV]^+$

1-butyl-3-methylpyrrolidinium acetate in the presence of water and $NaHCO_3$, [C_1C_4Pyrro][OAc] + H_2O + $NaHCO_3$

^{1}H NMR (insert NMR, DMSO-d6, ppm): δ 0.99 (t, *J* = 7.4 Hz, 3H), **1.14-1.18 (m)**, 1.41 (sext, J = 7.4 Hz, 2H), 1.75-1.83 (m, 2H), *1.83* (s, 3H), 2.27 (s, 3H), **3.10 (s, 3H)**, 3.40-3.44 (m, 2H), 3.54-3.63 (m, 4H), **5.01 (s, H(H_2O))**. ^{13}C NMR (insert NMR, DMSO-d6, ppm): δ 12.5, **18.5**, 20.3, 23.5, **24.3**, 46.7, ***62.5***, *62.9*, **158.4**, 175.9.

1-butyl-3-methylpyrrolidinium acetate in the presence of water and $NaHCO_3$, saturated with carbon dioxide, [C_1C_4Pyrro][OAc] + H_2O + $NaHCO_3$ + CO_2

^{1}H NMR (insert NMR, DMSO-d6, ppm): δ 0.99 (t, *J* = 7.4 Hz, 3H), **1.14-1.18 (m)**, 1.41 (sext, *J* = 7.4 Hz, 2H), 1.75-1.83 (m, 2H), *1.85* (s, 3H), 2.25 (s, 3H), **3.09 (s, 3H)**, 3.37-3.40 (m, 2H), 3.54-3.63 (m, 4H), **5.00 (s, H(H_2O))**. ^{13}C NMR (insert NMR, DMSO-d6, ppm): δ 12.5, **18.5**, 20.3, 23.4, **24.3**, 46.8, ***62.7***, *63.0*, **158.6**, 176.7.

Figure S-1

^{1}H NMR spectra (upper plot) and ^{13}C NMR spectra (lower plot) of $[C_1C_4Pyrro][OAc]$ in the presence of $NaHCO_3$.

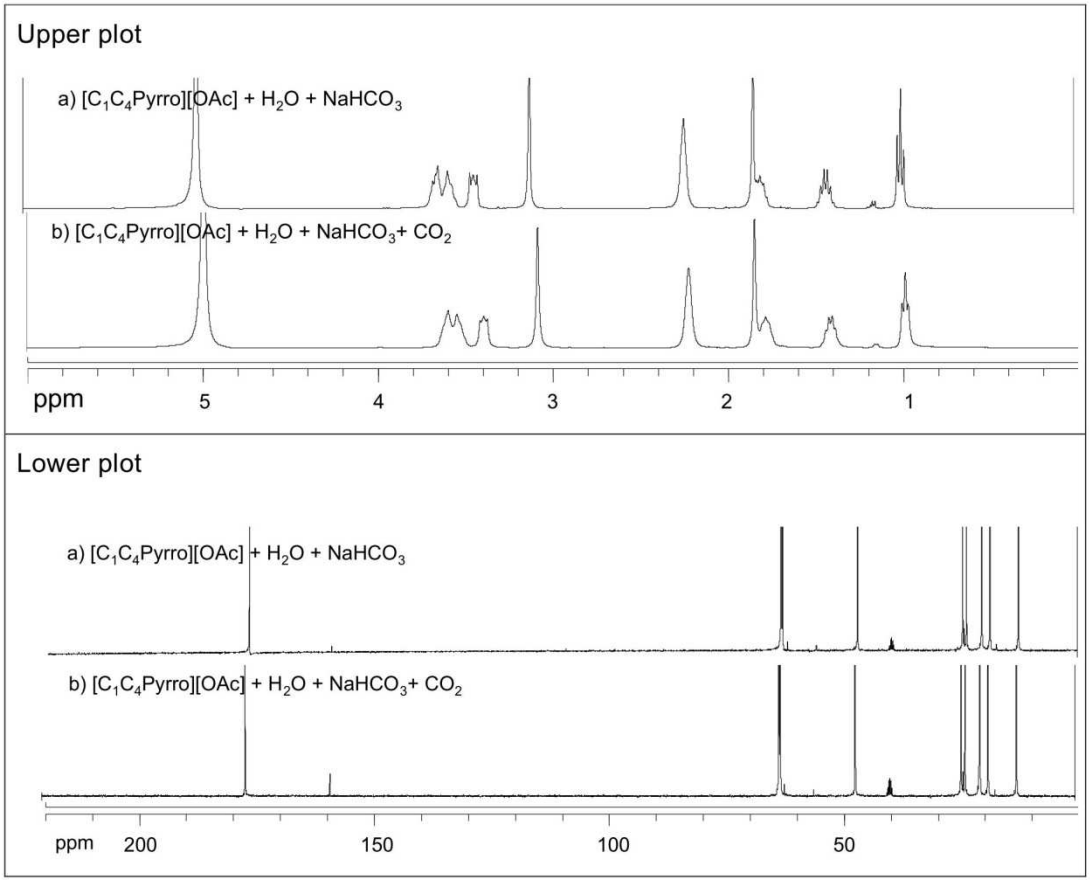

Table S- 2

Experimental Densities, ρ, of the ionic liquids $[C_1C_4Im][LEV]$ and $[C_1C_4Pyrro][OAc]$ + water mixtures between 293 K and 353 K and up to 25 MPa.

T/K	$\rho/kg\cdot m^{-3}$	$\delta/\%$	T/K	$\rho/kg\cdot m^{-3}$	$\delta/\%$
		$[C_1C_4Im][LEV]$			
	p = 0.10 ± 0.01 MPa				
303.11	1096.4	0.005			
313.17	1090.3	-0.003			
323.22	1084.2	-0.007			
333.17	1078.0	0.006			
		$[C_1C_4Pyrro][OAc]$+water (x_{water}=0.4077)			
	p = 0.10 ± 0.01 MPa			p = 0.50 ± 0.01 MPa	
293.47	1020.0	0.003	293.32	1019.2	0.045
303.15	1014.4	0.010	303.22	1014.2	-0.006
313.22	1009.1	-0.031	313.22	1009.3	-0.062
323.17	1003.1	0.008	323.18	1003.2	-0.010
333.17	997.3	0.015	333.18	997.5	0.011
343.17	991.8	0.005	343.17	991.9	0.011
353.11	986.3	-0.009	353.11	986.4	0.010
	p = 1.00 ± 0.01 MPa			p = 2.50 ± 0.01 MPa	
293.32	1019.7	0.022	293.31	1020.4	0.010
303.22	1014.5	-0.010	303.22	1015.0	-0.013
313.23	1009.1	-0.035	313.24	1009.4	-0.022
323.17	1003.1	0.006	323.19	1003.3	0.018
333.19	997.3	0.017	333.20	997.6	0.020

343.18	991.8	0.007	343.18	992.1	0.001
353.11	986.4	-0.007	353.13	986.6	-0.014
	p = 5.00 ± 0.01 MPa			p = 10.00 ± 0.01 MPa	
293.30	1021.2	0.005	293.27	1022.7	0.000
303.22	1015.8	-0.013	303.23	1017.2	-0.012
313.25	1010.1	-0.016	313.26	1011.5	-0.012
323.20	1004.1	0.021	323.20	1005.5	0.023
333.20	998.4	0.018	333.23	999.9	0.023
343.19	992.9	0.003	343.20	994.5	0.000
353.13	987.5	-0.018	353.13	989.1	-0.020
	p = 15.00 ± 0.01 MPa			p = 20.00 ± 0.01 MPa	
293.26	1024.4	-0.001	293.27	1026.1	-0.002
303.22	1019.0	-0.013	303.22	1020.7	-0.012
313.27	1013.3	-0.010	313.28	1015.1	-0.010
323.21	1007.4	0.024	323.21	1009.2	0.025
333.23	1001.8	0.021	333.23	1003.7	0.020
343.20	996.4	0.000	343.21	998.3	0.000
353.14	991.0	-0.020	353.14	993.0	-0.021
	p = 25.00 ± 0.01 MPa				
293.26	1027.8	-0.002			
303.23	1022.4	-0.014			
313.30	1016.8	-0.009			
323.22	1011.0	0.026			
333.23	1005.5	0.019			
343.22	1000.2	0.001			
353.13	994.9	-0.022			

293.26	1027.8	-0.002			
[C_1C_4Pyrro][OAc]+water (x_{water}=0.6028)					
	p = 0.10 ± 0.01 MPa			p = 0.50 ± 0.01 MPa	
293.31	1026.7	0.020	293.32	1027.2	-0.001
303.18	1021.4	-0.029	303.19	1021.6	-0.014
313.15	1015.4	-0.008	313.15	1015.5	0.003
323.19	1009.3	0.010	323.19	1009.4	0.016
333.17	1003.5	0.010	333.18	1003.7	0.006
343.10	997.7	0.006	343.11	997.8	0.006
353.18	991.9	-0.010	353.20	992.1	-0.016
	p = 1.00 ± 0.01 MPa			p = 2.50 ± 0.01 MPa	
293.31	1027.1	-0.004	293.29	1027.2	-0.028
303.21	1021.4	-0.010	303.22	1021.4	-0.018
313.15	1015.4	0.003	313.15	1015.7	0.008
323.19	1009.3	0.017	323.19	1009.9	0.035
333.18	1003.5	0.005	333.19	1004.1	0.036
343.10	997.7	0.007	343.09	998.4	0.050
353.21	992.0	-0.017	353.21	992.6	-0.084
	p = 5.00 ± 0.01 MPa			p = 10.00 ± 0.01 MPa	
293.28	1028.1	-0.007	293.28	1029.3	-0.006
303.22	1022.3	-0.010	303.21	1023.6	-0.012
313.14	1016.3	0.003	313.14	1017.7	0.004
323.19	1010.3	0.019	323.20	1011.6	0.020
333.19	1004.5	0.007	333.21	1005.9	0.008
343.08	998.7	0.006	343.08	1000.2	0.006
353.20	993.0	-0.019	353.20	994.6	-0.020

	p = 15.00 ± 0.01 MPa			p = 20.00 ± 0.01 MPa	
293.28	1031.0	-0.008	293.28	1032.6	-0.008
303.21	1025.3	-0.011	303.21	1026.9	-0.011
313.15	1019.4	0.005	313.15	1021.1	0.005
323.20	1013.4	0.020	323.20	1015.2	0.021
333.22	1007.7	0.009	333.24	1009.5	0.008
343.09	1002.1	0.006	343.10	1003.9	0.010
353.21	996.5	-0.022	353.19	998.4	-0.024
	p = 25.00 ± 0.01 MPa				
293.27	1034.2	-0.011			
303.23	1028.5	-0.009			
313.16	1022.7	0.007			
323.20	1016.9	0.022			
333.23	1011.3	0.008			
343.11	1005.7	0.003			
353.20	1000.2	-0.020			
	$[C_1C_4Pyrro][OAc]$+water (x_{water}=0.8027)				
	p = 0.10 ± 0.01 MPa			p = 0.50 ± 0.01 MPa	
293.14	1036.8	0.011	293.13	1037.0	0.011
303.16	1030.4	-0.013	303.22	1030.5	-0.014
313.15	1023.6	0.000	313.15	1023.7	-0.001
323.17	1016.9	-0.002	323.15	1017.0	0.000
333.14	1010.2	-0.001	333.14	1010.3	0.001
343.17	1003.5	0.003	343.18	1003.6	0.003
353.16	996.8	0.002	353.14	997.0	0.000
	p = 1.00 ± 0.01 MPa			p = 2.50 ± 0.01 MPa	

293.13	1036.9	0.004	293.14	1037.1	0.006
303.22	1030.3	-0.008	303.22	1030.5	-0.011
313.16	1023.6	0.003	313.16	1023.8	-0.001
323.17	1016.9	0.004	323.15	1017.1	0.005
333.09	1010.4	-0.007	333.17	1010.4	0.005
343.17	1003.6	0.002	343.17	1003.7	0.001
353.14	996.9	0.002	353.17	997.1	-0.004
	p = 5.00 ± 0.01 MPa			p = 10.00 ± 0.01 MPa	
293.15	1037.7	0.003	293.14	1038.8	0.003
303.21	1031.1	-0.008	303.22	1032.3	-0.007
313.17	1024.4	-0.002	313.16	1025.7	-0.003
323.15	1017.7	0.007	323.13	1019.0	0.008
333.15	1011.1	0.003	333.16	1012.4	0.005
343.19	1004.5	0.002	343.19	1005.9	0.001
353.15	997.9	-0.006	353.15	999.4	-0.006
	p = 15.00 ± 0.01 MPa			p = 20.00 ± 0.01 MPa	
293.15	1040.3	0.002	293.15	1043.8	0.045
303.18	1033.9	-0.007	303.19	1037.3	-0.001
313.16	1027.3	-0.002	313.17	1031.0	-0.051
323.13	1020.7	0.007	323.14	1024.4	-0.083
333.15	1014.2	0.005	333.15	1015.9	0.078
343.20	1007.6	0.002	343.17	1009.4	0.032
353.14	1001.2	-0.007	353.14	1003.1	-0.020
	p = 25.00 ± 0.01 MPa				
293.15	1043.3	-0.003			
303.19	1036.9	-0.003			

313.20	1030.5	-0.002
323.16	1023.9	0.012
333.15	1017.6	0.005
343.18	1011.2	0.001
353.17	1004.8	-0.009

5. RESULTATS ET CONCLUSIONS

5.1 Caractérisation des systèmes

Les mesures de caractérisation des liquides ioniques purs préalables aux mesures d'absorption de gaz sont regroupées dans le Tableau 4. La quantité d'eau mesurée correspond à la quantité d'eau présente après dégazage du liquide ionique étudié.

Tableau 4. Caractéristiques des liquides ioniques purs.

Liquide ionique	T_{fus}/ K	$T_{déc}$/ K	Quantité d'eau / ppm	Limite miscibilité avec eau (x_{H2O})
$[C_1C_2Im][OAc]$		423	500	Miscible
$[C_1C_4Im][OAc]$		433	600	Miscible
$[C_1C_4Pyrro][OAc]$	353	518	518	Miscible
$[C_1C_4Im][LEV]$		448	365	Miscible
$[C_1C_4Im][eFAP]$		580	10	0.20 à 303 K
$[C_1C_4Pyrro][eFAP]$		503	15	Non mesurée
$[P_{66614}][eFAP]$		473	< 5	0.22 à 303 K

5.2 Masse volumique

La masse volumique des différents systèmes liquides ioniques purs et liquides ioniques + eau a été déterminée en fonction de la température et de la pression. L'utilisation du modèle de contribution de groupe développé par Jacquemin et al.[63,64] a également permis de prédire la densité du $[C_1C_4Pyrro][OAc]$ pur.

Les masses volumiques des différents systèmes étudiés, à 303.15 K et à pression atmosphérique sont regroupées dans la figure suivante.

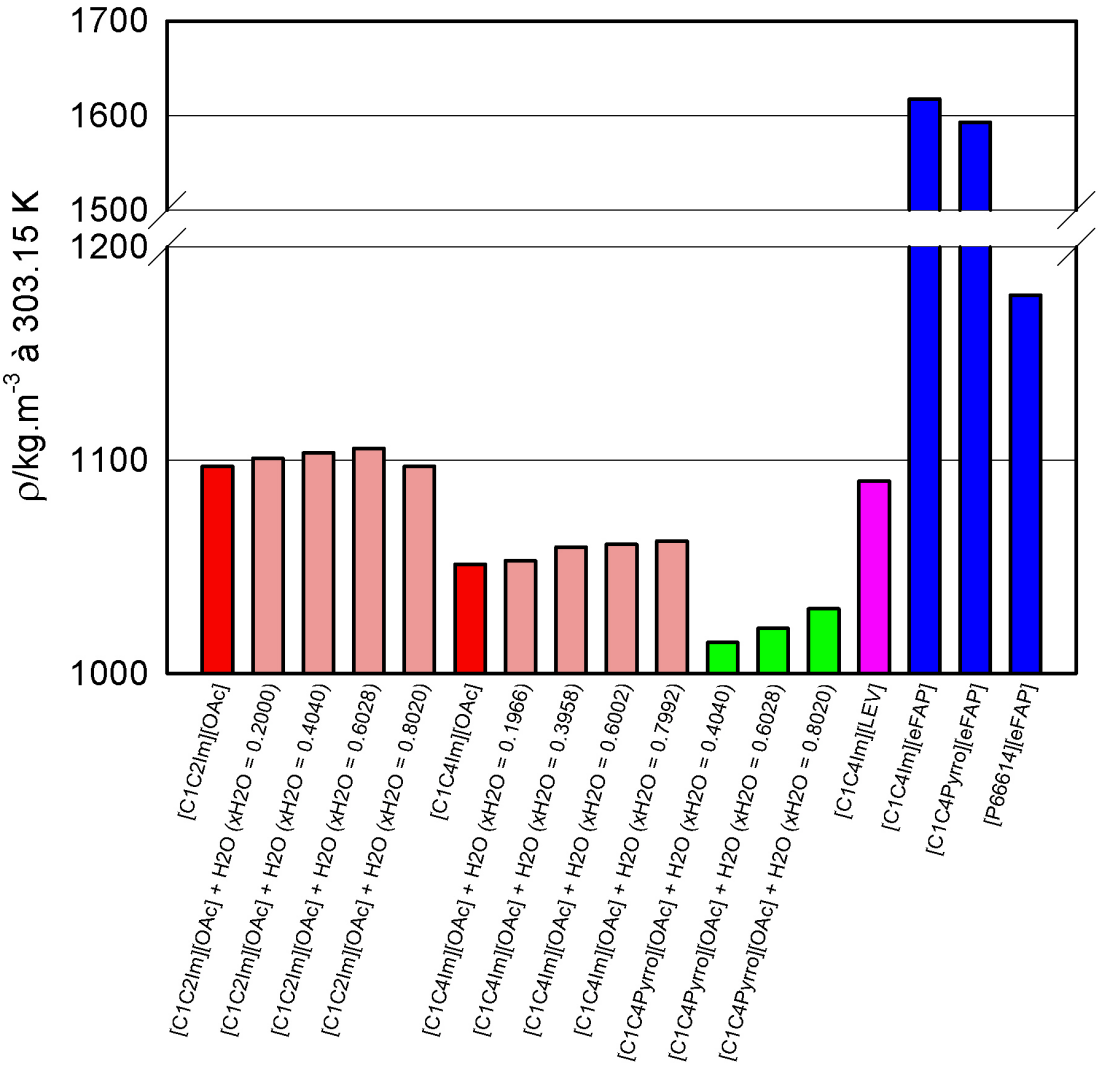

Figure 18. Densité des liquides ioniques purs et des mélanges binaires liquide ionique + eau à 303.15 K et à pression atmosphérique.

La masse volumique des liquides ioniques possédant un anion identique varie en fonction du cation présent. En effet, la diminution de la longueur de la chaine alkyle des cations imidazolium entraîne une augmentation de la densité, celle ci étant 4.37 % plus élevée dans le $[C_1C_2Im][OAc]$ que dans le $[C_1C_4Im][OAc]$. Les liquides ioniques contenant un cation imidazolium ou pyrrolidinium présentent une masse volumique supérieure aux liquides ioniques possédant un cation de type phosphonium. C'est le cas des liquides ioniques avec l'anion eFAP, la masse volumique du $[P_{66614}][eFAP]$ étant 26.08 et 27.22 % inferieure à celle du $[C_1C_4Pyrro][eFAP]$ et du $[C_1C_4Im][eFAP]$, respectivement. Les liquides ioniques avec un cation imidazolium restent toutefois légèrement plus denses que ceux avec un cation pyrrolidinium, que ce soit dans le cas des liquides ioniques avec un anion eFAP ou un anion OAc.

A cation équivalent, les liquides ioniques les plus denses sont ceux possédant l'anion eFAP suivi par les liquides ioniques avec anion LEV puis l'anion OAc, la masse volumique du $[C_1C_4Im][eFAP]$ étant 48.37 et 53.88 % plus importante que celle du $[C_1C_4Im][LEV]$ et du $[C_1C_4Im][OAc]$, respectivement.

L'ajout d'eau entraîne une augmentation de la masse volumique dans les deux systèmes $[C_1C_4Im][OAc]$ + eau et $[C_1C_4Pyrro][OAc]$ + eau, ceci jusqu'à la fraction maximale d'eau étudiée. Le cas du système $[C_1C_2Im][OAc]$ + eau diffère légèrement, l'augmentation de la masse volumique se faisant jusqu'à une fraction molaire d'eau de 0.6 avant de rediminuer pour les fractions molaires d'eau plus élevées.

5.3 Viscosité

La viscosité des différents systèmes liquides ioniques purs et liquides ioniques + eau a été déterminée à pression atmosphérique et en fonction de la température.

Comme précédemment, les valeurs de viscosités des différents systèmes, à 303.15 K et à pression atmosphérique, sont regroupées dans la figure ci dessous.

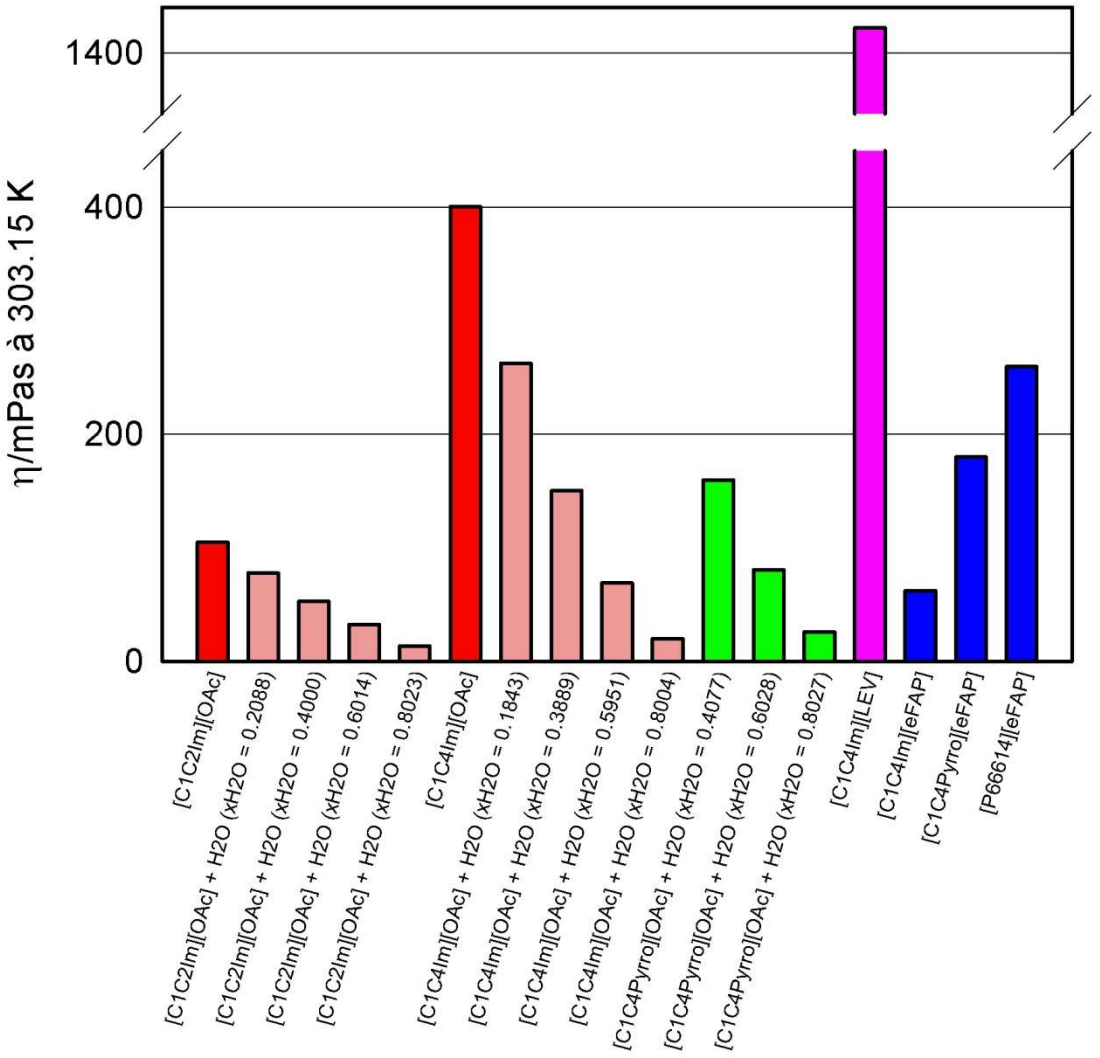

Figure 19. Viscosité des liquides ioniques purs et des mélanges binaires liquide ionique + eau à 303.15 K et à pression atmosphérique.

Parmi les liquides ioniques possédant un même cation, les plus visqueux sont les liquides ioniques contenant l'anion carboxylate et plus particulièrement le levulinate, la viscosité des liquides ioniques avec l'anion eFAP étant nettement plus faible. Ainsi,

le $[C_1C_4Im][LEV]$ est 3.6 et 23.1 fois plus visqueux que le $[C_1C_4Im][OAc]$ et que le $[C_1C_4Im][eFAP]$, respectivement.

A anion identique, les liquides ioniques avec un cation pyrrolidinium ou phosphonium sont plus visqueux que ceux avec un cation de type imidazolium. Le $[P_{66614}][eFAP]$ est 1.4 et 4.2 fois plus visqueux que le $[C_1C_4Pyrro][eFAP]$ et le $[C_1C_4Im][eFAP]$.

La présence d'eau entraîne une diminution de la viscosité dans les trois systèmes liquides ioniques + eau étudiés. Le système $[C_1C_4Pyrro][OAc]$ + eau est le plus visqueux des trois, la viscosité de ce système étant 1.06 et 3.03 fois plus importante que celle des systèmes $[C_1C_4Im][OAc]$ + eau et $[C_1C_2Im][OAc]$ + eau pour une fraction molaire d'eau donnée et égale à 0.4.

5.4 Absorption et propriétés thermodynamiques des gaz

Les mesures d'absorption de gaz ont été effectuées dans une gamme de températures comprises entre 303.15 et 353.15 K et à des pressions proches de la pression atmosphérique, les conditions pouvant varier en fonction des contraintes liées aux différents systèmes étudiés.

L'ensemble des mesures d'absorption de gaz effectuées sont regroupées dans le tableau ci-dessous.

Tableau 5. Systèmes solvant-solutés étudiés

Système	Gaz
$[C_1C_2Im][OAc]$	CO_2
$[C_1C_2Im][OAc]$ + eau	CO_2
$[C_1C_4Im][OAc]$	CO_2, N_2, N_2O
$[C_1C_4Im][OAc]$ + eau	CO_2
$[C_1C_4Im][LEV]$	CO_2
$[C_1C_4Pyrro][OAc]$	CO_2
$[C_1C_4Pyrro][OAc]$ + eau	CO_2
$[C_1C_4Im][eFAP]$	CO_2, N_2, N_2O, C_2H_6
$[C_1C_4Pyrro][eFAP]$	CO_2, N_2, N_2O, C_2H_6
$[P_{66614}][eFAP]$	CO_2, N_2, N_2O, C_2H_6

Les caractéristiques des gaz utilisés figurent ci-dessous.

Tableau 6. Caractéristiques des gaz utilisés

Gaz	Pureté (fraction molaire)	Fournisseur
Dioxyde de carbone (CO_2)	0.99995	AGA / Linde Gaz
Azote (N_2)	0.998	SAGA
Protoxyde d'azote (N_2O)	0.995	Linde
Ethane (C_2H_6)	0.995	AGA / Linde Gaz

Les résultats d'absorption de gaz sont exprimés en fraction molaire de gaz, chaque fraction molaire de gaz étant associée à une pression expérimentale d'équilibre. Deux cas de figure sont alors possibles. Premièrement, l'absorption de dioxyde de carbone dans le système étudié est liée uniquement à des phénomènes de type physique. Il est alors possible de calculer les constantes de Henry à partir des données expérimentales d'absorption puis de recalculer les fractions molaires de gaz à

1 bar. La connaissance des constantes de Henry donne également accès aux propriétés thermodynamiques de solvatation telles que l'énergie de Gibbs, l'enthalpie et l'entropie de solvatation. Dans le deuxième cas, l'absorption de dioxyde de carbone est liée à la fois aux phénomènes de solubilité mais également à la réaction chimique entre le gaz et le liquide ionique. L'application de la seule loi de Henry dans ce second cas ne permet pas de décrire correctement le comportement de l'absorption du dioxyde de carbone, la constante d'équilibre de la réaction chimique devant également être prise en compte. Les résultats d'absorption n'étant pas ramené à un bar dans ce cas, nous considérerons par la suite que la variation de la pression expérimentale d'équilibre n'a pas d'influence significative sur les valeurs d'absorption dans de tels systèmes afin de pouvoir comparer les différents résultats obtenus.

5.4.1 Absorption de gaz dans les liquides ioniques avec anions eFAP

Les résultats de solubilité à 303.15 K des différents gaz étudiés dans les liquides ioniques avec l'anion eFAP sont présentés dans les deux graphiques suivants. Afin de supprimer l'influence de la différence de masse molaire des différents liquides, les résultats préalablement exprimés en fraction molaire de gaz sont calculés en fraction massique.

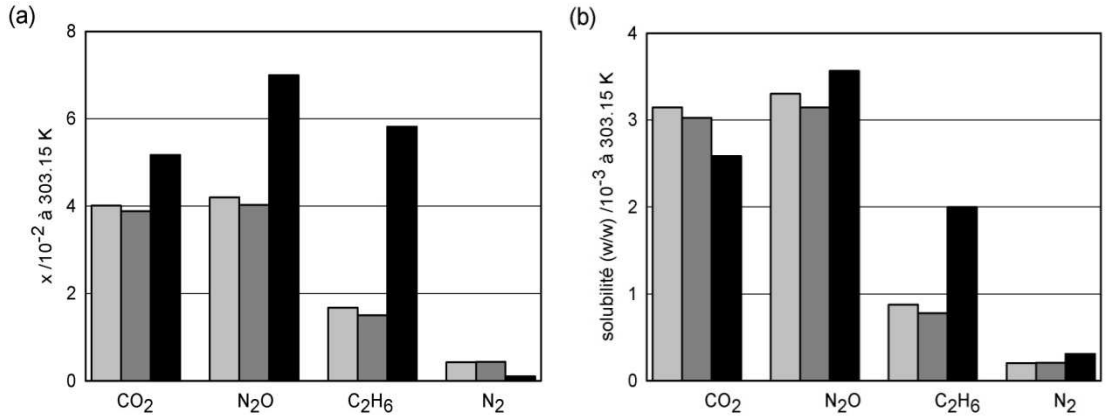

Figure 20. Solubilité de dioxyde de carbone, de protoxyde d'azote, d'éthane et d'azote exprimée en fraction molaire de gaz (a) et en fraction massique (b) dans les liquides ioniques avec anion eFAP, à 303.15 K et à 1 bar: ■, [C_1C_4mim][eFAP]; ■, [C_1C_4Pyrro][eFAP]; ■, [P_{66614}][eFAP].

Le dioxyde de carbone et le protoxyde d'azote sont les deux gaz les plus solubles dans les trois liquides ioniques. L'éthane est deux à trois fois moins soluble que les deux gaz précédents. La solubilité de l'azote est un ordre de grandeur inferieur aux deux gaz les plus solubles.

Dans le cas des systèmes ne réagissant pas chimiquement, les propriétés thermodynamiques de solvatation ont été calculées et figurent dans le tableau suivant.

Tableau 7. Propriétés thermodynamiques de solvatation du dioxyde de carbone, du protoxyde d'azote, de l'éthane et de l'azote des liquides ioniques avec anion eFAP.

Gaz	$-\Delta_{sol}H$ / kJ·mol^{-1}	$-\Delta_{sol}S$ / J·mol^{-1}·K^{-1}
	[C_1C_4Im][eFAP]	
CO_2	12.5 ± 0.1	68.0 ± 0.5
N_2O	11 ± 4	63 ± 9
C_2H_6	10 ± 1	68 ± 2
N_2	4 ± 1	58 ± 4
	[C_1C_4Pyrro][eFAP]	
CO_2	12.5 ± 0.3	68.1 ± 0.9
N_2O	12.0 ± 0.2	66.0 ± 0.6
C_2H_6	8 ± 1	61 ± 3
N_2	4 ± 1	58 ± 3
	[P_{66614}][eFAP]	
CO_2	9.7 ± 0.2	56.7 ± 0.6
N_2O	10.5 ± 0.2	56.9 ± 0.8
C_2H_6	12 ± 1	62 ± 3
N_2	4 ± 3	52 ± 8

La solubilité plus importante du dioxyde de carbone et du protoxyde d'azote dans les liquides ioniques [C_1C_4Im][eFAP] et [C_1C_4Pyrro][eFAP] est expliquée par des valeurs d'enthalpies plus favorables que pour l'éthane et l'azote. La différence de solubilité des différents gaz dans le [P_{66614}][eFAP] est essentiellement contrôlée par le terme entropique.

Les interactions entre l'éthane et le liquide ionique sont plus favorables dans le [P_{66614}][eFAP] que dans les deux autres liquides ioniques ce qui explique la solubilité plus importante de ce gaz dans le [P_{66614}][eFAP]. A l'inverse, ce sont les contributions entropiques qui contrôlent la solubilité de l'azote, le [P_{66614}][eFAP] présentant une valeur d'entropie plus négative que le [C_1C_4Im][eFAP] et le [C_1C_4Pyrro][eFAP].

5.4.2 Absorption de gaz dans les liquides ioniques avec anions carboxylates

Les résultats d'absorption des différents gaz dans les systèmes basés sur les anions carboxylates sont regroupés dans la Figure 21.

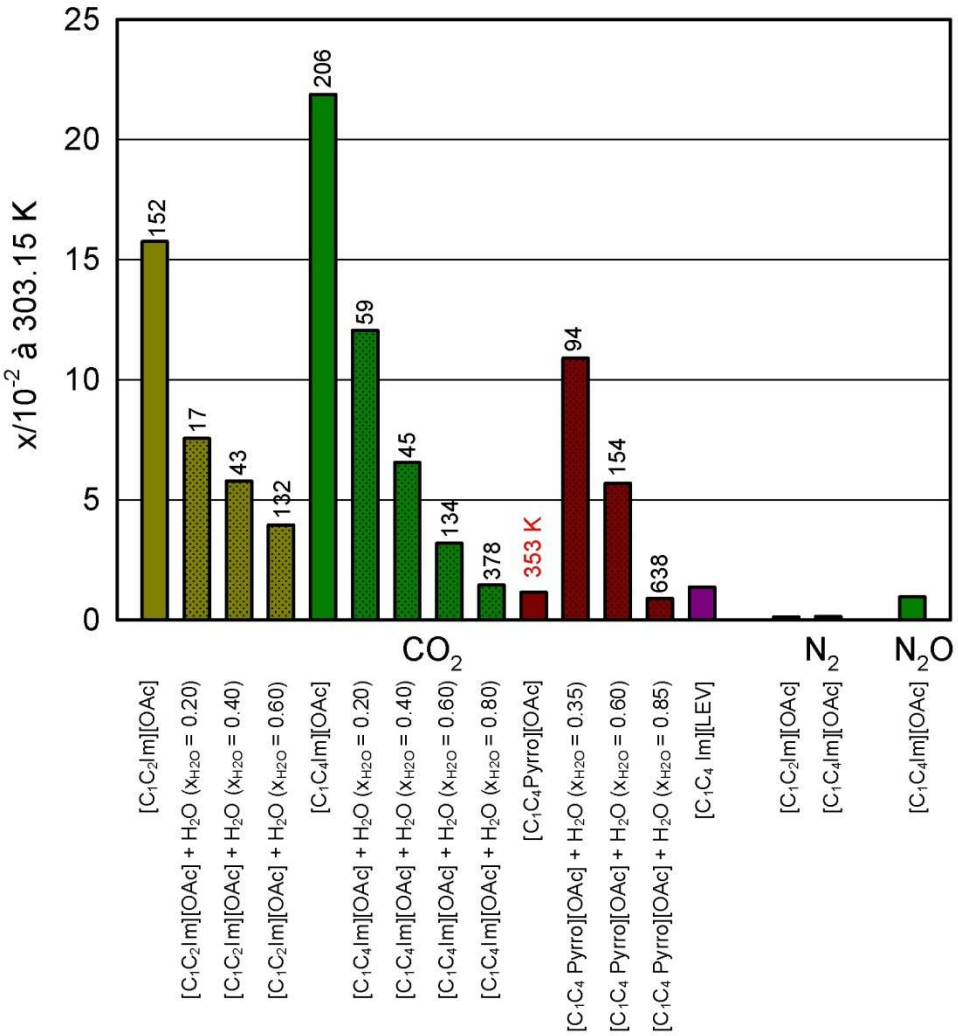

Figure 21. Absorption de dioxyde de carbone, de protoxyde d'azote et d'azote exprimée en fraction molaire de gaz dans les liquides ioniques avec anion carboxylate, à 303.15 K et à 1 bar. (L'absorption de dioxyde de carbone dans le [C_1C_4Pyrro][OAc] est mesurée à 353 K (en rouge) et les valeurs en noir correspondent aux pressions d'équilibre lorsque la fraction molaire de gaz n'est pas ramenée à 1 bar).

L'absorption de dioxyde de carbone dans le [C_1C_2Im][OAc] et le [C_1C_4Im][OAc] est un ordre de grandeur supérieure à celle dans le [C_1C_4Pyrro][OAc] et le [C_1C_4Im][LEV]. L'augmentation de la quantité d'eau dans les systèmes [C_1C_2Im][OAc] + eau, [C_1C_4Im][OAc] + eau et [C_1C_4Pyrro][OAc] + eau entraîne une diminution de

l'absorption de dioxyde de carbone. La comparaison de l'absorption du dioxyde de carbone dans le $[C_1C_2Im][OAc]$ et le $[C_1C_4Im][OAc]$ montre qu'elle augmente avec la longueur de la chaine alkyle, que ce soit dans les liquides ioniques purs ou dans les systèmes liquides ioniques + eau.

L'absorption plus importante de dioxyde de carbone dans les cinq systèmes $[C_1C_2Im][OAc]$, $[C_1C_4Im][OAc]$, $[C_1C_2Im][OAc]$ + eau, $[C_1C_4Im][OAc]$ + eau et $[C_1C_4Pyrro][OAc]$ + eau est expliquée par l'existence de réaction chimique avec le gaz, cette réaction étant différente en présence ou en absence d'eau.

L'absorption de gaz dans le $[C_1C_4Pyrro][OAc]$ pur étant uniquement physique, la réaction chimique entre le dioxyde de carbone et les liquides ioniques purs implique le cation imidazolium.

L'absorption du protoxyde d'azote et de l'azote dans le $[C_1C_4Im][OAc]$ est un ordre et deux ordres de grandeur inférieure à celle du dioxyde de carbone.

5.4.3 Comparaison de l'absorption de gaz dans les différents systèmes étudiés

L'absorption de dioxyde de carbone dans les liquides ioniques $[C_1C_2Im][OAc]$ et $[C_1C_4Im][OAc]$ est supérieure d'un ordre de grandeur à celle dans les liquides ioniques basés sur l'anion eFAP, cette différence étant due aux différences dans les mécanismes contrôlant l'absorption. A l'inverse, l'absorption de protoxyde d'azote est environ quatre fois plus élevée dans les liquides ioniques avec un anion eFAP que dans le $[C_1C_4Im][OAc]$. L'absorption de l'azote est quand à elle environ trois fois plus importante dans le $[C_1C_2Im][OAc]$ et le $[C_1C_4Im][OAc]$ que dans les liquides ioniques avec l'anion eFAP.

Par conséquent, la sélectivité des liquides ioniques de type imidazolium acétate pour l'absorption de dioxyde de carbone par rapport au protoxyde d'azote est bien meilleure, environ quinze fois supérieure à celle des liquides ioniques avec anion eFAP. La sélectivité pour l'absorption de dioxyde de carbone par rapport à l'azote est quand à elle du même ordre de grandeur pour les deux familles de liquides ioniques étudiés.

Références

1 GIEC, Changements climatiques 2007, Rapport de synthèse, http://www.ipcc.ch/pdf/assessment-report/ar4/syr/ar4_syr_fr.pdf.

2 Protocole de Kyoto, http://unfccc.int/resource/docs/convkp/kpeng.pdf.

3 Captage et stockage géologique de CO_2 CSC, Techniques de l'ingénieur, **2011**, *IN 115*, 1-14.

4 Anhelen, M.; Yan, J.; De Smedt, G., *Oil Gas Sci. Technol.* **2005**, *60*, 485.

5 Eide, L.; Bailey, D. W., *Oil Gas Sci. Technol.* **2005**, *60*, 475.

6 Bailey, D. W.; Feron, P. H. M., *Oil Gas Sci. Technol.* **2005**, *60*, 461.

7 Keskin, S.; Kayrak-Talay, D.; Akman, U.; Hortacsu, O. *J. Supercrit. Fluids* **2007**, *43*, 150.

8 Crosthwaite, J. M.; Muldoon, M. J.; Dixon, J. K.; Anderson, J. L.; Brennecke, J. F. *J. Chem. Thermodyn.* **2005**, *37*, 559.

9 Domanska, U. Ionic Liquids in Chemical Analysis, Koel, M. (Ed.), Taylor & Francis Group, New York, **2009**, 1-71.

10 Coleman, D.; Gathergood, J.A., *Chem. Soc. Rev.*, **2010**, *39*, 600.

11 Seddon, K. R.; Stark, A.; Torres, M. J. *Pure Appl. Chem.* **2000**, *72*, 2275.

12 Seki, S.; Kobayashi, T.; Kobayashi, Y.; Takei, K.; Miyashiro, H.; Hayamizu, K.; Tsuzuki, S.; Mitsugi, T.; Umebayashi, Y. *J. Mol. Liq.* **2010**, *152*, 9-13.

13 Trulove, P. C.; Mantz, R. A. Ionic liquids in synthesis 2nd ed., Wasserscheid, P.; Welton, T. (Eds.), Wiley-VCH Verlag, **2008**, 56.

14 Holbrey, J. D.; Rogers, R. D. Ionic liquids in synthesis 1st ed, Wasserscheid, P.; Welton, T. (Eds.), Wiley-VCH Verlag, **2003**, 41.

15 Maase, M. Ionic liquids in synthesis 1st ed, Wasserscheid, P.; Welton, T. (Eds.), Wiley-VCH Verlag, **2003**, 663.

16 Almantariotis, D.; Gefflaut, T.; Pádua, A. A. H.; Coxam, J.-Y.; Costa Gomes, M. F. *J. Phys. Chem. B* **2010**, *114*, 3608.

17 Blanchard, L. A.; Hancu, D.; Beckman, E.J.; Brennecke, J. F., *Nature* **1999**, *399*, 2829.

18 Ionic liquids in synthesis 1st ed., Wasserscheid, P.; Welton, T., *Wiley-VCH Verlag*, **2003**, 81.

19 Hasib-ur-Rahman, M.; Siaj, M.; Larachi, F. *Chem. Eng. Process*. **2010**, *49*, 313.

20 Karadas, F.; Atilhan, M.; Aparicio, S., *Energ. Fuel*, **2010**, *24*, 5817.

21 Ramdin, M.; W. De Loos, T.; Vlugt, J. H., *Ind. Eng. Chem. Res.* **2012**, *51*, 8149.

22 Zhao, Z.; Dong, H.; Zhang X., *Chinese J. Chem. Eng.*, **2012**, *20*, 120.

23 Ignat'ev, N. V.; Welz-Biermann, U.; Kucheryna, A.; Bissky, G.; Willner, H. *J. Fluorine Chem.* **2005**, *126*, 1150.

24 Maginn, E.J., Quaterly Technical Report to DOE. USA., 2005.

25 Muldoon, M. J.; Aki, S. N. V. K.; Anderson, J. L.; Dixon, J. K.; Brennecke, J. F. *J. Phys. Chem. B* **2007**, *111*, 9001.

26 Yokozeki, A.; Shiflett, M. B.; Junk, C. P.; Grieco, L. M.; Foo, T. *J.Phys.Chem. B* **2008**, *112*, 16654.

27 Blath, J.; Christ, J.; Deubler, N. ; Hirth, T.; Schiestel, T. *Chem. Eng. J.* **2011**, *172*, 167.

28 Zhang, X.; Liu, Z.; Wang, W. *AIChE J*. **2008**, *54*, 2717.

29 Zhang, X.; Huo, F. ; Liu, Z.; Wang, W.; Shi, W.; Maginn, E. J. *J. Phys. Chem. B* **2009**, *113*, 7591.

30 Shiflett, M.B; Kasprzak, D.J; Junk, C.P.; Yokozeki, A., *J. Chem. Thermodyn.* **2008**, *40*, 25.

31 Shiflett, M.B. Yokozeki, A., *J. Chem. Eng. Data*, **2009**, *54*, 108.

32 Carvalho, P.J.; Alvarez, V.H.; Schroder, B.; Gil, A.M.; Marrucho, I.M.; Aznar, M. Santos, L.M.N.B.F.; Coutinho, J.A.P., *J. Phys. Chem.* **2009**, *113*, 6803.

33 Shi, W.; R. Myers, C.; R. Luebke, D.; Steckel, J. A.; Sorescu, D. C., *J. Phys. Chem. B* **2012**, *116*, 283.

34 Tommassi, I.; Sorrentino, F., *Tetrahedron lett.* **2006**, *47*, 6453.

35 Wang, C.; Luo, H.; Luo, X.; Li, H.; Dai, S. *Green Chem.* **2010**, *12*, 2019.

36 Rodríguez, H.; Gurau, G.; Holbrey, J. D.; Rogers, R. D., *Chem. Commun.* **2011**, *47*, 3222.

37 Johansson, K. M.; Izgorodina E. I.; Forsyth M.; MacFarlane D. R.; Seddon K. R., *Phys. Chem. Chem. Phys.*, **2008**, *10*, 2972.

38 Hollóczki, O.; Gerhard, D.; Massone, K.; Szarva, L.; Németh, B.; Veszprémi, T.; Nyulászi, L., *New J. Chem.* **2010**, *34*, 3004.

39 Gurau, G.; Rodriguez, H.; Kelley, S. P.; Janiczek, P.; Kalb, R. S.; Rogers, R. D., *Angew. Chem.* **2011**, *50*, 12024.

40 Besnard, M.; Cabaço, M. I.; Chavez, F. V.; Pinaud, N.; Sebastiao, P. J.; Coutinho, J. A. P.; Danten, T., *Chem. Commun.* **2012**, *48*, 1245.

41 Blath, J.; Deubler, N.; Hirth, T.; Schiestel, T., *Chem. Eng. J.* **2012**, *181*, 152.

42 Shiflett, Y.; Elliott B. A.; Lustig, S. R.; Sabesan, S.; Kelkar, M. S.; Yokozeki, A., *Chem. Phys. Chem.* **2012**, *13*, 1806.

43 Cabaço, M. I.; Besnard, M.; Danten, Y.; Coutinho, J. A.; *J. Phys Chem B.* **2011**, 115, 3538.

44 Yoshizawa-Fujita, M.; Johansson, K.; Newman P. MacFarlane, D.R.; Forsyth M., *Tetrahedron Lett.* **2006**, *47*, 2755.

45 D. Chinn, D.Q. Vu, M.S. Driver, L.C. Boudreau., US Patent US20,060,251,558A1, **2006**, November 9; US20,050,129,598A1, **2005**, June 16.

46 Wang, G.; Hou, W.; Xiao, F.; Geng, J.; Wu, Y.; Zhang, Z., *J. Chem. Eng. Data,* **2011**, *56*, 1125.

47 Davis Jr, J. H.; Gordon, C. M.; Hilgers, C.; Wasserscheid, P.; Ionic liquids in synthesis 2nd ed., Wasserscheid, P.; Welton, T. (Eds.), Wiley-VCH Verlag, **2008**, 7.

48 Lagourette, B. ; Boned, C.; Saint-Guirons, H.; Xans, P.; Zhou, H. *Meas. Sci. Technol.* **1992**, *3*, 699.

49 Schilling, G.; Kleinrahm, R.; Wagner, W. *J. Chem. Thermodyn.* **2008**, *40*, 1095.

50 Fandino, O.; Pensado, A.S.; Lugo, L.; Comunas, M.J.P.; Fernandez, J. J*. Chem. Eng. Data* **2005**, 50, 939.

51 Jacquemin, J.; Husson, P.; Padua, A. A. H.; Majer, V., *Green Chemistry,* **2006**, *8*, 172.

52 Jacquemin, J.; Husson, P.; Majer, V.; Cibulka, I., *J. Chem. Eng. Data* **2007**, *52*, 2204.

53 Adamson, A. W. A Textbook of Physical Chemisty, 2nd. Ed., Academic Press, New York, **1973**, p. 411-430.

54 Husson, P.; Pison, L.; Jacquemin, J.; Costa Gomes, M. F., *Fluid Phase Equilibr*. **2010**, *294*, 98.

55 Jacquemin, J.; Husson, P.; Majer V.; Costa Gomes, M.F., *Fluid Phase Equilibr.* **2006**, *240*, 87.

56 Jacquemin, J.; Costa Gomes, M.F.; Husson P.; Majer V., *J. Chem. Thermodyn.* **2006**, *38*, 490.

57 Dymond, J. H.; Smith, E. B. The Virial Coefficient of Pure Gases and mixtures, Oxford University Press Oxford, UK, **1980**.

58 Prausnitz, J. M.; Lichtenthaler, R. N.; Azevedo, E. G. Molecular Thermodynamics of Fluid-Phase Equilibria, 3rd Ed., Upper Saddle River, NJ, **1999**, p. 583-634.

59 Smith, J.M.; Ness, H.C.V.; Abott, M.M.; Introduction to Chemical Engineering Thermodynamics, MacGraw-Hill, New York, 1996.

60 Costa Gomes, M. F.; Padua, A. A. H. Developments And Applications in Solubility, RSC, **2007**, 153.

61 Costa Gomes, M. F.; Padua, A. A. H., *Pure Appl. Chem.,* **2005**, *77*, 653.

62 Hildebrand, J. H.; Prausnitz, J. M.; Scott, R. L. *Van Nostrand Reinhold: New York* **1970**, 111.

63 Jacquemin, J.; Ge, R.; Nancarrow P.; Rooney, D. W.; Costa Gomes, M. F.; Padua, A. A. H.; Hardacre, C. *J. Chem. Eng. Data*. **2008**, *53*, 716.

64 Jacquemin, J.; Nancarrow, P.; Rooney, D. W.; Costa Gomes, M. F.; Husson, Majer, V.; P.; Padua, A. A. H.; Hardacre, C. *J. Chem. Eng. Data*., **2008**, *53*, 2133

Liste des symboles

Alphabet latin/abréviations

^{13}C	: carbone 13
A_i	: paramètres ajustables de l'équation empirique de corrélation de l'absorption de gaz
A	: constante du densimètre à tube vibrant
ACACIA	: Amélioration du Captage du CO_2 Industriel et Anthropique
AMVn	: Automated Micro Viscosimeter
B	: constante du densimètre à tube vibrant
bFAP	: tris(nonafluorobutyl)trifluorophosphate
BG	: ballon de gaz
BF_4	: tetrafluoroborate
B_{ii}	: second coefficient du viriel du composé i
B_{ij}	: second coefficient du viriel croisé du mélange i + j
C_1	: connexion mobile, connexion rotulex
C_1C_1Im	: 1-3-dimethylimidazolium
C_1C_2Im	: 1-ethyl-3-methylimidazolium
C_1C_3Im	: 1-propyl-3-methylimidazolium
C_1C_4Im	: 1-butyl-3-methylimidazolium
C_1C_5Im	: 1-pentyl-3-methylimidazolium
C_1C_6Im	: 1-hexyl-3-methylimidazolium
C_2C_2Im	: 1-3-ethylimidazolium
C2	: carbone en position 2 sur un cycle imidazolium
CAS	: Chemical Abstracts Service
CH_4	: méthane
C_i	: connexion mobile, connexion rotulex
CO_2	: dioxyde de carbone
COSMO RS	: COnductor like Screening MOdel for Realistic Solvents
DBU	: 1,8-diazabicyclo[5.4.0]undec-7-ene
DFT	: Density Functional Theory
DSC	: calorimétrie différentielle à balayage
EC	: cellule d'équilibre
eFAP	: tris(pentafluoroethyl)trifluorophosphtate
ETT	: S-ethyl-N,N,N',N'-tetramethylthiouronium
f_{ij}	: fugacité du composant i dans la phase j
FAP	: tris(pentafluoroalkyl)trifluorophosphate
FUI	: Fonds Unique Interministériel
GDF	: Gaz de France
GES	: gaz à effet de serre
$GtCO_2eq$	: milliards de tonnes-équivalent dioxyde de carbone
ICCF	: Institut de Chimie de Clermont Ferrand
IDA	: iminiodiacétate
Im	: imidazolium
IRTF	: Infrarouge à Transformée de Fourier
ISB	: isobutyrate

k : constante de calibration
K : Kelvin
K_H : constante de Henry
LB : ballon de gaz
LEV : levulinate
LI : liquide ionique
LCOMS : Laboratoire de Chimie Organométallique de Surface de Lyon
LMOPS : Laboratoire Matériaux Organiques à Propriétés Spécifiques de Lyon
LSA : Laboratoire de Sciences Analytiques de Lyon
m : masse
M : masse molaire, manomètre
MPa : megapascal
MTBD : 1,3,4,6,7,8-hexahydro-1-methyl-2H-pyrimido[1,2-a]pyrimidine
n : nombre de mole
N_{2224} : triethylbutylammonium
N_2O : protoxyde d'azote
NIST : National Institute of Standards and Technology
NTf_2 : bis(trifluoromethylsulfonyl)imide
O_3 : ozone
OAc : acétate
OT : bulleur
p : pression
P_{66614} : trihexyl(tetradecyl)phosphonium
p_{eq} : pression d'équilibre
PF_6 : hexafluorophosphate
pFAP : tris(heptafluoropropyl)trifluorophosphate
PFC : hydrocarbures perfluorés
PG : générateur de pression
PID : proportionnel intégral dérivé
ppm : partie par million
pVT : méthode de saturation à volume constant
PRG : pouvoir de réchauffement global
PRO : propionate
PRT : sonde de température
Pyrro : pyrrolidinium
R : constante universelle des gaz parfaits
RMN : résonance magnétique nucléaire
RPT : Resonant Pressure Transducers
SCH : Schlenk
SG : seringue en verre étanche aux gaz
SF_6 : hexafluorure de soufre
T : température en ℃ / K
t_1 : temps de chute
TFA : trifluoroacétate
TMA : trimethylacétate
TB : thermorégulateur
T_{fus} : température de fusion
$T_{déc}$: température de décomposition
TP : piège froid
TS : tube enroulé en forme de spirale
V : volume
V_{EC} : volume cellule d'équilibre

V_i	: vannes à piston
VG	: jauge de pression
V_m	: volume molaire
V_m^E	: volume molaire d'excès
VP	: pompe à vide
x_i	: fraction molaire du constituant i
Z_i	: facteur de compressibilité du composé i
Z_{ij}	: facteur de compressibilité de la solution i+j

Alphabet grec

ρ	: masse volumique
τ	: période de vibration
σ	: écart type
η	: viscosité
Φ	: coefficient de fugacité du composé i
$\Delta_{sol}G$	: énergie de Gibbs de solvatation
$\Delta_{sol}H$	: enthalpie
$\Delta_{sol}S$	: entropie